Indoleamine 2,3-dioxygenase 1 versus *Toxoplasma gondii* - host species determines success

Inaugural dissertation

for the attainment of the title of doctor
in the Faculty of Mathematics and Natural Sciences
at the Heinrich Heine University Düsseldorf

presented by

Christoph-Martin Ufermann
from Berlin

Düsseldorf, November 2021

from the Institute of Medical Microbiology and Hospital Hygiene
at the Heinrich Heine University Düsseldorf

Published by permission of the
Faculty of Mathematics and Natural Science at
Heinrich Heine University Düsseldorf

Supervisor: Prof. Dr. Walter Däubener

Co-supervisor: Prof. Dr. Lutz Schmitt

Date of oral examination: April 6th, 2022

Parts of this thesis have been published in:

Katrin Spekker-Bosker †, **Christoph-Martin Ufermann** †, Marco Maywald, Albert Zimmermann, Andreas Domröse, Claudia Woite, Walter Däubener and Silvia Kathrin Eller, hCMV-Mediated Immune Escape Mechanisms Favor Pathogen Growth and Disturb the Immune Privilege of the Eye. International Journal of Molecular Sciences 2019 DOI:10.3390/ijms20040858

> **C-MU** designed and performed experiments, analyzed data and wrote the manuscript (contribution: 30 %). CW assisted with the experiments. MM and AZ performed experiments, analyzed data and wrote the manuscript. AD wrote the manuscript. KS-B, WD and SE conceptualized the study, performed experiments, analyzed and validated all data, prepared figures and wrote the manuscript.

Katrin Spekker-Bosker †, **Christoph-Martin Ufermann** †, Maike Oldenburg, Walter Däubener and Silvia Kathrin Eller, Interplay between IDO1 and iNOS in human retinal pigment epithelial cells. Medical Microbiology and Immunology 2019 DOI:10.1007/s00430-019-00627-4

> **C-MU** designed and performed experiments, analyzed data and wrote the manuscript (contribution: 35 %). MO performed experiments. KS-B, WD and SE conceptualized the study, performed experiments, analyzed data, prepared figures and wrote the manuscript.

Christoph-Martin Ufermann †, Andreas Domröse †, Timo Babel, Anne Tersteegen, Sevgi Can Cengiz, Silvia Kathrin Eller, Katrin Spekker-Bosker, Ursula Regina Sorg, Irmgard Förster and Walter Däubener, Indoleamine 2,3-Dioxygenase Activity During Acute Toxoplasmosis and the Suppressed T Cell Proliferation in Mice. Frontiers in Cellular and Infection Microbiology 2019 DOI:10.3389/fcimb.2019.00184

> **C-MU** designed and performed experiments, analyzed all data, prepared figures and wrote the manuscript (contribution: 50 %). AD designed and performed experiments, prepared figures and wrote the manuscript. TB, AT, SC, SE and KS-B assisted with and performed experiments. US supervised animal experiments. WD and IF conceived and supervised the study. WD designed experiments and wrote the manuscript.

---

† shared first authorship.

Abstract

A primary acute infection with the zoonotic parasite *Toxoplasma gondii* (*T. gondii*) is usually asymptomatic or is accompanied with mild flu-like symptoms in immunocompetent healthy individuals. Here, a type 1 T helper cell (Th1) immune response is triggered that controls the acute infection and drives *T. gondii* to establish a chronic infection; thus *T. gondii* persists lifelong in its host. A clinically significant manifestation of an acute or reactivated chronic infection is ocular toxoplasmosis. Characteristic for a Th1 response is the induction of interferon gamma (IFN-γ) production via activated lymphocytes (e.g. T cells). IFN-γ plays an essential role in inhibiting the growth of pathogenic microorganisms by induction of a plethora of cell-autonomous effector molecules that are differentially regulated. This includes enzymes like the tryptophan degrading enzyme indoleamine 2,3-dioxygenase 1 (IDO1) that eventually leads to kynurenine production and the nitric oxide (NO) producing inducible NO synthase (iNOS). Both enzymes show extremely diverse roles including microbial defense and immune regulation.

The aim of this thesis is to further extend the knowledge on antimicrobial and immunosuppressive capacity of IDO1 using both *in vitro* and *in vivo* approaches.

Ocular toxoplasmosis was addressed by using a human retinal pigment epithelium (hRPE) cell line. Here, specific emphasis is on IDO1 and iNOS activity directed against *T. gondii* and *Staphylococcus aureus*. Furthermore, the immunosuppressive potential of hRPE specific IDO1 was analyzed. IDO1 activity inhibited pathogen growth and lymphocyte proliferation efficiently, whereas iNOS activity interfered with the antimicrobial effector function and immunosuppressive capacity of IDO1 in hRPE cells.

An experimental murine infection model was used to analyze the role of murine IDO1 (mIDO1) during the acute phase of toxoplasmosis *in vivo*. Here, C57BL/6J mice deficient for mIDO1 ($IDO^{-/-}$) and control mice (WT) were infected with *T. gondii* tachyzoites.

The course of the acute infection was not altered in $IDO^{-/-}$ mice. Parasite loads were comparable in the analyzed organs, even though mIDO1 was highly expressed in lung of WT mice and was absent in $IDO^{-/-}$ mice. Murine guanylate binding proteins – IFN-γ induced effector proteins – and miNOS, were detected in both genotypes in a comparable pattern. Interestingly, NO production by miNOS activity increased in absence of mIDO1 and parasite proliferation was increased by miNOS inhibition *ex vivo* in the absence of mIDO1 in different cell types.

Different T cell populations showed clear activation phenotypes in WT and IDO$^{-/-}$ mice. The lymphocyte proliferation response to *ex vivo* mitogen stimulation was drastically impaired at day seven post infection. This hyporesponsiveness of the lymphocytes was independent of mIDO1 but instead dependent on miNOS activity and interleukin-2 deprivation.

Conclusively, IDO1 is capable to inhibit the growth of pathogenic microorganisms (e.g. *T. gondii*) and thereby contributes as an effector mechanism to cell-autonomous immunity. Furthermore, the immunosuppressive capacity of IDO1 was demonstrated. Nevertheless, antimicrobial and immunosuppressive activity of IDO1 depend both on the context in which host and pathogen encounter one another (i.e. host species and pathogen species).

Zusammenfassung

Eine akute Primärinfektion mit dem zoonotischen Parasit *Toxoplasma gondii* (*T. gondii*) verläuft bei immunkompetenten gesunden Personen in der Regel asymptomatisch oder wird von leichten grippeähnlichen Symptomen begleitet. Hier wird eine Typ-1 T-Helferzell-Immunreaktion (Th1) ausgelöst, die die akute Infektion kontrolliert. Folglich etabliert sich eine chronische Infektion, wodurch *T. gondii* lebenslang in seinem Wirt persistiert. Eine klinisch bedeutsame Manifestation einer akuten oder reaktivierten chronischen Infektion ist die okuläre Toxoplasmose. Charakteristisch für eine Th1-Antwort ist die Induktion der Produktion von Interferon gamma (IFN-γ) durch aktivierte Lymphozyten (z. B. T-Zellen). IFN-γ spielt eine wesentliche Rolle bei der Hemmung des Wachstums pathogener Mikroorganismen durch die Induktion einer Vielzahl von zellautonomen Effektormolekülen, die unterschiedlich reguliert werden. Dazu gehören Enzyme wie das Tryptophan abbauende Enzym Indolamin-2,3-Dioxygenase 1 (IDO1), das schließlich zur Produktion von Kynurenin führt, und die Stickstoffmonoxid (NO) produzierende induzierbare NO-Synthase (iNOS). Beide Enzyme haben äußerst vielfältige Funktionen, unter anderem in der mikrobiellen Abwehr und der Immunregulation.

Ziel dieser Arbeit ist es, das Wissen über das antimikrobielle und immunsuppressive Potential von IDO1 mit Hilfe von *in vitro*- und *in vivo*-Ansätzen zu erweitern.

Zur Untersuchung der okulären Toxoplasmose wurde eine Zelllinie des menschlichen retinalen Pigmentepithels (hRPE) verwendet. Hier liegt der Schwerpunkt auf der IDO1- und iNOS-Aktivität, gerichtet gegen *T. gondii* und *Staphylococcus aureus*. Außerdem wurde das immunsuppressive Potenzial der hRPE-spezifischen IDO1 analysiert. Die IDO1-Aktivität hemmte das Erregerwachstum und die Lymphozytenproliferation effizient, während die iNOS-Aktivität die antimikrobielle Effektorfunktion und die immunsuppressive Kapazität von IDO1 in hRPE-Zellen beeinträchtigte.

Ein experimentelles Mausinfektionsmodell wurde verwendet, um die Rolle der murinen IDO1 (mIDO1) während der akuten Phase der Toxoplasmose *in vivo* zu analysieren. Dabei wurden C57BL/6J-Mäuse, denen mIDO1 fehlt ($IDO^{-/-}$), und Kontrollmäuse (WT) mit *T. gondii* Tachyzoiten infiziert.

Der Verlauf der akuten Infektion war bei $IDO^{-/-}$ Mäusen unverändert. Die Parasitenbelastung in den untersuchten Organen war vergleichbar, obwohl mIDO1 in der Lunge von WT-Mäusen stark exprimiert wurde und in $IDO^{-/-}$ Mäusen fehlte. Murine Guanylat-bindende Proteine – weitere IFN-γ-induzierte Effektormoleküle – und miNOS

wurden in beiden Genotypen in einem vergleichbaren Maß nachgewiesen. Interessanterweise stieg die NO-Produktion durch miNOS-Aktivität in Abwesenheit von mIDO1 an, und die Parasitenproliferation wurde durch miNOS-Hemmung *ex vivo* in Abwesenheit von mIDO1 in verschiedenen Zellen gefördert.
Verschiedene T-Zell-Populationen aus infizierten WT und $IDO^{-/-}$ Mäusen zeigten einen deutlichen Aktivierungsphänotyp. Die *ex vivo* Mitogen stimulierte Proliferation von Lymphocyten war am siebten Tag nach der Infektion drastisch beeinträchtigt. Diese reduzierte Proliferation der Lymphozyten war jedoch unabhängig von mIDO1 und wurde durch miNOS-Aktivität und den Entzug von Interleukin-2 beeinflusst.

IDO1 ist folglich in der Lage, das Wachstum von pathogenen Mikroorganismen (z. B. *T. gondii*) zu hemmen und trägt somit als Effektormechanismus zur zellautonomen Immunität bei. Darüber hinaus besitzt IDO1 ein immunsuppressives Potential. Diese antimikrobielle und die immunsuppressive Wirkung von IDO1 hängen jedoch von dem Kontext ab, in dem Wirt und Erreger aufeinandertreffen (d. h. von der Art des Wirts und der Art des Erregers).

Table of contents

1. Introduction

Perpetual exposition to microorganisms poses a challenge that requires a defense system that ensures the integrity of the body. The complex immune system conveys this very essential ability by discriminating between self and non-self. Immune responses that convey innate and adaptive immunity differ significantly. Fast and antigen-unspecific innate immune responses are required to prevent initial colonization by and the spread of pathogens in the body. Thereby gaining time for the induced adaptive immune response to develop. Development of an adaptive immune response takes days; however, is highly antigen-specific and thus extremely efficient in limiting and killing pathogenic microorganisms. Microorganisms are not per se disease causing and thus pathogenic (e.g. commensal bacteria). They are categorized in four large groups: viruses, bacteria, fungi and parasites [Janeway 2019 pp. 1-11]. A prominent pathogenic unicellular eukaryote with a parasitic lifestyle is the apicomplexan parasite *Toxoplasma gondii* (*T. gondii*).

1.1 Toxoplasma gondii – a ubiquitous species with many strains

T. gondii was named by Nicolle and Manceaux who were the first to describe this parasite. They identified *T. gondii* in a hamster-like rodent (*Ctenodactylus gundi*) used for leishmaniasis research in their laboratory in Tunis, Tunisia [Nicolle and Manceaux 1909].

T. gondii belongs to the protozoan phylum Apicomplexa that is comprised of thousands of species that all have a parasitic lifestyle in common [Adl *et al.* 2007]. The genus *Toxoplasma* contains only one species, namely *T. gondii*, with diverse strains that differ in global distribution and vary in virulence. Virulence of *T. gondii* was first determined in infection experiments with outbred Swiss mice. *T. gondii* strains are defined as either highly virulent (lethal dose < 10 tachyzoites) or non-virulent (lethal dose > 1000 tachyzoites) [Sibley and Boothroyd 1992]. *T. gondii* strains are assorted into three main clonal linages based on polymerase chain reaction - restriction fragment length polymorphisms [Sibley and Boothroyd 1992; Howe and Sibley 1995]. More recently a fourth clonal linage, namely type 12 that is common in North America, has been identified [Khan *et al.* 2011]. Type I and type II strains are more frequent in humans in comparison to type III strains [Howe and Sibley 1995]. Type I strains comprise all highly virulent strains (e.g. the RH strain, originally isolated from a patient with fatal

encephalitis [Sabin 1941]). The non-virulent strains are type II (e.g. ME49 strain, originally isolated from sheep [Lunde 1983]) and type III (e.g. CTG strain, originally isolated from a cat [Pfefferkorn *et al.* 1977]) strains [Howe and Sibley 1995]. Global diversity of *T. gondii* has recently been analyzed and revealed 15 haplogroups that comprise six major clades [Su *et al.* 2012].

1.1.1 Stage conversion as key to infection, pathogenesis and transmission

T. gondii is an obligate intracellular parasite that can infect all nucleated cells of warm-blooded organisms [Dubey 2009a]. Here, the intruder resides within the so called parasitophorous vacuole (PV), an intracellular compartment that is surrounded by a membrane. Sexual reproduction is restricted to the intestine of its definite hosts, which are members of the Felidae family (e.g. cats) [Jackson and Hutchison 1989] (Figure 1 A). As a matter of fact, only very recently it has been shown that this species specificity is based exclusively on the absence of delta-6-desaturase, an enzyme required for the initial and rate limiting step of linoleic acid conversion to arachidonic acid, in the cat's intestine [Martorelli Di Genova *et al.* 2019]. Martorelli Di Genova *et al.* hypothesized that the absence of intestinal delta-6-desaturase leads to a buildup of nutritional linoleic acid, which in turn acts as a signaling molecule triggering sexual development of *T. gondii* [Martorelli Di Genova *et al.* 2019]. Cats finally shed *T. gondii* oocysts with their feces into the environment where these oocysts sporulate und become infectious [Dubey *et al.* 1970]. Asexual replication by a process called endodyogeny [Goldman *et al.* 1958; Sheffield and Melton 1968] is performed by two stages. Rapid proliferating tachyzoites that lyse and egress in order to invade new host cells present one asexually replicating stage (Figure 1 C). This phase of rapid proliferation, host cell rupture, and invasion correspond to the acute stage of an infection that is known as the lytic cycle. Tachyzoites disseminate and convert into another asexually replicating stage, called bradyzoites. Bradyzoites are metabolically less active and are able to form tissue cysts in many organs, however predominantly in brain and muscle tissue [Dubey 1998], representing the chronic stage of infection (Figure 1 A & C).

1.1.2 Epidemiology and clinical manifestation of toxoplasmosis

Toxoplasmosis is a zoonotic disease of major medical and veterinary importance. *T. gondii* infects domestic animals (e.g. ovine and porcine species) with severe effects

on survival of the hosts (including their offspring) (Figure 1 A). Approximately one-third of the human population has been infected with *T. gondii* [Dubey 2009b]. In the German population prevalence of *T. gondii* is, depending on demographic factors, relatively high (seroprevalence: 49.1 %) [Wilking *et al.* 2016].

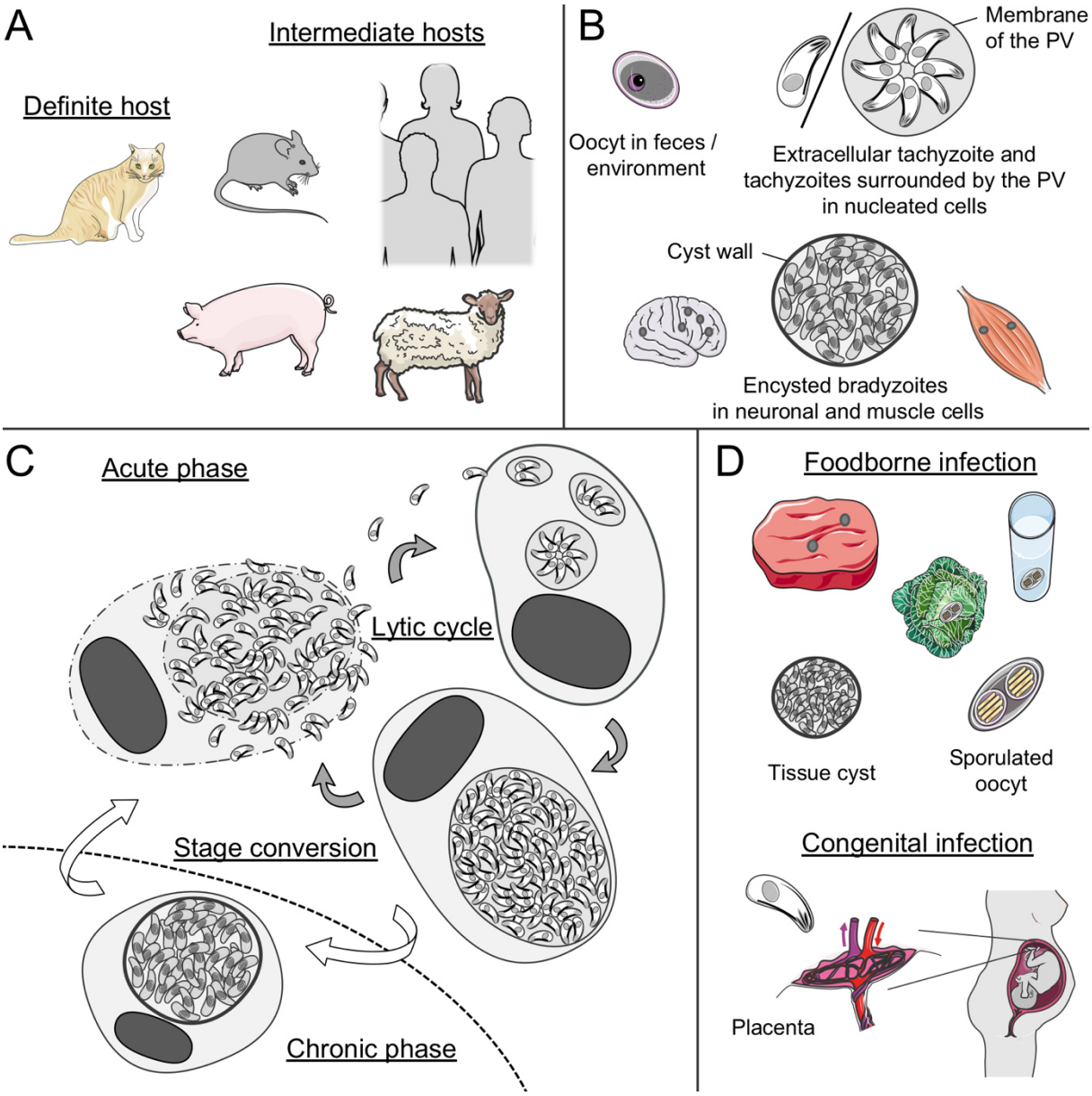

Figure 1: *Toxoplasma gondii* - hosts, asexual replication and transmission routes.

A, Illustration of exemplary hosts. **B**, Different *Toxoplasma gondii* (*T. gondii*) stages and their occurrence. Sexual replication of *T. gondii* takes place in feline enterocytes. In intermediate hosts, replication is restricted to clonal proliferation in nucleated cells. **C**, Schematic illustration of the asexual replication of *T. gondii*. During the acute phase tachyzoites invade host cells actively, reside within a parasitophorous vacuole (PV), proliferate rapidly until the host cell is lysed in order to egress and to start over again. Conversion to metabolically less active bradyzoites that form tissue cysts is characteristic for the chronic phase of infection. **D**, Human toxoplasmosis is predominantly a foodborne infection; however, tachyzoites can cross the placental barrier and thus can be vertically transmitted. Section **C** is adapted and redrawn from [Zhang *et al.* 2013a].

T. gondii is transmitted to humans via food consumption – undercooked meat that contains tissue cysts or water and vegetables contaminated with sporulated oocysts – or by vertical transmission (Figure 1 D). However, postnatally acquired *T. gondii* infections are the predominant cause of human toxoplasmosis [Schlüter *et al.* 2014]. According to the world health organization (WHO), toxoplasmosis contributes significantly to the overall burden of foodborne infectious diseases [WHO 2015] and thus is an important public health issue [Torgerson and Mastroiacovo 2013].

A primary acute infection is usually asymptomatic or is accompanied with mild flu-like symptoms in immunocompetent healthy individuals. Here, the infection is adequately controlled by the host immune system leading to stage conversion from the acute into the chronic stage of infection, resulting in lifelong persistence in its host (Figure 1 C). However, during fetal development and in immunocompromised individuals (e.g. after organ transplantations) a primary acute infection or reactivation of a chronic infection can be fatal. Clinically significant manifestations of this zoonosis are congenital toxoplasmosis, toxoplasma encephalitis and ocular toxoplasmosis [Montoya and Liesenfeld 2004]. Vertical transmission of the parasite occurs in pregnant women with primary acute toxoplasmosis (Figure 1 D). Clinical manifestations in neonates with congenital toxoplasmosis vary greatly and include cranial calcification, hydrocephalus and epilepsies [MacAuley *et al.* 1994]. Brain abscesses and lesions are characteristic for toxoplasmic encephalitis, which is a life-threatening manifestation as a result of reactivation of the chronic infection during immunosuppression, for instance in patients with acquired immune deficiency syndrome (AIDS) [Luft *et al.* 1983]. Primary acute infection or reactivation of chronic tissue cysts from congenital infection can lead to ocular toxoplasmosis (Figure 2 B - D) [Talabani *et al.* 2010]. *T. gondii* usually infects the cells of the neuronal retina and of the retinal pigment epithelium and therefore causes inflammation of the retina (retinitis) (Figure 2 A). A toxoplasmic retinochoroiditis develops, if the retinitis affects the underlying choroid [Maenz *et al.* 2014]. Ocular toxoplasmosis is an important cause of irreversible visual impairment [Pleyer *et al.* 2019]. Being the most frequent form of infectious posterior uveitis [Maenz *et al.* 2014] ocular toxoplasmosis represents up to 85 % (4.2 % in Germany [Jakob *et al.* 2009]) of all cases [Talabani *et al.* 2010].

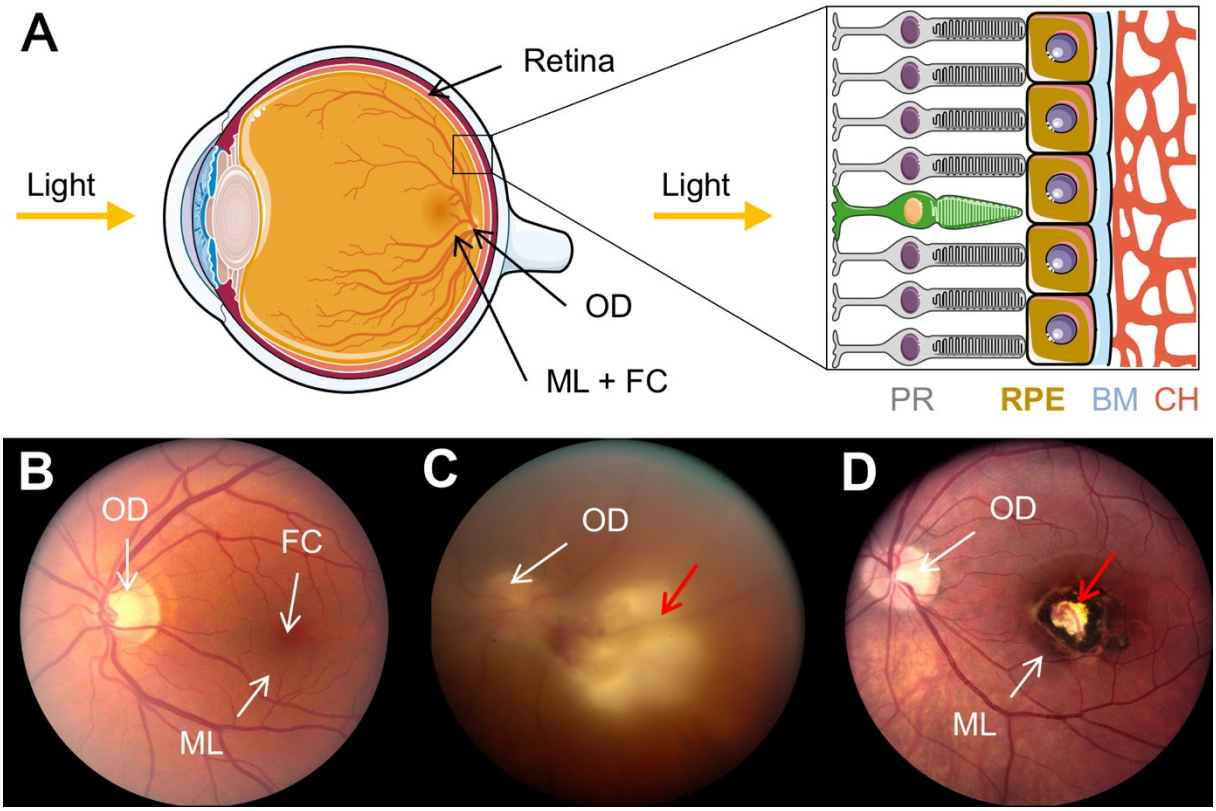

Figure 2: Ocular toxoplasmosis - Schematic illustration of the retina and fundus photography's.

A, Schematic illustration of the human eye and the different layers of the retina, consisting of the neuronal retina (here only photoreceptors (PR)), retinal pigment epithelium (RPE), Bruch's membrane (BM) and the underlying choroid (CH). Fundus photography's of (**B**) a healthy retina, (**C**) a retina during primary acquired acute toxoplasmosis and (**D**) a scarred retina from congenital toxoplasmosis. **C** & **D**, Red arrows point to the lesion caused by the lytic nature of the rapidly replicating tachyzoites and the scar in the macula lutea. **B** - **D**, Fundus photography's were re-used with permission from [AAPOS 2020]. All rights remain with the American Association of Pediatric Ophthalmology & Strabismus (AAPOS). Permission for re-use granted by Scott, Christina (Client Services Coordinator, AAPOS). (OD - optic disc; ML - macula lutea; FC - fovea centralis).

1.2 The host's counterattack: The immune response against the intracellular intruder *T. gondii*

Immune responses elicited by a *T. gondii* infection have been studied in a large variety of host species, with murine models being the most studied *in vivo* model. Here, immune responses against experimental infections with the tachyzoite stage are most frequently analyzed [Munoz *et al.* 2011]. *In vitro* models that address antiparasitic activity against *T. gondii* have been expanded to a large variety of hosts, including murine, ovine and bovine species, and humans to name a few, as well as different cell types (e.g. mesenchymal stem cells, macrophages, endothelial cells) [Mukhopadhyay *et al.* 2020; Spekker *et al.* 2013; Sibley *et al.* 1991; Däubener *et al.* 2001].

1.2.1 Sensing and innate immune cell activation

The first line of defense is posed by anatomical barriers (e.g. skin and mucosa) that hinder pathogen entrance, antimicrobial molecules (e.g. defensins and lysozymes) that are secreted to inhibit or even kill microorganism and commensal flora that limit colonization of pathogenic microorganisms by competition [Janeway 2019 pp. 42-43]. However, once this first line of defense is overcome, *T. gondii* is not residing safe and sound within its host, but rather faces a hostile environment with a plethora of antimicrobial weapons.

Infected and apoptotic cells, free parasites and its secreted molecules are taken up by phagocytic cells of the innate immune system. These cells include monocytes, macrophages, granulocytes and dendritic cells (DCs). Pathogen associated molecular patterns (PAMPs) are recognized with a set of highly conserved receptors, so called pattern recognition receptors (PRRs). PRR engagement increase phagocytic activity by macrophages and induces production of proinflammatory cytokines and chemokines by antigen presenting cells (APCs) thereby activating accessory non-immune cells and attracting additional leukocytes [Mogensen 2009]. Profilin, an actin binding protein involved in *T. gondii* gliding motility and host cell invasion [Plattner *et al.* 2008], is sensed by uninfected murine DCs via endosomal Toll-like receptor (TLR) 11 and 12 [Yarovinsky 2005; Andrade *et al.* 2013]. TLRs are PRRs integrated into membranes that are exposed to the extracellular milieu or to the endosomal lumen (Figure 3). Ligand engaged TLRs, like TLR11/12 with profilin, signal via the adaptor molecule myeloid differentiation primary response 88 (MyD88) that activates interferon response factor (IRF), a class of transcription factors, which in turn induce interleukin (IL)-12 production and secretion [Arancibia *et al.* 2007; Raetz *et al.* 2013]. TLR7/9, which are located in endosomes, are nucleic acid sensors that have been implicated to be involved in *T. gondii* sensing as well. In contrast to mice many other hosts (e.g. ovine species and humans) lack TLR11/12 and likely rely on other sensing mechanisms [Gazzinelli *et al.* 2014]. PRRs on the cell surface, like TLR2/4, can sense *T. gondii* surface glycosylphosphatidylinositol and have been described to contribute to host defense [Debierre-Grockiego *et al.* 2007]. Secreted molecules from *T. gondii* have been shown to trigger MyD88 and nuclear factor κB (NFκB) independent of receptor activation resulting in IL-12 and tumor necrosis factor-alpha (TNF-α) production by monocytes (Figure 3) [Rosowski *et al.* 2011; Braun *et al.* 2013].

Inflammasome activation has been described as a sensing pathway of *T. gondii* infected human and murine monocytes and macrophages [Wang *et al.* 2020]. Here, the nucleotide-binding oligomerization domain-like receptors NLRP1 [Witola *et al.* 2011; Ewald *et al.* 2013] and NLRP3 [Gov *et al.* 2017; Gorfu *et al.* 2014], which are cytosolic PRRs, are activated ultimately resulting in IL-1β and IL-18 production (Figure 3). These cytokines in turn induce interferon gamma (IFN-γ) production by neutrophils and contribute to IFN-γ production by T cells and natural killer (NK) cells, another leukocyte of the innate immune system [Sturge *et al.* 2013; López-Yglesias *et al.* 2019].

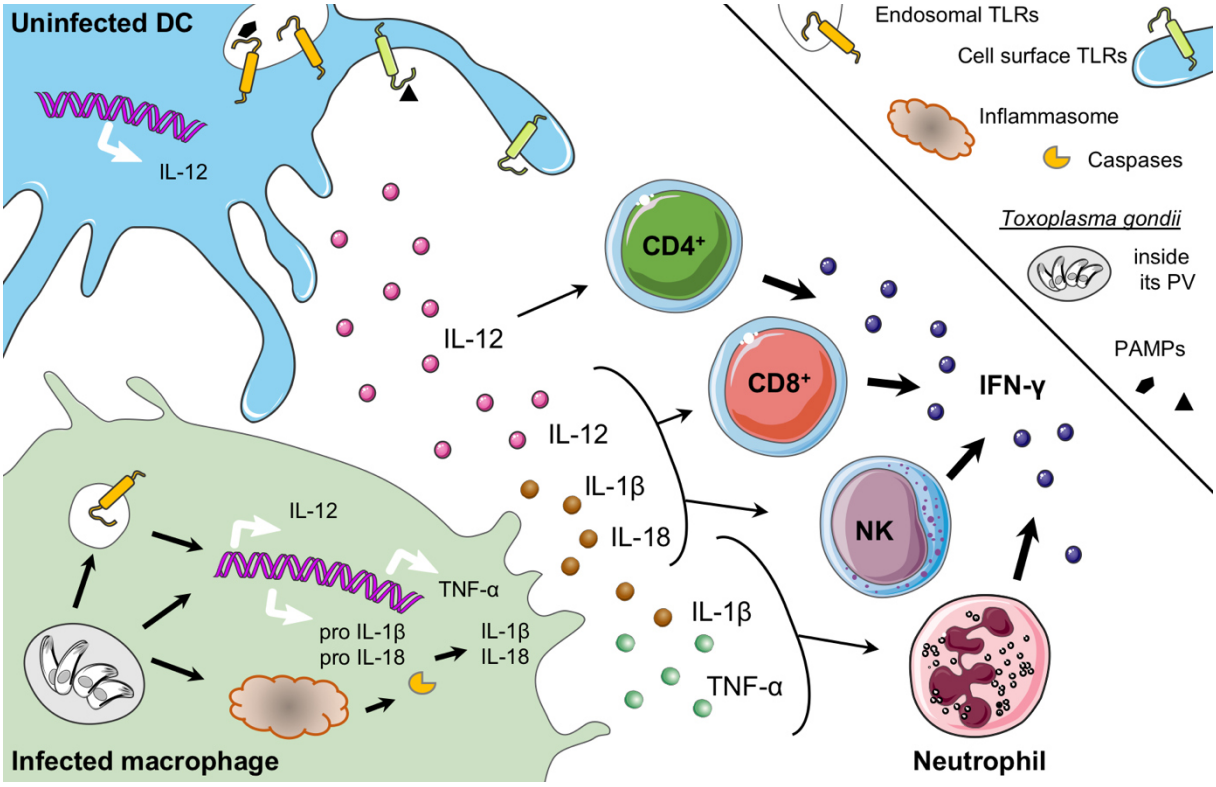

Figure 3: Proinflammatory cytokine induction during acute toxoplasmosis.
Pattern recognition receptor (PRRs) dependent and independent induction of proinflammatory cytokine production during the initial encounter of innate immune cells with *Toxoplasma gondii* (*T. gondii*) and the concomitant activation of IFN-γ production by innate and adaptive immune cells. Uninfected antigen presenting cells (APCs), like dendritic cells (DCs), sense extracellular or intracellular pathogen associated molecular patterns (PAMPs) of *T. gondii* via Toll like receptors (TLRs) on the cell surface and in endosomes respectively, activating IL-12 production. IL-12 and TNF-α production is induced by parasite derived molecules independent of receptor activation in infected monocytes (here a macrophage). Cytosolic PRRs can be activated leading to inflammasome activation. Inflammasome activated caspases in turn activate pro IL-1β and pro IL-18 and thus secretion of their active form. Adapted and redrawn from [Mukhopadhyay *et al.* 2020]. (PV, parasitophorous vacuole; IL-12/-1β/-18, interleukin-12/-1β/-18; TNF-α, tumor necrosis factor alpha; IFN-γ, interferon gamma; CD, cluster of differentiation; $CD4^+$/$CD8^+$, CD4 / CD8 positive T cells; NK, natural killer cell).

Recently, a novel mechanism has been identified by which human and murine monocytes indirectly sense *T. gondii* and are recruited to the site of infection. Here, S100A11, an alarmin produced in a caspase-1 dependent manner in infected cells, is released from lysed host cells leading to recruitment of monocytes in a chemokine ligand 2 (CCL2) dependent manner, independent of IL-12 and IFN-γ [Safronova *et al.* 2018]. Neutrophils that are recruited via chemokine receptor 1 (CCR1) [Khan *et al.* 2001] to the site of infection do not only produce cytokines. They directly contribute to limit parasite movement and thus dissemination by formation of neutrophil extracellular traps consisting of nuclear DNA fibers and associated enzymes and peptides with antimicrobial potential [Diaz-Goldines *et al.* 2019; Abdallah *et al.* 2012]. NK cells that are recruited to the site of infection in a CCR5-dependent manner [Kahn *et al.* 2006] are predominantly required for IFN-γ production since perforin-deficient mice that lack cytotoxicity by NK cells, but have a functional IFN-γ production, survived an infection with a type II *T. gondii* strain [Denkers *et al.* 1997].

During acute toxoplasmosis, ligand sensing by PRRs activates the innate immune system. IL-12 from DCs and macrophages in concert with IL-1β, IL-18 and TNF-α from monocytes and macrophages lead to a robust production of IFN-γ by innate immune cells (e.g. NK cells, neutrophils) as well as by adaptive immune cells (e.g. $CD4^+$ and $CD8^+$ T cells). IFN-γ that is produced in the early phase of infection is required to induce numerous effector mechanisms that help to control the acute phase [Yarovinsky 2014], whereas IFN-γ produced by the adaptive immune cells are required for the control of the chronic phase of infection [Khan 2019].

1.2.2 Type 1 T helper cell driven adaptive immune response against *T. gondii*

The key players of the adaptive immune system are B cells and T cells. Their targets are recognized in an antigen-specific manner by receptors that, in contrast to the highly conserved PRRs of innate immune cells, develop through somatic recombination. Somatic recombination is a process of gene rearrangement that takes place in B cell and T cell development in primary lymphoid organs (bone marrow and thymus respectively), which will result in a unique receptor that will bind a specific antigen and thereby increases diversity and specificity of the receptor repertoire [Janeway 2019 pp. 15-17; 175-191]. Both B cells and T cells are important lymphocytes required for

the control of the chronic phase of a *T. gondii* infection; however, during the acute phase B cells poses a less important role than T cells. Therefore, the following sections focus on the type 1 T helper cell (Th1) driven adaptive immune response induced during acute toxoplasmosis [Gazzinelli *et al.* 1994], with specific emphasis on selected T cell subsets (CTL, Th1, Treg) and T cell activation.

1.2.2.1 T cells - $CD3^+$ lymphocytes

The T cell receptor (TCR) is critical for activation, differentiation and effector function of the T cell. The TCR consists of two chains with constant and variable regions. The latter contain complementary determining regions that are shaped during somatic recombination, determining the specificity of the TCR for an epitope of an antigen that the TCR binds. Endogenous or exogenous antigens are processed by proteasomal or endosomal degradation and are presented as small peptide fragments on class I or class II major histocompatibility complex (MHCI and MHCII respectively) molecules. The interaction of the TCR with the peptide presented on MHC molecules is stabilized by interaction of cluster of differentiation (CD) 8 and CD4 molecules on the T cell with MHCI and MHCII on the interacting cell, respectively. The TCR lacks transmembrane domains and thus relies on other molecules, including CD3 molecules, for signal transduction. Together with the TCR these signal transducing molecules make up the TCR complex [Nikolich-Žugich *et al.* 2004; Clambey *et al.* 2014]. Hence, T cells ($CD3^+$ lymphocytes) can be discriminated from all other leucocytes by detection of CD3 on the cell surface.

The process of antigenic T cell activation and concomitant differentiation and clonal expansion is exemplarily described for Th1 cells in section 1.2.2.2. Th1 cells are a subgroup of CD4 expressing ($CD4^+$) effector T cells, so called T helper cells, that are induced during infections with intracellular pathogens (e.g. *T. gondii*) [Zhu *et al.* 2010; Gazzinelli *et al.* 1994]. Additional effector T cells are introduced in section 1.2.2.3.

1.2.2.2 Type 1 T helper cell differentiation

Development of naïve $CD4^+$ T cells into the appropriate, antigen-specific $CD4^+$ effector T cell requires three signals (Figure 4). (i), Antigen-specific TCR activation by the TCR engaging a peptide:MHCII complex on the APC. (ii), A costimulatory signal mediated by CD28 or CD40L on the T cell with CD80/CD86 or CD40 on the DC. CD28-dependent costimulation induces IL-2 expression as well as several activation

markers (compare Table 1, p. 11), like the high affinity IL-2 receptor (CD25). (iii), A lineage specific cytokine stimulus [Janeway 2019 p. 368].

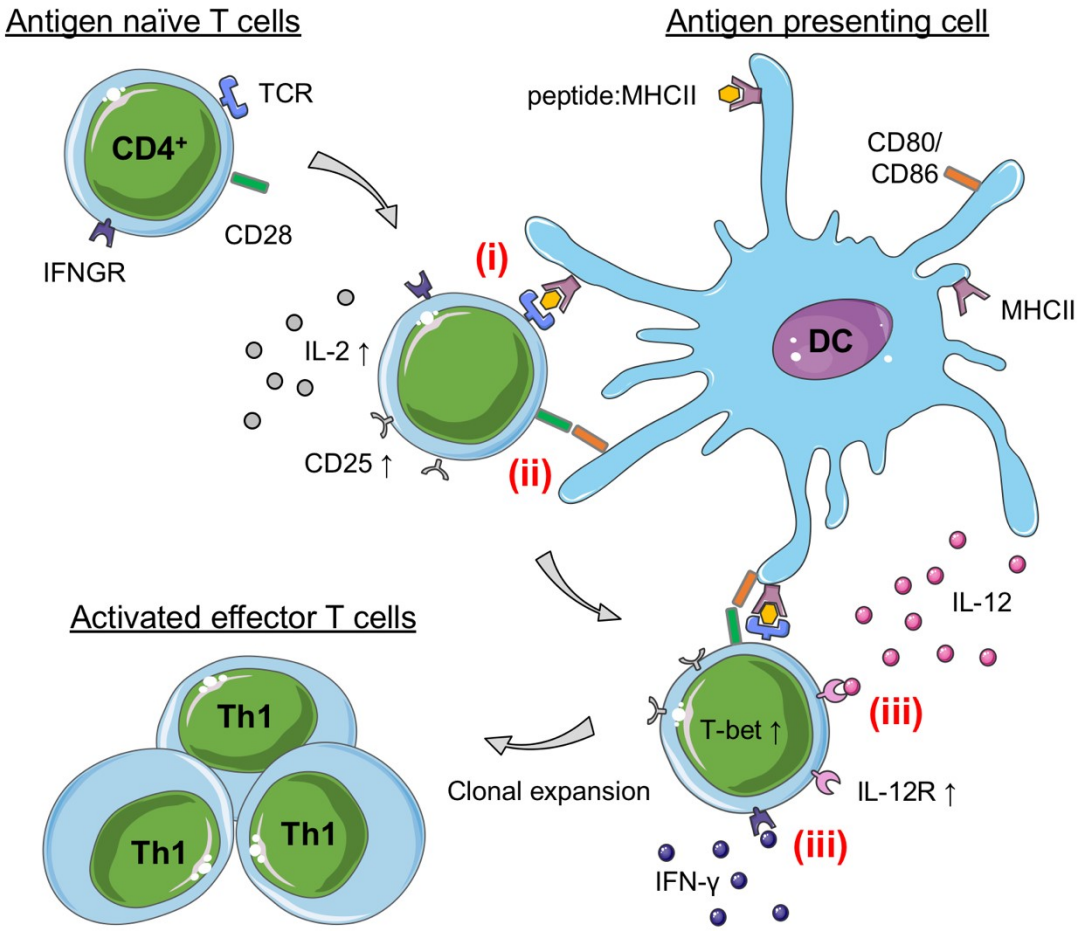

Figure 4: Th1 cell differentiation.
Type 1 T helper (Th1) cell development requires three signals. **(i)** Presentation of processed antigen as a peptide on MHCII (peptide:MHCII) by dendritic cells (DCs) to antigen naïve $CD4^+$ T cells. **(ii)** Costimulation by interaction of CD28 on T cells with CD80/CD86 on DCs. Activation of T cell receptor (TCR) and CD28 on T cells induces interleukin (IL)-2 receptor (CD25) expression and IL-2 production. **(iii)** Stimulation of T cells with cytokines specific for the Th1 lineage. Binding of interferon gamma (IFN-γ) to its receptor complex (IFNGR) leads to expression of the inducible subunit of the IL-12 receptor (IL-12R) and induces the transcription factor T-bet. Antigen presenting DCs produce IL-12 that induces IL-12R signaling in T cells leading to further increased T-bet expression. Eventually resulting in clonal expansion of the activated effector Th1 cells. Adapted and redrawn from [Ng *et al.* 2013]. (MHCII, class II major histocompatibility complex; CD, cluster of differentiation).

Th1 cell differentiation requires IL-12 and IFN-γ that are, as elaborated above (section 1.2.1), produced in response to sensing *T. gondii* and its associated PAMPs by different immune cells. IFN-γ binding to its receptor on $CD4^+$ T cells during antigen presentation induces expression of the Th1 specific transcription factor T-bet. Furthermore, the inducible subunit of the IL-12 receptor is expressed. Now IL-12 can further elevate T-bet expression completing the Th1 differentiation and clonal expansion of the

activated effector T cells [Mullen *et al.* 2001; Ng *et al.* 2013; Janeway 2019 pp. 366-370].

1.2.2.3 Effector T cells

Based on their effector function T cells can be grouped into different subsets. T cells with a cytotoxic function, so called cytotoxic T lymphocytes (CTLs), express CD8 molecules ($CD8^+$ T cells) on their surface [Zhu *et al.* 2010; Golubovskaya and Wu 2016]. During acute toxoplasmosis, CTLs produce IFN-γ that contributes to the containment of the acute *T. gondii* infection. During chronic toxoplasmosis the antigen specific CTLs are essentially required due to their cytotoxic capacity. Here, CTLs destroy all nucleated cells that present the CTLs specific antigen on MHCI molecules [Suzuki *et al.* 2010].

$CD4^+$ T cells are a large subset of T cells that have diverse effector functions. T helper cells (Th cells), a subset of $CD4^+$ T cells, assist leukocytes in immunologic processes. Currently, there are seven Th cell subsets (Th1 / 2 / 9 / 17 / 22, regulatory T cells and T follicular helper cells) described that are all characterized by different cytokine profiles for induction and effector function. [Zhu *et al.*2010; Golubovskaya and Wu 2016].

Th1 cells produce IFN-γ [Gazzinelli *et al.* 1994] that fuels cell-autonomous effector mechanisms that will be introduced in section 1.2.4. Furthermore, Th1 cells increase costimulatory molecule expression as well as produce IL-2 thereby supporting CTLs during chronic toxoplasmosis [Denkers *et al.* 1996; Bhadra *et al.* 2011].

Regulatory T cells (Tregs) are another subset of Th cells that have important immunoregulatory functions. $CD4^+$ T cell differentiation to Tregs and their function relies on the transcription factor forkhead box P3 (FOXP3) [Fontenot *et al.* 2003; Hori *et al.* 2003]. Tregs are involved in self-tolerance and modulate immune responses by suppression of T cell responses or APC´s capacity to activate antigen-naïve T cells [Zhu *et al.* 2010; Golubovskaya and Wu 2016]. The following table (Table 1) provides a short overview of molecules that are expressed by activated T cells relevant in the context of the here addressed topic.

Table 1: Activation markers - Molecules that can be found on / in activated T cells.

Molecule	On / in [1]	Function	Reference
CD25	Activated effector T cells, Tregs*	High affinity interleukin-2 receptor.	Liao *et al.* 2011

Molecule	On / in [1]	Function	Reference
Ki-67	Proliferating T cells	Cell cycle regulated gene involved in chromosomal integrity during mitosis.	Sun and Kaufmann 2018; Soares *et al.* 2010
CD44	Activated effector T cells	Cell-adhesion molecule (receptor for hyaluronic acid).	Schumann *et al.* 2015
L-selectin (CD62L)	Antigen-naïve T cells	Required for T cell entry into secondary lymphoid organs, absent on activated effector T cells.	Sprent and Surh 2011
CD69	Activated effector T cells	Receptor that is involved in regulating/shaping of immune responses.	Cibrián and Sánchez-Madrid 2017
OX40 (CD134)	Activated effector T cells, Tregs	Receptor that provides costimulatory signals to CD4 T cells.	Paterson *et al.* 1987; Croft *et al.* 2009
CTLA4 (CD152)	Activated T cells and Tregs	Ligand to CD80/86 (required for costimulation) and therefore negatively influences activation of T cells.	Chikuma 2017
PD-1 (CD279)	Activated T cells	Ligand binding inhibits TCR complex signaling.	Agata *et al.* 1996; Riley 2009
GITR (CD357)	Activated T cells, Tregs*	Costimulatory molecule that modulates suppressive function.	Ronchetti *et al.* 2015

[1] Only cell populations relevant in the context of this thesis are shown herein. The markers are not necessarily exclusive for the respective cell population. * Murine FOXP3$^+$ regulatory T cells (Tregs) express this marker independent of the activation status. (CD, cluster of differentiation; CTLA4, cytotoxic T lymphocyte antigen 4; GITR, glucocorticoid-induced tumor necrosis factor receptor related protein; PD-1, programmed cell death-1).

1.2.3 The type II interferon: IFN-γ

In contrast to type I interferons, which comprise several IFNs with IFN-α (which can be further subdivided) and IFN-β being the most prominent ones, type II interferons comprise only one cytokine, namely IFN-γ [Platanias 2005].

In the context of toxoplasmosis, all host species have in common that the proinflammatory IFN-γ contributes essentially to the hosts successful encounter with the intruder *T. gondii*. For example, mice treated with IFN-γ neutralizing antibodies or genetically engineered mice that are deficient for IFN-γ or its receptor are highly susceptible to *T. gondii* and succumb to acute toxoplasmosis [Suzuki *et al.* 1988; Scharton-Kersten *et al.* 1996; Yap and Sher 1999].

IFN-γ increases phagocytic activity and TLR expression by innate immune cells as well as antigen-presentation via MHC [Boehm *et al.* 1997; Schroder *et al.* 2003]. Furthermore, IFN-γ activates cytotoxic immune cells (NK cells and CTLs) and induces downstream effector mechanisms with antimicrobial effector functions in hematopoietic and non-hematopoietic cells [Sasai and Yamamoto 2019]. These so called IFN-γ effector mechanisms will be introduced in detail in sections 1.2.4 and 1.3.

1.2.3.1 IFN-γ signaling pathway

IFN-γ is active as a dimerized molecule that binds to its distinct receptor, the IFN-γ receptor (IFNGR) complex. The IFNGR complex consists of the ligand binding IFN-γR1 and the signal transmitting IFN-γR2 that signals via the JAK/STAT pathway [Pestka *et al.* 1997]. Cytoplasmic Janus kinases (JAKs) are associated to the cytokine bond receptor complex resulting in phosphorylation of JAKs, which enables attachment of signal transducer and activator of transcription 1 (STAT1). STAT1 then is phosphorylated (pSTAT1) and translocate as a homodimer from the cytosol into the nucleus. Here, pSTAT1 acts as a transcription factor and binds to IFN-γ-activated sequence (GAS) promoter elements thereby induce expression of interferon stimulated genes (ISGs; e.g. antimicrobial effector mechanisms that will be introduced in sections 1.2.4 below) as well as other transcription factors, like IRF1. IRF1 then binds to interferon-stimulated response element (ISRE) promoter regions to induce respective genes. [Bromberg and Darnell 2000; Pestka *et al.* 2004; MacMicking *et al.* 2012].
Regulation of signaling is mediated by tyrosine phosphatases that dephosphorylate activated JAKs and STATs or by inhibitors like suppressor of cytokine signaling (SOCS) that are induced by IFN-γ as a negative regulator of signaling. SOCS proteins interfere with cytokine mediated receptor signaling by binding to the phosphorylated tyrosine motives of JAKs and receptors or lead to degradation of JAKs and STATs via ubiquitination [Seif et al 2017].

1.2.4 Close-up on cell-autonomous immunity: IFN-γ effector mechanisms

The first line of defense posed by antimicrobial effector mechanisms of not only hematopoietic (e.g. macrophages) but also non-hematopoietic (e.g. fibroblasts, endothelial cells) cells against pathogens are collectively contributing to cell-autonomous immunity [MacMicking 2012]. This section focuses on antimicrobial effector mechanisms induced by IFN-γ, so called IFN-γ effector mechanisms that are very potent against *T. gondii* and thus highly relevant in the context of acute toxoplasmosis. Induction of these genes relies on IFN-γ signaling via the transcription factor STAT1 as described in section 1.2.3.1 [Lieberman *et al.* 2004]. IFN-γ activated cells can locally inhibit growth of pathogens or even kill pathogens to slow down their dissemination and thus gain time for the antigen-specific immune response that will eventually provide immunity [MacMicking 2012; Janeway 2019 pp. 445-452].

IFN-γ induced effector mechanisms act in different ways, including nutritional starvation and inactivation of enzyme function by catabolic enzymes and molecules that target and accumulate at the PV ultimately leading to parasite death. (Figure 5). The catabolic enzyme indoleamine 2,3-dioxygenase 1 (IDO1) degrades the essential amino acid tryptophan (L-tryptophan) (Figure 5) and thereby starves the tryptophan auxotroph *T. gondii* resulting in proliferation inhibition [Pfefferkorn 1984]. Section 1.3 focuses in detail on the function of the catabolic enzyme IDO1 and thus IDO1's impact on *T. gondii* and the host.

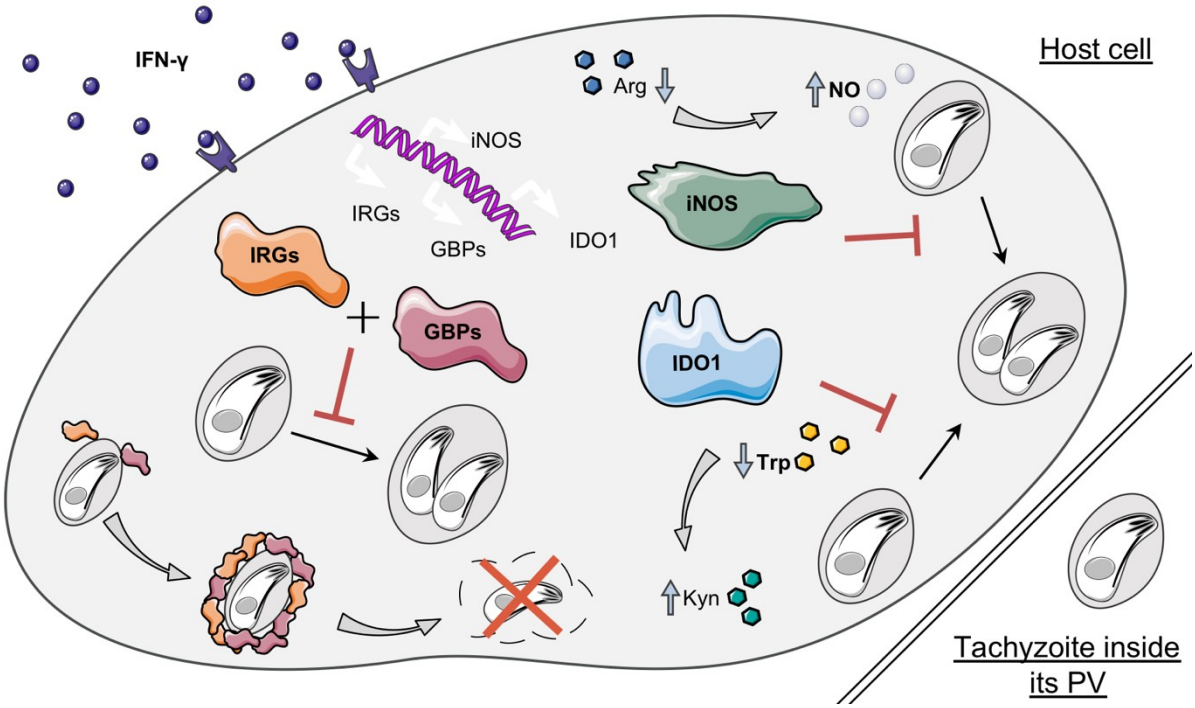

Figure 5: IFN-γ effector mechanisms directed against *T. gondii*.
Cell-autonomous effector mechanisms induced by interferon-gamma (IFN-γ) pose different modes of action against the intracellular parasite *Toxoplasma gondii* (*T. gondii*). Immunity related GTPases (IRGs) and guanylate binding proteins (GBPs) target and accumulate at the parasitophorous vacuole (PV) ultimately leading to parasite death [Martens *et al.* 2005; Yamamoto *et al.* 2012; Steffens *et al.* 2020]. Inhibition of parasite growth is achieved by starving *T. gondii* for tryptophan via indoleamine 2,3-dioxygenase 1 (IDO1) that degrades tryptophan (Trp) to kynurenine (Kyn) or by production of toxic nitric oxide (NO) from arginine (Arg) via inducible NO synthase (iNOS) [Pfefferkorn 1984; Adams *et al.* 1990].

1.2.4.1 Inducible nitric oxide synthase

Another group of catabolic enzymes degrade the essential amnio acid L-arginine and thereby produce nitric oxide (NO) (Figure 5). There are three isozymes of NO synthases (NOSs), namely neuronal NOS (nNOS; NOS1), inducible NOS (iNOS; NOS2) and endothelial NOS (eNOS; NOS3). nNOS and eNOS are low-output (meaning they produce low quantities of NO) NOSs that are constitutively expressed

in neural tissues and endothelium, and are involved in synaptic plasticity and vasodilation [Förstermann *et al.* 1998; Tenopoulou and Doulias 2020]. iNOS produces high quantities of NO upon induction by proinflammatory cytokines (e.g. combinations of IFN-γ, TNF-α and IL-1β) in hematopoietic and non-hematopoietic cells thereby contributing to the defense against pathogenic microorganisms [MacMicking 2012].
NO interacts with heme and non-heme iron of proteins thus affecting their function. Furthermore, NO interacts with reactive oxygen species causing the formation of highly toxic peroxynitrite that target thiols in proteins, induce lipid oxidation and damages DNA [Cooper 1999; Prolo *et al.* 2013].
In the context of toxoplasmosis, iNOS induction requires at least IFN-γ and TNF-α as shown in murine macrophages leading to production of NO and concomitant inhibition of parasite growth (Figure 5) [Adams *et al.* 1990; Sibley *et al.* 1991]. Interestingly, even though murine macrophages inhibit parasite growth via murine iNOS (miNOS); this mechanism seems to be redundant during the acute phase but rather important in the chronic stage of infection. Mice deficient for miNOS survived the acute infection with a type II strain, however succumbed during chronic infection due to toxoplasmic encephalitis [Scharton-Kersten *et al.* 1997].

1.2.4.2 IFN-inducible GTPases

IFN-inducible guanosine triphosphatases (GTPases) are of great relevance during acute infection. In general, GTPases hydrolyze guanosine triphosphate and guanosine diphosphate (GDP) to GDP and guanosine monophosphate, respectively [Legewie *et al.* 2019]. Thereby modifying cell membranes in the context of structural changes (e.g. remodeling and fusion of cellular membranes) [Praefcke and McMahon 2004]. p47 and p65 GTPase family members, namely immunity related GTPases (IRGs) and guanylate binding proteins (GBPs) respectively, are of great relevance in cell-autonomous defense. Both IRGs and GBPs are described to accumulate at the PV, even in a collaborative fashion, eventually leading to disruption of the integrity of the PV and thus the death of *T. gondii* (Figure 5) [Martens *et al.* 2005; Hunn *et al.* 2008; Yamamoto *et al.* 2012; Selleck *et al.* 2013; Steffens *et al.* 2020].
IRGs are highly abundant in mice (21 IRGs), whereas in humans there is only one IRG, known as IRM, that is not IFN-inducible [Hunn *et al.* 2011]. In contrast, GBPs have been shown to be important in order to control *T. gondii* in mice (11 mGBPs) [Degrandi *et al.* 2012; Yamamoto *et al.* 2012] and humans (seven hGBPs) [Tretina *et al.* 2019].

However, in the later the role and function of human GBPs (hGBPs) are vague and seem to be different from murine GBPs (mGBPs). hGPBs are described to be recruited to the PV in haploid fibroblast-like leukemia cells but are dispensable for the control of *T. gondii* [Oshima *et al.* 2014]. In a human lung epithelial cell line (A549) hGBP1 inhibits *T. gondii* (type II) via an unknown mechanism but independent of hGBP1 recruitment to the PV [Johnston *et al.* 2016]. Induction of apoptosis via hGBP1 in IFN-γ stimulated and *T. gondii* infected human macrophages has recently been shown [Fisch *et al.* 2019].

1.3 Tryptophan degrading enzymes

Tryptophan degrading enzymes and their diverse involvement in antimicrobial and immunosuppressive actions and thus their implication in health and disease have been extensively reviewed by Yeung and colleagues who have provided an elaborated collection of literature of this research field from the last decades [Yeung *et al.* 2015].
Tryptophan is an essential amino acid required for protein synthesis as well as synthesis of the neurotransmitter serotonin. However, the majority of tryptophan (approximately 95 %) is metabolized via the kynurenine pathway [Takikawa 2005]. The first and rate-limiting step of the kynurenine pathway is initiated by one of three heme-dioxygenases that oxidize the pyrrole ring of the indole moiety of tryptophan yielding N-formylkynurenine that is converted to stable kynurenine. Kynurenine is either excreted through urine or further catabolized resulting in many different biologically active kynurenine pathway metabolites (e.g. anthranilic acid, xanthurenic acid, picolinic acid, nicotinamide adenine dinucleotide) [Thomas and Stocker 1999].
Dietary tryptophan and steroid hormones induce tryptophan 2,3-dioxygenase (TDO) in the liver where it regulates tryptophan homeostasis [Schmike *et al.* 1965; Knox 1966]. Indoleamine 2,3-dioxygenase 1 (IDO1) is a TDO analog – as it evolved independently of TDO – that is expressed in many different organs and cell types. Infection independent IDO1 expression is reported in different organs and tissues, e.g. murine epididymis and prostate or human and murine female reproductive organs (including placenta) during pregnancy [Dai *et al.* 2010; Sedlmayr *et al.* 2002]. Proinflammatory cytokine dependent induction of IDO1 is of great relevance in infection and inflammation, as further elaborated in section 1.3.2 [Takikawa *et al.* 1988; Takikawa *et al.* 1999].

Indoleamine 2,3-dioxygenase 2 (IDO2) has been described recently as an IDO1 homolog that has evolved by gene duplication [Ball *et al.* 2007]. In comparison to IDO1 IDO2 has a lower tryptophan affinity and its expression pattern is different [Austin *et al.* 2009; Ball *et al.* 2007]. IDO2 protein can be detected in kidney, epididymis, testis and liver. Interestingly, in epididymis IDO2 and IDO1 are both expressed, however, in different cells suggesting that the isozymes might have non-redundant roles with yet to be defined functions [Ball *et al.* 2007]

1.3.1 Cytokine dependent induction of IDO1

IDO1 expression is mainly induced by the proinflammatory cytokine IFN-γ. The promoter region of IDO1 contains GASs and ISREs that are activated by IFN-γ induced transcription factors STAT1 and IRF1, respectively [Chon *et al.* 1995; Sotero-Esteva *et al.* 2000]. TNF-α and other cytokines have been shown to act in concert with IFN-γ to multiply IDO1 induction in many different cells, including glioblastoma cells, astrocytes and brain microvascular endothelial cells [Däubener *et al.* 1996; Däubener *et al.* 2001]. This synergistic effect might be due to increased signaling, since TNF-α induces the NFκB pathway eventually enhancing IRF1 and STAT1 expression that act as additional IDO1 activators as well as lead to increased IFNGR expression, which, in turn, acts as a positive feedback loop [Robinson *et al.* 2003].

1.3.2 IDO1 activity: starving and suppressing

IDO1 induction leads to degradation of tryptophan to N-formylkynurenine that is readily converted to kynurenine as the main metabolite in a dose dependent manner [Pfefferkorn *et al.* 1986]. Pfefferkorn and colleagues were the first to describe IDO induction as a cell-autonomous effector mechanism by showing that *T. gondii* growth was inhibited in IFN-γ stimulated human foreskin fibroblasts by this very same mechanism (Figure 5) [Pfefferkorn 1984; Pfefferkorn *et al.* 1986]. As *T. gondii* is an auxotroph for tryptophan this cell-autonomous mechanism impairs parasite growth by starvation, as supplementation of excess tryptophan rescues *T. gondii* growth. Other kynurenine pathway metabolites did affect *T. gondii* growth, if added at high concentration to the cell culture system, however, lower concentrations that are more likely to be reached by IDO activity had no effect on parasite proliferation [Pfefferkorn *et al.* 1986]. Since then, many other cell types have been shown to express IDO1 upon cytokine stimulation causing parasite growth inhibition, including glioblastoma cells,

astrocytes, brain microvascular endothelial cells and lung cells (HBE4-E6/E7 and A549) just to name a few [Däubener 1996; Däubener *et al.* 2001; Heseler *et al.* 2008]. Besides of *T. gondii,* many other pathogens have been shown to be controlled by IDO1 induction, either by tryptophan starvation or by kynurenine pathway metabolites. IDO1 mediated tryptophan depletion inhibits other intracellular pathogens like *Neospora caninum* [Spekker *et al.* 2009] a parasite that leads to abortion in cattle, viruses like Herpes simplex virus [Adams *et al.* 2004] and Measles virus [Obojes *et al.* 2005] or *Chlamydia* (*C.*) spp. like *C. pneumoniae* and *C. trachomatis* [Mehta *et al.* 1998; Roshick *et al.* 2006] that cause infections of the lung and the genital tract. Extracellular growth of commensal bacteria is inhibited by IDO1-mediated tryptophan depletion as shown for *Streptococcus agalactiae* (group B *Streptococcus*) [MacKenzie *et al.* 1998] and *Staphylococcus aureus* (*S. aureus*) [Hucke *et al.* 2004] both able to cause severe sepsis. Not tryptophan starvation by IDO1 activity but rather the production of kynurenine pathway metabolites affects *Listeria monocytogenes* as well *Trypanosoma cruzi* [Nino-Castro *et al.* 2014; Knubel *et al.* 2010].

While the immune system needs to be able to mount potent antimicrobial effector functions, it needs to minimize tissue damage. This balance between immunity and tolerance must be adequately adjusted, as dysfunction can have fatal consequences. IDO1 has, despite its antimicrobial capacity, potent immunosuppressive properties [Grohmann *et al.* 2003]. The first group of scientists that have identified IDO activity as an important immunosuppressive mechanism were Munn and colleagues. They showed that inhibition of IDO with 1-methyl tryptophan (1-MT) during murine pregnancy resulted in T cell mediated fetus rejection in allogeneic but not syngeneic mating experiments [Munn *et al.* 1998]. The mode of action that was suggested to induce tolerance in this context is tryptophan depletion by IDO1-positive APCs during T cell activation and thus inhibition of T cell proliferation [Munn *et al.* 1999; Munn *et al.* 2002; Mellor and Munn 2004]. Furthermore, kynurenine pathway metabolites have been implicated to inhibit T cell responses [Grohmann *et al.* 2003; Bauer *et al.* 2005]. Direct inhibition of effector T cells by IDO1 activity can be achieved through different mechanisms, including cell cycle arrest [Munn *et al.* 1999], cell death [Lee *et al.* 2010], apoptosis [Fallarino *et al.* 2002] or interference with glucose metabolism consequently inhibiting T cell proliferation [Eleftheriadis *et al.* 2014]. Indirect T cell suppression can

be achieved by activation of suppressive Tregs by IDO1-positive DCs [Sharma *et al.* 2007].

1.4 Objectives

Tryptophan degrading enzymes and their antimicrobial and immunosuppressive capacity have been extensively studied. This thesis aims to extend this knowledge by using both, *in vitro* and *in vivo* approaches. The former addresses IDO1 effector functions in human retinal pigment epithelium (hRPE) cells against *T. gondii* in the context of human ocular toxoplasmosis, whereas the latter addresses the role of IDO1 in experimental acute murine toxoplasmosis.

In ocular toxoplasmosis, *T. gondii* targets different cells of the retina, including the cells of the RPE that bear important functions, including diffusive light absorption, nutrient and oxygen transport [Strauss 2005]. For the *in vitro* approach the cell line ARPE19 is used to analyze the capacity of the RPE cell layer to respond to proinflammatory stimulation with specific emphasis on the IFN-γ induced cell-autonomous effector mechanisms IDO1 and iNOS. Consequently, the stimulated hRPE cells are analyzed with regard to their antimicrobial capacity against *T. gondii*. Furthermore, this *in vitro* model is expanded to address intraocular infections caused by disseminated bacteria, so called endogenous bacterial endophthalmitis (EBE) [Coburn *et al.* 2015]. Here, the usually commensal bacterium *S. aureus* – that can cause EBE – is utilized. Furthermore, the immunosuppressive capacity of IDO1 in hRPE cells is evaluated in co-culture experiments with stimulated T cells.

An experimental murine infection model is used to analyze the role of mIDO1 during the acute phase of toxoplasmosis *in vivo*. Here, C57BL/6J mice deficient for mIDO1 ($IDO^{-/-}$) and appropriate control mice (WT) are infected with a high dose of *T. gondii* tachyzoites. In order to identify the role of mIDO1 in mice, infection associated symptoms are documented, expression of the effector molecules mIDO1, miNOS and mGBPs as well as infection associated alterations of tryptophan and kynurenine concentrations are analyzed. Consequently, the antimicrobial effector function of mIDO1 is identified by comparison of the parasite load between the genotypes. In addition, *ex vivo* analysis of the antimicrobial effector function of mIDO1 is performed with different cells isolated from infected mice.

Concomitant with an acute *T. gondii* infection in mice the T cell proliferation response to *ex vivo* mitogen stimulation is drastically impaired [Chan *et al.* 1986]. Hence, mitogen stimulation experiments are performed to reveal the contribution of the immunosuppressive potential of mIDO1 in this context. Furthermore, activation markers on T cell subset, including Tregs, are analyzed and compared between genotypes.

2. Materials

The origin of cell, microbes and mouse lines used in the experiments are collected in this section. Furthermore, the origin of antibodies, oligonucleotides, chemical reagents, enzymes, the composition of media and buffers, technical equipment and disposables that were used are collected herein.

2.1 Antibodies

In addition to the antibodies for immunoblot (Table 2) and flow cytometry experiments (Table 3) an anti-human CD3ε monoclonal antibody (clone: OKT3) produced with a hybridoma cell line (CRL-8001™; ATCC® Manassas, VA, USA) was used for stimulation of human peripheral blood lymphocytes. MACS® cell separation antibodies were part of a commercial kit (Table 9).

Table 2: Primary and secondary antibodies for immunoblots.

Name	Antibody	Dilution	Order no.; Manufacturer
hβ-actin	rabbit anti-β-actin	1:5000 [a]	Sigma [1]
hIDO	mouse anti-IDO	1:500 [a]	Merck [2]
rabbit IgG	HRP-linked goat anti-rabbit IgG	1:10000 [b]	Dianova [3]
mouse IgG	HRP-linked goat anti-mouse IgG	1:10000 [b]	Dianova [3]
mβ-actin	mouse anti-β-actin (8H10D10), mAb	1:10000 [c]	3700S; Cell Signaling [4]
mIRF-1	rabbit anti-IRF-1 (D5E4) XP®, mAb	1:1000 [d]	8478; Cell Signaling [4]
mSTAT1	rabbit anti-Stat1, pAb	1:1000 [d]	9172S; Cell Signaling [4]
mpSTAT1	rabbit anti-phospho-Stat1 (Tyr701) (58D6), mAb	1:1000 [d]	9167S; Cell Signaling [4]
mSTAT3	rabbit anti-Stat3 (79D7), mAb	1:2000 [d]	4904S; Cell Signaling [4]
mpSTAT3	rabbit anti-phospho-Stat3 (Tyr705) (D3A7) XP®, mAb	1:1000 [d]	9145S; Cell Signaling [4]
mIDO1	rabbit anti-IDO, pAb	1:500 [d]	AB9900; Chemicon® Merck [2]
miNOS	rabbit anti-iNOS (1131-1144), pAb (LOT no.: D00040543)	1:1000 [d]	482728; CalBiochem®, Merck [2]
mGBP2	rabbit anti-mGBP2, pAb [Degrandi *et al.* 2007]	1:1000 [d]	courtesy of Dr. Degrandi, HHU [5]
mGBP7	rabbit anti-mGBP7, pAb [Legewie *et al.* 2019]	1:1000 [d]	courtesy of Dr. Degrandi, HHU [5]
mouse IgG	HRP-linked horse anti-mouse IgG	1:2000 [e]	7076S; Cell Signaling [4]
rabbit IgG	HRP-linked goat anti-rabbit IgG	1:2000 [e]	7074S; Cell Signaling [4]

mAb/pAb, monoclonal/polyclonal antibody; IgG, immunoglobulin G; HRP, horseradish peroxidase [a] 0.5 % skim milk powder (MP) in tris buffered saline (TBS); [b] 0.5 % MP in phosphate buffered saline; [c] 5 % MP in TBS with 0.1 % Tween® 20 (TBS-T); [d] 5 % bovine serum albumin (BSA) in TBS-

T; [e] 1 % MP in TBST-T; [1] St. Louis, Missouri, USA; [2] Darmstadt, GER; [3] Hamburg, GER; [4] Cambridge, UK;[5] Düsseldorf, GER

Table 3: Fluorochrome-conjugated antibodies for flow cytometry.

Antigen	Clone	Fluorochrome	Order no.	Company
CD3	17A2	Alexa Fluor® 700	100216	BioLegend® [1]
CD4	RM4-5	FITC	553047	BD Biosciences [2]
CD8a	53-6.7	Alexa Fluor® 700	100730	BioLegend® [1]
CD11b	M1/70	BV™ 510	101245	BioLegend® [1]
CD19	1D3	PerCP-Cy™5.5	551001	BD Biosciences [2]
CD25	PC61	BV™ 421	102034	BioLegend® [1]
CD44	IM7	BV™ 605	103047	BioLegend® [1]
CD62L	MEL-14	PE/Cy7	104418	BioLegend® [1]
CD69	H1.2F3	PE/Cy7	104512	BioLegend® [1]
CD95 (FAS-R)	Jo2	PE	554258	BD Biosciences [2]
CD127	A7R34	BV™ 650	135043	BioLegend® [1]
CD134 (OX-40)	OX-86	BV™ 605	119419	BioLegend® [1]
CD152 (CTLA4)	UC10-4B9	PE/Dazzle™ 594	106318	BioLegend® [1]
CD279 (PD-1)	29F.1A12	BV™ 711	135231	BioLegend® [1]
CD357 (GITR)	DTA-1	APC	126312	BioLegend® [1]
FoxP3	MF-14	PE	126404	BioLegend® [1]
Ki-67	16A8	APC	652406	BioLegend® [1]
TCRb	H57-597	BV™ 650	109251	BioLegend® [1]
CD16/32 (Fc-block)	93	unconjugated	14016185	Thermo Fisher [3]

APC, allophycocyanin; BV™, Brilliant Violet™; Cy, cyanine; FITC, fluorescein isothiocyanate; PE, phycoerythrin; PERCP, peridinin chlorophyll protein. [1] San Diego, CA, USA; [2] Heidelberg, GER; [3] Carlsbad, CA, USA

2.2 Oligonucleotides

All oligonucleotides listed in this section were ordered from Metabion International AG (Planegg, GER) as purified, desalted, lyophilized stocks that were dissolved in UltraPure™ distilled water [c = 100 pmol/µL] upon arrival and were stored at -20°C.

In-house bred indoleamine 2,3-dioxygenase 1 (mIDO1) -deficient ($IDO^{-/-}$) mice, originally bought from the Jackson Laboratory (Table 13), were genotyped with primers for polymerase chain reaction (PCR) as listed in Table 4. The primers are specific for a sequence of mIDO1 or a sequence of the neomycin cassette (nc) that was originally introduced to delete exons 3 to 5 of mIDO1 [Mellor *et al.* 2003].

Table 4: Primers for PCR-based genotyping of in-house bred $IDO^{-/-}$ mice.

Primer	Sequence [5´ → 3´]	Amplicon
mIDO1-forward	TGGAGCTGCCCGACGC	427 base pairs

Primer	Sequence [5´ → 3´]	Amplicon
mIDO1-reverse	TACCTTCCGAGCCCAGACAC	
nc-forward	CTTGGGTGGAGAGGCTATTC	280 base pairs
nc-reverse	AGGTGAGATGACAGGAGATC	

Based on a protocol from the Jackson Laboratory (no. 005867; version 2.0; Nov. 29th 2010).

The “Universal Probe Library Assay Design Center” from Roche was used to design the oligonucleotide/probe sets for quantitative real-time PCR (qPCR). The Universal Probe Library is based on short hydrolysis probes that are labeled at the 5' end with fluorescein and at the 3' end with a dark quencher dye. Furthermore, the probes contain locked nucleic acids for high specificity and thermal stability. The sequences of the Universal Probe Library probes detect 8- and 9-mer motifs that are in combination with the respective PCR primes specific for one transcript. The optimal combination of PCR primers and probes for the transcript of interest were suggested by the design center and are listed in Table 5 and Table 6.

Table 5: Oligonucleotide/probe sets for human gene expression analysis.

Gene of interest	Gene ID	Probe	Sequence [5´ → 3´]	
hIDO1	ENSG0 0000131203	#9	fw	CGCCTTGCACGTCTAGTTCT
			rv	TTGGCAGTAAGGAACAGCAAT
hIDO2	ENSG0 0000188676	#4	fw	TTCCTCACCATGGGTTATGTC
			rv	GAAGGGCAAGATTCCTTGG
hiNOS (NOS2)	ENSG0 0000007171	#16	fw	TCTTCCTGGTTTGACTGTCCTTA
			rv	GCTCAGATGTTCTTCACTGTGG
heNOS (NOS3)	ENSG0 0000164867	#67	fw	GACTGAAGGCTGGCATCTG
			rv	CCATGTTACTGTGCGTCCAC
hnNOS (NOS1)	ENSG0 0000089250	#39	fw	TGGGAGACTGAGGTGGTTCT
			rv	GTACTCAGTGCATCCCGTTTC
hβ-actin	ENSG0 0000075624	#64	fw	CCAACCGCGAGAAGATGA
			rv	CCAGAGGCGTACAGGGATAG

fw, forward; rv, reverse

Table 6: Oligonucleotide/probe sets for murine gene expression analysis.

Gene of interest	Gene ID	Probe	Sequence [5´ → 3´]	
mIDO1	ENSMUSG0 0000031551	#2	fw	GGGCTTCTTCCTCGTCTCTC
			rv	TGGATACAGTGGGGATTGCT
mIDO2	ENSMUSG0 0000031549	#12	fw	GTCCTTGGGGAGATACCACA
			rv	CCAAGGCTTGTAATGATCTGG
mTDO	ENSMUSG0 0000028011	#67	fw	CAATGACTGCTTTGGACTTCAAT
			rv	GCCGGAACTGTAGACTCTGG

Gene of interest	Gene ID	Probe	Sequence [5´ → 3´]	
miNOS (NOS2)	ENSMUSG0 0000020826	#13	fw	CTTTGCCACGGACGAGAC
			rv	TGTACTCTGAGGGCTGACACA
mGBP2	ENSMUSG0 0000028270	#17	fw	TGAGTACCTGGAACATTCACTGAC
			rv	AGTCGCGGCTCATTAAAGC
mβ-actin	ENSMUSG0 0000029580	#106	fw	TGACAGGATGCAGAAGGAGA
			rv	CGCTCAGGAGGAGCAATG

fw, forward; rv, reverse

To determine the parasite load in tissues of *T. gondii* ME49-infected mice the following oligonucleotides specific for the 35-fold repetitive B1 (*Tg*B1) gene [Burg *et al.* 1989] were used.

Table 7: Oligonucleotides for the detection of the *Toxoplasma gondii* B1 gene.

Primer	Sequence [5´ → 3´]
*Tg*B1-forward	GCTAAAGGCGTCATTGCTGTT
*Tg*B1-reverse	GGCGGAACCAACGGAAAT
*Tg*B1-probe	6-FAM-ATCGCAACGGAGTTCTTCCCAGACGT-BHQ-1

FAM, fluorescein; BHQ, Black hole quencher®

2.3 Reagents, enzymes and commercial kits

All reagents, chemicals, enzymes and commercial kits that were used for this thesis are listed in the following two tables.

Table 8: Reagents and chemicals.

Reagent	Manufacturer
Acetic acid (96 %)	Merck, Darmstadt, GER
Acetonitril LiChrosolv® gradient grade	Merck, Darmstadt, GER
Agarose	BD Biosciences, Heidelberg, GER
Beta mercaptoethanol	Roth, Karlsruhe, GER
Betaplate™ scint	PerkinElmer Inc. Waltham, MA, USA
Bovine serum albumin	Sigma-Aldrich, Munich, GER
Chloroform	Merck, Darmstadt, GER
Class B ODN1826 (CpG B)	Invivogen; San Diego, CA, USA
Concanavalin A (ConA) [2 mg/mL]	Sigma-Aldrich, Munich, GER
Difco™ skim milk	BD Biosciences, Heidelberg, GER
Dimethylsulfoxid (DMSO)	Merck, Darmstadt, GER
4-(dimethylamino) benzaldehyd	Merck, Darmstadt, GER
DNase/RNase-free distilled water (UltraPure™)	Thermo Fisher Scientific Inc., Carlsbad, CA, USA
deoxynucleoside triphosphates (dNTPs) [10 mM each]	Thermo Fisher Scientific Inc., Carlsbad, CA, USA
Dithiothreitol (DTT) [0.1 mM]	Invitrogen, Carlsbad, CA, USA

Reagent	Manufacturer
Dulbecco's phosphate buffered saline (DPBS)	Life Technologies, Carlsbad, CA, USA
eBioscience™ fixable viability dye eFluor™780	Thermo Fisher Scientific Inc., Carlsbad, CA, USA
Erythrocyte lysis buffer	Morphisto GmbH, Frankfurt am Main, GER
Ethanol absolute	Merck, Darmstadt, GER
Ethidium bromide (1 %)	Merck, Darmstadt, GER
Ethylenediaminetetraacetic acid (EDTA)	Fluka Chemie AG, Seelze, GER
FACS Clean solution	BD Biosciences, Heidelberg, GER
FACS Flow™ solution	BD Biosciences, Heidelberg, GER
FACS Shutdown solution	BD Biosciences, Heidelberg, GER
Fetal bovine serum (FBS) BioWhittaker®, Lot N°: 9SB003	Lonza, Basel, CH
Ficoll® Paque plus	GE Healthcare, Chicago, IL, USA
First-strand buffer (5×)	Invitrogen, Carlsbad, CA, USA
Glycerin	Merck, Darmstadt, GER
Glycerol (85 %)	Merck, Darmstadt, GER
Hydrochloric acid (25 %)	Roth, Karlsruhe, GER
Interferon gamma (rh) [2x10^5 U/mL in IMDM]	R&D Systems Inc., Minneapolis, MN, USA
Interferon gamma (rm) [2x10^5 U/mL in IMDM]	R&D Systems Inc., Minneapolis, MN, USA
Interleukin-1 beta (rh) [2x10^4 U/mL in IMDM]	R&D Systems Inc., Minneapolis, MN, USA
Interleukin-2 (rh) [100 µg/mL / 2.1x10^6 U/mL in 100 mM acidic acid with 1 % BSA]	R&D Systems Inc., Minneapolis, MN, USA
Iscove's modified Dulbecco's medium (IMDM)	Gibco, Grand Island, NY, USA
Isopropyl alcohol	Merck, Darmstadt, GER
Kynurenine (L-)	Sigma-Aldrich, Munich, GER
MassRuler™ DNA ladder mix	Thermo Fisher Scientific Inc., Carlsbad, CA, USA
Methanol	Merck, Darmstadt, GER
Methanol HPLC gradient grade	Merck, Darmstadt, GER
1-methyl-L-tryptophan (1-L-MT)	Merck, Darmstadt, GER
N-(1-naphthyl)ethylenediamine dihydrochrloride	Merck, Darmstadt, GER
N^G-monomethyl-L-arginine [5 mg/mL] in IMDM	Merck, Darmstadt, GER
3-nitro-L-tyrosine	Merck, Darmstadt, GER
NuPage® MOPS SDS running buffer (20×)	Novex by life technologies Carlsbad, CA, USA
NuPage® transfer buffer (20×)	Novex by life technologies Carlsbad, CA, USA
Oligo(dT)12-18 primer	Thermo Fisher Scientific Inc., Carlsbad, CA, USA
Penicillin/streptomycin (P/S)	Biochrom, Berlin, GER
Percoll®	Sigma-Aldrich, Munich, GER
Phosphate buffered saline (PBS; 10×)	Gibco, Grand Island, NY, USA
Pierce™ ECL western blotting substrate	Thermo Fisher Scientific Inc., Carlsbad, CA, USA
PageRuler™ protein ladder (10-180 kDa)	Thermo Fisher Scientific Inc., Carlsbad, CA, USA
Polymerase (high fidelity)	Roche, Basel, CH
Proteinase inhibitor cocktail tablets	Roche, Basel, CH
RPMI 1640 medium (w 2 g/L $NaHCO_3$;	PAN Biotech, Aidenach, GER

Reagent	Manufacturer
w/o L-glutamine and L-tryptophan)	
SignalFire™ ECL reagent	Cell Signaling Technology, Cambridge, UK
Sodium acetate	Merck, Darmstadt, GER
Sodium dodecyl sulfate (SDS)	Roth, Karlsruhe, GER
Sulfonamide	Sigma-Aldrich, Munich, GER
SuperSignal® West Dura extended duration substrate	Thermo Fisher Scientific Inc., Carlsbad, CA, USA
^{3}H-thymidine (37 MBq/mL)	PerkinElmer Inc. Waltham, MA, USA
TRI Reagent®	Merck, Darmstadt, GER
Trichloroacetic acid (TCA)	Merck, Darmstadt, GER
Tris(hydroxymethyl)aminomethane (TRIS)	Roth, Karlsruhe, GER
Trypan blue (0.4 %)	Sigma-Aldrich, Munich, GER
Trypsin/EDTA (0.05 %)	Gibco, Grand Island, NY, USA
Tryptophan (L-)	Sigma-Aldrich, Munich, GER
Tumor necrosis factor alpha (rh) [2x10^{4} U/mL in IMDM]	R&D Systems Inc., Minneapolis, MN, USA
Tween® 20	Merck, Darmstadt, GER
VLE RPMI 1640 medium, very low endotoxin with stable L-glutamine	Biochrom, Berlin, GER
^{3}H-uracil (37 MBq/mL)	PerkinElmer Inc. Waltham, MA, USA

rh, recombinant human; rm, recombinant murine

Table 9: Enzymes and commercial kits.

Product	Company
CD3ε MicroBead kit, mouse	Miltenyi Biotec, Bergisch Gladbach, GER
Collagenase [100 mg/mL]	Sigma-Aldrich, Munich, GER
Cyto-Fast™ Fix/Perm buffer set	Biolegend, San Diego, CA, USA
DNase [3000 U/mL]	Roche, Basel, CH
Lung dissociation kit, mouse	Miltenyi Biotec, Bergisch Gladbach, GER
M-MLV reverse transcriptase [200 U/µL]	Invitrogen, Carlsbad, CA, USA
Pierce™ BCA protein assay kit	Thermo Fisher Scientific Inc., Carlsbad, CA, USA
Proteinase K [200 µg/mL]	Qiagen, Venlo, NL
RNAse-out [40 U/µL]	Invitrogen, Carlsbad, CA, USA
Takyon NoRox Probe MasterMix dTTP	Eurogentec, Lüttich, BE
True-Nuclear™ transcription factor buffer set	Biolegend, San Diego, CA, USA

2.4 Media and buffers

Iscove's modified Dulbecco's medium with 4 mM L-glutamine, 25 mM HEPES and phenol red (IMDM; Gibco) supplemented with 5 % (v/v) heat-inactivated fetal bovine serum (FBS; BioWhittaker®) was used as the standard cell culture medium for the cultivation of mammalian cells. Freshly isolated murine cells for *ex vivo* experiments

were cultured in standard cell culture medium supplemented with penicillin (100 U/mL) and streptomycin (100 µg/mL). Murine bone marrow cells were cultured in macrophage colony-stimulating factor (M-CSF)-supplemented medium composed of VLE RPMI 1640 medium, 10 % (v/v) heat-inactivated FBS and 15 % (v/v) M-CSF (L929 cell conditioned medium; batch tested).

All buffers used within this thesis are listed in the following table (Table 10).

Table 10: Buffers.

Buffer	Composition
Digestion buffer (fresh)	10 mg/mL Collagenase, 180 U/mL DNase in PBS
Ehrlich reagent (fresh)	1.2 % 4-(dimethylamino) benzaldehyde in acetic acid
FACS buffer (4 °C)	5 % FBS, 2 mM EDTA in PBS
Griess reagent A (RT)	0.1 % *N*-(1-naphthyl)ethylenediamine dihydrochloride in ddH_2O
Griess reagent B (RT)	2.5 % sulfonamide in 15 % hydrochloric acid
Lysis buffer (pH 8.5) (RT)	100 mM Tris/HCl, 5 mM EDTA (pH 8), 0.2 % SDS, 200 mM NaCl in ddH_2O
MACS®-buffer (4 °C)	2 mM EDTA, 0.5 % BSA in PBS
Protein loading buffer (5×; RT)	10 % SDS, 30mM Tris/HCL (pH6,8), 45 % glycerin, 25 % β-mercaptoethanol, 0.15 % bromphenol blue in ddH_2O
Proteinase lysis buffer (fresh)	1 % proteinase K (200 µg/mL) in lysis buffer (pH 8.5)
Rinsing buffer (4 °C)	3 % FBS in PBS
Running buffer (1×; RT)	5 % NuPage® MOPS SDS running buffer (20×) in ddH_2O
Sodium acetate buffer (RT)	50 mM sodium acetate in ddH_2O (pH4.2, adj. with acetic acid)
Stop buffer (4 °C)	10 mM EDTA in PBS
TAE buffer (RT)	40 mM Tris, 1 mM EDTA, 40 mM acetic acid in ddH_2O
TBS-T (RT)	150 mM NaCl, 10 mM Tris HCl pH8, 0.1 % Tween® 20 in ddH_2O
Transfer buffer (1×; RT)	5 % NuPage® transfer buffer (20×), 20 % methanol in ddH_2O

Buffers had to be prepared fresh or could be stored at 4 °C or room temperature (RT).

2.5 Equipment and disposables

The technical equipment, plasticware and other disposables that were used in this thesis are collected in this section.

Table 11: Devices.

Equipment / Devices	Company
Agarose gel electrophoretic chambers Mini-Sub® / Sub-Cell® GT System	Bio-Rad Laboratories, Hercules, CA, USA
Analytic scale Chyo JL-180	Chyo Balance Corporation, JP
Axio Observer	Carl ZEISS, Oberkochen, GER
BD LSRFortessa™	BD Biosciences, Heidelberg, GER
Blotting chamber (semi dry)	Peqlab Biotechnologie GmbH, Erlangen, GER
Cell counter Cellometer® Auto T4	Nexelcom™ Bioscience, Lawrence, MA, USA

Equipment / Devices	Company
Cell counting chamber Neubauer Improved	Paul Marienfeld GmbH & Co. KG, Lauda Königshofen, GER
Cell harvester Basic96 harvester	Skatron Instruments Inc., Sterling, VA, USA
Centrifuge Eppendorf 5415C (rotor: F45-18-11)	Eppendorf AG, Hamburg, GER
CFX96 Touch™ RT PCR Detection System & C1000 Touch™ Thermal Cycler Chassis	Bio-Rad Laboratories, Hercules, CA, USA
Consort gel electrophoresis power supply E861	Consort BVBA, Turnhout, BE
Drying chamber Binder E28	Binder GmbH, Tuttlingen, GER
Electric flake ice maker SPR 165	NordCap®, Munich, GER
Elix® water purification system	Merck, Darmstadt, GER
Freezer -20°C	Liebherr, Bulle FR, CH
Freezer -80°C Revco	Welabo, Düsseldorf, GER
gentleMACS™ Octo Dissociator	Miltenyi Biotec, Bergisch Gladbach, GER
Heat sealer LKB Wallac 1295-012	LKB instruments Inc., Mount Waverley, VIC, AU
Hera Safe HS18 laminar flow	Thermo Fisher Scientific Inc., Carlsbad, CA, USA
Heraeus BB 6220 CO_2 incubator	Thermo Fisher Scientific Inc., Carlsbad, CA, USA
Hettich Universal 32 R (rotor: 1653)	Hettich, Tuttlingen, GER
Light box LKB Wallac 1295-013	LKB instruments Inc., Mount Waverley, VIC, AU
Liquid nitrogen tank Arpege 110	Air Liquide Medical GmbH, Düsseldorf, GER
Liquid scintillation counter LKB Wallac 1205 Betaplate™	LKB instruments Inc., Mount Waverley, VIC, AU
Magnetic stirrer and heating unit RCT basic IKAMAG®	IKA®-Werke GmbH & Co. KG, Staufen, GER
Manu-Cart® 55mm cartidge holder for LiChroCART® 55-2 HPLC-Cartidge	Merck, Darmstadt, GER
Micro centrifuge Eppendorf 5417R (rotor: F45-30-11)	Eppendorf AG, Hamburg, GER
Micro centrifuge Eppendorf MiniSpin® (rotor: F45-12-11)	Eppendorf AG, Hamburg, GER
Microplate reader Tecan Sunrise™	Tecan Group Ltd., Männedorf, CH
Microwave	Bosch, Gerlingen-Schillerhöhe, GER
MidiMACS™ Separator and MultiStand	Miltenyi Biotec, Bergisch Gladbach, GER
Molecular Imager® Gel Doc™ XR+ System	Bio-Rad Laboratories, Hercules, CA, USA
Peltier thermal cycler PTC-200 MJ Research	Bio-Rad Laboratories, Hercules, CA, USA
Peqlab gel chamber	Peqlab Biotechnologie GmbH, Erlangen, GER
Percellys® Minilys® tissue homogenizer	Bertin Technologies, Montigny-le-Bretonneux, Frau
pH meter MP 225	Mettler Toledo, Columbus, OH, USA
Power supply peqPOWER 250	Peqlab Biotechnologie GmbH, Erlangen, GER
Purospher® STAR RP-18 endcapped (3 µm) LiChroCART® 55-2 HPLC-cartridge	Merck, Darmstadt, GER
Purospher® STAR RP-18 endcapped (5 µm) (4-4) guard column	Merck, Darmstadt, GER

Equipment / Devices	Company
Refrigerator	Liebherr, Bulle FR, CH
Sample bagging support LKB Wallac 1295-011	LKB instruments Inc., Mount Waverley, VIC, AU
Scale Sartorius 1209 MP	Sartorius AG, Göttingen, GER
Sorvall RC4 (rotor: LH-4000W; adaptors: 15 mL/50 mL disposable conical tubes)	Thermo Fisher Scientific Inc., Carlsbad, CA, USA
spectrophotometer NanoDrop® ND-1000	Thermo Fisher Scientific Inc., Carlsbad, CA, USA
System Gold® 106 detector UV/VIS	Beckman Coulter, Krefeld, GER
System Gold® 126 solution module	Beckman Coulter, Krefeld, GER
System Gold® 508 auto sampler	Beckman Coulter, Krefeld, GER
Thermal Cycler C1000TM	Bio-Rad Laboratories, Hercules, CA, USA
Thermomixer comfort (1.5 mL block)	Eppendorf AG, Hamburg, GER
Ultrasonic bath Bransonic 32	Bransonic, Hayward, CA, USA
Vacuum diaphragm pump ME 8SI	Vacuubrand GmbH & Co. KG, Wertheim, GER
Vortex VF2	Janke&Kunkel (IKA), Staufen in Breisgau, GER
Water bath Laktoherm 1	Dinkelberg, Neu-Ulm, GER
Water bath GFL 1002	GFL mbH, Burgwedel, GER
XCELL SureLock Mini-Cell	Invivogen, San Diego, CA, USA

Table 12: Plasticware and other disposables.

Item	Company
4titude® - FrameStar® Break-A-Way PCR plate	Brooks Life Sciences, Chelmsford, MA, USA
4titude® - Strips of 8 flat optical caps	Brooks Life Sciences, Chelmsford, MA, USA
Beveled tips 200 µL TipOne®	Starlab, Hamburg, GER
Canula sterican® 18/23/25/27G	B. Braun Melsungen AG, Melsungen, GER
Cell counting chamber SD100 slide	Nexelcom™ Bioscience, Lawrence, MA, USA
Cell culture dishes 94×16 mm non-treated	Greiner Bio-One GmbH, Frickenhausen, GER
Cell culture flasks 25/75/162 cm^2 tissue culture treated and ventilated (Corning®)	Corning Inc., Corning, NY, USA
Centrifugation tubes 0.5/1.5 mL	Eppendorf AG, Hamburg, GER
Centrifugation tubes 15 mL Cellstar® tubes	Greiner Bio-One GmbH, Frickenhausen, GER
Centrifugation tubes 2 mL Safe-lock tubes	Eppendorf AG, Hamburg, GER
Centrifugation tubes 50 mL	Sarstedt® AG & Co. KG. Nümbrecht, GER
Round-bottom polypropylene tube, 5 mL	Corning Inc., Corning, NY, USA
gentleMACS™ C Tubes	Miltenyi Biotec, Bergisch Gladbach, GER
Graduated filter tips 10/20/200/1000 µl TipOne®	Starlab, Hamburg, GER
MACS® LD Column	Miltenyi Biotec, Bergisch Gladbach, GER
Microtiter plates 6/12/96 wells, flat (F), round (U), conically shaped (V) bottom (Costar®)	Sigma-Aldrich, Munich, GER
Millex® GV 0.22 µm	Merck, Darmstadt, GER
Nitrocellulose blotting membrane, Amersham™ Protran TM 0.1 µm	GE Healthcare, Chicago, IL, USA
NuPage 4 %–12 % and 10 % Bis-Tris gel	Life Technologies, Carlsbad, CA, USA

Item	Company
Nylon sieves 70/100 µm	Corning Inc., Corning, NY, USA
Parafilm®	Pechiney Plastic Packaging, Chicago, IL, USA
Percellys® lysing kit CK28	Bertin Technologies, Montigny-le-Bretonneux, FRA
PP Screw cap 9mm, natural rubber	VWR International GmbH, Darmstadt, GER
Printed glass fiber filter mat A 1205-401	PerkinElmer Inc. Waltham, MA, USA
Reagent reservoir 100 mL disposable	VWR International GmbH, Darmstadt, GER
Sample bag for Betaplate™ 1205-411	PerkinElmer Inc. Waltham, MA, USA
Serological plastic pipettes 5/10/25/50 mL (Costar®)	Sigma-Aldrich, Munich, GER
Syringes Omnifix® 5/10/20 mL	B. Braun Melsungen AG, Melsungen, GER
Sterile filter Sarstedt Filtropur S 0.2 µm	Sarstedt® AG & Co. KG. Nümbrecht, GER
Topsert TPX-short thread integrated insert falcon ND9	VWR International GmbH, Darmstadt, GER
Whatman, Grade 3 CHR	GE Healthcare, Chicago, IL, USA

2.6 Cell lines, pathogenic microorganisms and mouse lines

The cell lines, pathogens (e.g. parasites, bacteria or viruses) and mouse lines used in experiments for this thesis are listed in the following.

Table 13: Cell lines, pathogenic microorganisms and mouse lines.

Name	Species and cell type	Order no.	Origin
hRPE	*Homo sapiens*, retinal pigment epithelium cell line (ARPE-19)	CRL-2302™	ATCC® [1]
HFF	*Homo sapiens*, foreskin fibroblast (HFF-1)	SCRC-1041™	ATCC® [1]
Glioblastoma cell line	*Homo sapiens,* glioblastoma cell line (86HG39) [Bilzer *et al.* 1991]	courtesy of Dr. T. Blitzer and Dr. W. Wechsler, Institute of Neuropathology, HHU [2]	
RAW 264.7	*Mus musculus,* macrophage cell line (RAW264.7)	TIB-71™	ATCC® [1]
T. gondii ME49	*Toxoplasma gondii*, apicomplexan parasite, type II strain ME49, tachyzoite	50611™	ATCC® [1]
S. aureus	*Staphylococcus aureus*, tryptophan-auxotrophic isolate [Heseler *et al.* 2008]	Institute of Medical Microbiology and Hospital Hygiene, HHU[2]	
hCMV	human cytomegalovirus, endotheliotropic strain TB40/E [Sinzger *et al.* 1999]	courtesy of Dr. A. Zimmermann, Institute of Virology, HHU [2]	
C57BL/6J mouse (wild type, WT)	*Mus musculus*, C57BL/6J inbred mouse (C57BL/6JRj)	000664	Janvier Labs [3]
mIDO1 deficient C57BL/6J mouse ($IDO^{-/-}$)	*Mus musculus*, C57BL/6J inbred mouse deficient for indoleamine 2,3-dioxygenase 1 (B6.129-$Ido1^{tm1Alm}$/J)	005867	Jackson Laboratory [4]

[1] Manassas, VA, USA; [2] Düsseldorf, GER;[3] Le Genest-Saint-Isle, FRA; [4] Bar Harbor, ME, USA

3. Methods

3.1 Cultivation of mammalian cells and pathogens

All cells were cultured in fetal bovine serum (FBS)-supplemented Iscove's modified Dulbecco's medium (IMDM) unless otherwise indicated and were kept in a humidified Heraeus BB 6220 CO_2 incubator (37 °C, 5 % CO_2).

3.1.1 Propagation of mammalian cells

Human foreskin fibroblasts (HFFs), human retinal pigment epithelium (hRPE) cells, human glioblastoma cells and Raw 264.7 cells were cultured in culture flasks with IMDM supplemented with 5 % (v/v) heat-inactivated FBS. Cells were passaged frequently (e.g. when 90 % – 100 % confluency had been reached) using 0.05 % trypsin/EDTA for detachment. Confluent HFF monolayers served as host cells for the cultivation of *T. gondii* tachyzoites (section 3.1.3) and human cytomegalovirus (section 3.1.5).

3.1.2 Isolation of human peripheral blood lymphocytes

Human peripheral blood lymphocytes (PBLs) were isolated from blood of healthy donors using Ficoll® Paque Plus density gradient centrifugation according to the manufacturer's protocol. In brief, heparinized blood was diluted with phosphate buffered saline (PBS) in equal parts and was layered on top of Ficoll® Paque Plus. The lymphocyte layer was collected after gradient centrifugation (400×*g,* RT, 35 min). Lymphocytes were washed with PBS three times (80×*g*, RT, 10 min), resuspended in RPMI 1640 medium, counted and adjusted to the desired cell concentration. PBL were used for the experiments shortly after isolation.

3.1.3 *T. gondii* serial passages *in vitro* and purification of tachyzoites

T. gondii strain ME49 tachyzoites were maintained *in vitro* by serial passages in HFF cells. HFF cell monolayers were infected for 42-48 h to yield highly parasitized host cells. Parasitized host cells were harvested in PBS by scraping them off. Intracellular parasites were released by serial cannula passages (2×23 G cannula and 2×27 G cannula). After purification by differential centrifugation (85×*g*, RT, 5 min and 780×*g*, RT, 5 min) tachyzoites were counted and adjusted to the desired concentration (for *in vitro* experiments: 2×10^6 tachyzoites per mL in RPMI 1640 medium; for *in vivo*

experiments: 5×10^5 tachyzoites per mL in PBS). The parasites were used immediately for the experiments.

Toxoplasma lysate antigen (TLA) was prepared from freshly isolated tachyzoites. The parasite number was adjusted in PBS and parasites were lysed by three freeze/thaw cycles (liquid nitrogen for 5 min and 37°C water bath for 5 min).

3.1.4 Cultivation of *S. aureus* and determination of its growth

The *S. aureus* isolate used herein was originally obtained from a routine diagnostic specimen and is a tryptophan-auxotrophic strain. *S. aureus* was grown on brain heart infusion (HBI) agar with 5 % sheep blood in an incubator (37 °C, 5 % CO_2) overnight. For hRPE infection experiments a single colony was picked, resuspended in PBS and serially diluted. Colony-forming units (cfu) of the dilution used for the inoculation of hRPE cultures was determined on HBI agar overnight. *S. aureus* growth in hRPE cultures was determined 24 hours post infection (hpi) by measurement of the optical density (OD) of the resuspended cultures at 620 nm.

3.1.5 Cultivation of human cytomegalovirus

The human cytomegalovirus (hCMV) strain TB40/E used herein was reconstituted from its bacterial artificial chromosome (BAC) clone TB40/E-BAC4 [Sinzger *et al.* 2008] and was provided by Dr. A. Zimmermann (Institute of Virology, HHU, Düsseldorf). hCMV stocks were prepared as described by [Le *et al.* 2008]. In brief, HFF cells were infected with hCMV and supernatants were collected when all host cells showed complete cytopathic phenotype. hRPE cells were used in a standard plaque assay to determine the virus titer of the hCMV stocks. The hCMV stocks (6×10^6 plaque forming units) were stored at -80 °C until further use.

3.2 Simulation of an inflammatory state *in vitro*

For stimulation of an inflammatory state *in vitro* human retinal pigment epithelium (hRPE) cells were supplemented with recombinant human interferon gamma (IFN-γ), interleukin-1 beta (IL-1β), tumor necrosis factor alpha (TNF-α), the IDO inhibitor 1-methyl-L-tryptophan (1-L-MT), the NOS inhibitor N^G-monomethyl-L-arginine (N^GMMA) and L-tryptophan (Trp) as indicated in the figure legends (Figure 6 - Figure 9).

For gene expression experiments hRPE cells were seeded in 6-well plates (10^6 cells per well) and remained untreated or stimulated with proinflammatory cytokines for 24 h.

For IDO and iNOS activity tests hRPE cells were seeded as triplicates in 96-well F-bottom plates (3×10^4 cells per well) and remained untreated or stimulated with proinflammatory cytokines for 72 h.

For *T. gondii* and *S. aureus* infection experiments or PBL co-cultivation experiments hRPE cells were pre-stimulated in 96-well plates for 72 h as indicated in the figure legends (Figure 8 & Figure 9). Pre-stimulated hRPE cultures were infected with freshly prepared *T. gondii* tachyzoites (in RPMI 1640 medium; 2×10^4 tachyzoites per well) or *S. aureus* (in PBS; 10-100 cfu per well).

Freshly prepared PBLs (in RPMI 1640 medium; 1.5×10^5 PBLs per well) were added to the pre-stimulated cultures for co-cultivation experiments. PBL proliferation was stimulated with an anti-human CD3ε antibody as indicated in the figure legends (Figure 8 & Figure 9).

hRPE cells pre-infected with hCMV for stimulation experiments were prepared by seeding 3×10^4 hRPE cells per well of 96-well plates and addition of hCMV stock (multiplicity of infection: 2; Figure 9). Freshly infected hRPE cells were centrifuged (960×*g*, RT, 30 min acceleration: 8 brake: 5) and then stimulated with proinflammatory cytokines. The hCMV-infected and stimulated cells were incubated for 72 h before the cultures were used in infection or co-cultivation experiments. hCMV infection was verified by microscopic observation of the cytopathic phenotype.

3.3 Experimental infection *in vivo*

3.3.1 Animal model and experimental infection

mIDO1-deficient ($IDO^{-/-}$) mice were bred and kept under specific pathogen-free (SPF) conditions in the Central Animal Care and Research Facility of the Heinrich Heine University Düsseldorf. These in-house bred mice were genotyped by PCR as described in section 3.5.1. For wild type (WT) controls C57BL/6J mice were ordered from Janvier Labs. WT mice were treated equally to $IDO^{-/-}$ mice upon arrival. All experiments were performed with age- and sex-matched groups. Mice were infected intraperitoneally (ip) with 10^5 *T. gondii* ME49 tachyzoites in 200 µL PBS unless

otherwise indicated. Uninfected (naïve) control mice and infected mice were kept under SPF conditions and were checked daily (compare Table 14).

Mice were euthanized by cervical dislocation for sample collection or when the termination criterion (more than 16 points, compare Table 14) was reached.

All experiments involving living animals were performed in the Central Animal Care and Research Facility of the Heinrich Heine University Düsseldorf and in strict compliance with the German Animal Welfare Act. The experimental protocol was authorized by the North Rhine-Westphalia State Agency for Nature, Environment and Consumer Protection (permit numbers 84-02.04.2013.A271 and 84-02.04.2016.A508). All efforts were made to minimize animal harm during the experiments.

Table 14: Assessment criteria for *in vivo* experiments.

Criteria	Assessment result	Evaluation
Bodyweight	unchanged / increased	0 points
	reduction < 5 %	1 point
	reduction 5 – 10 %	5 points
	reduction 11 - < 20 %	10 points
	reduction ≥ 20 %	20 points
Appearance	normal (smooth shiny fur, clean anus, clear eyes)	0 points
	fur defects (reduced or excessive body care)	1 point
	unkempt fur and anus, cloudy eyes, increased muscle tone	5 points
	scruffy fur and dirty anus, abnormal posture, cloudy eyes, high muscle tone	10 points
	cramps, palsies of extremities or torso musculature, breathing noises, cold body	20 points
Behavior	normal (sleeping, reaction to contact, curios and explores the cage, social contact)	0 points
	slight changes to normal behavior	1 point
	unusual behavior (e.g. no flight behavior)	5 points
	self-isolation, lethargy, strong hyperkinetic, coordination difficulties	10 points
	auto aggression (e.g. self-amputation), signs of pain during handling	20 points

Infection experiments with bradyzoites (ip infection) or cysts (oral infection) were performed by the research group (RG) Pfeffer (Institute of Medical Microbiology and Hospital Hygiene, HHU, Düsseldorf, GER) and RG Förster (LIMES, University Bonn, Bonn, GER), respectively. The protocols were authorized by the North Rhine-Westphalia State Agency for Nature, Environment and Consumer Protection (permit numbers 84-02.04.2013.A495 and 81-02.04.2018.A094). Data from lymphocyte proliferation experiments with splenocytes received from RG Pfeffer and RG Förster are illustrated in Figure 20B.

3.3.2 Sample collection

Blood samples were taken from euthanized mice by cardiac puncture. Sera were generated from clogged blood samples (4 °C overnight) in two centrifugation steps (each 20000×*g*, 4 °C, 10 min). Organs (lung, brain, liver, spleen and mesenteric lymph nodes (MLNs)) were collected and washed in PBS. Cell isolation from murine tissues was performed as described below (section 3.3.3). Tissue homogenates were prepared from lung, liver and brain in PBS using the Percellys® system. All samples were stored at -80 °C for further processing.

3.3.3 Murine cell isolation

For *ex vivo* lymphocyte proliferation experiments cells from spleen and MLNs were isolated by incubation in digestion buffer for 30 min at 37 °C. Digested tissues were passed through 70 µm nylon sieves followed by erythrocyte lysis.

Ex vivo parasite proliferation experiments were performed using lung cells and peritoneal exudate cells (PECs) isolated from infected mice sacrificed for sample collection.

Lung cells were isolated with a lung dissociator kit and a gentleMACS™ Octo Dissociator according to the manufacturer's instructions. The cells were passed through 70 µm nylon sieves and purified with a 30 % / 70 % Percoll®-gradient. The lung cell layer was collected after centrifugation (1090×*g*, 4 °C, 35 min). Lung cells were washed with PBS thrice (540×*g*, 4 °C, 10 min).

PECs were isolated according to the protocol from Ray and Dittel [Ray and Dittel 2010]. In brief, rinsing-buffer was injected with a 27 G cannula into the abdomen of mice euthanized for sample collection. The abdomen was massaged, and the solution was collected with a 25 G cannula. PECs were washed once (350×*g*, 4 °C, 10 min) with PBS.

Bone marrow derived macrophages (BMDMs) for *in vitro T. gondii* infection experiments were differentiated from bone marrow cells isolated from hind legs provided by RG Murray (Max Plank Institute of Biochemistry, Martinsried, GER). Hind legs were shipped in PBS at 4 °C. Femurs and tibias were isolated, disinfected in 70 % ethanol for 3 min and the bone marrow was flushed out using cell culture medium. The solution was centrifuged (350×*g*, 4 °C, 5 min), erythrocytes were lysed, and cells were filtered through 100 µm nylon sieves. BMDM differentiation with M-CSF was performed according to [Scheu *et al.* 2008]. In brief, 1.5×10^6 bone marrow cells were resuspended

in 10 mL M-CSF supplemented medium and cultured in non-treated cell culture dishes at 37 °C and 10 % CO_2. Fresh medium (5 mL, M-CSF supplemented) was added to the cultures on day three. The cells were ready for stimulation experiments on day six.

All murine cells, except BMDMs, were resuspended in medium (IMDM with 5 % FBS, 100 U/mL penicillin 100 µg/mL streptomycin) for *in vitro* experiments. Cells for separation or flow cytometry experiments were resuspended in MACS® buffer (section 3.7.2) or in FACS buffer (section 3.7.3), respectively. Cells were counted either manually using trypan blue (0.4 %) and a Neubauer Improved Cell counting chamber or automatically using trypan blue (0.2 %), a SD100 counting chamber slide and an automated cell counter (Cellometer® Auto T4). Cells for *in vitro* experiments were seeded in low evaporation lid, 96-well, F-bottom plates. Splenocytes were seeded in triplicates and MLN cells were seeded in duplicates with 3×10^5 cells per well unless otherwise indicated. Lung cells and PECs were seeded in duplicates as 1×10^5 cells per well. BMDM were resuspended in M-CSF-supplemented medium and were seeded in triplicates as 3×10^4 cells per well.

3.3.4 Stimulation of murine cells *ex vivo*

Lymphocyte proliferation was stimulated using the mitogen concanavalin A (ConA; 1 µg/mL) and the class B oligonucleotide ODN1826 (CpG B; 0.1 µM) as indicated in the figures (Figure 20 - Figure 22). Recombinant human interleukin-2 (IL-2; 5 ng/mL which is equivalent to 105 U/mL) and the NOS inhibitor N^G-monomethyl-L-arginine (N^GMMA; 100 µg/mL) were supplemented as indicated in the figures (Figure 18, Figure 20, Figure 21).

BMDMs were stimulated with recombinant murine IFN-γ (mIFN-γ, gradient from 30 U/mL- 0.04 U/mL) as indicated in the figure (Figure 19).

3.4 Proliferation assays

3.4.1 Lymphocyte proliferation

Lymphocyte proliferation was determined by the ^{3}H-thymidine incorporation method. In brief, ^{3}H-thymidine (7.4 kBq per well) was added 48 h after lymphocyte stimulation. Cultivation was stopped and cells were lysed by freezing after an additional 24 h of

cultivation. Incorporated ^{3}H-thymidine was detected with liquid scintillation spectrometry and measured as counts per minute (cpm).

3.4.2 Parasite proliferation

T. gondii tachyzoite proliferation was determined by the ^{3}H-uracil incorporation method as described [Pfefferkorn *et al.* 1977]. In brief, ^{3}H-uracil (12.3 kBq per well) was added 24 h post cultivation of lung cells and PECs from infected mice. *In vitro* infected cultures were supplemented with ^{3}H-uracil 24 h (BMDM) or 48 h (hRPE cells) post infection. ^{3}H-uracil incorporation was stopped and cells were lysed by freezing after an additional 24 h of cultivation. Incorporated ^{3}H-uracil was detected with liquid scintillation spectrometry and was measured as cpm.

3.5 PCR-based methods

3.5.1 Genotyping of in-house bred mice

In-house bred IDO$^{-/-}$ mice were genotyped with a PCR approach as described in the following. The primers (listed in Table 4) specific for a segment of the mIDO1 sequence or a segment of the neomycin cassette that was originally introduced to delete exons 3 to 5 of mIDO1 [Mellor *et al.* 2003]. A 427 bp product will be generated from the intact WT mIDO1 gene, whereas a 280 bp PCR product will be generated from the neomycin cassette/mIDO1 construct. DNA was isolated from tail cuts or ear punches by proteinase K digestion. Samples were incubated with proteinase lysis buffer at 56 °C and 1100 rpm on a thermo-shaker for 90 min. DNA was precipitated with isopropyl alcohol and washed with 70 % ethanol. Extracted DNA was dissolved in UltraPure™ distilled water. Each 25 µL PCR reaction contained 1.5 µL DNA template,1.5 µL Taq polymerase, 0.5 µL dNTPs, 2.5 µL buffer (10×), 0.5 µL primer (0.4 µM each) and 17 µL UltraPure™ distilled H_2O. The PCR conditions were defined as 2 min at 94 °C, 30 cycles of each 94 °C for 15 s followed by 57 °C for 30 s and 72 °C for 1 min and a final step at 72 °C for 7 min on a PTC-200 thermal cycler. DNA loading dye (6×) was added to the PCR product. The samples and controls (15 µL per pocket) as well as the MassRuler™ DNA ladder (7 µL per pocket) were loaded on an agarose gel (1.5 % agarose, 0.002 % ethidium bromide in TAE-buffer) and run at 100 V for approximately 50 min. Separated DNA fragments were documented and analyzed with the Molecular Imager® Gel Doc™ XR+ System.

3.5.2 Relative quantification of gene expression

Total RNA was extracted according to the TRI Reagent® protocol. In brief, total RNA was extracted from hRPE cells (approximately 10^6 cells) and murine tissues (50 µL lung / liver / brain homogenate) with 500 µL TRI Reagent® and 100 µL chloroform followed by precipitation with isopropyl alcohol. Extracted RNA was dissolved in UltraPure™ distilled water (hRPE: 50 µL; lung: 40 µL; liver: 50 µL; brain: 30 µL) and RNA concentration was determined with a NanoDrop® spectrophotometer. Reverse transcription of 1.5 µg total RNA to complementary DNA (cDNA) was performed with M-MLV reverse transcriptase and oligo(dT) 12-18 primers according to the manufacturer´s instructions. PCR primers were designed using the “Universal Probe Library Assay Design Center” and are listed in Table 5 and Table 6. qPCR was performed with the Takyon NoRox Probe MasterMix dTTP on a BioRad CFX96 Touch Real-Time PCR Detection system. Quality of qPCR analysis was verified by technical replicates for each sample in each run. Each well of a multiplate 96-well PCR plate contained 5 µL cDNA template, 12.5 µL Takyon NoRox Probe Master Mix dTTP, 0.3 µL primer (10 µM each), 0.5 µL probe (10 µM) and 6.4 µL UltraPure™ distilled H_2O for a total reaction volume of 25 µL. The PCR conditions were 7 min at 95 °C and 40 cycles of each 94 °C for 20 s and 60 °C for 1 min.

The qPCR data was analyzed with the comparative CT (cycle threshold) method also known as the $2^{-\Delta\Delta CT}$ method. $2^{-\Delta\Delta CT}$ can be used to compare the gene expression in two different samples (e.g. untreated versus treated or naïve versus infected), with each sample relating to an internal control gene.

3.5.3 Parasite load determination

DNA was extracted from murine tissue homogenates by proteinase K digestion. In brief, 500 µL proteinase lysis buffer was added to murine tissue homogenates (20 µL lung / liver / brain homogenate) and was incubated at 56 °C and 1100 rpm on a thermo-shaker for 90 min. DNA was precipitated with 500 µL isopropyl alcohol and washed with 500 µL 70 % ethanol. Extracted DNA was dissolved in UltraPure™ distilled water (lung: 50 µL; liver: 100 µL; brain: 30 µL) and the DNA concentration was adjusted to 100 ng/µL. The qPCR was performed with the above (section 3.5.2) mentioned detection system. For parasite quantification a standard curve with adjusted *T. gondii* genomic DNA concentrations was established and was used in parallel on each plate. The oligonucleotides and the template specific probe that were used herein (Table 7)

bind to a sequence segment of the *T. gondii* B1 gene that is commonly used in diagnostics [Pelloux 1998]. Quality of qPCR analysis was verified by technical replicates for each sample in each run. Each well of a multiplate 96-well PCR plate contained 5 µL DNA template, 12.5 µL Takyon NoRox Probe Master Mix dTTP, 2.5 µL primer (3 µM each), 2.5 µL probe (2 µM) for a total reaction volume of 25 µL. The PCR conditions were defined as 10 min at 95 °C and 45 cycles of each 95 °C for 15 s and 60 °C for 1 min.

3.6 Measurement of enzyme activity

3.6.1 Kynurenine detection as a measure of IDO activity

The enzymatic activity of IDO directly correlates with the concentration of kynurenine in supernatants of tissue culture cells. The measurement of kynurenine can be used to determine IDO1 activity [Däubener *et al.* 1994]. Therefore, Ehrlich reagent was used to determine the relative kynurenine content in cell culture supernatants. In brief, 10 µL trichloroacetic acid (30 %) was added to 160 µL cell culture supernatant in 96-well V-bottom plates and was incubated in a water bath at 60 °C for 30 min. Clear supernatant (100 µL) was collected after centrifugation (780×*g*, RT, 10 min) and 100 µL Ehrlich reagent was added. The absorbance was measured at 492 nm after 5 min incubation.

3.6.2 Nitrite detection as an indirect measure of NOS activity

Nitric oxide (NO) production was measured via the Griess assay [Ding *et al.* 1988]. Nitrite is measured as a stable breakdown product of NO. In brief, 100 µL cell culture supernatant was transferred from each well into wells of a 96-well F-bottom plate after 72 h of *in vitro* cultivation. Freshly prepared Griess reagent (equal parts of A and B) was added as 100 µL to each sample. Absorbance was measured at 540 nm after 15 min incubation. The nitrite content was calculated by extrapolation from a sodium nitrite standard curve assayed parallel to each measurement.

3.6.3 Detection of free tryptophan and kynurenine via HPLC analysis

High-performance liquid chromatography (HPLC) analysis was used to quantify total free tryptophan and kynurenine in murine serum and lung, liver and brain tissue. Protein precipitation was done with trichloroacetic acid (2.5 % final concentration). Measurement quality was monitored with 3-nitro-L-tyrosine (2.5 µg/mL for lung, liver,

and brain samples; 10 µg/mL for sera) that was used to spike all samples. Analysis was performed with a System Gold® HPLC system. For separation, a reverse phase C18 column cartridge with an adequate guard column was used. The mobile phase consisted of 50 mM sodium acetate with 5 % or 2 % acetonitrile for tryptophan and kynurenine analysis, respectively, using a flowrate of 0.5 mL/min. All eluents were vacuum degassed and filtrated (2 µm pore size). The absorbance was measured at 280 nm for tryptophan and 360 nm for kynurenine. Concentrations were determined with calibration curves using highly pure L-tryptophan and L-kynurenine.

3.7 Immuno-based methods

3.7.1 Protein detection by immunoblotting

Murine lung homogenates were incubated with proteinase inhibitor at 4°C for 30 min. Cell lysates from *in vitro* experiments were prepared by three freeze/thaw cycles (liquid nitrogen for 5 min and 37°C water bath for 5 min). Clear supernatants were generated by differential centrifugation (450×*g*, 4 °C, 15 min; 18000×*g*, 4 °C, 15 min). The protein content was determined with the Pierce™ BCA protein assay kit according to the manufacturer's instructions. Samples were adjusted to 1 µg protein per µL sample with UltraPure™ distilled water and protein loading buffer (5×). Samples were stored at 4 °C. Protein separation was done with NuPAGE Novex Bis-Tris mini gels in an appropriate electrophoresis system (150 V for 60 min–75 min). A pre-stained protein ladder for protein size estimation was used on every gel. The protein amount (10 µg or 30 µg per lane) and gel type (4 %–12 % or 10 % Bis-Tris gels) used for protein separation are indicated in the figure legends (Figure 6, Figure 14, Figure 17, Appendix A). Proteins were semi-dry blotted on nitrocellulose membranes (110 mA/blot) for 2 h. Membranes were blocked in 5 % (w/v) skim milk powder in TBS-T at RT for 1 h. The antibodies in Table 2 were used for specific protein detection as described therein. Primary antibodies were incubated at 4 °C overnight. The peroxidase-conjugated, secondary antibodies were incubated at RT for 1 h. The membranes were washed thrice with TBS-T for 5 min between each of the steps mentioned above. Labeled proteins were detected by enhanced chemiluminescence with different substrate solutions. SignalFire™ ECL reagent was used for mIRF1, mpSTAT1 and mpSTAT3. SuperSignal® West Dura extended duration substrate was

used for miNOS. Pierce™ ECL western blotting substrate was used for every other labeled protein.

3.7.2 Cell separation - MACS® technology

Splenocytes were isolated according to section 3.3.3 and resuspended in MACS® buffer. Splenic T cells and non-T cells were separated with the CD3ε MicroBead kit according to the manufacturer's instructions. In brief, splenocytes were incubated with a biotinylated anti-CD3ε antibody and washed in MACS® buffer (350×*g*, 4 °C, 10 min), followed by an incubation with a magnetic bead-linked anti-biotin antibody. Labelled and washed cells were passed through a LD-column in a magnetic field. All non-T cells passed through the column, whereas the anit-CD3ε MicroBead-labeled T cells where enriched within the column. The eluted T cells and the non-T cells were counted and plated as 1.5×10^5 cells of each cell type per well in single or co-cultivation experiments.

3.7.3 Flow cytometry

Flow cytometry experiments were performed to analyze effector T cells and regulatory T cells. Therefore, the following effector T cell and regulatory T cell panels were designed. The antibodies used herein are listed in Table 3. The antibody concentrations for surface and intracellular staining's were optimized for each panel by titration and fluorescence minus one (FMO) controls.

Splenocytes were isolated according to section 3.3.3 and resuspended in FACS buffer. An Fc-block against CD16/CD32 was performed (4 °C, 10 min) to minimize unspecific antibody binding. Cell staining took place in 96-well U-bottom plates. Stained cells were resuspended in 200 µL FACS buffer and transferred into round-bottom tubes for acquisition on a BD LSRFortessa™ flow cytometer. The analysis of flow cytometry data was performed with FlowJo™.

3.7.3.1 Effector T cell panel

Surface staining against CD4 (1:400), CD19 (1:100), CD152 (1:50) CD62L (1:100), CD8a (1:100), CD25 (1:100), CD11b (1:100), CD44 (1:200), TCRb (1:100), CD279 (1:200), CD95 (1:100) as well as viability staining with eFluor™780 (1:5000) was done at 4 °C in the dark for 30 min. The cells were washed in PBS (350×*g*, 4 °C, 5 min) and treated according to the instructions of the Cyto-Fast™ Fix/Perm buffer set from Biolegend. Intracellular staining against Ki-67 (1:400) was done at RT in the dark for

20 min. The gating strategy for Th cells ($CD4^+$ T cells) and CTLs ($CD8^+$ T cells) stained with the effector T cell panel is illustrated in the appendix (Appendix B, p. 120).

3.7.3.2 Regulatory T cell panel

Surface staining against CD4 (1:400), CD19 (1:100), CD152 (1:50) CD69 (1:100), CD3 (1:100), CD25 (1:100), CD11b (1:100), CD134 (1:100), CD127 (1:50), CD279 (1:50), CD357 (1:100) as well as viability staining with eFluor™780 (1:5000) was done at 4 °C in the dark for 30 min. The cells were washed in PBS (350×*g*, 4 °C, 5 min) and treated according to the instructions of the True-Nuclear™ transcription factor buffer set from Biolegend. Intracellular staining against FOXP3 (1:100) was done at RT in the dark for 30 min. The detailed gating strategy Tregs ($CD4^+$ $CD25^+$ $FOXP3^+$ T cells) is illustrated in the appendix (Appendix C p. 121).

3.8 Software

The software used within this thesis and the respective application purposes are listed in the following.

Table 15: Software and application purposes.

Software (version)	Application purpose
MouseBase (4.2)	Database for mouse breeding purposes.
Cellometer® Auto T4 Software (3.3.5.11)	Automated bright field cell counting with the Cellometer® Auto T4.
NanoDrop™1000 Operating Software (3.8.1)	Measurement of nucleic acid concentration and purity with the NanoDrop™ 1000 spectrophotometer.
Magellan™ (7.2)	Microplate reader setup and photometric data acquisition on the Tecan Sunrise™.
32Karat™ (8.0)	Setup, acquisition and analysis of high-performance liquid chromatography data on the System Gold® HPLC system.
Universal Probe Library Probe Finder (2.53)	Design of oligonucleotide/probe sets for gene expression analyses.
Bio-Rad CFX Manager™ (3.1)	Setup of the CFX 96 Touch Real-Time PCR Detection System and acquisition as well as analysis of qPCR data.
BD FACSDiva™	Setup of the BD LSRFortessa™ and acquisition of flow cytometry data.
FlowJo™ V (10.6.1)	Analysis of flow cytometry data.
ChemoStar V60+ (0.4.33.0)	Chemiluminescence imaging of immunoblots on the iNTAS ECL Chemostar analyzer.
Microsoft® Excel 2016	Raw data collection and preparation.
GraphPad Prism (8.4.2)	Data analysis and illustration.
Servier Medical Art [Servier 2017]	Cartoons for design of graphics of this thesis. Original cartoons were modified. Usage according to CC BY 3.0 license*.
Microsoft® PowerPoint	Design of figures and graphics.

* Creative Commons Attribution 3.0 Unported License (https://creativecommons.org/licenses/by/3.0/)

3.9 Statistical analysis

Sample numbers and experimental repeats are indicated in the respective figure legends. For data illustration different graph types are used. Data are presented as scattered dot blots consisting of data points with the respective mean or median as indicated. For bar charts and others, mean or median with standard deviation (SD) or standard error of the mean (SEM) are used as indicated. Violin plots represent data distribution (thickness of the plot), range from the smallest to the largest data point and include the median as well as the interquartile range (IQR, from 1st to 3rd quartile), compare Figure 23.

Statistical analyses were performed with GraphPad Prism 8 software. To determine whether the mean difference between two independent groups was significantly different the Students *t*-test (unpaired, two-tailed) was used. For the comparison of three or more independent groups the analysis of variance (ANOVA) was applied. The One-way ANOVA was applied when one categorical independent variable was used. The Two-way ANOVA was applied when two categorical independent variables were used. All ANOVAs performed herein were corrected for multiple comparison by the Tukey´s post hoc test, as the variance between the respective groups were homogeneous. Differences in survival of a *T. gondii* infection was analyzed with the log-rank test. The statistical tests used are indicated in the respective figure legends. For all experiments p values < 0.05 were considered significant and are illustrated with asterisks (*) and pound signs (#) as indicated.

4. Results

4.1 Antimicrobial and immunosuppressive capacity of hRPE cells

The eye is a target of several pathogens, including the apicomplexan parasite *T. gondii*. Ocular toxoplasmosis usually manifests as a retinitis. An *in vitro* approach with a human retinal pigment epithelial (hRPE) cell line, namely ARPE19, was used to address relevant questions concerning ocular toxoplasmosis.

4.1.1 Expression of the effector proteins IDO1 and iNOS upon stimulation with proinflammatory cytokines

Initially, a qPCR approach was used to analyze the capacity of hRPE cells to express cell-autonomous effector mechanisms. Therefore, hRPE cells were stimulated with proinflammatory cytokines and the expression of antimicrobial effector molecules was analyzed.

Relative mRNA expression of IDO1 was strongly increased (1.6×10^6-fold) after IFN-γ (500 U/mL) stimulation compared to the unstimulated control (Figure 6A). Costimulation with additional IL-1β and TNF-α (100 U/mL each) supplementation did not further increase IDO1 expression. IFN-γ stimulation also resulted in expression of iNOS (777-fold). However, IFN-γ stimulation in combination with IL-1β [Spekker-Bosker *et al.* 2019a] or both IL-1β and TNF-α increased (7.3×10^4-fold) iNOS expression even stronger compared to the unstimulated control (Figure 6A). The relative expression of iNOS was not affected by supplementation using N^GMMA (Figure 6A). Analysis of the expression of the IDO1- and iNOS-isozymes, namely IDO2, nNOS and eNOS, were included to provide insights into their inducibility by the cytokines used herein. Relative mRNA expression of IDO2 and eNOS was slightly increased by cytokine stimulation ranging between 13-fold up to 20-fold change increases, which is equivalent to 0.0013 % of the relative expression of IDO1 or 0.027 % of iNOS. Expression of nNOS was not detectable in hRPE cells after stimulation with cytokines (Figure 6A).

Stimulation of hRPE cells with proinflammatory cytokines not only induced IDO1 expression on the transcriptional level but also on protein level as illustrated via an immunoblot (Figure 6B). However, IDO1 protein expression was not drastically altered

when hRPE cells were costimulated with IFN-γ, IL-1β and TNF-α or *N*^{G}MMA (Figure 6B).

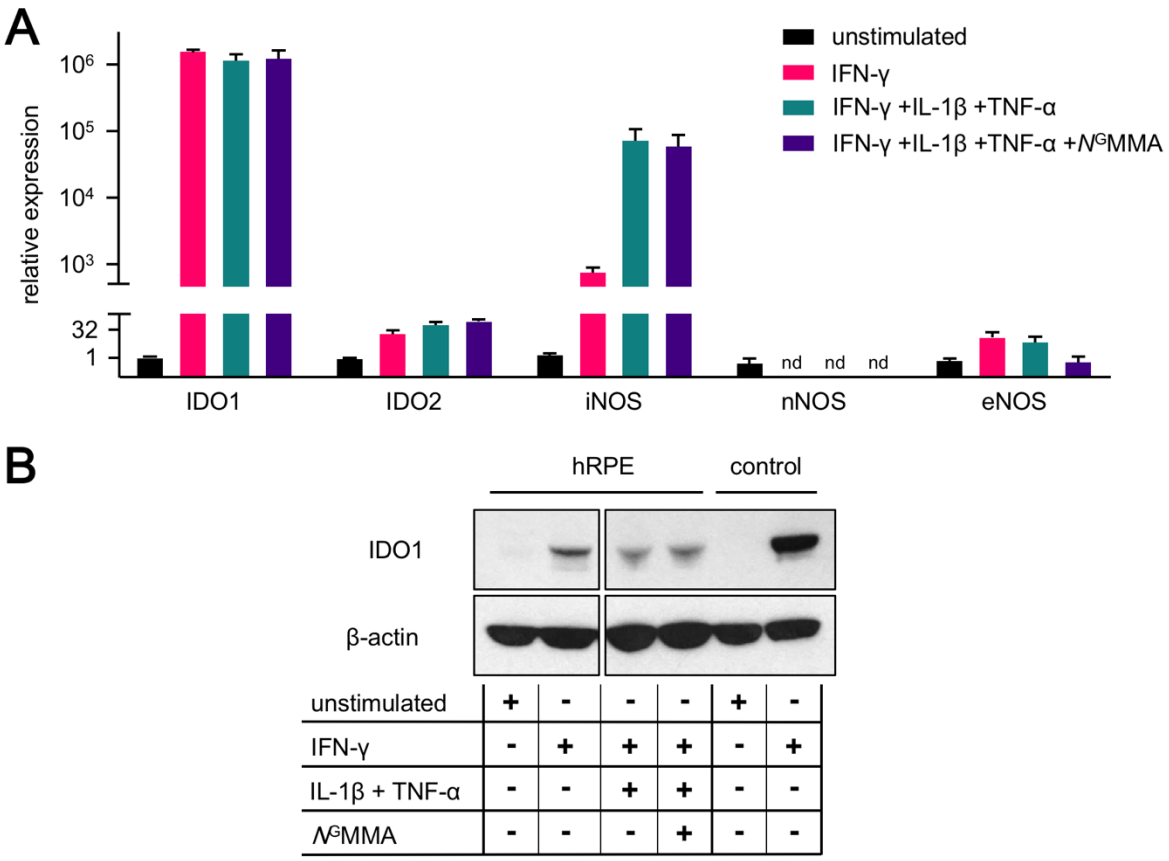

Figure 6: Stimulus dependent induction of IDO and iNOS mRNA expression in hRPE cells.

A, Relative mRNA expression of indoleamine 2,3-dioxygenase 1 (IDO1) and 2 (IDO2), neuronal (nNOS), inducible (iNOS) and endothelial nitric oxide synthase (eNOS) in human retinal pigment epithelium (hRPE) cells as determined by quantitative real-time PCR. Data were normalized to β-actin and were represented on a log-10 scale as relative expression (mean values ± SEM) of duplicate measurements (n = 2). **B**, Immunoblot analysis of IDO1 and β-actin protein expression of cell cultures. **A & B**, hRPE cells and human glioblastoma cells (control) remained unstimulated or were stimulated with combinations of interferon gamma (IFN-γ, 500 U/mL), interleukin-1 beta (IL-1β, 100 U/mL), tumor necrosis factor alpha (TNF-α, 100 U/mL) and the NOS inhibitor *N*^{G}-monomethyl-L-arginine (*N*^{G}MMA, 100 µg/mL) for 24 hours. S hours. Protein samples (30 µg/lane) and protein marker were run on a 10 % Bis-Tris gel(nd – not detected). This figure is modified from [Spekker-Bosker *et al.* 2019a], which is published under the liberal Creative Commons Attribution 4.0 International (CC BY 4.0) license.

Next, enzyme activities of the induced antimicrobial effector proteins were analyzed. The activity of tryptophan degrading enzymes, like IDO1, can be measured in the supernatant of cell cultures by detection of kynurenine, the product of tryptophan degradation. Thus, hRPE cells were stimulated with varying concentrations of IFN-γ in

a cell culture system with excess tryptophan. IDO1 activity was clearly induced in a dose dependent manner in hRPE cells (Figure 7A).

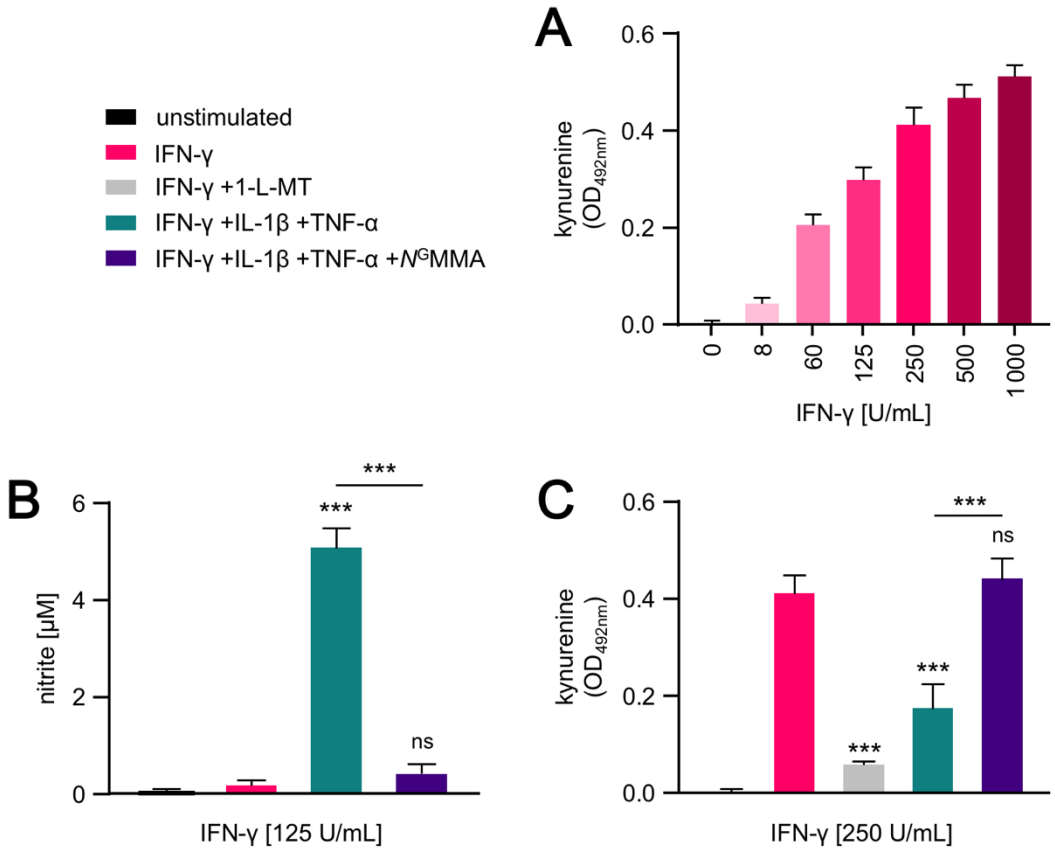

Figure 7: Activity of IDO1 and iNOS in stimulated hRPE cells and the interference with one another.

Indoleamine 2,3-dioxygenase 1 (IDO1) as well as inducible nitric oxide synthase (iNOS) activity was evaluated indirectly by accumulation of (**A, C**) kynurenine and (**B**) nitrite in the supernatant of human retinal pigment epithelium (hRPE) cell cultures. The kynurenine and nitrite content were determined by using Ehrlich´s and Griess reagent, respectively. hRPE cells remained unstimulated or were stimulated with (**A**) different concentrations of interferon gamma (IFN-γ) alone or with (**B, C**) combinations of IFN-γ, interleukin-1 beta (IL-1β, 100 U/mL), tumor necrosis factor alpha (TNF-α, 100 U/mL), the IDO inhibitor 1-methyl-L-tryptophan (1-L-MT, 1.5 mM) and the NOS inhibitor N^G-monomethyl-L-arginine (N^GMMA, 100 µg/mL) as indicated for 72 hours. Data are represented as mean values ± SEM of triplicate measurements (n = 2 - 4) and analyzed using a one-way ANOVA corrected for multiple comparison by the Tukey´s post hoc test. ***p ≤ 0.001 indicate significant differences compared to the IFN-γ stimulated dataset, if not otherwise indicated (**B**, **C**). (ns - not significant). This figure contains modified data from [Spekker-Bosker *et al.* 2019a], which is published under the liberal Creative Commons Attribution 4.0 International (CC BY 4.0) license.

Supplementation with the IDO inhibitor 1-methyl-L-tryptophan (1-L-MT) significantly reduced IDO1 activity in hRPE cells by 85 % (Figure 7C). Measurement of NOS activity can be achieved by detection of nitrite, a primary stable and nonvolatile breakdown product of nitric oxide, in the supernatant of cell cultures. IFN-γ stimulation was not

sufficient to induce detectable iNOS activity (Figure 7B), even though transcripts were induced by IFN-γ alone (Figure 6A). In experiments with higher hRPE cell numbers (10× more cells) costimulation with IFN-γ and IL-1β resulted in measurable iNOS activity [Spekker-Bosker *et al.* 2019a] as expected from the qPCR analysis. Nevertheless, costimulation with IFN-γ, IL-1β and TNF-α showed significant iNOS activity, which could be abrogated with the competitive inhibitor N^GMMA (Figure 7B). Costimulation of hRPE cells with IFN-γ, IL-1β and TNF-α did not only led to production of nitrite, but further reduced IDO1 activity by 57 %. This phenotype could be reversed by inhibition of iNOS with N^GMMA, which completely restored IDO1 activity (Figure 7C).

4.1.2 IDO1 mediates pathogen and lymphocyte growth control in hRPE cells

Following the relevance of the IFN-γ induced effector proteins - identified above – in regard to control of pathogen growth and lymphocyte proliferation was investigated. In addition to infection with the parasite *T. gondii*, this hRPE *in vitro* model was extended to address intraocular infections caused by disseminated bacteria, so called endogenous bacterial endophthalmitis (EBE) [Coburn *et al.* 2015]. Therefore, an isolate of *S. aureus* – usually a commensal bacterium – that can cause EBE was used. Since the hRPE bares important functions for the establishment and maintenance of the immune privilege of the eye [Streilein *et al.* 2002] co-cultivation with activated T cells were also included in the analysis. Thus, hRPE cell cultures were pre-stimulated with proinflammatory cytokines before infection with *T. gondii*, inoculation with *S. aureus* or co-cultivation with human lymphocytes.

Intracellular growth of *T. gondii* tachyzoites was measured via incorporation of ^{3}H-uracil. Proliferation of *T. gondii* tachyzoites in unstimulated hRPE cells served as a positive control and therefore was defined as 100 % growth (Figure 8A). IFN-γ stimulation and subsequent IDO1 induction led to a significant reduction (of 82 %) of *T. gondii* tachyzoite proliferation to 18 %. Supplementation of excess tryptophan restored parasite proliferation drastically (to 85 %). Induction of the antimicrobial effector mechanism iNOS by stimulation of hRPE cells with IFN-γ, IL-1β and TNF-α improved parasite proliferation significantly (by 33 % compared to IFN-γ stimulated hRPE), which could be reversed with the competitive NOS inhibitor N^GMMA.

Nevertheless, in the presence of iNOS parasite proliferation was by far not optimal (51 % of the positive control).

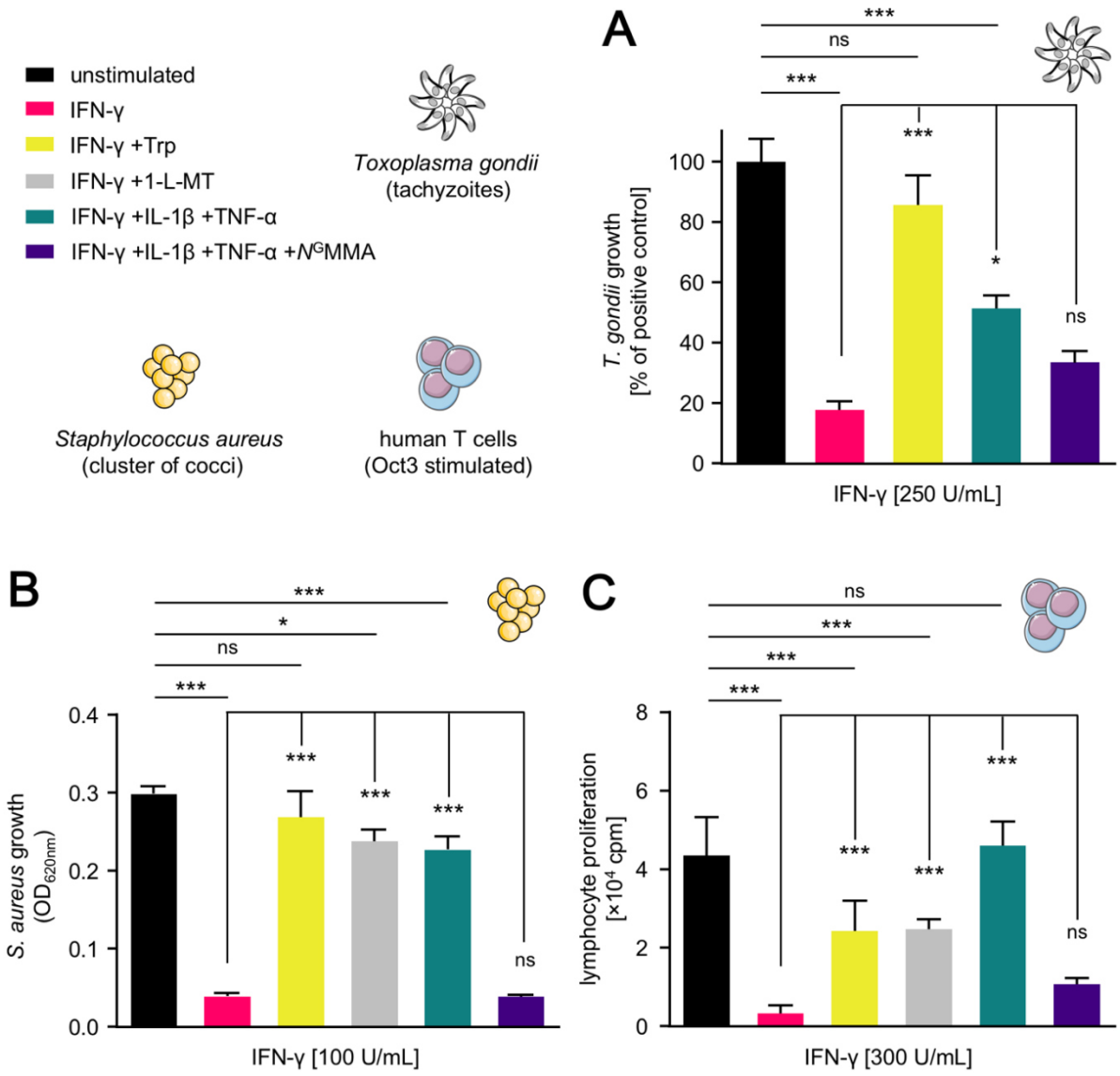

Figure 8: iNOS reduces the capacity of IDO1 to inhibit pathogen growth and lymphocyte proliferation in hRPE cell cultures.

Proliferation and growth of (**A**) *Toxoplasma gondii* tachyzoites, (**B**) *Staphylococcus aureus* and (**C**) anti-CD3 activated human lymphocytes in pre-stimulated human retinal pigment epithelium (hRPE) cell cultures. Proliferation and growth were determined using (**A**) the ^{3}H-uracil and (**C**) the ^{3}H-thymidine incorporation assays or (**B**) via measurement of the optical density (OD) at 620 nm. hRPE cells remained unstimulated or were pre-stimulated with combinations of interferon-gamma (IFN-γ), interleukin-1 beta (IL-1β, 100 U/mL), tumor necrosis factor alpha (TNF-α, 100 U/mL), the indoleamine 2,3-dioxygenase inhibitor 1-methyl-L-tryptophan (1-L-MT, 1.5 mM), the nitric oxide synthase inhibitor N^{G}-monomethyl-L-arginine (N^{G}MMA, 100 µg/mL) and additional L-tryptophan (Trp, 100 µg/mL) as indicated for 72 hours. Data were represented as mean values ± SEM of triplicate measurements (n = 2-4). *p ≤ 0.05; ***p ≤ 0.001 indicate significant differences determined using a one-way ANOVA corrected for multiple comparison by the Tukey´s post hoc test (cpm - counts per minute; ns - not significant). This figure contains modified data from [Spekker-Bosker *et al.* 2019a] and [Spekker-Bosker *et al.* 2019b], which are published under the liberal Creative Commons Attribution 4.0 International (CC BY 4.0) license.

S. aureus growth in pre-stimulated hRPE cell cultures was measured by optical density (Figure 8B). IFN-γ induced IDO1 production abrogated *S. aureus* growth by 86 %. Excess tryptophan as well as 1-L-MT, an IDO inhibitor, supplementation restored bacterial growth drastically (to 90 % and 80 %, respectively). In addition, stimulation of hRPE cells with IFN-γ, IL-1β and TNF-α and subsequent induction of iNOS favored bacterial growth significantly (77 %). This phenotype was completely reversable by inhibition of iNOS with N^GMMA.

Proliferation of human lymphocytes was analyzed by detection of incorporated ^{3}H-thymidine into anti-CD3 activated and proliferating T cells (Figure 8C). Lymphocyte proliferation in IFN-γ pre-stimulated hRPE cell cultures was highly impaired (by 92 %) compared to lymphocyte proliferation in unstimulated hRPE cell cultures. Excess tryptophan as well as 1-L-MT supplementation attenuated this phenotype, however restored lymphocyte proliferation to only about 56 % of the positive control (lymphocyte growth in unstimulated hRPE). hRPE cell cultures with induced iNOS activity were able to restore lymphocyte proliferation completely (107 %). iNOS inhibition with N^GMMA again reversed the observed phenotype. Lymphocyte proliferation was again impaired (25 % of the positive control).

4.1.3 hCMV interferes with the antimicrobial and immunosuppressive milieu of stimulated hRPE cultures

The host specific human cytomegalovirus (hCMV) usually causes asymptomatic infections but will persist livelong [Zuhair *et al.* 2019]. Similar to *T. gondii*, hCMV is highly prevalent (up to 83 %) in the human population and causes similar clinical manifestations in the eye of predominantly immunosuppressed patients [Zuhair *et al.* 2019; Melendez-Munoz *et al.* 2019]. Due to the high prevalence of both, *T. gondii* and hCMV, simultaneous infections with these pathogens are likely. Thus, the consequences of a hCMV infection in regard to the establishment and control of infections with other opportunistic pathogens, that are targeting the eye, were analyzed in the following *in vitro* model.

IFN-γ induced IDO1 activity in hCMV infected hRPE cell cultures was significantly reduced (58 % in comparison to the non-hCMV infected IFN-γ stimulated hRPE cell cultures; Figure 9A). This reduced IDO1 activity had drastic consequences for the control of *T. gondii* proliferation and *S. aureus* growth, which resulted in an unhindered

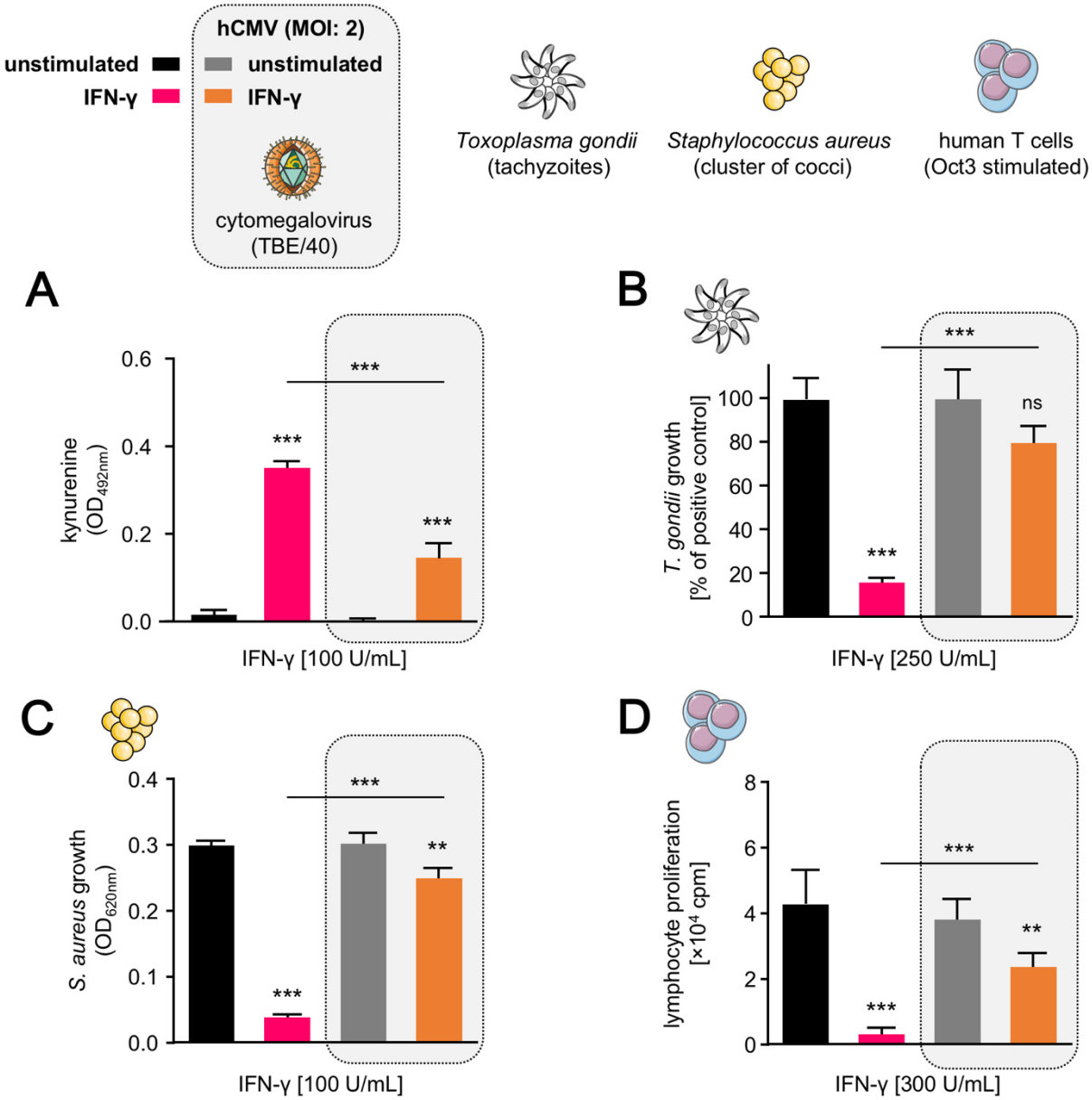

Figure 9: hCMV infection of hRPE cells diminishes the antimicrobial and immunosuppressive milieu.

Indoleamine 2,3-dioxygenase 1 (IDO1) activity and its antimicrobial and immunosuppressive capacity are reduced in cytomegalovirus infected hRPE cells. hRPE cell cultures remained either uninfected or were infected with the human cytomegalovirus strain TBE/40 (MOI: 2) before stimulated with interferon gamma (IFN-γ) for 72 hours. IDO1 activity was evaluated by measurement of (**A**) kynurenine accumulation in the supernatant of human retinal pigment epithelium (hRPE) cell cultures. Proliferation and growth of (**B**) *Toxoplasma gondii* tachyzoites, (**C**) *Staphylococcus aureus* and (**D**) anti-CD3 activated human lymphocytes in pre-stimulated human retinal pigment epithelium (hRPE) cell cultures were determined using (**B**) ^{3}H-uracil and (**D**) ^{3}H-thymidine incorporation assays or (**C**) via measurement of the optical density (OD) at 620 nm. Data are represented as mean values ± SEM of triplicate measurements (n = 4) and were analyzed using a one-way ANOVA corrected for multiple comparison by the Tukey´s post hoc test. **p ≤ 0.01; ***p ≤ 0.001 indicate significant differences to the respective unstimulated dataset, if not otherwise indicated. (MOI - multiplicity of infection; cpm - counts per minute; ns - not significant). This figure contains modified data from [Spekker-Bosker *et al.* 2019b], which is published under the liberal Creative Commons Attribution 4.0 International (CC BY 4.0) license.

proliferation of *T. gondii* tachyzoites (Figure 9B) or a slightly significant reduction of *S. aureus* growth (to 83 %) in IFN-γ stimulated cultures (Figure 9C). In addition to the interference of the hCMV infection with the antimicrobial properties of IFN-γ stimulated hRPE cell cultures, their suppressive properties were also affected. Even though activated human T cells showed reduced proliferation (63 % of the positive control) in IFN-γ stimulated and hCMV infected hPRE cells they exhibited a significantly better proliferation (63 % versus 8 %) compared to T cells that were cultured in non-hCMV infected IFN-γ stimulated hPRE cell cultures (Figure 9D).

Conclusively, IDO1 is induced upon IFN-γ stimulation in hRPE cells, whereas iNOS activity required additional IL-1β and TNF-α stimulation. Interestingly, only IDO1 inhibited *T. gondii* and *S. aureus* growth in hRPE cell cultures sufficiently. iNOS only marginally inhibited pathogen growth, but instead interfered with IDO1 activity and IDO1 mediated pathogen control and its immunosuppressive capacity. Furthermore, co-infection experiments revealed that the IFN-γ induced antimicrobial and immunosuppressive milieu in hRPE cell cultures was interrupted by hCMV.

4.2 Antimicrobial role of mIDO1 in mice

To identify the role of tryptophan degrading enzymes during the acute phase of toxoplasmosis an experimental *in vivo* model was utilized. Here, C57BL/6J mice deficient for mIDO1 ($IDO^{-/-}$) and appropriate control mice (WT) were infected intraperitoneal (ip) with *T. gondii* tachyzoites, representing the rapidly proliferating stage during an acute *T. gondii* infection.

4.2.1 Lack of mIDO1 does not influence toxoplasmosis associated symptoms and survival of acute murine toxoplasmosis

WT and $IDO^{-/-}$ mice were infected with 10^5 *T. gondii* tachyzoites and were scored for infection associated signs according to the assessment criteria in Table 14 (p. 34) on a daily basis. If a termination criterion was reached (methods section 3.3.1), the animals were euthanized and killed painlessly in accordance with animal welfare standards. Figure 10 illustrates the survival of infected and control mice (Figure 10A), as well as the underlying scoring (Figure 10B) and weight changes (Figure 10C) of these animals. Each symbol in Figure 10B & C represents the determined value of one

mouse at the specific time point and the lines represent the respective mean of these values per genotype.

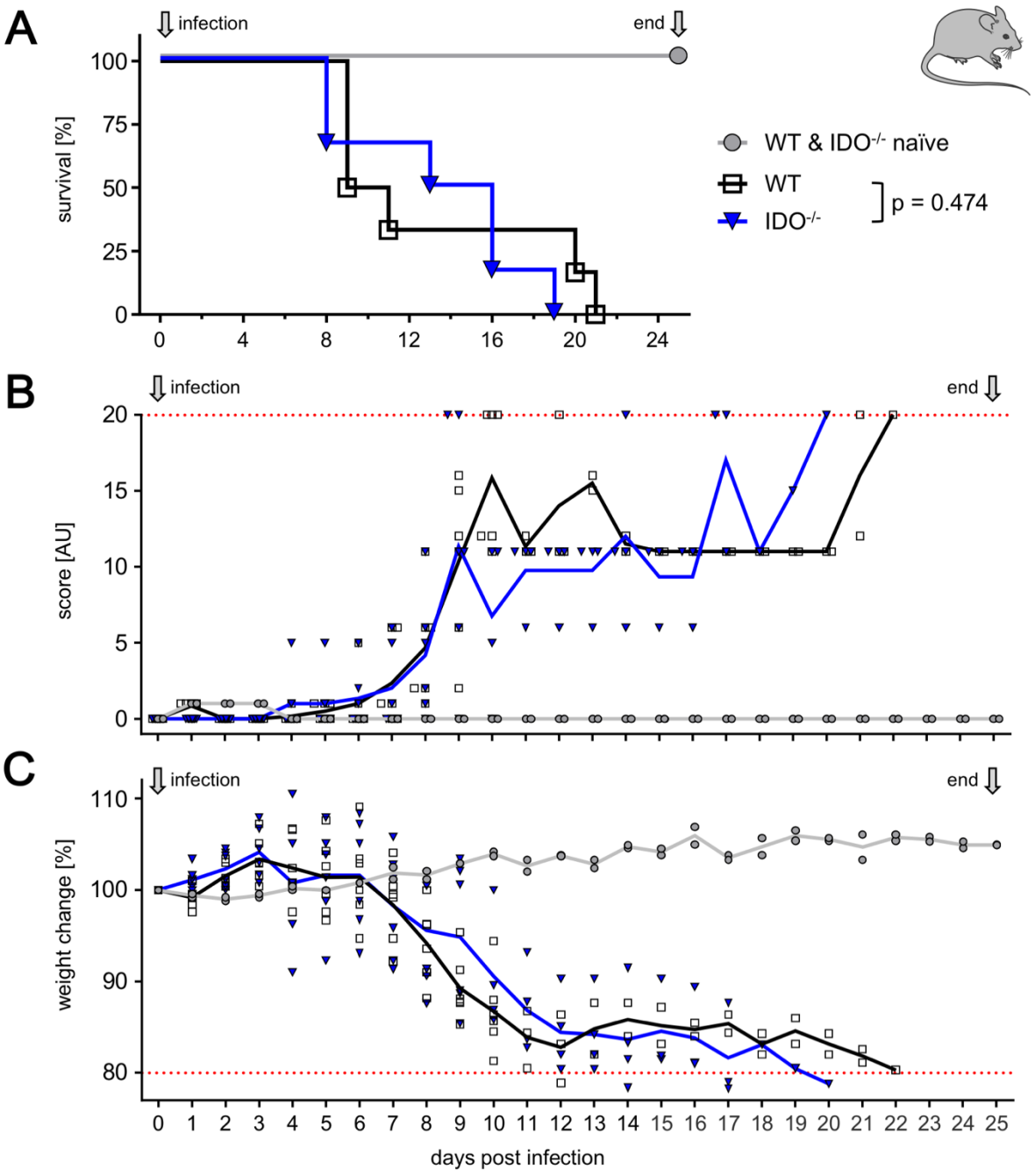

Figure 10: IDO $^{-/-}$ and WT mice show comparable susceptibility during experimental toxoplasmosis.

A, Survival of naïve and *Toxoplasma gondii* (*T. gondii*; ME49 strain) infected wild type (WT) and indoleamine 2,3-dioxygenase 1-deficient (IDO$^{-/-}$) mice, including their corresponding (**B**) scores and (**C**) relative weight changes are shown. **A**, Survival of *T. gondii* infected WT and IDO$^{-/-}$ mice is comparable as tested using the log-rank test. **B** & **C**, Solid lines depict mean values of the individual scores or relative weight changes that are represented as staggered or aligned symbols, respectively. Mice were sacrificed when the threshold (scattered lines) for weight loss (= 20 %) or score (= 20) was reached. Data origin from one experiment with naïve (WT, n = 1; IDO$^{-/-}$, n = 1) and *T. gondii* (intraperitoneal dose: 10^5 tachyzoites) infected WT (n = 6) and IDO$^{-/-}$ (n = 6) mice. (AU - arbitrary units).

The first weight loss of an infected mouse was observed at four days post infection (dpi). However, from six dpi and onward mice from both infected genotypes ($IDO^{-/-}$ and WT mice) increasingly lost weight and showed additional signs of infection (Figure 10B & C). The first mice reached termination criteria by eight dpi ($IDO^{-/-}$) and nine dpi (WT). By that time, infected mice had already lost on average of 10 % body weight and were scored with 5 to 10 points. Half of the infected mice were alive until nine dpi (WT) and 13 dpi ($IDO^{-/-}$). The last mouse of each genotype fulfilling termination criteria survived until 19 dpi ($IDO^{-/-}$) and 21 dpi (WT), respectively.
This data was generated in an experiment in the context of congenital toxoplasmosis in which mice were meant to be immunized for an infection experiment. The chosen infection dose was lethal for all mice; however, it showed that mIDO1 deficiency does not influence the survival of these infected mice. From here on infected mice had been euthanized not later than nine dpi.

Abnormal increases in organ size (e.g. lymphadenitis, splenomegaly) have been reported during toxoplasmosis in otherwise healthy individuals [Carme *et al.* 2002]. In wild type mice, *T. gondii* induced splenomegaly's have been published before [Chen *et al.* 2017]. Thus, infection associated organomegalies were analyzed in $IDO^{-/-}$ mice next. Here, organ weights of spleen, lung, liver as well as brain – predominantly targeted by *T. gondii* to develop into tissue cysts – from WT and $IDO^{-/-}$ mice were documented and analyzed. The organ weights were normalized to the corresponding mouse body weight at infection start, since a global body weight loss was observed during infection (Figure 11).
A splenomegaly was clearly observed in both genotypes as documented by weight measurements. Relative mean spleen weights of naïve mice were at 4 ±1 mg/g and 4.3 ±0.9 mg/g for WT and $IDO^{-/-}$ mice, respectively. During the initial phase of the infection spleen weights increased drastically. Relative mean spleen weights reached 7.1 ±3.1 mg/g (178 %) and 6.6 ±1.5 mg/g (153 %) for WT and $IDO^{-/-}$ mice at three dpi. By seven dpi the relative spleen weights had tripled with means at 11.6 ±2.5 mg/g (290 %) for WT and 13.6 ±2.6 mg/g (316 %) $IDO^{-/-}$ mice.
Relative lung weights were stable during infection (naïve: 9.6 mg/g, 3 dpi: 10.6 mg/g, 7 dpi: 9.9 mg/g) in WT mice. Lungs of $IDO^{-/-}$ mice showed a trend towards an increase in relative lung weight (naïve: 8.3 mg/g, 3 dpi: 9.6 mg/g, 7 dpi: 10.7 mg/g). One specimen in particular ($IDO^{-/-}$ at 7 dpi, 15.7 mg/g relative lung weight) had a strikingly

heavy lung (369 mg). Based on the acquired data the lung of a mouse with 23.5 g body weight would be expected to weigh 195 mg – 252 mg.

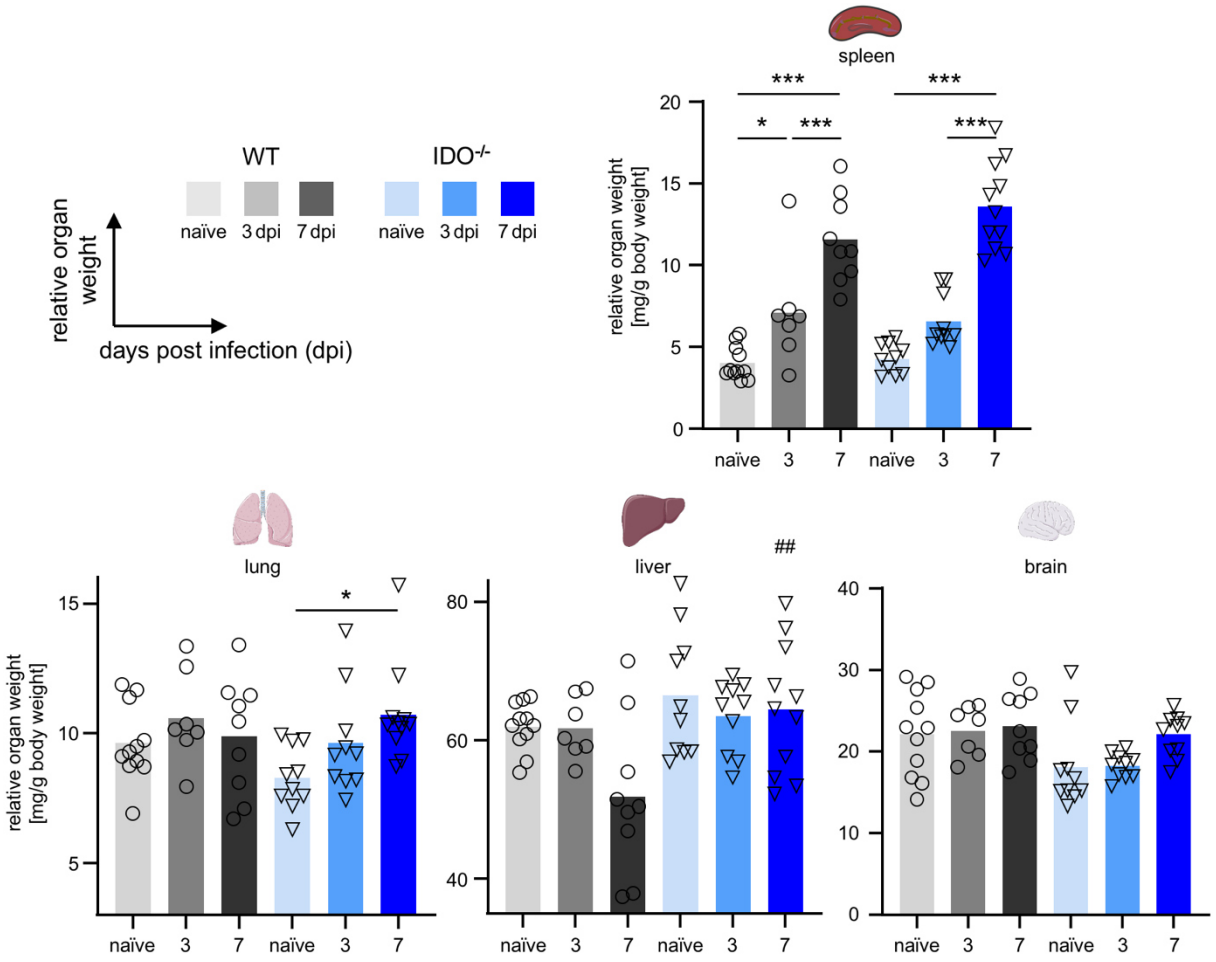

Figure 11: Spleen but not lung, liver and brain weights increase drastically during *T. gondii* infection.

Organs were collected from naïve wild type (WT) and indoleamine 2,3-dioxygenase 1-deficient (IDO$^{-/-}$) (WT n = 11; IDO$^{-/-}$ n = 10) or *Toxoplasma gondii* (*T. gondii*; ME49 strain) infected (3 dpi, WT n = 7; IDO$^{-/-}$ n = 10 | 7 dpi, WT n = 9; IDO$^{-/-}$ n = 11) mice. The organ weights were normalized to the corresponding mouse body weight at infection start. Dot plots depict relative organ weights from two (3 dpi) and three (7 dpi) independent experiments. Bars depict the respective mean values. The data was analyzed using a one-way ANOVA corrected for multiple comparison by the Tukey´s post hoc test. $^{\#\#}p \leq 0.01$ indicates significant differences between genotypes at the same time point. $^{*}p \leq 0.05$; $^{***}p \leq 0.001$ indicate significant differences between time points of the same genotype. (dpi - days post infection).

Relative liver weights were stable in IDO$^{-/-}$ mice throughout the observed period (64.8 ±7.9 mg/g for naïve mice and at three dpi and seven dpi). In WT mice, relative liver weights dropped from 61.9 ±3.7 mg/g (naïve and three dpi) to 51.8 ±10.6 mg/g at seven dpi.

Relative mean brain weights were stable in WT (means at 22.6 ±4.2 mg/g) and IDO$^{-/-}$ (means at 19.6 ±3.8 mg/g) mice throughout the observed period.

Splenomegaly associated with *T. gondii* infection was clearly observed in WT mice and comparable in IDO$^{-/-}$ mice. Other organomegalies were not as prominent; however, IDO$^{-/-}$ mice showed a trend for increased lung weights during infection.

4.2.2 mIDO1 is induced and active during acute murine toxoplasmosis

IFN-γ is the major cytokine induced during a *T. gondii* infection [Gazzinelli *et al.* 1993; Hunter *et al.* 1994]; thus, expression of IFN-γ induced cell-autonomous effector mechanisms were analyzed using a qPCR approach. In addition to the expression of the effector molecules mGBP2, miNOS and mIDO1 (Figure 12) two other tryptophan degrading enzyme, namely murine IDO2 (mIDO2) and murine TDO (mTDO) were included in the analysis (Figure 13). The expression of the genes of interest are relative to the expression of an internal control (murine β-actin) of samples from infected mice compared to samples of naïve mice.

qPCR analysis of lung samples (Figure 12A) showed that mIDO1 mRNA expression was strongly induced in lungs of *T. gondii* infected WT mice (3 dpi: 79.4-fold; 7 dpi: 95.3-fold) and was absent in lung samples of infected IDO$^{-/-}$ mice. Relative mRNA expression of mGBP2 was equally induced in both genotypes at three dpi (WT: 16.2-fold; IDO$^{-/-}$: 10.4-fold) and seven dpi (WT: 26.5-fold; IDO$^{-/-}$: 25-fold). miNOS expression was weakly induced at three dpi (WT: 1.1-fold; IDO$^{-/-}$: 2.1-fold), but more prominent at seven dpi (WT: 4.3-fold; IDO$^{-/-}$: 5.6-fold).

Analysis of liver samples (Figure 12B) showed no mIDO1 expression at three dpi in both genotypes. At seven dpi mIDO1 mRNA expression was induced (13.7-fold) in WT livers, whilst some samples showed weak (1.9-fold) and others very high (93-fold) mIDO1 induction.

Relative mGBP2 mRNA expression was equally induced in both genotypes at three dpi (WT: 14.5-fold; IDO$^{-/-}$: 14-fold) and seven dpi (WT: 25-fold; IDO$^{-/-}$: 33.4-fold). miNOS expression was weakly induced (WT: 1.9-fold; IDO$^{-/-}$: 2.4-fold) in liver at three dpi as well; however, at seven dpi relative miNOS expression increased by 22.5-fold and 21.2-fold in liver of WT and IDO$^{-/-}$ mice.

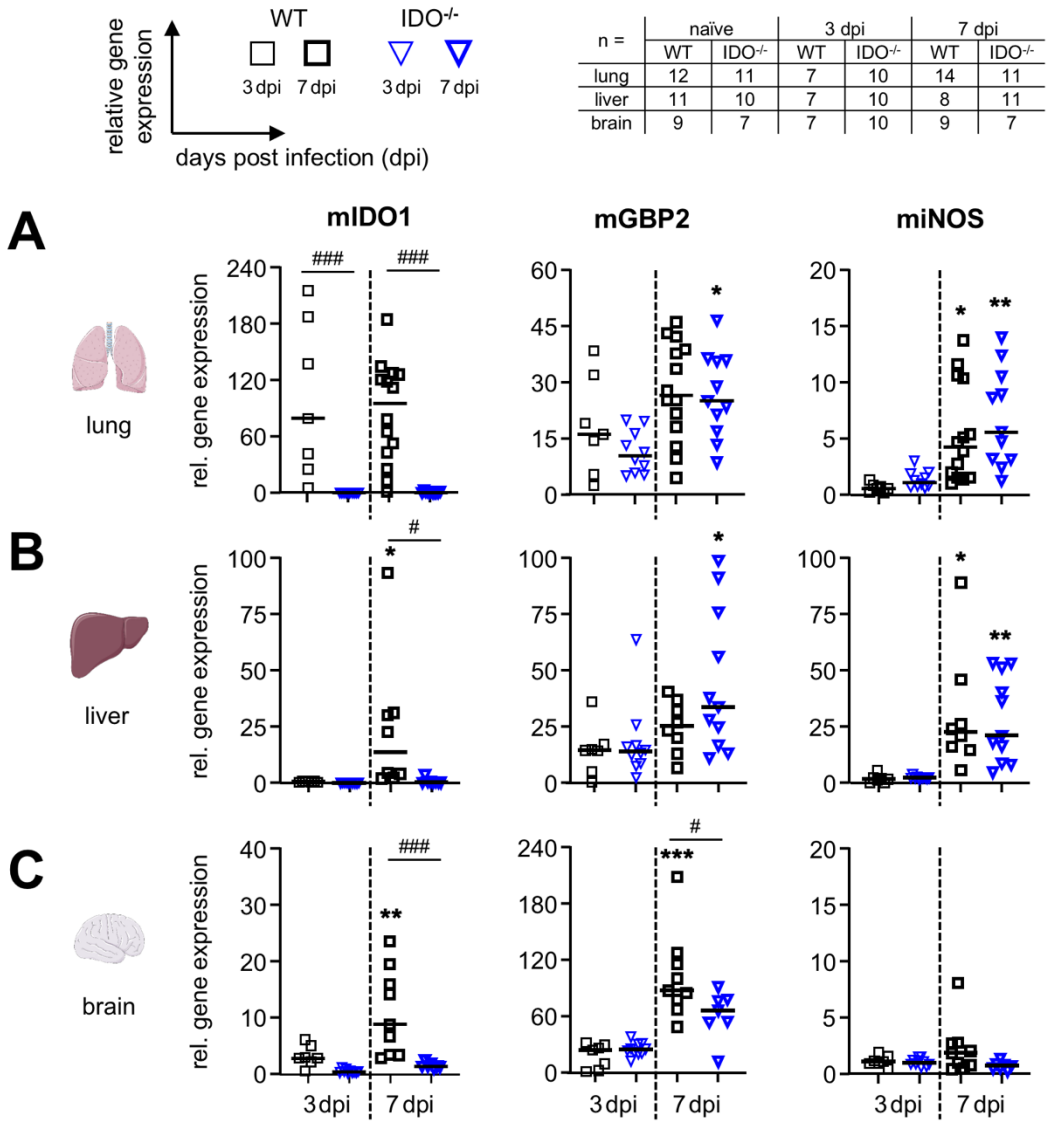

Figure 12: mGBP2 and miNOS expression is not elevated in IDO$^{-/-}$ mice.
Relative mRNA expression of murine indoleamine 2,3-dioxygenase 1 (mIDO1), guanylate binding protein 2 (mGBP2) and inducible nitric oxide synthase (miNOS) in (**A**) lung, (**B**) liver and (**C**) brain tissue from wild type (WT) and indoleamine 2,3-dioxygenase 1 deficient (IDO$^{-/-}$) mice during T*oxoplasma gondii* (*T. gondii*; ME49 strain) infection. Quantitative real-time PCR (qPCR) data was analyzed using the $2^{-\Delta\Delta CT}$ method. Here, expression of the gene of interest is relative to the expression of an internal control (β-actin) of samples from infected mice compared to samples from naïve mice. The data is illustrated in scattered dot plots (each dot represents one mouse) and the median. The table summarizes the number of samples (n) from two (3 dpi) and three (7 dpi) independent experiments. Data were analyzed using a one-way ANOVA corrected for multiple comparison by the Tukey´s post hoc test. $^{\#}p \leq 0.05$; $^{\#\#\#}p \leq 0.001$ indicate significant differences between genotypes at the same time point. $^{*}p \leq 0.05$; $^{**}p \leq 0.01$; $^{***}p \leq 0.001$ indicate significant differences between time points of the same genotype. (dpi - days post infection). This figure contains data from [Ufermann *et al.* 2019], which is published under the liberal Creative Commons Attribution 4.0 International (CC BY 4.0) license.

Analysis of brain samples (Figure 12C) showed that mIDO1 mRNA expression increased in brains of WT mice over time from 2.5-fold (3 dpi) up to 8.9-fold (7 dpi). In

contrast, brains of IDO$^{-/-}$ mice showed no mIDO1 expression. mGBP2 expression in brains of WT and IDO$^{-/-}$ mice increased from 24.4-fold to 100.9-fold and 24.7-fold to 66.6-fold, respectively. Relative expression of miNOS was increased only in the brain of WT mice at seven dpi by 1.9-fold and was not induced in brains of IDO$^{-/-}$ mice.

Next, the expression of the isozymes mIDO2 and mTDO was analyzed in order to identify possible compensatory mechanisms for the lack of mIDO1 in the IDO$^{-/-}$ mice (Figure 13).

First, cycle thresholds (CTs) of mIDO2 (Figure 13A) and mTDO (Figure 13B) were compared with the CTs of mβ-actin in samples of naïve WT and IDO$^{-/-}$mice. CTs are inversely related to amplicon abundance, thus the smaller the CT value the more amplicon is present. If no signal was present in the qPCR after 40 cycles the CT was defined as '40'. mβ-actin CT values in WT and IDO$^{-/-}$ mouse samples are consistent within the same organ and do not differ between genotypes.

mIDO2 transcripts were not detected in lungs of naïve mice (WT: CT_{mIDO2}=39.7, $CT_{m\beta\text{-actin}}$=22.8; IDO$^{-/-}$: CT_{mIDO2}=40, $CT_{m\beta\text{-actin}}$=22.9), but were clearly abundant in livers of WT (CT_{mIDO2}=31.3, $CT_{m\beta\text{-actin}}$=24.3) and IDO$^{-/-}$ (CT_{mIDO2}=32.1, $CT_{m\beta\text{-actin}}$=24.2) mice (Figure 13A). Brains from WT mice had a weak mIDO2 expression (CT_{mIDO2}=38.4, $CT_{m\beta\text{-actin}}$=19.5), which was absent in brains from IDO$^{-/-}$ mice (CT_{mIDO2}=39.7, $CT_{m\beta\text{-actin}}$=19) (Figure 13A).

Even more abundant were mTDO transcripts in organs of naïve mice (Figure 13B). mTDO was highly expressed in liver (WT: CT_{mTDO}=26.8, $CT_{m\beta\text{-actin}}$=24.3; IDO$^{-/-}$: CT_{mTDO}=27, $CT_{m\beta\text{-actin}}$=24.2) and measurable in lung (WT: CT_{mTDO}=37.1, $CT_{m\beta\text{-actin}}$=22.8; IDO$^{-/-}$: CT_{mTDO}=35.8, $CT_{m\beta\text{-actin}}$=22.9) and brain (WT: CT_{mTDO}=32, $CT_{m\beta\text{-actin}}$=19.5, IDO$^{-/-}$: CT_{mTDO}=31.9, $CT_{m\beta\text{-actin}}$=19) samples of both genotypes.

Next, changes in expression of mIDO2 (Figure 13C) and mTDO (Figure 13D) due to *T. gondii* infection was analyzed. Few specimens from both genotypes showed slight increases of mIDO2 and mTDO transcripts. However, this had no impact on the mean relative expression of mIDO2 and mTDO, which were not altered by a *T. gondii* infection.

Consequently, this indicates that mIDO2 and mTDO are expressed predominantly in murine liver and that their expression is unaffected by an infection with *T. gondii*.

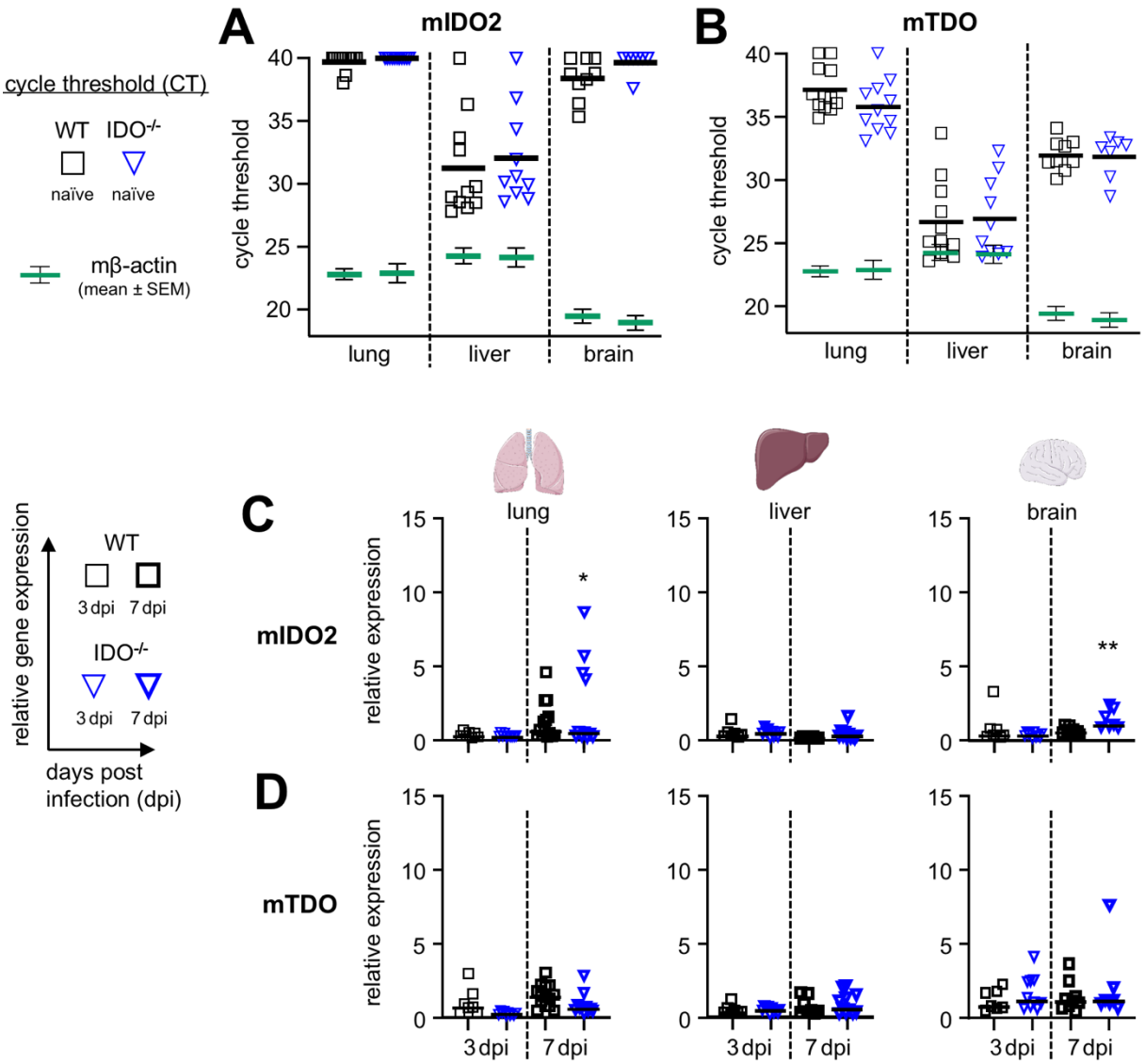

Figure 13: mIDO2 and mTDO transcripts in liver of naïve mice and weakly increased mIDO2 transcripts during infection in IDO$^{-/-}$ mice.

Expression of (**A**, **C**) murine indoleamine 2,3-dioxygenase 2 (mIDO2) and (**B**, **D**) murine tryptophan 2,3-dioxygenase (mTDO) in lung, liver and brain tissue from wild type (WT) and indoleamine 2,3-dioxygenase 1 deficient (IDO$^{-/-}$) mice during *Toxoplasma gondii* (*T. gondii*; ME49 strain) infection. **A** & **B**, Cycle thresholds (CTs) as mean values of duplicate measurements from quantitative real-time PCR (qPCR) experiments are shown as scattered dot plots (each dot represents one mouse) for mIDO2 and mTDO and the mean values ± SEM of the respective murine beta-actin (mβ-actin) CT in organs of naïve WT and IDO$^{-/-}$ mice. **C** & **D**, Relative mRNA expression of mIDO2 and mTDO were determined with the $2^{-\Delta\Delta CT}$ method. Here, expression of the gene of interest is relative to the internal control (mβ-actin) of samples from infected mice compared to samples of naïve mice. Data are illustrated in scattered dot plots (each dot represents one mouse) including the median. Data was analyzed using a one-way ANOVA corrected for multiple comparison by the Tukey´s post hoc test. *$p \leq 0.05$; **$p \leq 0.01$ indicate significant differences between time points of the same genotype. (dpi - days post infection). This figure contains data from [Ufermann *et al.* 2019], which is published under the liberal Creative Commons Attribution 4.0 International (CC BY 4.0) license.

The qPCR analysis demonstrated that mIDO1, mGBP2 and miNOS expression were induced upon infection with *T. gondii*, whereas mIDO2 and mTDO expression was independent of a *T. gondii* infection. Furthermore, relative mRNA expression of mGBP2 and miNOS was comparable in both genotypes. WT lungs – out of all organs – showed the most intense mIDO1 mRNA expression upon infection. Thus, protein expression in lung tissues from WT and IDO$^{-/-}$ mice, two per time point and genotype, was analyzed with immunoblots (Figure 14).

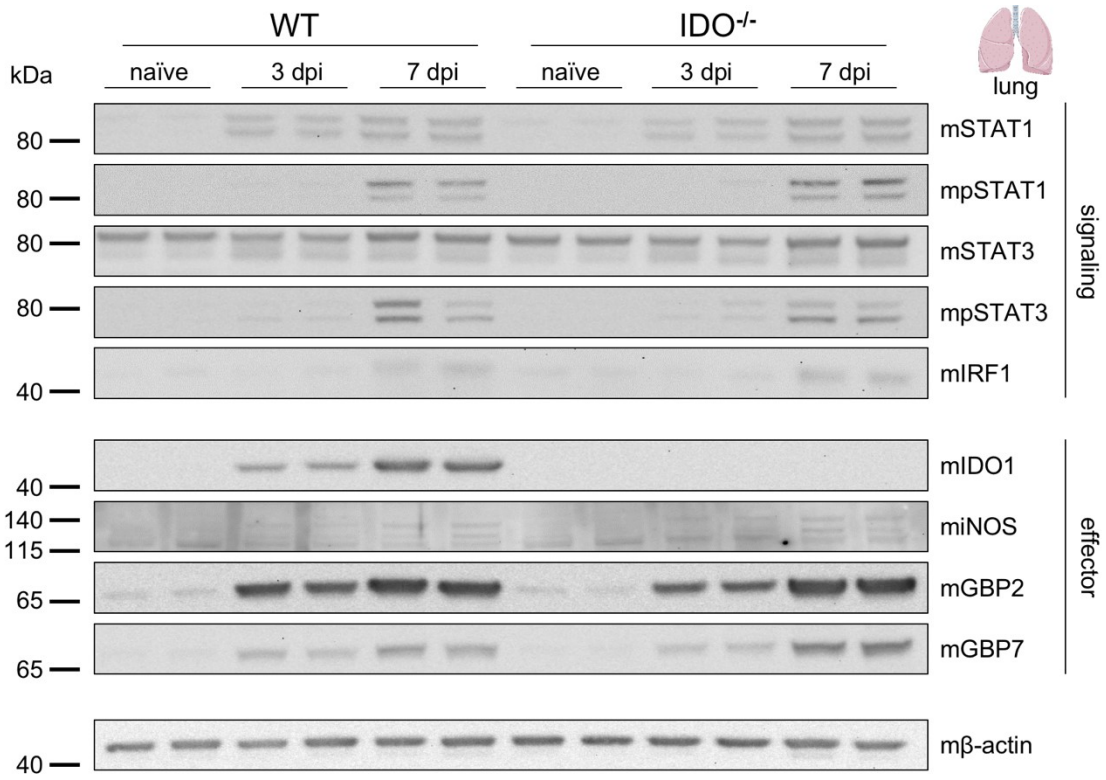

Figure 14: Comparable protein expression of IFN-γ - regulated molecules in lungs of WT and IDO$^{-/-}$ mice during *T. gondii* infection.

Immunoblot analysis of proteins involved in interferon-gamma (IFN-γ) signaling and IFN-γ induced effector molecules in lungs of naïve and *Toxoplasma gondii* (*T. gondii*; ME49 strain) infected wild type (WT) and indoleamine 2,3-dioxygenase 1 deficient (IDO$^{-/-}$) mice. Protein expression of murine signal transducer and activator of transcription 1 (mSTAT1) and 3 (mSTAT3), their phosphorylated forms (mpSTAT1, mpSTAT3), interferon regulatory factor 1 (mIRF1), IDO, inducible nitric oxide synthase (miNOS), guanylate binding protein 2 (mGBP2) and 7 (mGBP7) were analyzed in lungs of naïve and infected WT and IDO$^{-/-}$ mice on day three and seven post infection. Samples (10 µg/lane) and protein marker were run on 4 %–12 % Bis-Tris gels. Protein marker bands are indicated with a line and the band size in kilo dalton (kDa) on the left side of each blot. Lung samples origin from two independent experiments. (dpi - days post infection).

Expression of IFN-stimulated genes, like the cell-autonomous effector molecules that were analyzed by qPCR beforehand, require IFN-γ signaling via mpSTAT1 and mIRF1. In contrast to mpSTAT1, mSTAT3 activation induces immune regulatory genes and

dampens the Th1-mediated inflammatory response. These transcription factors involved in IFN-γ signaling were therefore included into immunoblot analysis (Figure 14, upper panel). mSTAT1 increased during the course of infection, whereas mSTAT3 was expressed equally strong in naïve lungs and at three and seven dpi. The phosphorylated and thus activated STATs (mpSTAT1 and mpSTAT3) were slightly present at three dpi and clearly present at seven dpi in lungs of both genotypes. mIRF1 was weakly present at seven dpi in both genotypes.
IFN-γ induced cell-autonomous effector proteins that are known to be required for control and clearance of *T. gondii* were detected in both genotypes in the same pattern; except for mIDO1, which was, as expected, absent in lungs of IDO$^{-/-}$ mice (Figure 14, lower panel). mIDO1 protein expression increased in the lungs of WT mice during the course of infection. miNOS was poorly detectable (compare Appendix A, p. 119). Nevertheless, a band at the expected protein size of miNOS (130 kilo dalton (kDa)) was, next to several other bands (compare Appendix A, p. 119), present in both genotypes at seven dpi (Figure 14, lower panel). mGBPs were slightly detectable in lung samples of naïve mice of both genotypes. mGBP2 was more prominent than mGBP7 while the protein band intensities of both mGBPs massively increased during the course of infection (Figure 14, lower panel). mβ-actin protein expression, which was comparable between genotypes and infection status, was included in the analysis as an internal control.

Expression of proteins involved in IFN-γ signaling and IFN-γ induced effector proteins, except for mIDO1, were comparable in both genotypes indicating that there was no obvious compensation for the missing mIDO1 in IDO$^{-/-}$ mice. Analysis of mIDO1 activity in WT mice and thus the impact of the missing mIDO1 in IDO$^{-/-}$ mice on the systemic distribution of tryptophan and kynurenine – the substrate and product of tryptophan degrading enzymes – was explored next. Tryptophan is an essential amino acid that *T. gondii* is auxotrophic for [Pfefferkorn 1984]. Furthermore, tryptophan is required by activated T cells during proliferation [Mellor and Munn 1999]. Here, the abundance of the amino acid and its metabolite during the initial phase of an acute murine toxoplasmosis was analyzed with HPLC (Figure 15).

As nutrients in general, tryptophan is distributed throughout the body via the blood. Thus, serum samples were included in the HPLC analysis (Figure 15A). The

tryptophan concentrations in serum were comparable between WT and IDO$^{-/-}$ mice.

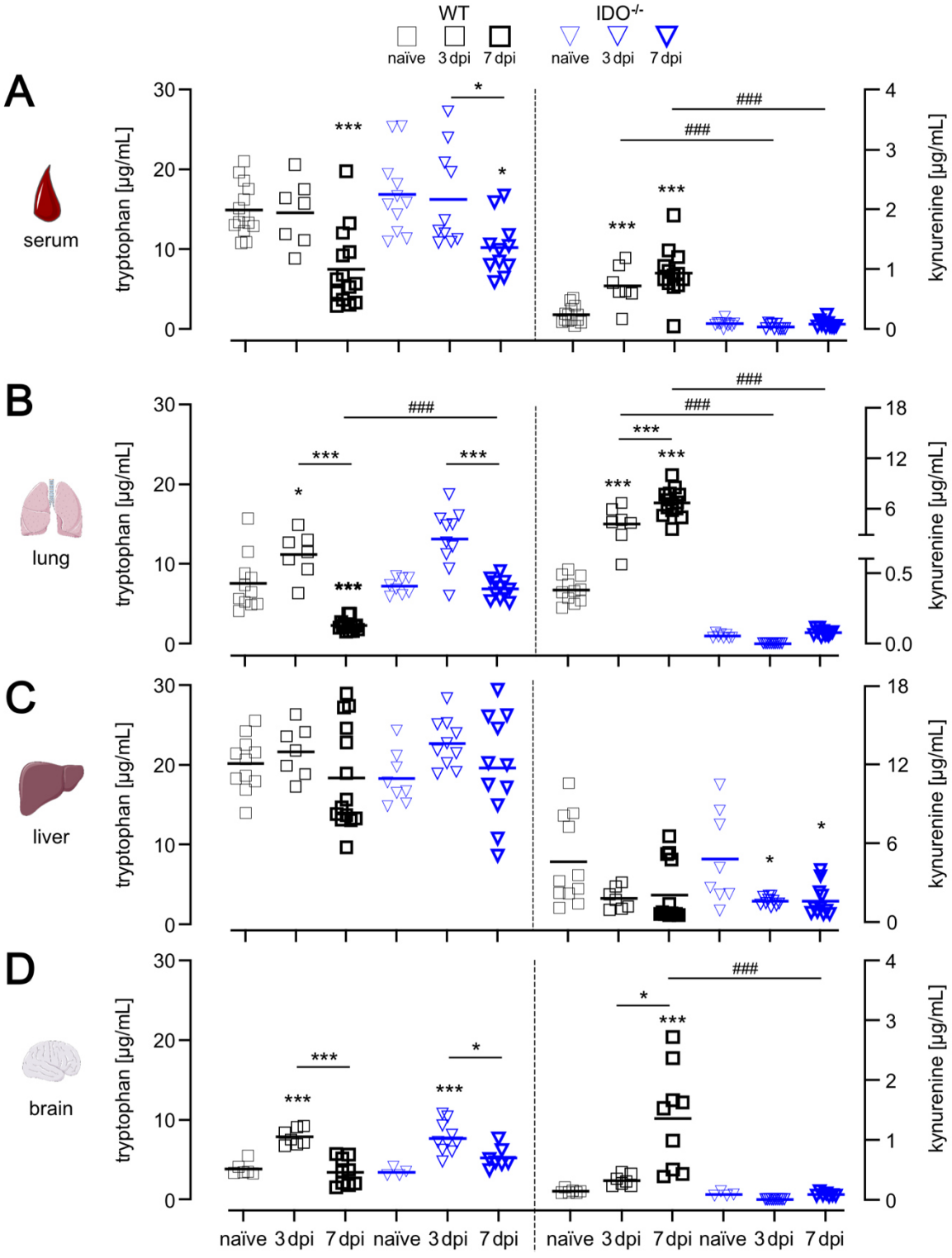

Figure 15: Abrogated kynurenine production during *T. gondii* infection in IDO$^{-/-}$ mice.

Free tryptophan and kynurenine were measured by high-performance liquid chromatography in (**A**) serum, (**B**) lung, (**C**) liver and (**D**) brain samples collected from naïve and *Toxoplasma gondii* (*T. gondii;* ME49 strain) infected wild type (WT) and indoleamine 2,3-dioxygenase 1 deficient (IDO$^{-/-}$) mice at day three and seven post infection. Samples are from two (3 dpi) and five (7 dpi) independent experiments. Means of duplicate measurements of a

single tissue sample are shown in scattered dot plots and the overall mean. Data were analyzed using one-way ANOVA corrected for multiple comparison by the Tukey´s post hoc test. ###p ≤ 0.001 indicate significant differences between genotypes at the same time point. *p ≤ 0.05; ***p ≤ 0.001 indicate significant differences to the naïve group of the same genotype, if not otherwise indicated. (dpi - days post infection). This figure contains data from [Ufermann *et al.* 2019], which is published under the liberal Creative Commons Attribution 4.0 International (CC BY 4.0) license.

Naïve WT and IDO$^{-/-}$ mice possess a mean tryptophan concentration of 15 µg/mL and 16.7 µg/mL in serum. At seven dpi the serum tryptophan concentration had dropped significantly by 36 % in WT (9.6 µg/mL) and 38.9 % in IDO$^{-/-}$ (10.2 µg/mL) mice (Figure 15A, left side). However, only in WT mice the serum kynurenine concentration increased, from 0.2 µg/mL in naïve WT mice to 0.7 µg/mL (250 %) at 3dpi and to 0.9 µg/mL (350 %) at 7dpi, while in IDO$^{-/-}$ mice the mean serum kynurenine concentration remained low (0.1 µg/mL) and close to the detection limit (Figure 15A, right side).

Mean tryptophan concentrations in lung tissue were comparable in naïve WT and IDO$^{-/-}$ mice (Figure 15B, left side). Interestingly, the concentration of tryptophan increased in lungs of both genotypes from 7.7 µg/mL and 7.3 µg/mL in naïve WT and IDO$^{-/-}$ mice to 11.3 µg/mL and 13.4 µg/mL at three dpi. At seven dpi the mean tryptophan concentration in lung tissue dropped again. In WT mice by 78.8 % to 2.4 µg/mL, which is even below the level detected in naïve mice. In IDO$^{-/-}$ mice the mean tryptophan concentration in lung tissue dropped by 47.8 % to 7 µg/mL, which is equivalent to the level detected in naïve mice (Figure 15B, left side). As in serum, the kynurenine concentration in lung tissue only increased in WT mice; however, much more drastic from 0.4 µg/mL to 4.2 µg/mL (950 %) at three dpi and 6.7 µg/mL (1575 %) at seven dpi. Kynurenine concentrations were very low (0-0.1 µg/mL) and close to the detection limit in lungs of IDO$^{-/-}$ mice (Figure 15B, right side).

Tryptophan homoeostasis is regulated by liver specific mTDO activity (compare Figure 13). Thus, in addition liver samples were analyzed (Figure 15C). Mean tryptophan concentrations in liver tissue stayed constant throughout the observed period in WT (naïve: 20.2 µg/mL; 3 dpi: 21.7 µg/mL; 7dpi: 18.3 µg/mL) and IDO$^{-/-}$ (naïve: 18.3 µg/mL; 3 dpi: 22.7 µg/mL; 7 dpi: 19.6 µg/mL) mice (Figure 15C, left side). The mean kynurenine concentrations were comparable in naïve WT (4.6 µg/mL) and IDO$^{-/-}$ (4.8 µg/mL) mice and were reduced by 54.3 % and 66.7 % in infected WT and IDO$^{-/-}$ mice at seven dpi (Figure 15B, right side).

HPLC analysis of brain tissue was performed (Figure 15D), since the brain is one of the main targets of *T. gondii* and induced mIDO1 expression was observed in WT mice upon *T. gondii* infection (Figure 12C). Similar to lung tissue, the mean tryptophan concentration in brain tissue first increased before it dropped again during infection (Figure 15D, left side). In detail, the mean tryptophan concentrations in brain tissue were comparable in naïve mice (WT: 3.9 µg/mL; $IDO^{-/-}$: 3.5 µg/mL). These concentrations increased to 7.9 µg/mL (102.6 %) and 7.7 µg/mL (120 %) at three dpi and dropped to the level of naïve mice (WT: 3.5 µg/mL; $IDO^{-/-}$: 5.2 µg/mL) at seven dpi. The mean kynurenine concentration was only increased in brain tissue of WT mice (from 0.1 µg/mL to 1.4 µg/mL) at seven dpi (Figure 15D, right side).

This HPLC analysis revealed that the tryptophan concentration in lung tissue had increased at three dpi independent of the genotype and had dropped again at seven dpi. In WT mice the tryptophan concentration in lung tissue dropped significantly below the level of naïve mice, whereas in $IDO^{-/-}$ mice the tryptophan concentration in lung tissue was significantly higher than in the WT at seven dpi and did not drop below the level of naïve mice. Furthermore, this HPLC analysis clearly showed that the increase in the kynurenine concentration during the course of the infection was dependent on the presence of mIDO1.

4.2.3 Unaltered parasite load in $IDO^{-/-}$ mice

The previously analyzed organs were subjected to qPCR analyses to analyze the impact of the missing mIDO1 in $IDO^{-/-}$ mice on the parasite load during the initial phase of a *T. gondii* infection. The presence of parasites was verified by detection of the genomic repeats of the *Tg*B1 gene, a 35-fold repetitive gene in the *T. gondii* genome. Absolute quantification, thus calculation of the parasite load was performed with a standard curve. The parasite loads in organs of WT and $IDO^{-/-}$ mice are illustrated as parasites per µg DNA (Figure 16). As expected, no parasites could be detected in any sample from naïve mice (data not shown). The mean parasite load in lung samples of infected WT mice increased from 1.55×10^3 parasites/µg DNA at three dpi to 2.29×10^5 parasites/µg DNA at seven dpi. The mean parasite load in lung samples of infected $IDO^{-/-}$ mice were not significantly different compared to the WT samples and increased from 3.24×10^3 parasites/µg DNA at three dpi to 1.78×10^5 parasites/µg DNA at seven dpi (Figure 16A). The mean parasite load in liver samples from infected WT

mice increased from 7.77×10^3 parasites/µg DNA at three dpi to 4.71×10^5 parasites/µg DNA at seven dpi. The mean parasite loads in liver samples from infected IDO$^{-/-}$ mice were not significantly different compared with the infected WT samples and increased from 7.18×10^3 parasites/µg DNA at three dpi to 4.04×10^5 parasites/µg DNA at seven dpi (Figure 16B).

Some brain samples (WT, 3 dpi: n=3; IDO$^{-/-}$, 3 dpi: n=1, 7 dpi n=1) showed no presence of the *Tg*B1 gene yet, even though the other organs (lung and liver) of the respective mice were positive for the *Tg*B1 gene. The mean parasite load in brain tissue of infected WT mice was at 315 parasites/µg DNA at three dpi and increased to 8.15×10^3 parasites/µg DNA at seven dpi. The mean parasite load in brains of infected IDO$^{-/-}$ mice was not significantly different compared to the WT samples and increased from 527 parasites/µg DNA at three dpi to 5.57×10^4 parasites/µg DNA at seven dpi (Figure 16C).

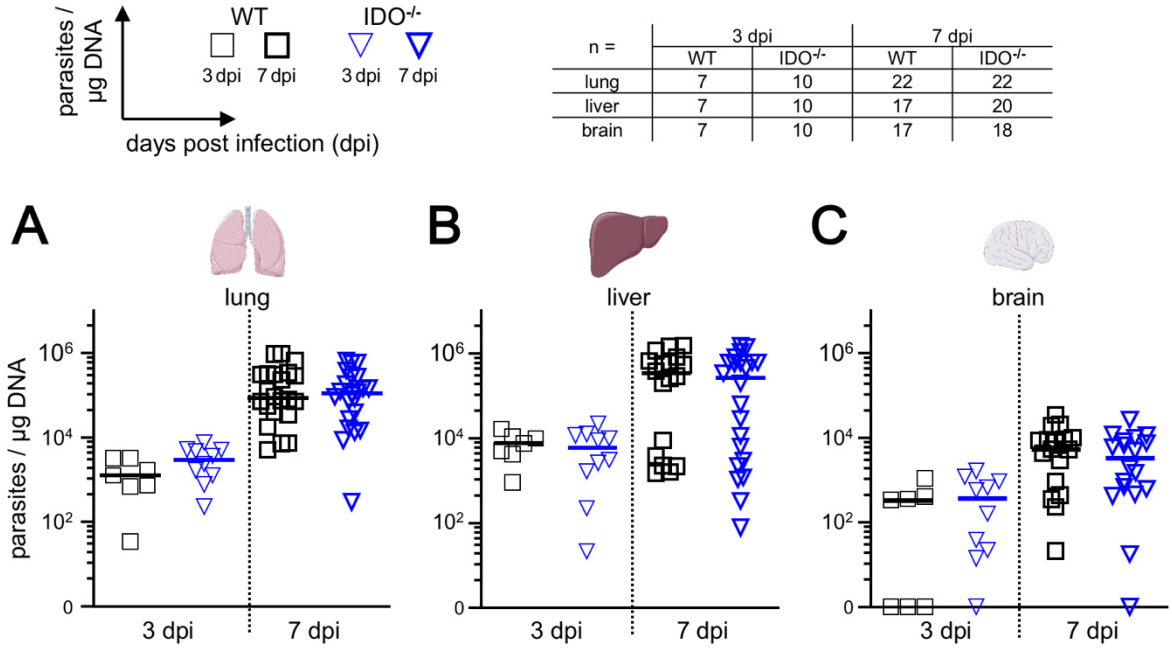

n =	3 dpi		7 dpi	
	WT	IDO$^{-/-}$	WT	IDO$^{-/-}$
lung	7	10	22	22
liver	7	10	17	20
brain	7	10	17	18

Figure 16: Comparable parasite loads in WT and IDO$^{-/-}$ mice.
Detection of the *Toxoplasma gondii* (*T. gondii*) B1 gene in samples of infected wild type (WT) and indoleamine 2,3-dioxygenase 1 deficient (IDO$^{-/-}$) mice. Organs were collected on day three and seven post infection with *T. gondii* (ME49 strain). The parasite loads are illustrated as parasites per µg DNA in (**A**) lung, (**B**) liver and (**C**) brain tissue. The table summarizes the number of samples (n) from two (3 dpi) and five (7 dpi) independent experiments. Means of duplicate measurements of a single tissue sample are shown in scattered dot plots. Data are analyzed using a one-way ANOVA corrected for multiple comparison by the Tukey´s post hoc test. Differences between genotypes at the same time point were not significant. (dpi - days post infection). This figure contains data from [Ufermann *et al.* 2019], which is published under the liberal Creative Commons Attribution 4.0 International (CC BY 4.0) license.

In conclusion, dissemination of *T. gondii* and thus parasite load increased during the course of infection. The parasite load was highest in liver (close proximity to the site of infection) and lower in lung and brain, which are organs upwards of the site of infection and towards the predominantly targeted location of *T. gondii*. However, the parasite load – independent of organ and time post infection – did not differ between WT and $IDO^{-/-}$ mice.

4.2.4 Cell-autonomous effector mechanisms in murine toxoplasmosis: mIDO1 can inhibit parasite growth

Upon infection with *T. gondii* potent cell-autonomous effector mechanism like miNOS are induced (Figure 12 & Figure 14). Interacting and interfering properties of iNOS and IDO have been reported before [Alberati-Giani *et al.* 1997; Däubener *et al.* 1999] and have also been demonstrated in hRPE cells in this thesis (section 4.1; Figure 7 & Figure 8). Thus, the role of miNOS in $IDO^{-/-}$ mice was further examined.

Therefore, an immunoblot analysis of lung tissue from WT and $IDO^{-/-}$ mice was performed. In this experiment, cytokine (IFN-γ, IL-1β, TNF-α) stimulated RAW 264.7 cells (murine macrophage cell line) served as a positive control. A band at the expected height of miNOS (130 kDa) was present at nine dpi in lung tissue of WT mice, but already on seven dpi in lungs of $IDO^{-/-}$ mice (Figure 17A). As an internal control, mβ-actin protein expression was included in the analysis and was detected in all samples.

In addition, NOS activity in murine cells from infected mice was analyzed using another approach. Therefore, splenocytes from infected WT and $IDO^{-/-}$ mice were isolated at seven dpi. NOS activity of primary isolated splenocytes was measured in the supernatant after 72 h of *ex vivo* cultivation. The mean nitrite concentration in splenocyte cultures was 76.1 % higher in $IDO^{-/-}$ splenocyte cultures (8.1 µM) than in WT splenocyte cultures (4.6 µM) (Figure 17B).

Next, *ex vivo* NOS activity and concomitant proliferation of *T. gondii* in cells isolated from lungs and peritoneal cavities of *T. gondii* infected mice was analyzed to elucidate the impact of the missing mIDO1 on NOS activity and parasite proliferation (Figure 18).

NOS activity was over all high in lung cell cultures; however, lung cells from IDO$^{-/-}$ mice produced significantly more nitrite (mean nitrite concentration of 68.8 µM) than lung cells from WT mice (mean nitrite concentration of 60.5 µM; Figure 18A, left side). Parasite proliferation was not detectable in cultures from both genotypes (Figure 18A, right side).

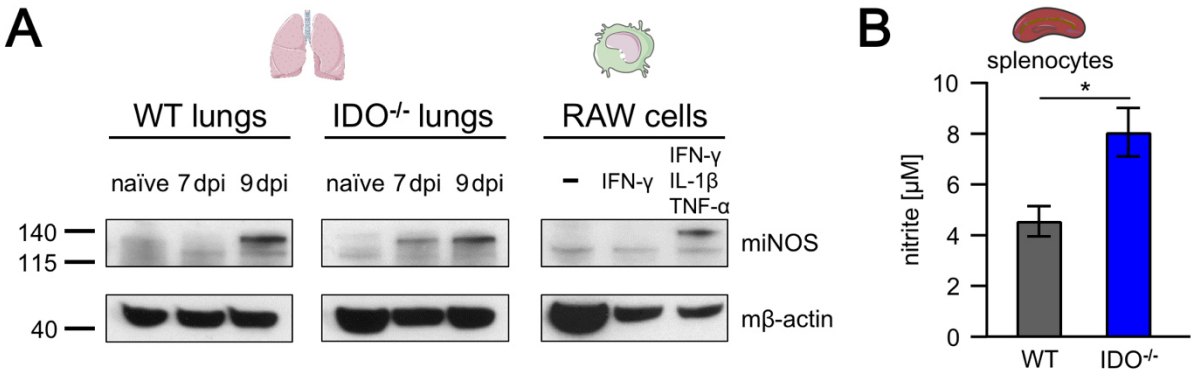

Figure 17: Increased miNOS activity in IDO$^{-/-}$ splenocytes.
A, Immunoblot analysis shows protein expression of murine inducible nitric oxide synthase (miNOS) and murine beta-actin (mβ-actin) in lung tissue of naïve and *Toxoplasma gondii* (*T. gondii;* ME49 strain) infected mice. Wild type (WT) and indoleamine 2,3-dioxygenase 1 deficient (IDO$^{-/-}$) mice were sacrificed on day seven and nine post infection. RAW 264.7 cells remained unstimulated (-) or were stimulated with the proinflammatory cytokines IFN-γ, IL-1β and TNF-α (as indicated; each 100 U/mL) as negative and positive controls respectively. Protein samples (20 µL/lane) and protein marker were run on a 10 % Bis-Tris gel. Protein marker bands are indicated with a line and the band size in kilo dalton (kDa) on the left side of each blot. **B**, miNOS activity of *ex vivo* splenocytes cultured in medium without additional stimulation for 72 hours. Splenocytes were isolated from *T. gondii* infected WT (n = 8) and IDO$^{-/-}$ (n = 10) mice on day 7 post infection. NOS activity was measured indirectly with the Griess reaction by detection of nitrite in the supernatant. Data were represented as means ± SEM of triplicate measurements. *p ≤ 0.05 indicates a significant difference determined with the Students *t*-test (unpaired, two-tailed). (dpi - days post infection; IFN-γ - interferon-gamma; IL-1β - interleukin-1beta; TNF-α - tumor necrosis factor-alpha). This figure contains data from [Ufermann *et al.* 2019], which is published under the liberal Creative Commons Attribution 4.0 International (CC BY 4.0) license.

Inhibition of NOS with *N*^{G}MMA resulted in a significant drop in the nitrite concentration to 14.5 µM and 12.4 µM in lung cell cultures from WT and IDO$^{-/-}$ mice (Figure 18A, left side). Concomitantly, parasite proliferation increased in lung cell cultures of both genotypes; however, parasite proliferation was significantly higher in lung cells from IDO$^{-/-}$ mice (mean proliferation WT: 70 cpm to 1007 cpm | IDO$^{-/-}$: 137 cpm to 2348 cpm; Figure 18A, right side).

A similar phenotype was observed in peritoneal exudate cells (PECs) that were isolated from *T. gondii* infected mice Figure 18B). NOS activity was higher in PEC cultures from

IDO$^{-/-}$ mice (mean nitrite concentration WT: 8.5 µM versus IDO$^{-/-}$: 17.1 µM) and could be inhibited with *N*^{G}MMA (WT: 1.4 µM | IDO$^{-/-}$: 2.3 µM; Figure 18B, left side). Parasite proliferation was again more prominent in cell cultures of IDO$^{-/-}$ mice when NOS was inhibited (mean proliferation WT: 1104 cpm to 1501 cpm | IDO$^{-/-}$: 351 cpm to 2151 cpm; Figure 18B, right side).

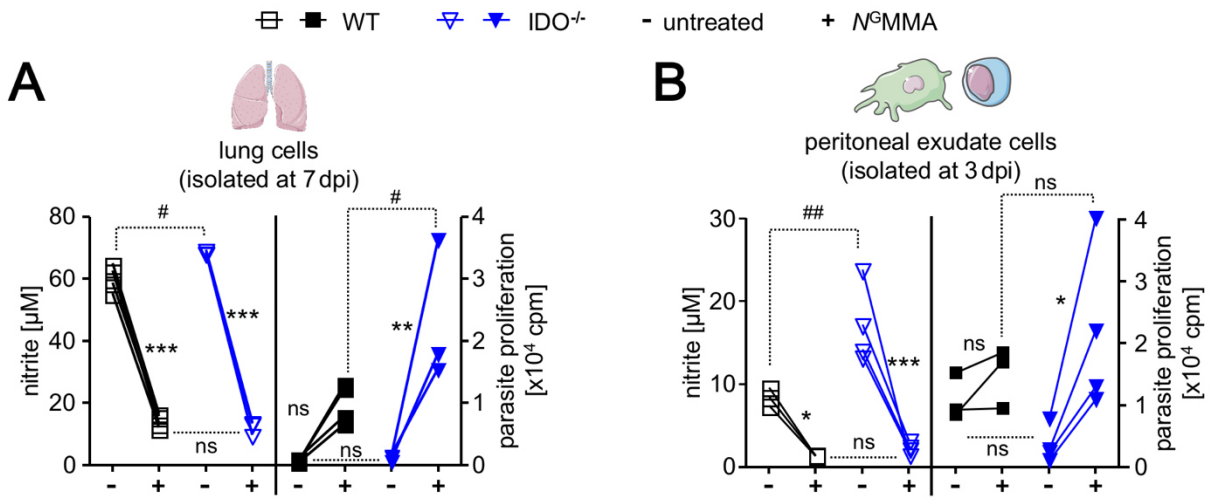

Figure 18: Increased parasite proliferation upon inhibition of NOS activity in peritoneal exudate and lung cells isolated from infected mice.

NOS activity and concomitant parasite proliferation in (**A**) lung cells (lungs collected 7 dpi: WT n = 4 | IDO$^{-/-}$ n = 3) and (**B**) peritoneal exudate cells (PECs collected 3 dpi: WT n = 3 | IDO$^{-/-}$ n = 4) isolated from *Toxoplasma gondii* (*T. gondii;* ME49 strain) infected mice. Wild type (WT) and indoleamine 2,3-dioxygenase 1 deficient (IDO$^{-/-}$) mice were sacrificed at 7 dpi (**A**) and 3 dpi (**B**). *Ex vivo* cell cultures remained untreated (-) or were supplemented with the NOS inhibitor *N*^{G}-monomethyl-L-arginine (*N*^{G}MMA, 100 µg/mL) (+). NOS activity was measured indirectly with the Griess reaction by detection of nitrite in the supernatant. Proliferation of *T. gondii* tachyzoites was determined with the ^{3}H-uracil incorporation assay. Each symbol represents the mean value of duplicate measurements from cells isolated from one animal. The mean values of untreated and *N*^{G}MMA supplemented cultures from one specimen were connected with a solid line. Data were analyzed using a one-way ANOVA corrected for multiple comparison by the Tukey´s post hoc test. $^{\#}p \leq 0.05$; $^{\#\#}p \leq 0.01$ indicate significant differences between genotypes at the same treatment. $^{*}p \leq 0.05$; $^{**}p \leq 0.01$; $^{***}p \leq 0.001$ indicate significant differences between treatments of the same genotype. (cpm - counts per minute; dpi - days post infection; ns - not significant).

These experiments show that mIDO1 indeed can inhibit *T. gondii* growth; however, other cell-autonomous effector mechanisms – as miNOS – are more intensely active than mIDO1.

Further, murine BMDMs were differentiated from bone marrow isolated from WT as well as mIDO1 and mIDO2 double knock out (mIDO1/2-KO) mice to have a glimpse on the control of parasite proliferation in murine BMDMs. BMDMs were activated by

stimulation with different concentrations of mIFN-γ (Figure 19). Parasites proliferated in unstimulated BMDMs from both genotypes comparably good (mean parasite proliferation in BMDMs from WT: 6.6×10^4; mIDO1/2-KO: 7.7×10^4). mIFN-γ stimulation resulted in a dose dependent decrease in parasite proliferation in BMDM cultures from both genotypes (Figure 19), indicating that murine BMDMs inhibit *T. gondii* growth in an IDO1/2 independent manner.

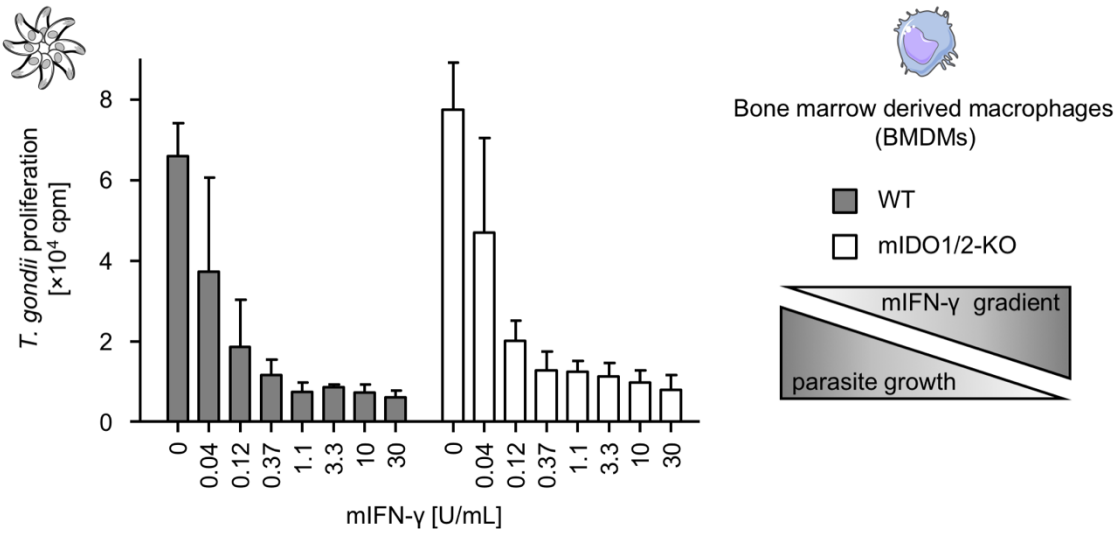

Figure 19: Comparable *T. gondii* proliferation in WT and IDO1/2-KO BMDMs *ex vivo*.

Parasite proliferation in stimulated bone marrow derived macrophages (BMDMs) differentiated from BM from wild type (WT, n = 2) and indoleamine 2,3-dioxygenase 1 and 2 knock out (mIDO1/2-KO, n = 2) mice. BMDM cultures were stimulated with a murine interferon-gamma (mIFN-γ) gradient as indicated. BMDMs were infected with 10^5 *Toxoplasma gondii* (*T. gondii*; ME49 strain) tachyzoites 24 hours post stimulation. Parasite proliferation was determined with the ^{3}H-uracil incorporation assay. Data were represented as mean values and SD of triplicate measurements of one experiment. Data was analyzed using a one-way ANOVA corrected for multiple comparison by the Tukey´s post hoc test. Parasite proliferation is not significantly different in mIDO1/2-KO BMDMs compared to WT BMDMs. (cpm -counts per minute).

In conclusion, mIDO1 is induced and active during murine toxoplasmosis in an organ, tissue and cell type specific manner. Neither other tryptophan degrading enzymes, nor other cell-autonomous effector mechanisms are excessively increased in order to compensate the lack of mIDO1 in IDO$^{-/-}$ mice. In an experimental setup miNOS was slightly, but significantly more active in cultures with cells of IDO$^{-/-}$ mice. Inhibition of miNOS resulted in a stronger parasite growth in cells of IDO$^{-/-}$ mice compared to WT mice, indicating that here – under the chosen experimental conditions – mIDO1 is capable to limit parasite growth as well. However, the parasite load – independent of organ and time post infection – was not different between WT and IDO$^{-/-}$ mice.

4.3 Immunosuppressive role of mIDO1 in mice

Concomitant with an acute toxoplasmosis lymphocyte proliferation response to *ex vivo* mitogen stimulation is drastically impaired [Chan *et al.* 1986]. There could be different mechanisms involved, including activated Tregs with their immunosuppressive potential to reduce immunopathology during the infection [Schmidt *et al.* 2012]. This is of special interest, since DCs can confer suppressive functions of Tregs in an IDO-dependent manner [Fallarino *et al.* 2003; Lippens *et al.* 2016]. Therefore, the proliferative responses of T cells isolated from *T. gondii* infected WT and IDO$^{-/-}$ mice were analyzed *ex vivo*.

4.3.1 Hyporesponsiveness of T cells during toxoplasmosis

Initial lymphocyte proliferation experiments were performed to test the suitability for the experimental *in vivo* infection model. This included different variables such as the time point post infection, the parasite stage and the route of infection (Figure 20).

First, the lymphocyte responsiveness to stimulation with the T cell mitogen ConA was tested in a time dependent manner (Figure 20A). Therefore, splenocytes from naïve and *T. gondii* tachyzoite infected WT mice were isolated at three-, seven- and ten-dpi. Proliferation was determined by measurement of incorporated ^{3}H-thymidine. *Ex vivo* ConA stimulation of cells from naïve mice resulted in a strong lymphocyte proliferation (mean proliferation: 7.6×10^{4} cpm). The responsiveness of splenocytes was clearly affected by the different time points. The proliferation response was slightly reduced at three dpi (mean proliferation: 5×10^{4} cpm) but was highly impaired at seven dpi (mean proliferation: 0.6×10^{4} cpm) and 10 dpi (mean proliferation: 0.08×10^{4} cpm; Figure 20A). Impaired T cell responsiveness can be caused by several factors. This includes lack of the cytokine IL-2 that is required for T cell proliferation [Gills and Smith 1977; Bachmann and Oxenius 2007], but also activity of miNOS [Albina *et al.* 1991; van der Veen 2001]. Supplementation of the ConA stimulated splenocyte cultures with additional IL-2 and the NOS inhibitor N^{G}MMA had no effect on cells from mice at 10 dpi. However, it resulted in a strong increase (approximately 900 %) in proliferation at seven dpi (mean proliferation: 5.4×10^{5} cpm; Figure 20A).

Second, WT mice were infected with different *T. gondii* stages via different routes. This included on the one hand the injection of tachyzoites, the rapid proliferating stage, present during the acute phase of infection and on the other hand the injection of bradyzoites, the persisting stage, enclosed in cysts during the chronic phase of

infection, into the peritoneum. To mimic the natural route of infection intact cysts were administered orally. Furthermore, lysed *T. gondii* tachyzoites (TLA) were injected into the peritoneum (Figure 20B). Mitogen stimulated T cell proliferation was analyzed at seven dpi, since the phenotype of interest was most prominent at this time point (Figure 20A). Illustrated lymphocyte proliferations are relative to the positive control (proliferation of lymphocytes from naïve mice). Lymphocytes from ip infected mice with

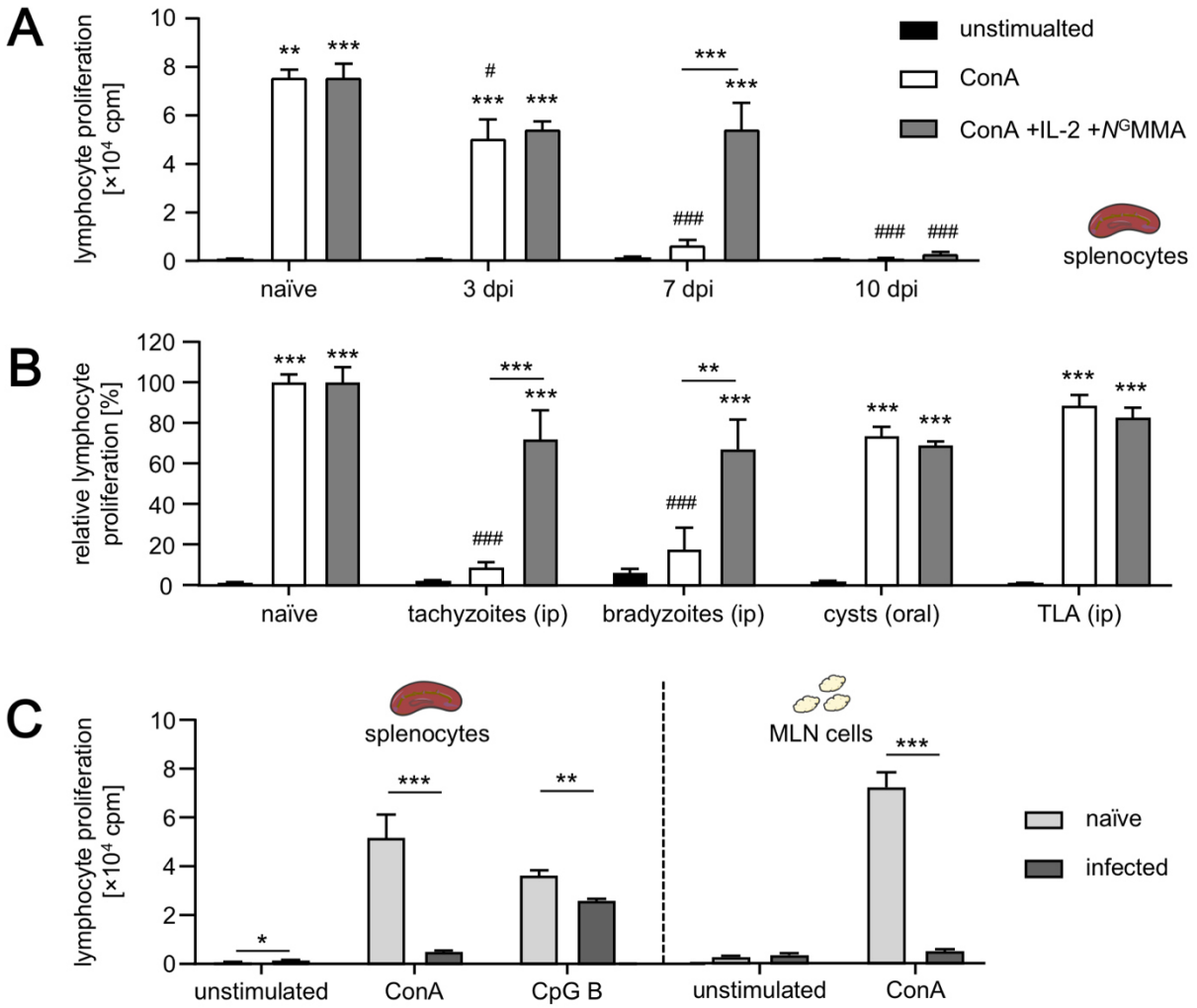

Figure 20: Impaired mitogen induced lymphocyte proliferation during *T. gondii* infection.

Lymphocyte proliferation of *ex vivo* mitogen stimulated (**A, B, C**) spleen and (**C**) mesenteric lymph node (MLN) cell cultures. **A**, Spleens were collected from naïve (n = 3) or *Toxoplasma gondii* (*T. gondii*; ME49 strain) infected wild type (WT) mice at three, seven and ten days post infection (dpi; each time point: n = 3). **B**, Spleens were collected from naïve (n = 3) or *T. gondii* tachyzoite (intraperitoneal (ip) dose: 10^5 tachyzoites; n = 3), bradyzoite (ip dose: 20 lysed cysts; n = 3) or cyst (oral dose: 20 cysts; n = 4) infected or *T. gondii* lysate antigen (TLA; ip dose equivalent to 10^5 tachyzoites; n = 3) injected WT mice at day seven post infection. **C**, Spleens and MLNs were collected from naïve (n = 7-9) and *T. gondii* infected (n = 7-9) WT mice at day seven post infection. Cell cultures remained unstimulated or were supplemented with the nitric oxide synthase inhibitor N^G-monomethyl-L-arginine (N^GMMA, 100 µg/mL) and interleukin-2 (IL-2, 5 ng/mL) as indicated. **A** & **B** & **C**, T cell and (**C**) B cell proliferation was stimulated *ex vivo* with concanavalin A (ConA; 1 µg/mL) and class B CpG

oligonucleotide ODN1826 (CpG B; 0.1 µM) respectively for 72 hours. Lymphocyte proliferation was determined using the ^{3}H-thymidine incorporation assay. Data were represented as mean values and SEM of triplicate measurements in (**A**, **C**) counts per minute (cpm) or (**B**) relative to the proliferation response of ConA stimulated cells from naïve mice. The data in **A** and **B** were analyzed using a two-way ANOVA corrected for multiple comparison by the Tukey´s post hoc test. $^{\#}p \leq 0.05$, $^{\#\#\#}p \leq 0.001$ indicate significant differences between equally treated cells from naïve and infected mice. $*p \leq 0.05$, $***p \leq 0.001$ indicate significant differences between treatments within the same group. The Student's t-test (unpaired, two-tailed) was used to analyze the data in **C**. $*p \leq 0.05 **p \leq 0.01$, $***p \leq 0.001$ indicate significant differences between equally stimulated cells from naïve and infected mice. This figure contains data from [Ufermann *et al.* 2019], which is published under the liberal Creative Commons Attribution 4.0 International (CC BY 4.0) license.

bradyzoites showed the same phenotype as lymphocytes from ip infected mice using tachyzoites. In detail, a weak proliferation response to ConA stimulation alone (tachyzoite (ip): 8.5 %; bradyzoite (ip): 17.6 %) was strongly increased by additional supplementation of IL-2 and N^{G}MMA (tachyzoite (ip): 71.7 %; bradyzoite (ip): 67 %). Lymphocytes isolated from orally infected mice with cysts responded properly (mean proliferation: 73.5 %) to ConA stimulation on seven dpi. Oral cyst administration and ip injection of TLA had no significant effect on lymphocyte responsiveness (mean proliferation: 73.4 % and 88.6 % respectively; Figure 20B).

Third, the responsiveness of splenic B cells and T cells, as well as of T cells from mesenteric lymph nodes (MLN) were analyzed to investigate if other lymphocytes subsets are also affected by the infection and if the T cell hyporesponsiveness is spleen specific (Figure 20C). B cell proliferation was stimulated with the TLR9 agonist class B CpG ODN1826 (CpG B). Splenocytes isolated from infected mice at seven dpi showed reduced proliferation to ConA (T cell mitogen) and CpG B (B cell mitogen) stimulation compared to splenocytes from naïve mice. In detail, ConA induced T cell proliferation was reduced by 90 % in cell cultures of infected mice (naïve: 5.1×10^{4} cpm versus infected: 0.5×10^{4} cpm). CPG B induced B cell proliferation was only reduced by 28 % in cell cultures of infected mice (naïve: 3.6×10^{4} cpm versus infected: 2.6×10^{4} cpm). T cell proliferation in MLN cell cultures from infected mice was even more reduced compared to splenocyte cultures. In detail, the mean T cell proliferation in MLN cell cultures was reduced to 7 % of naïve cultures (naïve: 7.2×10^{4} cpm | infected: 0.5×10^{4} cpm; Figure 20C).

These results concerning reduced T cell responses during acute toxoplasmosis are in line with previously published data [Haque *et al.* 1994]. The time point post infection

as well as the infection route critically affect splenic T cell responsiveness. This phenotype is not unique to splenic T cells since MLN T cells showed severe hyporesponsiveness, but also mitogen stimulated B cell responsiveness affected during *T. gondii* infection.

In sum, the results of these analyses indicate that the chosen experimental infection model serves as a suitable system to analyze T cell responsiveness. Hence, this experimental infection model was used to elucidate the contribution of mIDO1 to the hyporesponsiveness of splenic T cells during acute toxoplasmosis.

4.3.2 miNOS activity and IL-2 deprivation are the key players in murine toxoplasmosis associated T cell hyporesponsiveness

Splenocytes from naïve and *T. gondii* infected WT and IDO$^{-/-}$ mice were collected at seven dpi and stimulated with the mitogen ConA to induce lymphocyte proliferation. Splenic T cells from naïve mice proliferated comparably to ConA stimulation (Figure 21A). In detail, the proliferation of mitogen stimulated splenic T cells from both naïve genotypes was comparable (mean proliferation, WT: 5.1×10^4 cpm; IDO$^{-/-}$: 6.1×10^4 cpm). Splenic T cells from *T. gondii* infected mice showed strongly reduced (WT: 90 %; IDO$^{-/-}$: 92 %) proliferation responses to mitogen stimulation. IL-2 supplementation to ConA stimulated T cells did not increased proliferation (Figure 21A). Unstimulated splenocyte cultures from infected IDO$^{-/-}$ mice exhibited a stronger NOS activity then cultures from WT mice (Figure 21B), which was already illustrated in Figure 17B. miNOS has been described to impair T cell proliferation [Patton *et al.* 2002]. Thus, mitogen stimulated splenocyte cultures of both genotypes were supplemented with N^GMMA to inhibit miNOS. miNOS activity was determined by measurement of nitrite in the culture supernatant (Figure 21B). The nitrite content dropped by 76 % in cultures of both genotypes (WT: from 5.9 µM to 1.4 µM | IDO$^{-/-}$: from 9 µM to 2.2 µM) due to N^GMMA mediated NOS inhibition. Consequently, inhibition of NOS elevated mitogen induced T cell proliferation responses in cultures of both genotypes (mean proliferation, WT: 1.5×10^4 cpm; IDO$^{-/-}$: 1.8×10^4 cpm) significantly (Figure 21A). Combination of ConA stimulation with IL-2 supplementation and NOS inhibition further increased T cell proliferation to 3.1×10^4 cpm and 3.8×10^4 cpm in WT (60 % of naïve cultures) and IDO$^{-/-}$ (62 % of naïve cultures) cultures, respectively. However, the differences in proliferation responses of T cells from WT and IDO$^{-/-}$ mice remained not significant and below the level of cultures from naïve mice (Figure 21A).

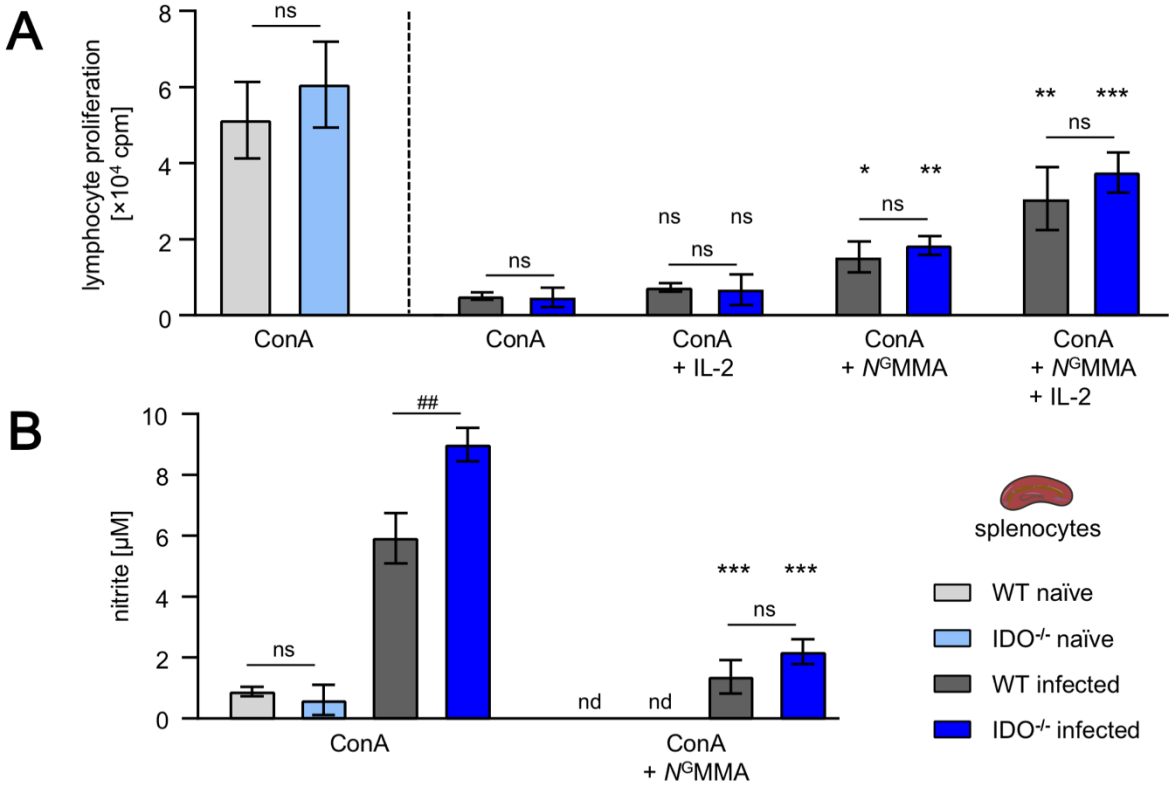

Figure 21: Splenic T cell responsiveness is affected by IL-2 availability and NOS activity and is independent of mIDO1.

A, Lymphocyte proliferation and **B,** nitric oxide synthase (NOS) activity of *ex vivo* mitogen stimulated splenocyte cultures. Spleens were collected from naïve wild type (WT, n = 7) and indoleamine 2,3-dioxygenase 1 deficient ($IDO^{-/-}$, n = 5) mice or *Toxoplasma gondii* (*T. gondii*; ME49 strain) infected WT (n = 8) and $IDO^{-/-}$ (n = 10) mice at day seven post infection. Splenic T cell proliferation was stimulated *ex vivo* with concanavalin A (ConA; 1 µg/mL). Cell cultures were supplemented with interleukin-2 (IL-2, 5 ng/mL) and the NOS inhibitor N^G-monomethyl-L-arginine (N^GMMA, 100 µg/mL) as indicated. **A**, Lymphocyte proliferation was determined using the ^{3}H-thymidine incorporation assay. **B**, NOS activity was measured indirectly with the Griess reaction by detection of nitrite in the supernatant. Data were represented as mean ± SEM values of triplicate measurements. Data were analyzed using a one-way ANOVA corrected for multiple comparison by the Tukey´s post hoc test. $^{\#\#}p \leq 0.01$ indicate significant differences between equally stimulated cells from different genotypes. $^*p \leq 0.05$; $^{**}p \leq 0.01$; $^{***}p \leq 0.001$ indicate significant differences to ConA stimulated cultures from infected mice of the same genotype. (cpm - counts per minute; ns - not significant, nd - not detected). This figure is modified from [Ufermann *et al.* 2019], which is published under the liberal Creative Commons Attribution 4.0 International (CC BY 4.0) license.

In sum, hyporesponsiveness of T cells was not different in cultures from $IDO^{-/-}$ mice and could be attenuated by IL-2 supplementation and inhibition of NOS. Thus, IL-2 deprivation and NOS activity significantly contribute to the hyporesponsiveness of T cells observed during acute murine toxoplasmosis, whereas mIDO1 does not.

In a different approach mitogen stimulation experiments of co-cultures composed of cells from naïve and infected WT mice were performed (Figure 22A).

Here, unprimed and primed cells (from naïve and infected WT mice respectively) were either stimulated alone (each 1.5×10^5 cells) or in co-cultures (1.5×10^5 unprimed and 1.5×10^5 primed cells). As expected, unprimed splenocytes proliferated (mean proliferation: 2.8×10^4 cpm), whereas the primed cells poorly proliferated (mean proliferation: 0.4×10^4 cpm). Interestingly, proliferation of mitogen stimulated co-cultures was comparable to unprimed cells (mean proliferation: 3.2×10^4 cpm; Figure 22A).

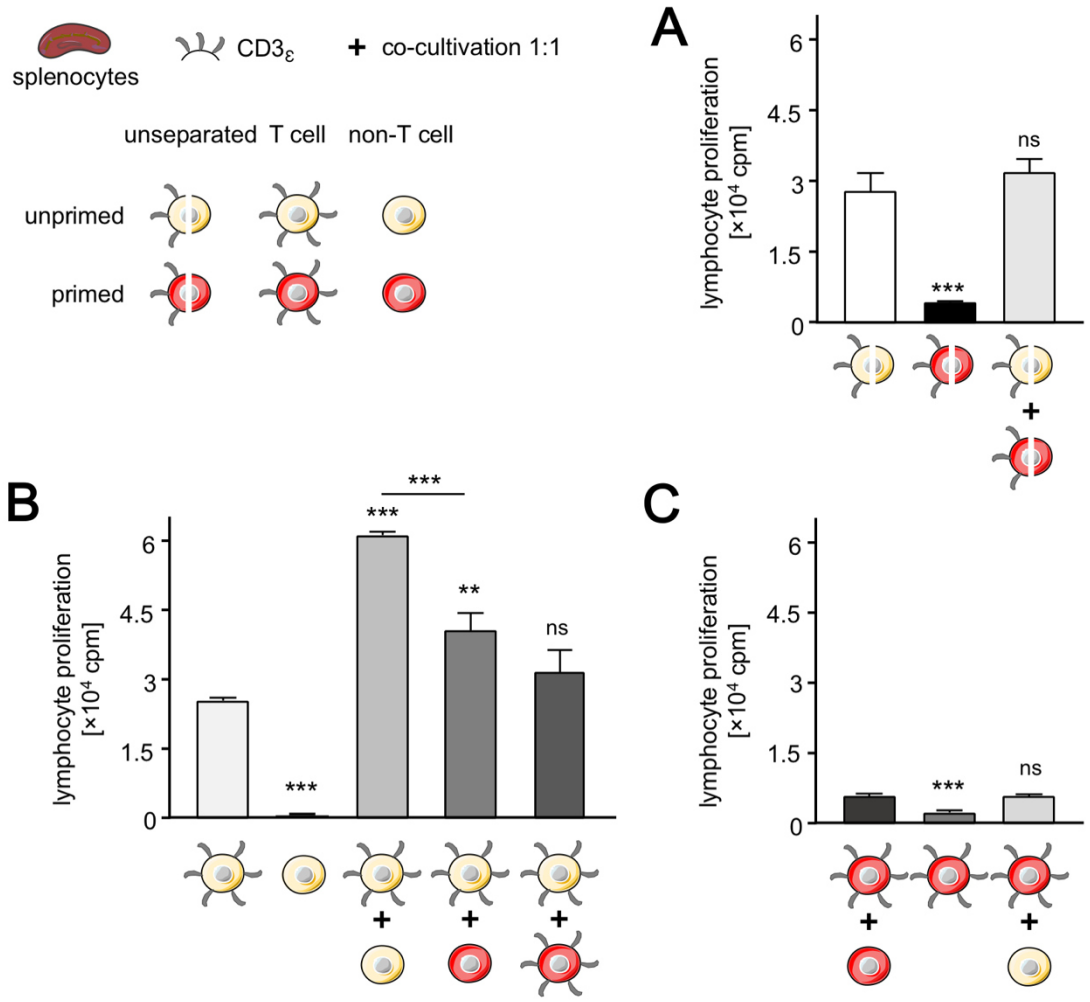

Figure 22: Unaltered proliferation of WT unprimed T cells in co-cultivation experiments with primed T cells.

Mitogen induced lymphocyte proliferation in splenocyte cultures from naïve (unprimed) and *Toxoplasma gondii* (*T. gondii*; ME49 strain) infected (primed) wild type (WT) mice. Spleens were collected from naïve (unprimed, n = 6) and *T. gondii* infected (primed, n = 6) mice at day seven post infection. Splenic T cell proliferation was stimulated *ex vivo* with the mitogen concanavalin A (1 µg/mL). Lymphocyte proliferation was determined with the ^{3}H-thymidine incorporation assay. **A**, Unprimed (1.5×10^5 cells) and primed (1.5×10^5 cells) splenocytes (unseparated) were stimulated alone or in co-cultures for 72 hours. **B** & **C**, $CD3_\varepsilon$ antibodies

and the MACS® technology were used to separate splenic T cells ($CD3_\varepsilon$ positive) and non-T cells ($CD3_\varepsilon$ negative) for additional co-cultivation experiments. **B**, Unprimed splenocytes were separated and stimulated alone (T cells and non-T cells, 1.5×10^5 cells each) or in co-cultures with different separated unprimed and primed cells (1.5×10^5 cells per group). **C**, Primed splenocytes were separated and stimulated alone (1.5×10^5 T cells) or in co-cultures with unprimed and primed non-T cells (1.5×10^5 cells per group). Data were represented as mean values ± SEM of triplicate measurements of two independent experiments. Data were analyzed using a one-way ANOVA corrected for multiple comparison by the Tukey´s post hoc test. **p ≤ 0.01; ***p ≤ 0.001 indicate significant differences based on comparison with the first dataset in each graph unless otherwise indicated. (cpm - counts per minute; MACS® - magnetic-activated cell sorting; ns - not significant).

Next, spleen cell populations were separated based on the presence of CD3ε on their surface. This resulted in a CD3ε enriched population – from here on referred to as T cells – and a CD3ε negative, thus T cell depleted, population – from here on referred to as non-T cells – that were used for the following mitogen induced proliferation experiments (Figure 22B & C). Mitogen stimulation with ConA – induced proliferation of unprimed T cells (mean proliferation: 2.5×10^4 cpm), whereas non-T cells did not proliferate (mean proliferation: 0.05×10^4 cpm; Figure 22B). Bystander help of accessory cells from unprimed non-T cells in co-cultures with unprimed T cells resulted in a 240 % increase of the lymphocyte proliferation (mean proliferation: 6.1×10^4 cpm) compared to stimulation of unprimed T cells alone (Figure 22B).

Unprimed non-T cells were then exchanged with primed non-T cells to elucidate if the bystander help of accessory cells from the primed non-T cell population is affected by the infection. This resulted in a significantly lower lymphocyte proliferation (mean proliferation: 4.1×10^4 cpm). Even though the capacity of the primed non-T cells to support efficient T cell proliferation was reduced the lymphocyte proliferation was still 60 % stronger compared to unprimed T cell cultures alone. This indicates that the bystander help of accessory cells in the primed non-T cell population was negatively affected by the infection.

Next, co-cultivation of primed and unprimed T cells was performed to check if T cells from naïve and infected mice would affect the proliferation of one another. Proliferation of stimulated co-cultures of unprimed and primed T cells (mean proliferation: 3.2×10^4 cpm) was comparable to unprimed T cell alone (Figure 22B). Primed T cells alone performed worse (mean proliferation: 0.2×10^4 cpm) than co-cultures of primed T cells and primed non-T cells (mean proliferation: 0.6×10^4 cpm; Figure 22C). Exchange of the primed non-T cells with unprimed non-T cells slightly elevated the proliferation response to the level of co-cultures of primed T cells and primed non-

T cells (Figure 22C), which indicates that the bystander help of accessory cells from unprimed non-T cells was not sufficient to enable a proper T cell proliferation response.

In sum, primed T cells did not respond properly to the mitogen stimulation and require IL-2 supplementation and NOS inhibition for improved proliferation. Bystander help of unprimed non-T cells is required for an efficient proliferation response of unprimed T cells; however, unprimed non-T cells only marginally improved the performance of the primed T cells. Primed non-T cells are not as efficient in bystander help as unprimed non-T cells are. Interestingly, primed T cells had no obvious adverse effect on proliferation of unprimed T cells. This data shows that not only T cells, but also non-T cells are negatively affected by a *T. gondii* infection.

4.3.3 During acute murine toxoplasmosis regulatory T cells express markers associated with a suppressive phenotype

T cells essentially contribute to the control of toxoplasmosis. Upon activation antigen-specific $CD4^+$ T cells (T helper cells) commit to the Th1 phenotype what is key for the efficient adaptive immune response. Activated antigen-specific $CD8^+$ T cells (cytotoxic T cells) contribute to killing infected cells. Furthermore, these activated T cells next to innate immune cells (e.g. NK cells and neutrophils) produce host-protective IFN-γ required to battle the *T. gondii* infection. Limiting an overwhelming proinflammatory response and thus reducing immune pathology is mediated by regulatory T cells (Tregs: $CD4^+$ $CD25^+$ $FOXP3^+$ T cells). Hence, a detailed examination of splenic T cell populations from naïve and *T. gondii* infected WT and $IDO^{-/-}$ mice was performed using flowcytometry analyses.

Splenic T helper cells ($CD4^+$ T cells) (Figure 23A-C) and cytotoxic T cells ($CD8^+$ T cells) were analyzed first (Figure 23D & E). The gating strategy is illustrated in the appendix (Appendix B, p. 120). The overall amount of naïve splenic $CD4^+$ T cells is not different between WT (2.1×10^7 $CD4^+$ T cells) and $IDO^{-/-}$ (2.2×10^7 $CD4^+$ T cells) mice (Figure 23A). During infection the overall number of $CD4^+$ T cells slightly dropped to 1.5×10^7 $CD4^+$ T cells and 1.6×10^7 $CD4^+$ T cells for WT and $IDO^{-/-}$ mice, respectively. Expression of activation and proliferation markers like the receptor for IL-2 (IL-2R, CD25) and Ki-67 on $CD4^+$ T cells significantly increased seven dpi compared to naïve mice (Figure 23B). In detail, the percentage of IL-2R positive T helper cells increased

from 5.7 % to 15.3 % in the WT and from 6.3 % to 15.2 % in IDO$^{-/-}$ mice. Ki-67 positive T helper cells increased from 3.5 % to 18.5 % in the WT and from 4.9 % to 13.7 % in IDO$^{-/-}$ mice. Neither the percentage of IL-2R-positive nor Ki-67-positive T helper cells were significantly different between WT and IDO$^{-/-}$ mice. Furthermore, activated effector (CD62L^{-} CD25^{+} CD279^{+} CD152^{+}) T helper cells from infected mice exhibited an increased mean fluorescent intensity (MFI) of CTLA4 (CD152) on the cell surface compared to naïve mice (Figure 23C).

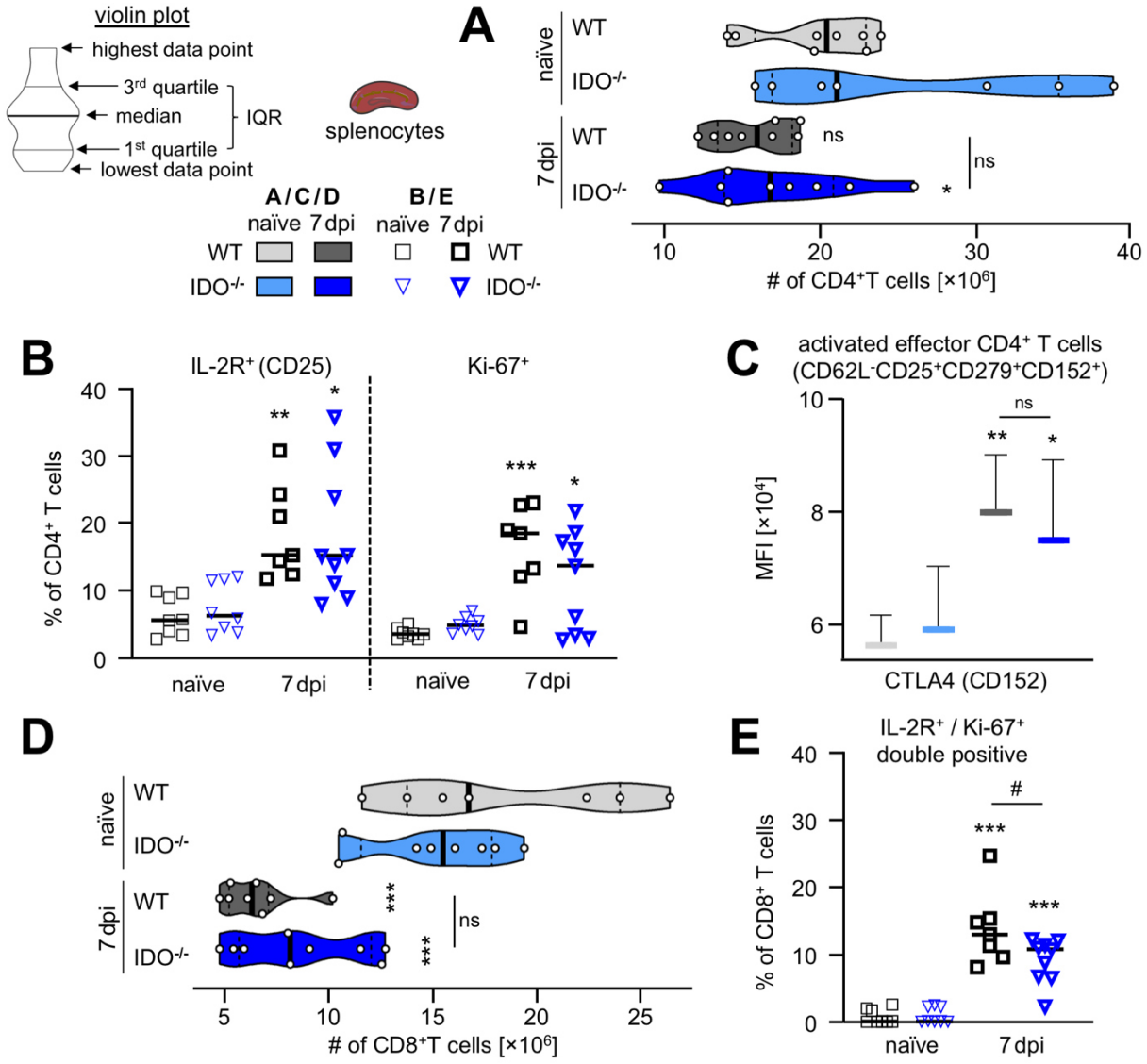

Figure 23: Elevated T cell activation and effector markers in *T. gondii* infected mice.

Flow cytometry analysis of splenic (**A**, **B**, **C**) T helper cells (CD4^{+} T cells) and (**D**, **E**) cytotoxic T cells (CD8^{+} T cells) isolated from naïve and *Toxoplasma gondii* (*T. gondii*; ME49 strain) infected wild type (WT, naïve n = 8 | 7 dpi n = 8) and indoleamine 2,3-dioxygenase 1 deficient (IDO$^{-/-}$, naïve n = 7 | 7 dpi n = 9) mice. Absolute splenic (**A**) CD4^{+} and (**D**) CD8^{+} T cell numbers are compared between genotypes and infection status and are illustrated via violin plots. Frequencies of (**B**) CD4^{+} T cells expressing the activation markers interleukin-2 receptor (IL-2R) or Ki-67 and frequencies of (**E**) CD8^{+} T cells double positive for IL-2R and Ki-67 are shown as scattered dot plots (each dot represents a sample from one mouse) and the median.

C, The mean fluorescence intensity (MFI) of cytotoxic T-lymphocyte-associated protein 4 (CTLA4) on activated effector T helper cells is shown as median values ± SEM. Data are pooled from three independent experiments and were analyzed using a one-way ANOVA corrected for multiple comparison by the Tukey´s post hoc test. $^{\#}p \leq 0.05$ indicate significant differences between equally treated genotypes. $^{*}p \leq 0.05$; $^{**}p \leq 0.01$; $^{***}p \leq 0.001$ indicate significant differences caused by infection within the same genotype. (ns - not significant; dpi - days post infection).

Prior to infection with *T. gondii*, cytotoxic T cells were highly abundant in spleens of WT (mean $CD8^+$ T cells: 1.7×10^7) and $IDO^{-/-}$ (mean $CD8^+$ T cells: 1.6×10^7) mice (Figure 23D). The overall number of splenic cytotoxic T cells had dropped by 65 % (mean $CD8^+$ T cells: 0.6×10^7) in WT and by 50 % (mean $CD8^+$ T cells: 0.8×10^7) in $IDO^{-/-}$ mice at seven dpi. However, these cytotoxic T cells showed clear signs of activation (Figure 23E). 13 % of WT and 10.8 % $IDO^{-/-}$ cytotoxic T cells were double positive for IL-2R and Ki-67 at seven dpi, whereas in naïve mice IL-2R and Ki-67 double positive cytotoxic T cells were scarce (WT: 0.2 % | $IDO^{-/-}$: 0.2 %; Figure 23E). There were significantly more cytotoxic T cells positive for IL-2R and Ki-67 in WT mice compared to $IDO^{-/-}$ cytotoxic T cells. This is predominantly due to one specimen that contained 24.6 % IL-2R and Ki-67 double positive cytotoxic T cells.

Splenic Tregs ($CD4^+$ $CD25^+$ $FOXP3^+$ T cells) were analyzed next (Figure 24). The detailed Treg gating strategy is illustrated in the appendix (Appendix C, p. 121). The absolute number of splenic Tregs are comparable between naïve WT and $IDO^{-/-}$ mice (WT: 0.24×10^6 Tregs | $IDO^{-/-}$: 0.45×10^6 Tregs) as well as *T. gondii* infected WT and $IDO^{-/-}$ mice (WT: 0.95×10^6 Tregs | $IDO^{-/-}$: 1×10^6 Tregs) (Figure 24A). The MFI of IL-2R on Tregs was comparable between WT and $IDO^{-/-}$ mice and was not altered by the infection (Figure 24B).

Not only significantly increased frequencies of Tregs expressed activation markers (e.g. CD69, OX40, CTLA4, PD-1), but also the abundance of these activation markers on the cell surface of the activated Tregs – expressed as MFI – was significantly increased at seven dpi (Figure 24C). In detail, the activation marker CD69 was detected on 33 % and 35 % of naïve WT and $IDO^{-/-}$ Tregs, respectively. Significantly more Tregs from $IDO^{-/-}$ mice (53 %) than WT mice (69 %) were positive for CD69 at seven dpi. Concomitant with that increase the MFI of CD69 increased from 1.1×10^3 to 5.9×10^3 on WT and from 1.3×10^3 to 6.6×10^3 $IDO^{-/-}$ Tregs (Figure 24C). The percentage

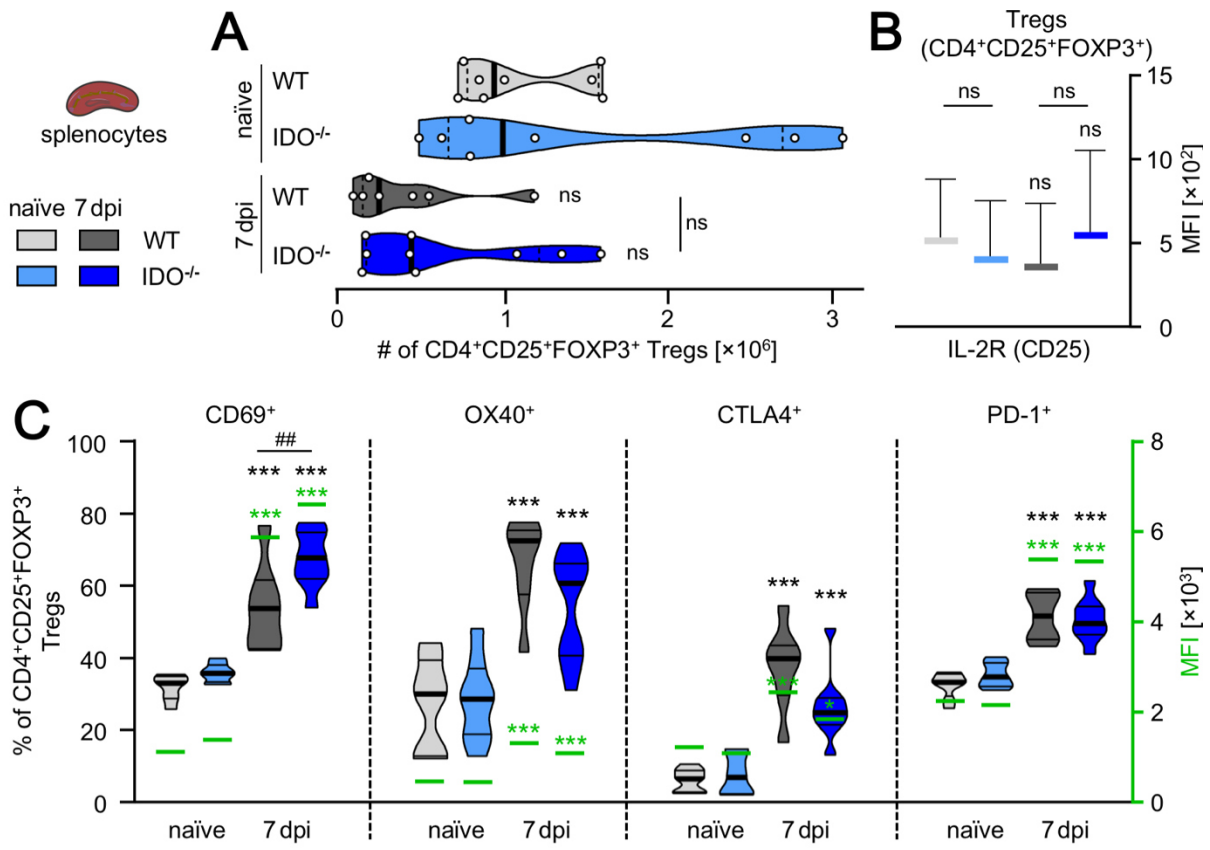

Figure 24: Increased expression of activation markers on regulatory T cells that are associated with a suppressive phenotype.

Flow cytometry analysis of splenic regulatory T cells (Tregs) isolated from naïve and *Toxoplasma gondii* (*T. gondii*; ME49 strain) infected wild type (WT, naïve n = 8 | 7 dpi n = 8) and indoleamine 2,3-dioxygenase 1 deficient (IDO$^{-/-}$, naïve n = 7 | 7 dpi n = 9) mice. **A**, Absolute splenic Treg numbers are compared between genotypes and infection status and are illustrated via violin plots. **B**, The mean fluorescence intensity (MFI) of the interleukin-2 receptor (IL-2R) on Tregs is shown as median ± SEM. **C**, Frequencies of Tregs expressing the activation markers CD69, OX40, cytotoxic T-lymphocyte-associated protein 4 (CTLA4) and programmed cell death protein 1 (PD-1) are depicted via violin plots (left axis) and the respective median MFI of the activation markers are shown as green lines (right axis). Data are pooled from three independent experiments and were analyzed using a one-way ANOVA corrected for multiple comparison by the Tukey´s post hoc test. $^{\#\#}p \leq 0.01$ indicate significant differences between equally treated genotypes. $^{*}p \leq 0.05$; $^{***}p \leq 0.001$ indicate significant differences caused by infection within the same genotype. For reasons of simplicity, differences that are not significant (ns) are not indicated in **C.** (dpi - days post infection).

of OX40 positive Tregs increased from 29 % and 28 % in naïve WT and IDO$^{-/-}$ mice to 72 % and 60 % at day seven post infection. The MFI of OX40 on these Tregs increased slightly (WT: from 0.5×10^3 to 1.3×10^3 | IDO$^{-/-}$: from 0.4×10^3 to 1.1×10^3; Figure 24C). The percentage of CTLA4 positive Tregs was increased almost seven times (6 % to 40 %) in the WT, whereas in IDO$^{-/-}$ mice the percentage of CTLA4 positive Tregs was only increased by four times (6 % to 25 %), however the differences between genotypes were not significant. The MFI of CTLA4 on these Tregs increased as well,

however not as strong in IDO$^{-/-}$ mice (from 1.1×10^3 to 1.8×10^3) compared to WT mice (from 1.2×10^3 to 2.4×10^3; (Figure 24C). Treg frequencies positive for PD-1 were comparable in WT (32 %) and IDO$^{-/-}$ mice (34 %) and further increased up to 51 % and 49 % at seven dpi. The MFI of PD-1 on these Tregs had almost tripled (WT: from 2.2×10^3 to 5.4×10^3 | IDO$^{-/-}$: from 2.1×10^3 to 5.3×10^3) at seven dpi compared to naïve mice (Figure 24C).

In sum, flowcytometric analysis revealed that splenic T cell populations (CD4$^+$, CD8$^+$ and Tregs) from WT and IDO$^{-/-}$ mice are not drastically different. As a response to *T. gondii* infection the analyzed T cell populations showed an activation associated phenotype that has not differed between WT and IDO$^{-/-}$ mice.

5. Discussion and Outlook

The results obtained in this thesis show that IDO1 is a potent antimicrobial effector molecule with immunosuppressive capacity in an *in vitro* model of human ocular toxoplasmosis. IFN-γ induced IDO1 in hRPE cells inhibited *T. gondii* and *S. aureus* growth, and restricted proliferation of activated lymphocytes, which was abrogated in the presence induced iNOS activity.

In an experimental acute murine toxoplasmosis model WT and IDO$^{-/-}$ mice were analyzed. Here, mIDO1 expression was highly induced in WT lung tissue and changes in tryptophan / kynurenine level were observed. However, IDO$^{-/-}$ mice showed no differences in toxoplasmosis associated symptoms, survival, parasite load or T cell activation and proliferation responses compared to WT mice. Furthermore, *ex vivo* analyses of different cells showed that miNOS activity was increased in the absence of mIDO1.

In the upcoming sections the results of the respective *in vitro* and *in vivo* models are discussed. Open questions regarding cell specific IDO1 expression, consequences of tryptophan starvation in the context of toxoplasmosis and a revolutionary *in vitro* model that opens the door for a variety of jet unanswered questions are provided in the outlook.

5.1 IDO1 in humans

5.1.1 Tryptophan degrading enzymes in hRPE cells

Infectious posterior uveitis due to ocular toxoplasmosis poses a risk of irreversible visual impairment [Pleyer *et al.* 2019]. Protection of the interior of the eye from pathogens and the preservation of the eye´s immune privilege is accomplished by the RPE cell monolayer [Detrick and Hooks 2020]. To address the contribution of the antimicrobial and immunosuppressive potential of IDO1, the hRPE cell line APRE19 was used in an *in vitro* model of ocular infections.

The results show that IDO1 was induced in a dose dependent manner following IFN-γ stimulation. Here, IDO1 activity efficiently inhibited *T. gondii* and *S. aureus* growth. Pathogen growth was rescued by inhibition of IDO and/or tryptophan supplementation. These results are in line with a report on cytokine stimulated primary hRPE cells

[Nagineni *et al.* 1996]. In their study, Nagineni and colleagues showed that inhibition of *T. gondii* by IFN-γ activated primary hRPE was dependent on IDO [Nagineni *et al.* 1996].

Liver specific TDO regulates tryptophan homeostasis [Schmike *et al.* 1965; Knox 1966]. Tetracycline induced expression of recombinant TDO in HeLa cells has been shown to be capable to inhibit *T. gondii* and *S. aureus* growth *in vitro* [Schmidt *et al.* 2009]. However, Bando and colleagues showed that native TDO expression in Huh7 cells, a human hepatocellular carcinoma cell line, was not involved in the inhibition of *T. gondii* growth [Bando *et al.* 2018]. Since IDO2 can degrade tryptophan as well [Yeung *et al.* 2015] and data on IDO2 effector function during infection is scarce, analysis of IDO2 in hRPE cells was included in this thesis.

In the ARPE19 cell line used herein, IDO2 was induced by cytokine stimulation and showed a 13-fold increase in relative expression. The contribution of IDO2 to the intense tryptophan degradation documented herein is likely marginal, since its increased relative expression is equivalent to only approximately 0.0013 % of the relative expression of IDO1 in this *in vitro* model. In addition, the substrate affinity of IDO2 is lower than that of IDO1 [Austin *et al.* 2009].

IDO1 and IDO2 have both been reported to be expressed in epididymis, however, in different cells [Ball *et al.* 2007]. Interestingly, Fukunaga *et al.* reported that IDO2 was upregulated in the absence of IDO1 in epididymis [Fukunaga *et al.* 2012]. Hence, IDO2 expression could be increased in hRPE cells in the absence of IDO1. However, that and weather IDO2 expression would contribute to limit pathogen growth in hRPE cells under these conditions remains to be elucidated.

To maintain the immune privilege of the eye, naïve RPE cells have been shown to produce several suppressive molecules like transforming growth factor beta (TGF β) or prostaglandin E2 (PGE2) [Sugita *et al.* 2006; Liversidge *et al.* 1993]. TGF β abrogates T cell activation by inhibition of TCR signaling or by interference with linage specific transcription factors [Chen et al 2003; Neurath et al 2002]. Whereas PGE2 inhibits T cell proliferation by inhibition of IL-2 production, as well as by inhibition of the transferrin receptor [Chouaib *et al.* 1985], consequently reducing the availability of iron [Fatima Macedo *et al.* 2004; Jennifer *et al.* 2020].

In the herein used cell line IFN-γ induced suppression of activated lymphocytes was clearly dependent on IDO1 mediated tryptophan depletion. This adds another

mechanism to RPE cells that potentially contributes to the immune privilege of the eye by preventing proliferation of undesirable T cells (e.g. specific for retinal proteins). Interestingly, supplementation of excess tryptophan and competitive inhibition of IDO1 with 1-L-MT did not fully restore the proliferation capacity of the activated T cells in this coculture system. Indicating, that kynurenine pathway metabolites might affect the proliferation capacity of activated T cells as well. Similar observations have been made in the context of tumor immunology. Here, IDO is hijacked as an immune escape mechanism by tumors leading to local tryptophan starvation and accumulation of kynurenine pathway metabolites that impair T cell functionality [Zamanakou *et al.* 2007]. One example of kynurenine pathway metabolites is kynurenic acid. Rad Pour *et al.* just recently reported that increased production of kynurenic acid by active IDO in melanoma cells contributed to dysfunction of tumor specific effector $CD4^+$ T cells [Rad Pour *et al.* 2019].
Hence, not only tryptophan starvation by, but also accumulation of kynurenine pathway metabolites following IDO activity are potential mechanism that could contribute to the immune privilege of the eye during inflammatory responses.

5.1.2 Regulation of IDO1 by iNOS in hRPE

Tryptophan degradation by human IDO1 contributed to the antimicrobial and immunosuppressive capacity of IFN-γ stimulated hRPE cells, as shown herein. Another potent antimicrobial enzyme, iNOS, has been described to be induced upon cytokine stimulation in primary RPE cells [Goureau *et al*. 1994].
In this thesis, relative expression of iNOS was already detectable on transcript level in the hRPE cell line ARPE19 following IFN-γ activation. However, enzyme activity, as measured by nitrite accumulation in the supernatant, was only measurable by additional stimulation with IL-1β and TNF-α. Here, iNOS drastically affected IDO1 functionality leading to increased growth of *T. gondii* and *S. aureus* as well as proliferation of activated lymphocytes.

Interference of NO, the product of iNOS activity, with IDO has been reported on transcription/translational and protein level before. In murine macrophages, miNOS inhibited mIDO mRNA expression, which was increased by inhibition of miNOS activity [Alberati-Giani *et al.* 1997]. This was not the case in hRPE cells used in this thesis. Here, iNOS activity did not affect IDO1 mRNA, since relative expression of IDO1 was

unaltered in the presence of iNOS activity. In the human cancer cell line RT4 Hucke *et al.* showed that, upon stimulation of iNOS, IDO activity was impaired and was accommodated by a reduced bacteriostatic and parasitostatic phenotype. This phenotype was dependent on NO, which inhibited IDO activity and lead to increased proteasomal degradation of IDO protein [Hucke *et al.* 2004]. Direct binding of NO to the heme prosthetic group of purified recombinant human IDO protein has been shown to inactivate IDOs catalytic activity [Samelson-Jones and Yeh 2006; Thomas *et al.* 2007]. Samelson-Jones and Yeh further showed that NO-binding induced conformational changes and suggested that these might contribute to enhance proteasomal degradation. However, here binding of tryptophan to the active site inhibited NO-binding to the enzyme [Samelson-Jones and Yeh 2006]. Whereas Thomas *et al.* showed that enzyme inactivation by NO binding to the heme prosthetic group occurred in the presence of tryptophan, resulting in an inactive nitrosylated IDO-tryptophan complex [Thomas *et al.* 2007]. The latter is likely the mode of action in hRPE cells used herein. Here, inhibition of IDO1 was dependent on iNOS activity, hence NO production as shown by inhibition of iNOS activity. However, here NO inactivated enzymatic activity in hRPE cells in the presence of tryptophan and did not lead to proteasomal degradation of IDO1 protein, since IDO1 protein content was unaltered.

T. gondii has evolved a vast array of effector molecules that interact with and manipulate its host cell. Interestingly, regulation of IDO1 by iNOS shown in hRPE cells in this thesis, has recently been shown to be exploited by *T. gondii* in a different *in vitro* model. Bando *et al.* showed that IFN-γ induced IDO1 in different human cell lines was abrogated in a coculture system with *T. gondii* infected human monocytes. In detail, *T. gondii* secreted the dense granule protein GRA15, which induced IL-1β production in the infected human monocytes. IL-1β then stimulated iNOS expression in IFN-γ stimulated hepatocytes (Huh7) and primary human neurons leading to drastically reduced IDO1 activity [Bando *et al.* 2018; Bando *et al.* 2019]. On one hand, this mechanistic exploitation by *T. gondii* poses a potential risk for the antimicrobial effectivity of IDO1 in hRPE cells. On the other hand, intrinsic regulation of IDO1 activity by iNOS dependent NO production poses a potential, post-transcriptional regulatory mechanism that might be of specific importance to the eye. Excessive IDO activity could be detrimental to the diverse, non-regenerative cells of the eye, since tryptophan

starvation could potentially lead to death of the differentiated cells of the retina causing severe irreversible visual impairment.

5.1.3 Active co-infections can favor one another

Inhibition of *T. gondii* growth is dependent on IFN-γ induced IDO in hRPE cells as shown in the herein used ARPE19 cell line, as well as in primary cells [Nagineni *et al.* 1996]. In these hRPE cells IFN-γ induced IDO drastically inhibits hCMV as well [Zimmermann *et al.* 2014; Bodaghi *et al.* 1999].

Due to the high prevalence of both, *T. gondii* and hCMV [Zuhair *et al.* 2019; Melendez-Munoz *et al.* 2019], simultaneous infections with these pathogens are likely. Although in the post-Highly Active Antiretroviral Therapy (HAART) era, ocular manifestations (e.g. lesions) of many opportunistic infections (e.g. hCMV and *T. gondii*) in HIV/AIDS patients – previously considered defining diseases for AIDS – have decreased [Sudharshan *et al.* 2020], they continue to be reported. In the case-report by Jehangir and colleagues an HIV patient with severe lethargy and confusion was examined revealing a reactivated *T. gondii* infection with an active hCMV co-infection causing severe lesions in the brain [Jehangir *et al.* 2014]. Thus, the consequences of an hCMV infection in regard to the establishment and control of infections with other opportunistic pathogens that are targeting the eye, were analyzed in this thesis.

IFN-γ stimulation of hCMV infected hRPE cells used herein resulted in a clearly reduced IDO1 activity compared to uninfected cells.

This is likely due to hCMVs capacity to interfere with IFN-γ signaling by manipulating pSTAT1 translocation as well as dephosphorylation and enhancing proteasomal degradation of JAK1 [Baron and Davignon 2008; Miller *et al.* 1998]. Inhibition of IFN-γ signaling and ultimately inhibition of the IFN-γ effector mechanism IDO1, as shown herein, had drastic consequences for the control of pathogen growth as well as proliferation of activated lymphocytes by hRPE cells. This implicates that an active hCMV infection would support the establishment / growth of other infections / pathogens.

As shown herein, hCMV inhibited IDO1-dependent antimicrobial effects not only against *T. gondii* but also against *S. aureus*. Additionally, the hCMV infection reduced the IDO1-dependent immunoregulatory capacity of ARPE19 cells. Hence, an active hCMV infection might be capable to promote intraocular infections by disseminated

bacteria and might favor development of autoreactive immunopathology in the eye that could otherwise be controlled in an IDO1-dependent manner.

5.2 Acute murine toxoplasmosis

In vitro approaches that address induction of mIDO1 and its antimicrobial effector function in IFN-γ activated murine cells have proven to be difficult and rather fruitless [Halonen *et al.* 1998; Meisel *et al.* 2011]. However, Silva *et al.* suggested, based on their infection experiments with diverse gene deficient mice, that mIDO could potentially contribute to the control of *T. gondii* in mice. This suggestion was based on their observation that WT and iNOS-KO mice that survived the acute phase of infection expressed mIDO mRNA and showed accompanied changes in tryptophan and kynurenine levels. Whereas IFN-γ-KO and IRF1-KO mice that quickly succumbed to the acute infection lacked mIDO mRNA and associated kynurenine reduction [Silva *et al.* 2002].

5.2.1 mIDO1 – induced but not effective

WT and IDO$^{-/-}$ mice were analyzed during the acute phase of infection to test the hypothesis by Silva *et al.* and indeed, IDO$^{-/-}$ mice lacked this increase in kynurenine levels as reported by Silva *et al.* [Silva *et al.* 2002]. This was especially prominent in the lung, where mIDO1 was strongly induced on transcriptional and protein level in WT mice during acute toxoplasmosis as shown herein. However, following infection with a high dose of *T. gondii* ME49 (type II strain) tachyzoites IDO$^{-/-}$ mice showed no differences in toxoplasmosis associated symptoms (i.e. weight loss) and survival compared to the respective WT mice. This result is in line with publications of infection experiments with different type II *T. gondii* strains, ME49 and Fukaya strain respectively, where similar observations were reported [Divanovic *et al.* 2012; Murakami *et al.* 2012]. Infection with 20 *T. gondii* ME49 cysts was comparable in IDO-KO and WT mice [Divanovic *et al.* 2012]. WT mice, IDO-KO mice and WT mice treated with the IDO inhibitor 1-MT were infected with 20 cysts of the *T. gondii* Fukaya strain. Lack of the IDO gene or its activity had no diverging effect on infection associated symptoms or survival as reported by Murakami and colleagues. Interestingly, here IDO gene deficiency or mIDO inhibition resulted in reduced expression of the *T. gondii* specific surface antigen 2 (*Tg*SAG2) mRNA in lung tissue, indicating a reduced parasite burden [Murakami *et al.* 2012]. With regard to the antimicrobial potential of

IDO this contradictory finding was explained with reduced suppression of the immune response in the absence of IDO activity [Murakami *et al.* 2012]. In the hands of Divanovic *et al. in vivo* blockade of mIDO by 1-MT treatment of WT mice had no effect on the acute phase of infection, but rather caused a profound phenotype during chronic toxoplasmosis. Here, the parasite load (i.e. cyst number) in brains of mice was significantly increased by 1-MT treatment, which eventually resulted in death of the 1-MT treated mice [Divanovic *et al.* 2012]. With the herein used experimental model of acute murine toxoplasmosis the absence of the mIDO1 gene and its consequences during the chronic phase of infection cannot be addressed, since all mice, irrespective of the genotype, would have succumb to the acute infection. However, contradictory to Murakami *et al.* 2012, who showed reduced *T. gondii Tg*SAG2 mRNA expression in IDO$^{-/-}$ mice and 1-MT treated WT mice, the parasite loads in organs from WT and IDO$^{-/-}$ mice were comparable in the infection model used in this thesis. Interestingly, Murakami's observation was only present at seven dpi and vanished at later time points [Murakami *et al.* 2012]. Though, it has to be considered that the herein intraperitoneal administered high infection dose is a strictly experimental scenario and that by simulation of a natural infection (i.e. oral gavage of a low amount of sporulated oocysts) potential contribution of mIDO1 activity to control the infection cannot be fully excluded. Nevertheless, the results of this thesis indicate that, despite the fact that mIDO1 is induced and functionally active in WT mice during toxoplasmosis, mIDO1 seems to be dispensable with regard to its antimicrobial effector function in mice.

During chronic toxoplasmosis mIDO1 and mIDO2 have both been shown to be induced comparably strong in the brain [Divanovic *et al.* 2012]. In addition to mIDO1, the expression of two other tryptophan degrading enzymes, namely mIDO2 and mTDO, was analyzed in this thesis. Herein, mIDO2 and mTDO were constitutively expressed in liver of both genotypes. Relative expression of mTDO was unchanged by the infection in all organs of both genotypes. Whereas the relative expression of mIDO2 was unchanged by the infection in the majority of lung tissues. In brain tissue mIDO2 expression was slightly, but significantly increased at seven dpi. However, kynurenine concentrations in serum, lung and brain tissues of infected IDO$^{-/-}$ mice were low and close to the detection limit and therefore similar to naïve mice. Hence, a compensatory induction of mIDO2 and mTDO and thereby masking the lack of mIDO1 in the experimental model used herein can be excluded.

Surprisingly tryptophan concentrations were elevated in lung and brain tissue at three dpi in both genotypes. What is even more astonishing is that at seven dpi not only in WT mice, but also IDO$^{-/-}$ mice, these tryptophan concentrations then dropped to or even below the tryptophan concentration of naïve mice in serum, lung and brain tissues. A similar observation was reported during acute toxoplasmosis in IFN-γ-KO and IRF-1-KO mice where serum tryptophan concentrations dropped below the level of the naïve mice [Silva *et al.* 2002]. This observation cannot be attributed to mIDO1 activity, since mIDO1 induction relies on IFN-γ as well as on effective IFN-γ signaling [Chon *et al.* 1995; Sotero-Esteva *et al.* 2000]. With regard to the serum tryptophan concentration IDO$^{-/-}$ and WT mice used herein showed the same phenotype as the IFN-γ-KO and IRF-1-KO mice published by Silva *et al.* underlining that mIDO1 is not responsible for the significant drop of the serum tryptophan concentration observed in WT mice during acute toxoplasmosis.

There are several scenarios that could possibly contribute to this drop in the serum tryptophan concentration. These scenarios were not considered in the analyses herein but should be addressed in future studies. They include reduced feed intake or nutrient absorption, metabolic pathways that utilize tryptophan, tryptophan elimination through urine and tryptophan syphoning into storages (in organs, tissues, cells), proteins and proliferating cells.

In accordance with other studies drastically reduced body weights were observed during acute murine toxoplasmosis in the *in vivo* model used in this thesis [Khan *et al.* 1997; Hatter *et al*. 2018; Melchor *et al.* 2020]. Behavioral changes were documented herein and deviated increasingly from normal behavior over the time of infection. However, a reduced feed intake was not explicitly documented. Amino acids, like tryptophan, are absorbed in the small intestine [Bröer and Fairweather 2018]. Severe inflammation of the small intestine during acute toxoplasmosis, as described for instance by Kahn and colleagues or Dias and colleagues, might hinder efficient absorption of nutrients and could therefore possibly contribute to the serum tryptophan drop in infected mice observed herein [Khan *et al.* 1997; Dias *et al.* 2014]. Thus, future studies should address the contribution of reduced feed intake or impaired nutrient absorption due to inflammatory damage of the small intestine during acute toxoplasmosis with regard to the observed serum tryptophan drop.

The melatonin synthesis pathway for instance utilizes tryptophan via serotonin to yield melatonin by several enzymatic steps that are independent of IDO1 [Zhao *et al.* 2019]. Interestingly, melatonin synthesis has recently been shown to be induced by *T. gondii* in human intestinal epithelial cells (Caco-2 cells) [Majumdar *et al.* 2019]. Here, in the absence of IDO1, melatonin protected *T. gondii* from reactive oxygen species and favored parasite growth [Majumdar *et al.* 2019]. Nevertheless, it remains to be shown whether melatonin synthesis is increased during acute toxoplasmosis *in vivo* and what consequences this would have on the parasite, the host and its serum tryptophan level. Since mouse urine was not analyzed herein and because tryptophan (8.35 ± 5.35 µg/g creatinine) can be detected in urine of healthy individuals [Oh *et al.* 2017], this tryptophan elimination pathway cannot be ruled out to be involved in the drop of serum tryptophan observed herein.

PD-1-deficient (PD-$1^{-/-}$) mice are unable to inhibit activated T cells and therefore exhibit a persistent T cell activation phenotype [Okazaki et al., 2013]. This phenotype leads to depletion of several serum amino acids, including tryptophan [Miyajima *et al.* 2017]. Miyajima and colleagues elegantly demonstrated that the serum amino acid depletion was dependent on activated T cells but independent of IFN-γ. Furthermore, they demonstrated that accumulation of tryptophan in lymph nodes was concomitant with increased expression of a sodium-ion-independent L-amino acid transporter (LAT) that is responsible for the transport of neutral amino acids (e.g. tryptophan), namely LAT1, in activated T cells [Miyajima *et al.* 2017]. LAT1 expression was furthermore accompanied with intracellular accumulation of tryptophan and increased protein biosynthesis in activated T cells [Miyajima *et al.* 2017]. It remains to be shown whether the siphoning of available tryptophan by the mechanisms published by Miyajima *et al.* are responsible for the serum tryptophan drop observed during acute murine toxoplasmosis. However, they likely contribute to this phenotype since, as shown herein, T cells from WT and $IDO^{-/-}$ mice exhibit activation phenotypes and the serum tryptophan drop were comparable between the genotypes.

Thus, it remains to be shown in future studies to what extend the scenarios elaborated above contribute to the serum tryptophan drop in the context of acute murine toxoplasmosis observed herein.

5.2.2 Other IFN-γ effector proteins contribute to the control of *T. gondii* in mice

Irrespective the fact that mIDO1 is induced and functionally active in WT mice during acute toxoplasmosis, infection associated symptoms and parasite loads were comparable in IDO$^{-/-}$ and WT mice. This indicates that other IFN-γ effector proteins induced during infection are substantially involved in limiting parasite growth *in vivo*. IFN-γ inducible mGBP's have previously been shown to contribute to parasite control *in vivo* [Kim *et al*. 2016a]. Infection experiments with specific mGBP-KO mice have shown that lack of a single mGBP has substantial consequences for the survival of these mice. For example, compared to WT counterparts' mice lacking mGBP1, mGBP2 or mGBP7 have recently been shown to be highly sensitive to infections with type II *T. gondii* parasites [Selleck *et al.* 2013; Degrandi *et al.*2012; Steffens *et al.* 2020].

In line with the published data on the role of mGBP's in murine toxoplasmosis, mGBP2 could be shown to be expressed on mRNA level in the herein analyzed organs of WT and IDO$^{-/-}$ mice. Furthermore, mGBP2 and mGBP7 proteins were detected in lungs of both WT and IDO$^{-/-}$ mice, without genotype specific differences. Protein band intensities of the analyzed mGBP's (mGBP2 and mGBP7) massively increased in the course of infection indicating that the mGBP protein content increases, likely to combat the intruder *T. gondii*.

5.2.3 Protein activities of miNOS and mIDO1 interfere *in vivo* and *ex vivo*

miNOS has been implicated to be of high relevance during the chronic phase of infection, rather than in the acute phase that was analyzed herein. This has been demonstrated by Scharton-Kersten and colleagues where miNOS deficient mice succumbed to toxoplasmic encephalitis during the chronic phase of infection [Scharton-Kersten *et al.* 1997]. Interestingly, Fujigaki *et al.* reported in an acute infection model with a type II *T. gondii* strain (20 cysts of the Fukaya strain administered ip) that inhibition of miNOS activity *in vivo* with N^GMMA increased parasite loads in brain but had no effect on parasite loads in lungs of treated WT mice and resulted in increased serum kynurenine concentration [Fujigaki *et al.* 2002]. Based hereon Fujigaki and colleagues suggested that miNOS and mIDO are cross regulated by one another in a cell or tissue specific fashion.

In order to investigate a possible reciprocal influence of mIDO1 and miNOS as suggested by Fujigaki and colleagues, analysis of miNOS was performed in the

experimental model used herein. Here, miNOS could be shown to be induced on transcriptional level in lung and liver and marginally in brain. Comparison of miNOS protein in lung samples of WT and IDO$^{-/-}$ mice at seven dpi and nine dpi indicated that miNOS protein was present in IDO$^{-/-}$ lungs prior to WT lungs. However, it has to be taken into account that miNOS protein detection in lung tissue at three dpi and seven dpi was inconsistent with the herein used antibody. Irrespective of this uncertainty, NO production *ex vivo* was significantly higher in splenocyte, lung cell and PEC cultures from infected IDO$^{-/-}$ mice than from their WT counterparts. These results are in line, with reports by Ye *et al.* and Ohtaki *et al.* that showed that in the absence of mIDO activity NO production was increased in cell culture systems with isolated murine lymphocytes and PECs, respectively [Ye *et al.* 2017; Ohtaki *et al.* 2009]. Ye and colleagues described increased NO production in mixed lymphocyte cultures from BALB/c and C57BL/6 mice that were treated with the IDO inhibitor 1-methyl-DL-tryptophan [Ye *et al.* 2017]. mIDO activity was increased in lipopolysaccharide (LPS) stimulated WT PECs when miNOS activity was pharmacologically inhibited and conversely, LPS stimulated PECs derived from IDO$^{-/-}$ mice showed increased NO production [Ohtaki *et al.* 2009]. Such a reciprocal influence of mIDO1 and miNOS as shown herein and by others [Ye *et al.* 2017; Ohtaki *et al.* 2009] might be of specific importance in the context of inflammation. Khan and colleagues observed reduced liver degeneration, less ulceration and necrosis of the distal small intestine in miNOS-KO mice infected with *T. gondii* in comparison to their WT counterparts [Khan *et al.* 1997]. Khan *et al.* concluded that the lack of NO and therefore its harmful nature was responsible for the less harmful manifestations during acute toxoplasmosis in miNOS-KO mice [Khan *et al.* 1997]. However, here it has to be considered that mIDO activity, which was not analyzed by Khan *et al.* could have potentially contributed to the reduced inflammatory damage to these tissues in miNOS-KO mice. Based on the results in this thesis, no precise statement can be made about the reciprocal influence of mIDO1 and miNOS, as it was not taken into account in detail during implementation of the experiments. Therefore, this topic should be considered in future studies.

5.3 Immunoregulatory property of IDO1

A continuously growing body of literature has underlined the importance of IDO1 as an enzyme with immunoregulatory properties in the fields of transplant medicine, tumor immunology and autoimmunity [reviewed by Löb *et al.* 2009].

For example, suppression of murine T cell responses by the local microenvironment created by a specific subset of DCs that express mIDO1 in tumor draining lymph nodes has been described [Munn et al, 2004]. Furthermore, clonal T cell proliferation *in vivo* was shown to be suppressed in an mIDO1 dependent manner by splenic DCs [Mellor *et al.* 2003]. In addition, mIDO mediates tolerance to self-antigens of apoptotic cells in the marginal zone of the spleen [Ravishankar *et al.* 2012].

Therefore, mitogen induced lymphocyte proliferation experiments were performed to reveal a possible contribution of mIDO1 and its suppressive capacity to the drastically reduced T cell responsiveness that has been described by Chan and colleagues during acute murine toxoplasmosis [Chan *et al.* 1986].

5.3.1 mIDO1 is not responsible for the impaired T cell responsiveness

By comparing the *ex vivo* mitogen stimulated lymphocyte proliferation responses of splenocytes from *T. gondii* infected WT and IDO$^{-/-}$ mice no direct involvement of mIDO1 could be observed, since proliferation responses were comparable between genotypes. Supplementation of IL-2 and inhibition of miNOS *in vitro* increased lymphocyte proliferation in response to mitogen stimulation of the splenocyte cultures from both genotypes. This is in line with data on purified CD4^{+} T cells isolated from *T. gondii* infected WT mice during the acute phase, as published by Khan and colleagues. Here they showed that IL-2 supplementation increased the T cell responsiveness drastically [Khan *et al.* 1996]. The splenocyte cultures used herein consisted of a broad variety of cells, including haematopoetic and non-haematopoietic cells. Hence, miNOS activity, for instance by macrophages as published by Albina and colleagues [Albina *et al.* 1991], contributed to the unresponsiveness of the lymphocytes.

Interestingly, mitogen induced proliferation of splenocyte cultures from WT mice infected orally with 20 *T. gondii* ME49 cysts were unaffected when isolated at seven dpi. This might be explained with a combination of the infection dose and the time post infection, since impaired T cell proliferation responses at seven dpi were indeed shown after oral infection of C57BL/6 mice with 50 *T. gondii* ME49 cysts [Salinas *et al.* 2014]. Hence, analysis of the lymphocyte proliferation responses from the orally infected mice used herein at a later time point might have resulted in a similar phenotype.

Co-cultivation experiments performed in this thesis, indicated that the impaired responsiveness of primed T cells isolated from infected mice could not be conferred to unprimed T cells isolated from naïve mice. Conversely bystander help by unprimed non-T cells for primed T cells had no effect on the proliferation response. Interestingly, Tregs were suggested by Salinas and colleagues to mediate suppression of T cell proliferation solely by IL-2 deprivation in a contact dependent manner. In trans-well experiments they showed that T cells could proliferate when physically separated from the Tregs whilst sharing the same cell culture medium [Salinas *et al.* 2014]. In addition, they performed co-cultivation experiments of Tregs isolated from infected mice with a T cell-cell line (CTLL-2) that produces IL-2 and relies on IL-2 for proliferation. Here, CTLL-2 cells showed reduced proliferation when cultured with purified Tregs from infected mice [Salinas *et al.* 2014].

Salinas and colleagues furthermore noted that T cells that were in contact with Tregs died off after several divisional rounds, “mainly in the last rounds of cell division detected in the assay” [Salinas *et al.* 2014]. This was not analyzed in detail herein, however, obvious signs of dead cells, such as a clear reduction in cell number, or an increase of detached or miss shaped cells were not observed prior to termination of the assay used herein. The continuous IL-2 deprivation of activated T cells due to competition with Tregs, as reported by Salinas *et al.* could likely induce apoptosis in T cells. Tregs have been shown to be capable of depriving effector $CD4^+$ T cells from cytokines, which eventually resulted in induction of apoptosis of the activated effector T cells *in vitro* and *in vivo* [Pandiyan *et al.* 2007]. Hence, continuous IL-2 deprivation of T cells *in vivo* and consequently induction of apoptosis in these T cells would explain, why lymphocyte proliferation responses could not be rescued by IL-2 supplementation and miNOS inhibition when splenocytes were isolated at ten dpi as shown herein. However, whether apoptosis of IL-2 deprived T cells is indeed induced at this time point post infection remains to be elucidated.

5.3.2 mIDO1$^{-/-}$ – impact on effector T cells and Tregs in acute toxoplasmosis

In addition to the analysis of the T cell responsiveness, abundance of T cell subsets, including Tregs, and the presence of activation markers on these T cell subsets were analyzed and compared between genotypes. This is of special interest, since DCs can confer suppressive functions of Tregs in an IDO-dependent manner [Fallarino *et al.* 2003; Lippens *et al.* 2016].

Analysis of Th ($CD4^+$ T cells) cells, CTLs ($CD8^+$ T cells) and Tregs ($CD4^+CD25^+FOXP3^+$ T cells) of naïve and *T. gondii* infected WT and $IDO^{-/-}$ mice revealed no differences between genotypes. Nevertheless, at seven dpi splenic $CD4^+$ and $CD8^+$ T cells and Tregs showed a strong trend towards a reduction in cell number in the spleen, which is in line with several publications. Zhang and colleagues for example compared Th cell and CTL populations during infection of BALB/c mice with the *T. gondii* strains ME49 and RH (a highly virulent type I strain). Here, Th cell and CTL populations were significantly reduced in the course of acute infection, which was more prominent during infection with the ME49 strain [Zhang *et al.* 2018]. With regard to Tregs during lethal oral infection with *T. gondii* ME49 cysts, Oldenhove and colleagues described a reduction in Treg numbers in several tissues, including spleen, MLN and small intestine lamina propria [Oldenhove *et al.* 2009]. Tenorio *et al.* showed a reduction in splenic Tregs during oral infection of C57BL/6J mice with 25 *T. gondii* ME49 cysts as well. Furthermore, they showed that the remaining Tregs exhibited an activation phenotype and analyzed their activation induced phenotype, revealing a clearly increased suppressive phenotype [Tenorio *et al.* 2011]. In accordance with the data by Tenorio *et al.* the remaining Tregs detected in spleen in the experimental infection model used herein showed a significant increase in expression of activation markers, indicating an activation like phenotype. Furthermore, Tenorio and colleagues could show that the activated Tregs were responsible for production of IL-10 detected in *in vivo*. The suppressive capacity of the activated Tregs regarding the unresponsiveness of mitogen stimulated T cells, however, was mediated in an IL-2 dependent manner, since neutralization of IL-10 *in vivo* had no impact on the suppressive phenotype described [Tenorio *et al.* 2011].

Interestingly, T cell suppression was dependent on IL-10 produced by lung resident Tregs in a murine model of a respiratory infection [Coleman *et al.* 2012]. The proportion of IFN-γ producing lymphocytes in cervical lymph nodes approximately doubled in $IL\text{-}10^{-/-}$ mice compared to the respective WT mice during *Bordetella pertussis* infection [Coleman *et al.* 2012]. Hence, the mode of action of Tregs on T cell suppression might differ in a tissue dependent manner.

5.4 It's all about the context – species specific relevance of IDO1

In this thesis the antimicrobial and immunosuppressive capacity of IDO1 was analyzed using both *in vitro* and *in vivo* approaches. IDO1 efficiently inhibited pathogen growth in human RPE cells, whereas in mice IDO1 had no significant effect on pathogen growth. These results indicate that the role of IDO1 as a potent effector mechanism depends on host species.

5.4.1 IDO1 - induced and hijacked

Apparently, not only tumors hijack IDO to take advantage of its catabolic and suppressive activity [Zamanakou *et al.* 2007; Rad Pour *et al.* 2019]. Some pathogenic microorganisms (e.g. uropathogenic *Escherichia coli* and *Mycobacterium tuberculosis*) are capable to benefit from the immunosuppressive action of IDO activity while at the same time withstand the tryptophan starvation and thereby circumvent eradication by the immune system [Loughman *et al.* 2012; Gautam *et al.* 2018].

Uropathogenic *Escherichia coli* for instance, induce IDO in epithelial cells of the urinary tract, thereby reducing the anti-bacterial immune response and enabling the colonization of the urinary epithelium [Loughman *et al.* 2012]. In experimental *Mycobacterium tuberculosis* (*M. tuberculosis*) infection studies, IDO1 is induced and active not only in mice but also in macaques [Gautam *et al.* 2018]. Administration of 1-D-MT reduced bacterial burden and clinical manifestations due to reduced immunosuppressive action of IDO1. In detail, more effector T cells with increased functionality (e.g. granzyme B expression by $CD8^+$ T cells) were recruited to the site of infection (i.e. non-necrotizing granulomas and necrotic tissue lesion). In addition, the $CD4^+$ T cell compartment of 1-D-MT treated macaques expressed increased levels of the proliferation marker Ki-67 compared to untreated animals [Gautam *et al.* 2018]. Furthermore, in characterization studies of vaccine candidates against tuberculosis Smith and colleagues showed that tryptophan auxotrophic *M. tuberculosis* mutants were avirulent even in severe combined immune-deficient mice that lack a functional adaptive immune response [Smith *et al.* 2001]. These results by Smith *et al.* implicate that mIDO1 has the potential to facilitate its antimicrobial potential by tryptophan starvation *in vivo*. In active and latent human tuberculosis, IDO1 is induced and active as shown by transcriptomic and metabolomic analyses [Collins *et al.* 2020]. Therefore, Collins and colleagues suggest that tryptophan catabolism fueled by IDO1 activity during tuberculosis could be used for the development of a tuberculosis biomarker that

could be facilitated to enable a patient specific therapy approach [Collins *et al.* 2020]. Interestingly, T cell mediated macrophage activation does facilitate inhibition of intracellular *M. tuberculosis* in an IDO-dependent manner *in vitro*, however, only when *M. tuberculosis* specific tryptophan biosynthesis is hindered [Zhang *et al.* 2013b].
This could be exploited by treatment regimens that specifically inhibit tryptophan biosynthesis in *M. tuberculosis*, however, development of such inhibitors requires ongoing effort. For instance, as shown by Abrahams and colleagues, who have illustrated their efforts in the drug discovery pipeline with regard to the analysis of inhibitors of mycobacterial tryptophan biosynthesis [Abrahams *et al.* 2017].
An extreme dependency on mIDO1 activity *in vivo* has been shown for the development of the apicomplexan parasite *Eimeria falciformis (E. falciformis). E. falciformis* infects the mouse caecum where it resides within intestinal epithelial cells and subverts the murine host defense along the IFN-γ/IDO1 axis, as shown by Schmid and colleagues. After all, *E. falciformis* relies on host derived xanthurenic acid that is produced along the kynurenine pathway downstream of mIDO1 to facilitate its lifecycle [Schmid *et al.* 2012; Schmid *et al.* 2013].

5.4.2 IDO1 – induced and effective

In accordance with the results of this thesis mIDO1 is strongly induced and active in lung tissue following infection with other pathogenic microorganisms; however, in contrast to the herein reported unaffected parasite growth, mIDO1 significantly impaired growth of pathogenic bacteria and fungi in other *in vivo* studies [Virok *et al.* 2019; Araujo *et al.* 2014]. Inhibition of mIDO with 1-MT in *C. muridarum* infected Balb/c mice resulted in an approximately 2-fold reduction of the *ex vivo* analyzed inclusion formation, a read-out for the detection of infective chlamydia [Virok *et al.* 2019].
Even more strikingly, mIDO essentially contributed to fungal clearance in pulmonary mycosis, caused by the pathogenic fungus *Paracoccidioides brasiliensis* (*P. brasiliensis*). In addition, mIDO activity protected the host of elevated tissue pathology due to an otherwise exuberating inflammatory response [Araujo *et al.* 2014]. Susceptible mice treated with the IDO inhibitor 1-MT exhibited sustained fungal growth, increased influx of DCs, myeloid and lymphoid cells. Furthermore, mIDO inhibition resulted in elevated tissue pathology and increased mortality during infection with *P. brasiliensis* [Araujo *et al.* 2014].

The previous two sections make it clear that the contrasting results of this thesis go hand in hand with the reports in the literature. The antimicrobial and immunosuppressive capacity of IDO1, as well as its consequences (i.e. harmful or beneficial) for both the host and the pathogen, clearly depend on the combination of species involved in each case. In the context of *T. gondii*, coevolution has intensively shaped defense mechanisms, especially of natural hosts (i.e. mice), as well as immune evasion strategies by *T. gondii*, which are briefly elaborated in the following paragraph.

5.4.3 Host manipulation – essential *T. gondii* precision tools for intracellular success

T. gondii invades host cells where the parasite resides within a PV shielding itself from cytosolic defense mechanisms. *T. gondii* secrets many effector molecules that help to shape the intracellular environment that surrounds its refuge thereby securing the nutritional demand within, integrity of and safety within the PV [Olson *et al.* 2020; Crawford *et al.* 2006; Pernas *et al.* 2014; Pernas *et al.* 2018; Peixoto *et al.* 2010; Rosowski et al 2012]. Specialized organelles, namely dense granules and rhoptries are the origin of GRA and ROP proteins that help convey these aims [Etheridge *et al.* 2014; Alaganan *et al.* 2013; Selleck *et al.* 2015; Kim *et al.* 2016b].

5.4.3.1 Manipulation of host cell signaling

Downregulation of host genes involved in MAPK signaling by for instance ROP38, contributes to active control of host cell apoptosis and proliferation, thereby assuring the safe refuge [Peixoto *et al.* 2010]. IFN-γ induced genes turn the host cell cytoplasm into a deadly trap outside the PV. However, all three clonal linages of *T. gondii* (type I, II and III) are capable to interfere with IFN-γ induced gene expression in their infected host cell [Rosowski et al 2012]. The dense granule effector protein *T. gondii* inhibitor of STAT1 transcription activity (*Tg*IST) translocates into the host cell nucleus where it binds to activated STAT1 molecules and reduces their recycling [Gay *et al.* 2016; Olias *et al.* 2016; Nast *et al.* 2018; Rosowski *et al.* 2014]. Consequently, *T. gondii* pre-infected host cells (e.g. HFF and Huh7) show impaired induction of effector mechanisms (e.g. IDO1) upon IFN-γ stimulation in a *Tg*IST dependent manner [Bando et al 2018]. Turnover of pSTAT1 was not analyzed in detail in this thesis, however *T. gondii* infected WT and IDO$^{-/-}$ mice clearly showed increased mpSTAT1 during the course of acute toxoplasmosis.

5.4.3.2 Nutritional dependencies

T. gondii resides within its PV but relies on numerous nutrients and metabolites from its host cell [Blume and Seeber 2018].

Early after infection *T. gondii* secretes a dense granule effector protein called mitochondrial association factor 1 (MAF1) that binds close-by host mitochondria to the PV, which is essential for optimal parasite growth [Pernas *et al.* 2014]. MAF1 interaction with host mitochondria is thought to enable improved fatty acid (FA) scavenging by *T. gondii*. Scavenging of host derived lipoic acid for instance, which is an important cofactor for numerous biosynthetic pathways, is a potential candidate with regard to MAF1 action [Crawford *et al.* 2006]. Interestingly, upon infection host cell mitochondria fuse and channel FA into β-oxidation, which enables competition of the host cell with *T. gondii* for FA [Pernas *et al.* 2018].

T. gondii is auxotrophic for tryptophan [Pfefferkorn 1984] and tryptophan starvation via host IDO1 activity has been confirmed in this thesis. The supply of tryptophan is achieved by *T. gondii* by manipulating active tryptophan transport via LAT1 in its host cell by an unknown mechanism [Olson *et al.* 2020]. Furthermore, *Tg*ApiAT5-3, a putative apicomplexan amino acid transporter (ApiAT) in *T. gondii* that transports large neutral amino acids (including tryptophan), has been identified in a multidisciplinary approach using bioinformatic, genetic, cell biologic and metabolic tools [Parker *et al.* 2019]. In this thesis, induction of IDO1 in hRPE cells resulted in tryptophan starvation and consequently inhibition of excessive parasite growth; however, to what extent host LAT1 and *Tg*ApiAT5-3 expression are regulated by *T. gondii* in hRPE cells in this context remains to be shown in future studies.

5.4.3.3 Attack and counterattack

In this thesis, analysis of murine lung tissue revealed that mGBP2 and mGBP7 are highly expressed during acute toxoplasmosis, which is in line with other publications [Degrandi *et al.*2012; Steffens *et al.* 2020]. In murine hosts, the vulnerability of *T. gondii* to these IFN-γ induced cell-autonomous effector mechanisms is reduced by secretion of GRA and ROP proteins by *T. gondii*. mIRGs turnover is increased by multi-protein complexes of PV bound GRA7 and associated ROP5, ROP17 and ROP18, whereas ROP18, ROP5 and ROP45 are described to affect mGBPs [Etheridge *et al.* 2014; Alaganan *et al.* 2013; Selleck *et al.* 2015; Kim *et al.* 2016b]. Variation in strain specific virulence of *T. gondii* in mice (i.e. of highly virulent type I strains [Mordue *et al.* 2001;

Lilue *et al.* 2013]) is largely due to polymorphisms in ROP5 and ROP18 [Behnke *et al.* 2011; Saeij *et al.* 2006]. High susceptibility of mice is conflicting with the role of mice as natural intermediate host of *T. gondii*, where encystation and persistence is key for a successful completion of the parasite's lifecycle (see section 1.1.1, pp. 2-3). In contrast to inbred laboratory mice, wild-derived mouse strains (in the following called 'wild mice') have highly polymorphic mIRG alleles (chromosome 11), making these wild mice impervious to infection with type I *T. gondii* strains [Lilue *et al.* 2013]. The highly polymorphic mIRGs in wild mice essentially contribute to the control of an acute murine toxoplasmosis in the wild, enabling encystation and persistence of the parasites and therefore explain the existence of these type I *T. gondii* strains in nature as further elaborated by Lilue and colleagues [Lilue *et al.* 2013].

In the light of coevolution of natural hosts and *T. gondii*, polymorphic ROP proteins and IFN-inducible GTPases depict an arms race of parasites attack and hosts' counterattack. In accidental host evolution is not fueling such an arms race, since accidental hosts are a 'dead-end' in the parasite's life-cycle. IFN-inducible GTPases like IRGs are almost completely absent in humans and GBPs are less important and act in a different mode of action in comparison to murine GBPs [Mukhopadhyay *et al.* 2020]. Similarly, parasite detection in mice is highly dependent on TLR11 and TLR12, which are absent in humans [Sasai and Yamamoto 2019]. Thus, the arms race during coevolution of mice and *T. gondii* has shaped recognition of and effective cell-autonomous effector mechanisms directed against *T. gondii*, as well as the parasites precision tools directed against these countermeasures. Hence, the differential importance of IDO1 in mice and humans during toxoplasmosis reported in this thesis.

5.5 Outlook

5.5.1 Which cells possess IDO1 activity in the lung?

Depending on the context, several different cell types that can be found in the lung have been shown to express IDO1 protein [Hayashi *et al.* 2004; Lee *et al.* 2007; Hansen *et al.* 2000; Gautam *et al.* 2018]. For example, in a mouse model of allergic disease suppression of lung inflammation and hyperreactivity was mediated by mIDO1 expressing lung epithelial cells rather than pulmonary DCs [Hayashi *et al.* 2004]. Whereas, during acute tuberculosis in macaques' APCs represented the IDO1-

expressing cell type [Gautam *et al.* 2018]. In allogeneic hematopoietic stem cell transplantation control of severe lethal pulmonary inflammation was mediated along the IDO-aryl hydrocarbon receptor-axis. In that study predominantly alveolar macrophages and epithelial cells were IDO1 positive [Lee *et al.* 2007]. Interestingly, in different murine models of malaria vascular endothelial cells in several organs, including the lung, were the primary site of IDO expression during infection with *Plasmodium berghi* [Hansen *et al.* 2000]. Whether vascular endothelial cells express mIDO1 during acute murine toxoplasmosis is of great interest; however, remains to be elucidated. Even though mIDO1 has been shown to be expressed in different tissues during acute murine toxoplasmosis, as shown herein, cell types responsible for mIDO1 expression remain to be identified in future studies.

5.5.2 How does *T. gondii* counteract tryptophan starvation?

Initially demonstrated by Pfefferkorn, *T. gondii* is a tryptophan auxotroph and relies on available tryptophan for optimal growth [Pfefferkorn 1984]. In this thesis, induction of IDO1 in hRPE cells resulted in tryptophan starvation and consequently inhibition of excessive parasite growth. Just recently, Parker and colleagues, as well as Olson and colleagues have shown that *T. gondii* actively imports tryptophan via *Tg*ApiAT5-3 and manipulates active tryptophan transport via LAT1 into its host cell [Parker *et al.* 2019; Olson *et al.* 2020]. These recent findings support the parasites capability to support its demand for tryptophan in order to grow optimally, even if tryptophan availability is scarce intracellularly. Therefore, it would be interesting to analyze the expression pattern of LAT1 in infected hRPE cells and of *Tg*ApiAT5-3 in *T. gondii* in future studies to evaluate the extent to which *T. gondii* manipulates hRPE cells and tryptophan transport during IFN-γ stimulation.

Furthermore, the results of this thesis have shown that mIDO1 is highly active in lung tissue, leading to local tryptophan deprivation during acute murine toxoplasmosis. In $IDO^{-/-}$ mice Murakami and colleagues reported reduced relative expression of *T. gondii* specific *Tg*SAG2 mRNA in lung tissue [Murakami *et al.* 2012]. Interestingly, *Tg*SAG2 proteins represent a family of surface proteins that are expressed by *T. gondii* in a stage specific (i.e. tachyzoite) manner [Lekutis *et al.* 2000]. Murakamis' report therefore indicates a reduction of actively proliferating parasites due to either growth stagnation or conversion of the rapidly proliferating tachyzoite stage to the less active bradyzoite stage.

In experiments with the intracellular bacterium *C. trachomatis* a similar observation of stage conversion has been made [Leonhardt *et al.* 2007]. Here, tryptophan starvation drove *C. trachomatis* into a persistent stage, which could be reversed by supplementation of tryptophan *in vitro* [Leonhardt *et al.* 2007].
Intriguingly, nutritional starvation can indeed drive stage conversion of *T. gondii*, from the tachyzoite stage into the bradyzoite stage, which exhibits reduced proliferation and an altered metabolism, as reviewed by Lüder and Rahmen [Lüder and Rahmen 2017]. For example, stage conversion of *T. gondii* has been shown by arginine starvation, which triggered cyst formation *in vitro* [Fox *et al.* 2004]. However, in their study arginine concentrations were as low as 5-10 µM [Fox *et al.* 2004]; in mammalian plasma arginine concentrations vary between 100 µM and 250 µM and more importantly, in human cells intracellular arginine concentrations are reported to range between 100 µM and 1000 µM [Wu and Morris 1998], rendering cyst formation by arginine starvation unlikely *in vivo*. Nevertheless, in the context of mIDO1 activity and tryptophan degradation it remains to be shown in future studies, if tryptophan starvation can drive *T. gondii* stage conversion from tachyzoite into bradyzoite stage both *in vitro* and *in vivo*.

5.5.3 What's next? Organoids as elegant *in vitro* models to study organ/tissue specific host-pathogen interactions.

Organoids are self-organized, three-dimensional, multicellular constructs that partially display architecture and function of the respective *in vivo* tissue and organ. Organoids are often stem cell-derived, meaning they were differentiated from embryonic, (induced) pluripotent or adult stem cells; however, they can be differentiated from primary isolated cells derived from biopsy samples as well [Hofer and Lutolf 2021]. Several different disciplines utilize organoids as superior *in vitro* models to address a large variety of topics. These include human disease models to study for instance Alzheimer's disease or cystic fibrosis [Park *et al.* 2018; Strikoudis, *et al.* 2019]. In preclinical drug development approaches organoids are facilitated in drug screening platforms [Zhou *et al.* 2017; Miranda and Cabral 2020]. Furthermore, drug screening approaches with patient derived organoids are used in oncology to identify the best possible treatment regime based on the disease characteristics, thereby contributing to precision medicine [Driehuis *et al.* 2019]. Just recently human cerebral organoids have been used as an important physiologic *in vitro* model of toxoplasmosis [Seo *et al.*

2020]. Here, invasion, proliferation and stage conversion of *T. gondii* could be recapitulated in human cerebral organoids [Seo *et al.* 2020].
The coronavirus disease 19 caused by the novel severe acute respiratory syndrome coronavirus 2 (SARS-CoV-2) has already caused millions of deaths with tremendous socio-economic impact on mankind [WHO, 2021; Nicola *et al.* 2020]. Human organoid models that are relevant in the context of toxoplasmosis have recently been used to better understand the infection by SARS-CoV-2 [Ramani *et al.* 2020; Han *et al.* 2021]. Lung organoids for instance, as published by Han *et al.* [Han *et al.* 2021], provide the opportunity to address questions in the context of mIDO1 and toxoplasmosis that could not be answered with standard *in vitro* models and without conducting *in vivo* models. Furthermore, protocols for multi-species organoid platforms, as published by Holthaus and colleagues, provide new tools to analyze zoonotic pathogens in different hosts helping to elucidate species specific differences in host-pathogen interaction and hurdles in drug development [Holthaus *et al.* 2021].
Protocols for the development of human retinal organoids with several different cell types, including RPE and photoreceptors, have been established [Wagstaff *et al.* 2021]. These retinal organoids are currently predominantly used in experimental therapeutic studies of human ocular diseases [Wagstaff *et al.* 2021].

Organoids have opened the door for the analysis of host-pathogen interactions that have not been possible in standard two-dimensional cell culture systems. Thereby, use of organoids contributes to a further reduction of *in vivo* models consequently helping to reduce the number of animals used in *in vivo* studies, and therefore complying with the 3Rs (Replacement, Reduction, Refinement) as specified by the EU directive 2010/63/EU [European Parliament and the Council of the EU 2010]. Data variation and outliers for instance, as observed in some of the experiments shown herein, are to some extend in the nature of the model. Organoids therefore offer greater complexity compared to classical cell culture systems, while likely exhibiting less variability compared to *in vivo* models. Thus, organoids offer an elegant approach to analyze intriguing questions in the context of toxoplasmosis.
Organoids in general will help to identify a possible cell tropism of *T. gondii* in an organ specific manner, host cell manipulation by *T. gondii* even of uninfected cells could be analyzed in a controlled complex three-dimensional microenvironment as well. Conversely, organoids offer an elegant way to analyze antimicrobial effector

mechanisms, like the herein addressed IDO1, iNOS and GBPs, in different cell types in concert in an *in vivo* relevant context. Are different effector mechanisms induced in different cells at the same time, how do they influence one another, and how is *T. gondii* affected by these. Human retinal organoids for instance could be used for the analysis of ocular toxoplasmosis to achieve a broader understanding of the different cell types in concert. Furthermore, multi-species organoid protocols of for instance lung organoids would help to decipher the species-specific differences of the host defense mechanisms IDO1 and iNOS including their reciprocal interaction in a cell specific manner, while at the same time evaluating *T. gondii* growth in the context of a three-dimensional organoid. Furthermore, this organoid system would allow for instance to investigate, if IDO1 dependent tryptophan starvation can possibly drive *T. gondii* stage conversion as elaborated in section 5.5.2. or would help to identify a lung cell specific tropism of *T. gondii*.

6. References

AAPOS. "Toxoplasmosis." American Association for Pediatric Ophthalmology and Strabismus. Last modified 05/05/2020, 2020. Accessed 12.10.2020, 2020. https://www.aapos.org/glossary/toxoplasmosis.

Abi Abdallah, D. S., Lin, C., Ball, C. J., King, M. R., Duhamel, G. E., and Denkers, E. Y. *Toxoplasma gondii* Triggers Release of Human and Mouse Neutrophil Extracellular Traps. *Infect Immun* 80, no. 2 (Feb 2012): 768-77. DOI:10.1128/IAI.05730-11.

Abrahams, K. A., Cox, J. A. G., Futterer, K., Rullas, J., Ortega-Muro, F., Loman, N. J., Moynihan, P. J., Perez-Herran, E., Jimenez, E., Esquivias, J., Barros, D., Ballell, L., Alemparte, C., and Besra, G. S. Inhibiting Mycobacterial Tryptophan Synthase by Targeting the Inter-Subunit Interface. *Sci Rep* 7, no. 1 (Aug 25 2017): 9430. DOI:10.1038/s41598-017-09642-y.

Adams, L. B., Hibbs, J. B., Jr., Taintor, R. R., and Krahenbuhl, J. L. Microbiostatic Effect of Murine-Activated Macrophages for *Toxoplasma gondii*. Role for Synthesis of Inorganic Nitrogen Oxides from L-Arginine. *J Immunol* 144, no. 7 (Apr 1 1990): 2725-9. https://www.ncbi.nlm.nih.gov/pubmed/2319133.

Adams, O., Besken, K., Oberdorfer, C., MacKenzie, C. R., Takikawa, O., and Daubener, W. Role of Indoleamine-2,3-Dioxygenase in Alpha/Beta and Gamma Interferon-Mediated Antiviral Effects against Herpes Simplex Virus Infections. *J Virol* 78, no. 5 (Mar 2004): 2632-6. DOI:10.1128/jvi.78.5.2632-2636.2004.

Adl, S. M., Leander, B. S., Simpson, A. G., Archibald, J. M., Anderson, O. R., Bass, D., Bowser, S. S., Brugerolle, G., Farmer, M. A., Karpov, S., Kolisko, M., Lane, C. E., Lodge, D. J., Mann, D. G., Meisterfeld, R., Mendoza, L., Moestrup, O., Mozley-Standridge, S. E., Smirnov, A. V., and Spiegel, F. Diversity, Nomenclature, and Taxonomy of Protists. *Syst Biol* 56, no. 4 (Aug 2007): 684-9. DOI:10.1080/10635150701494127.

Agata, Y., Kawasaki, A., Nishimura, H., Ishida, Y., Tsubata, T., Yagita, H., and Honjo, T. Expression of the Pd-1 Antigen on the Surface of Stimulated Mouse T and B Lymphocytes. *Int Immunol* 8, no. 5 (May 1996): 765-72. DOI:10.1093/intimm/8.5.765.

Alaganan, A., Fentress, S. J., Tang, K., Wang, Q., and Sibley, L. D. Toxoplasma Gra7 Effector Increases Turnover of Immunity-Related Gtpases and Contributes to Acute Virulence in the Mouse. *Proc Natl Acad Sci U S A* 111, no. 3 (Jan 21 2014): 1126-31. DOI:10.1073/pnas.1313501111.

Alberati-Giani, D., Malherbe, P., Ricciardi-Castagnoli, P., Kohler, C., Denis-Donini, S., and Cesura, A. M. Differential Regulation of Indoleamine 2,3-Dioxygenase Expression by Nitric Oxide and Inflammatory Mediators in IFN-Gamma-Activated Murine Macrophages and Microglial Cells. *J Immunol* 159, no. 1 (Jul 1 1997): 419-26. https://www.ncbi.nlm.nih.gov/pubmed/9200481.

Albina, J. E., and Henry, W. L., Jr. Suppression of Lymphocyte Proliferation through the Nitric Oxide Synthesizing Pathway. *J Surg Res* 50, no. 4 (Apr 1991): 403-9. DOI:10.1016/0022-4804(91)90210-d.

Andrade, W. A., Souza Mdo, C., Ramos-Martinez, E., Nagpal, K., Dutra, M. S., Melo, M. B., Bartholomeu, D. C., Ghosh, S., Golenbock, D. T., and Gazzinelli, R. T. Combined Action of Nucleic Acid-Sensing Toll-Like Receptors and Tlr11/Tlr12 Heterodimers Imparts Resistance to *Toxoplasma gondii* in Mice. *Cell Host Microbe* 13, no. 1 (Jan 16 2013): 42-53. DOI:10.1016/j.chom.2012.12.003.

Arancibia, S. A., Beltran, C. J., Aguirre, I. M., Silva, P., Peralta, A. L., Malinarich, F., and Hermoso, M. A. Toll-Like Receptors Are Key Participants in Innate Immune Responses. *Biol Res* 40, no. 2 (2007): 97-112. DOI:10.4067/s0716-97602007000200001.

Araujo, E. F., Loures, F. V., Bazan, S. B., Feriotti, C., Pina, A., Schanoski, A. S., Costa, T. A., and Calich, V. L. Indoleamine 2,3-Dioxygenase Controls Fungal Loads and Immunity in Paracoccidioidomicosis but Is More Important to Susceptible Than Resistant Hosts. *PLoS Negl Trop Dis* 8, no. 11 (Nov 2014): e3330. DOI:10.1371/journal.pntd.0003330.

Austin, C. J., Mailu, B. M., Maghzal, G. J., Sanchez-Perez, A., Rahlfs, S., Zocher, K., Yuasa, H. J., Arthur, J. W., Becker, K., Stocker, R., Hunt, N. H., and Ball, H. J. Biochemical Characteristics and Inhibitor Selectivity of Mouse Indoleamine 2,3-Dioxygenase-2. *Amino Acids* 39, no. 2 (Jul 2010): 565-78. DOI:10.1007/s00726-010-0475-9.

Bachmann, M. F., and Oxenius, A. Interleukin 2: From Immunostimulation to Immunoregulation and Back Again. *EMBO Rep* 8, no. 12 (Dec 2007): 1142-8. DOI:10.1038/sj.embor.7401099.

Ball, H. J., Sanchez-Perez, A., Weiser, S., Austin, C. J., Astelbauer, F., Miu, J., McQuillan, J. A., Stocker, R., Jermiin, L. S., and Hunt, N. H. Characterization of an Indoleamine 2,3-Dioxygenase-Like Protein Found in Humans and Mice. *Gene* 396, no. 1 (Jul 1 2007): 203-13. DOI:10.1016/j.gene.2007.04.010.

Bando, H., Lee, Y., Sakaguchi, N., Pradipta, A., Ma, J. S., Tanaka, S., Cai, Y., Liu, J., Shen, J., Nishikawa, Y., Sasai, M., and Yamamoto, M. Inducible Nitric Oxide Synthase Is a Key Host Factor for Toxoplasma Gra15-Dependent Disruption of the Gamma Interferon-Induced Antiparasitic Human Response. *mBio* 9, no. 5 (Oct 9 2018). DOI:10.1128/mBio.01738-18.

Bando, H., Lee, Y., Sakaguchi, N., Pradipta, A., Sakamoto, R., Tanaka, S., Ma, J. S., Sasai, M., and Yamamoto, M. Toxoplasma Effector Gra15-Dependent Suppression of IFN-Gamma-Induced Antiparasitic Response in Human Neurons. *Front Cell Infect Microbiol* 9 (2019): 140. DOI:10.3389/fcimb.2019.00140.

Bando, H., Sakaguchi, N., Lee, Y., Pradipta, A., Ma, J. S., Tanaka, S., Lai, D. H., Liu, J., Lun, Z. R., Nishikawa, Y., Sasai, M., and Yamamoto, M. Toxoplasma Effector Tgist Targets Host Ido1 to Antagonize the IFN-Gamma-Induced Anti-Parasitic Response in Human Cells. *Front Immunol* 9 (2018): 2073. DOI:10.3389/fimmu.2018.02073.

Baron, M., and Davignon, J. L. Inhibition of IFN-Gamma-Induced Stat1 Tyrosine Phosphorylation by Human Cmv Is Mediated by Shp2. *J Immunol* 181, no. 8 (Oct 15 2008): 5530-6. DOI:10.4049/jimmunol.181.8.5530.

Bauer, T. M., Jiga, L. P., Chuang, J. J., Randazzo, M., Opelz, G., and Terness, P. Studying the Immunosuppressive Role of Indoleamine 2,3-Dioxygenase: Tryptophan Metabolites Suppress Rat Allogeneic T-Cell Responses *in vitro* and *in vivo*. *Transpl Int* 18, no. 1 (Jan 2005): 95-100. DOI:10.1111/j.1432-2277.2004.00031.x.

Behnke, M. S., Khan, A., Wootton, J. C., Dubey, J. P., Tang, K., and Sibley, L. D. Virulence Differences in Toxoplasma Mediated by Amplification of a Family of Polymorphic Pseudokinases. *Proc Natl Acad Sci U S A* 108, no. 23 (Jun 7 2011): 9631-6. DOI:10.1073/pnas.1015338108.

Bhadra, R., Gigley, J. P., and Khan, I. A. Cutting Edge: Cd40-Cd40 Ligand Pathway Plays a Critical Cd8-Intrinsic and -Extrinsic Role During Rescue of Exhausted Cd8 T Cells. *J Immunol* 187, no. 9 (Nov 1 2011): 4421-5. DOI:10.4049/jimmunol.1102319.

Bilzer, T., Stavrou, D., Dahme, E., Keiditsch, E., Burrig, K. F., Anzil, A. P., and Wechsler, W. Morphological, Immunocytochemical and Growth Characteristics of Three Human Glioblastomas Established *in vitro*. *Virchows Arch A Pathol Anat Histopathol* 418, no. 4 (1991): 281-93. DOI:10.1007/BF01600156.

Blume, M. and Seeber, F. Metabolic interactions between *Toxoplasma gondii* and its host [version 1; peer review: 2 approved]. *F1000Research* (2018), 7(F1000 Faculty Rev):1719. DOI:10.12688/f1000research.16021.1.

Bodaghi, B., Goureau, O., Zipeto, D., Laurent, L., Virelizier, J. L., and Michelson, S. Role of IFN-Gamma-Induced Indoleamine 2,3 Dioxygenase and Inducible Nitric Oxide Synthase in the Replication of Human Cytomegalovirus in Retinal Pigment Epithelial Cells. *J Immunol* 162, no. 2 (Jan 15 1999): 957-64. https://www.ncbi.nlm.nih.gov/pubmed/9916720.

Boehm, U., Klamp, T., Groot, M., and Howard, J. C. Cellular Responses to Interferon-Gamma. *Annu Rev Immunol* 15 (1997): 749-95. DOI:10.1146/annurev.immunol.15.1.749.

Bröer, S. and Fairweather, S.J. Amino Acid Transport Across the Mammalian Intestine. In Comprehensive Physiology, D.M. Pollock (Ed.). (Dec 13 2018):343-73. DOI:10.1002/cphy.c170041.

Braun, L., Brenier-Pinchart, M. P., Yogavel, M., Curt-Varesano, A., Curt-Bertini, R. L., Hussain, T., Kieffer-Jaquinod, S., Coute, Y., Pelloux, H., Tardieux, I., Sharma, A., Belrhali, H., Bougdour, A., and Hakimi, M. A. A Toxoplasma Dense Granule Protein, Gra24, Modulates the Early Immune Response to Infection by Promoting a Direct and Sustained Host P38 Mapk Activation. *J Exp Med* 210, no. 10 (Sep 23 2013): 2071-86. DOI:10.1084/jem.20130103.

Bromberg, J., and Darnell, J. E., Jr. The Role of Stats in Transcriptional Control and Their Impact on Cellular Function. *Oncogene* 19, no. 21 (May 15 2000): 2468-73. DOI:10.1038/sj.onc.1203476.

Burg, J. L., Grover, C. M., Pouletty, P., and Boothroyd, J. C. Direct and Sensitive Detection of a Pathogenic Protozoan, *Toxoplasma gondii*, by Polymerase Chain Reaction. *J Clin Microbiol* 27, no. 8 (Aug 1989): 1787-92. DOI:10.1128/JCM.27.8.1787-1792.1989.

Carme, B., Bissuel, F., Ajzenberg, D., Bouyne, R., Aznar, C., Demar, M., Bichat, S., Louvel, D., Bourbigot, A. M., Peneau, C., Neron, P., and Darde, M. L. Severe Acquired Toxoplasmosis in Immunocompetent Adult Patients in French Guiana. *J Clin Microbiol* 40, no. 11 (Nov 2002): 4037-44. DOI:10.1128/jcm.40.11.4037-4044.2002.

Chan, J., Siegel, J. P., and Luft, B. J. Demonstration of T-Cell Dysfunction During Acute Toxoplasma Infection. *Cell Immunol* 98, no. 2 (Apr 1 1986): 422-33. DOI:10.1016/0008-8749(86)90301-1.

Chen, C. H., Seguin-Devaux, C., Burke, N. A., Oriss, T. B., Watkins, S. C., Clipstone, N., and Ray, A. Transforming Growth Factor Beta Blocks Tec Kinase Phosphorylation, Ca2+ Influx, and Nfatc Translocation Causing Inhibition of T Cell Differentiation. *J Exp Med* 197, no. 12 (Jun 16 2003): 1689-99. DOI:10.1084/jem.20021170.

Chen, X. Q., Zhou, C. X., Elsheikha, H. M., He, S., Hu, G. X., and Zhu, X. Q. Profiling of the Perturbed Metabolomic State of Mouse Spleen During Acute and Chronic Toxoplasmosis. *Parasit Vectors* 10, no. 1 (Jul 18 2017): 339. DOI:10.1186/s13071-017-2282-6.

Chikuma, S. Ctla-4, an Essential Immune-Checkpoint for T-Cell Activation. *Curr Top Microbiol Immunol* 410 (2017): 99-126. DOI:10.1007/82_2017_61.

Chon, S. Y., Hassanain, H. H., Pine, R., and Gupta, S. L. Involvement of Two Regulatory Elements in Interferon-Gamma-Regulated Expression of Human Indoleamine 2,3-Dioxygenase Gene. *J Interferon Cytokine Res* 15, no. 6 (Jun 1995): 517-26. DOI:10.1089/jir.1995.15.517.

Chouaib, S., Welte, K., Mertelsmann, R., and Dupont, B. Prostaglandin E2 Acts at Two Distinct Pathways of T Lymphocyte Activation: Inhibition of Interleukin 2 Production and Down-Regulation of Transferrin Receptor Expression. *J Immunol* 135, no. 2 (Aug 1985): 1172-9. https://www.ncbi.nlm.nih.gov/pubmed/2989362.

Cibrian, D., and Sanchez-Madrid, F. Cd69: From Activation Marker to Metabolic Gatekeeper. *Eur J Immunol* 47, no. 6 (Jun 2017): 946-53. DOI:10.1002/eji.201646837.

Clambey, E. T., Davenport, B., Kappler, J. W., Marrack, P., and Homann, D. Molecules in Medicine Mini Review: The Alphabeta T Cell Receptor. *J Mol Med (Berl)* 92, no. 7 (Jul 2014): 735-41. DOI:10.1007/s00109-014-1145-2.

Coburn, P. S., Wiskur, B. J., Astley, R. A., and Callegan, M. C. Blood-Retinal Barrier Compromise and Endogenous *Staphylococcus aureus* Endophthalmitis. *Invest Ophthalmol Vis Sci* 56, no. 12 (Nov 2015): 7303-11. DOI:10.1167/iovs.15-17488.

Coleman, M. M., Finlay, C. M., Moran, B., Keane, J., Dunne, P. J., and Mills, K. H. The Immunoregulatory Role of Cd4(+) Foxp3(+) Cd25(-) Regulatory T Cells in Lungs of Mice Infected with Bordetella Pertussis. *FEMS Immunol Med Microbiol* 64, no. 3 (Apr 2012): 413-24. DOI:10.1111/j.1574-695X.2011.00927.x.

Collins, J. M., Siddiqa, A., Jones, D. P., Liu, K., Kempker, R. R., Nizam, A., Shah, N. S., Ismail, N., Ouma, S. G., Tukvadze, N., Li, S., Day, C. L., Rengarajan, J., Brust, J. C., Gandhi, N. R., Ernst, J. D., Blumberg, H. M., and Ziegler, T. R. Tryptophan Catabolism Reflects Disease Activity in Human Tuberculosis. *JCI Insight* 5, no. 10 (May 21 2020). DOI:10.1172/jci.insight.137131.

Cooper, C. E. Nitric Oxide and Iron Proteins. *Biochim Biophys Acta* 1411, no. 2-3 (May 5 1999): 290-309. DOI:10.1016/S0005-2728(99)00021-3.

Crawford, M. J., Thomsen-Zieger, N., Ray, M., Schachtner, J., Roos, D. S., and Seeber, F. *Toxoplasma gondii* Scavenges Host-Derived Lipoic Acid Despite Its De Novo Synthesis in the Apicoplast. *EMBO J* 25, no. 13 (Jul 12 2006): 3214-22. DOI:10.1038/sj.emboj.7601189.

Croft, M., So, T., Duan, W., and Soroosh, P. The Significance of Ox40 and Ox40l to T-Cell Biology and Immune Disease. *Immunol Rev* 229, no. 1 (May 2009): 173-91. DOI:10.1111/j.1600-065X.2009.00766.x.

Dai, X., and Zhu, B. T. Indoleamine 2,3-Dioxygenase Tissue Distribution and Cellular Localization in Mice: Implications for Its Biological Functions. *J Histochem Cytochem* 58, no. 1 (Jan 2010): 17-28. DOI:10.1369/jhc.2009.953604.

Daubener, W., Posdziech, V., Hadding, U., and MacKenzie, C. R. Inducible Anti-Parasitic Effector Mechanisms in Human Uroepithelial Cells: Tryptophan Degradation Vs. No Production. *Med Microbiol Immunol* 187, no. 3 (Mar 1999): 143-7. DOI:10.1007/s004300050086.

Daubener, W., Remscheid, C., Nockemann, S., Pilz, K., Seghrouchni, S., Mackenzie, C., and Hadding, U. Anti-Parasitic Effector Mechanisms in Human Brain Tumor Cells: Role of Interferon-Gamma and Tumor Necrosis Factor-Alpha. *Eur J Immunol* 26, no. 2 (Feb 1996): 487-92. DOI:10.1002/eji.1830260231.

Daubener, W., Spors, B., Hucke, C., Adam, R., Stins, M., Kim, K. S., and Schroten, H. Restriction of *Toxoplasma gondii* Growth in Human Brain Microvascular Endothelial Cells by Activation of Indoleamine 2,3-Dioxygenase. *Infect Immun* 69, no. 10 (Oct 2001): 6527-31. DOI:10.1128/IAI.69.10.6527-6531.2001.

Daubener, W., Wanagat, N., Pilz, K., Seghrouchni, S., Fischer, H. G., and Hadding, U. A New, Simple, Bioassay for Human IFN-Gamma. *J Immunol Methods* 168, no. 1 (Jan 12 1994): 39-47. DOI:10.1016/0022-1759(94)90207-0.

Debierre-Grockiego, F., Campos, M. A., Azzouz, N., Schmidt, J., Bieker, U., Resende, M. G., Mansur, D. S., Weingart, R., Schmidt, R. R., Golenbock, D. T., Gazzinelli, R. T., and Schwarz, R. T. Activation of Tlr2 and Tlr4 by Glycosylphosphatidylinositols Derived from *Toxoplasma gondii*. *J Immunol* 179, no. 2 (Jul 15 2007): 1129-37. DOI:10.4049/jimmunol.179.2.1129.

Degrandi, D., Konermann, C., Beuter-Gunia, C., Kresse, A., Wurthner, J., Kurig, S., Beer, S., and Pfeffer, K. Extensive Characterization of IFN-Induced Gtpases Mgbp1 to Mgbp10 Involved in Host Defense. *J Immunol* 179, no. 11 (Dec 1 2007): 7729-40. DOI:10.4049/jimmunol.179.11.7729.

Degrandi, D., Kravets, E., Konermann, C., Beuter-Gunia, C., Klumpers, V., Lahme, S., Wischmann, E., Mausberg, A. K., Beer-Hammer, S., and Pfeffer, K. Murine Guanylate Binding Protein 2 (Mgbp2) Controls *Toxoplasma gondii* Replication. *Proc Natl Acad Sci U S A* 110, no. 1 (Jan 2 2013): 294-9. DOI:10.1073/pnas.1205635110.

Denkers, E. Y., Scharton-Kersten, T., Barbieri, S., Caspar, P., and Sher, A. A Role for Cd4+ Nk1.1+ T Lymphocytes as Major Histocompatibility Complex Class Ii Independent Helper Cells in the Generation of Cd8+ Effector Function against Intracellular Infection. *J Exp Med* 184, no. 1 (Jul 1 1996): 131-9. DOI:10.1084/jem.184.1.131.

Denkers, E. Y., Yap, G., Scharton-Kersten, T., Charest, H., Butcher, B. A., Caspar, P., Heiny, S., and Sher, A. Perforin-Mediated Cytolysis Plays a Limited Role in Host Resistance to *Toxoplasma gondii*. *J Immunol* 159, no. 4 (Aug 15 1997): 1903-8. https://www.ncbi.nlm.nih.gov/pubmed/9257855.

Detrick, B., Hooks, J. J. The RPE Cell and the Immune System. In: Klettner A., Dithmar S. (eds) Retinal Pigment Epithelium in Health and Disease. *Springer*, *Cham*. (2020):101-14 DOI:10.1007/978-3-030-28384-1_6.

Dias, R. R. F., Carvalho, E. C. Q. d, Leite, C.C.dS., Tedesco, R. C., Calabrese, K. dS., Silva, A. S., DaMatta, R. A., Sarro-Silva, M. dF. *Toxoplasma gondii* Oral Infection Induces Intestinal Inflammation and Retinochoroiditis in Mice Genetically Selected for Immune Oral Tolerance Resistance. *PLOS ONE* 9, no. 12 (2014):e113374. DOI:10.1371/journal.pone.0113374.

Diaz-Godinez, C., and Carrero, J. C. The State of Art of Neutrophil Extracellular Traps in Protozoan and Helminthic Infections. *Biosci Rep* 39, no. 1 (Jan 31 2019). DOI:10.1042/BSR20180916.

Ding, A. H., Nathan, C. F., and Stuehr, D. J. Release of Reactive Nitrogen Intermediates and Reactive Oxygen Intermediates from Mouse Peritoneal Macrophages. Comparison of Activating Cytokines and Evidence for Independent Production. *J Immunol* 141, no. 7 (Oct 1 1988): 2407-12. https://www.ncbi.nlm.nih.gov/pubmed/3139757.

Divanovic, S., Sawtell, N. M., Trompette, A., Warning, J. I., Dias, A., Cooper, A. M., Yap, G. S., Arditi, M., Shimada, K., Duhadaway, J. B., Prendergast, G. C., Basaraba, R. J., Mellor, A. L., Munn, D. H., Aliberti, J., and Karp, C. L. Opposing Biological Functions of Tryptophan Catabolizing Enzymes During Intracellular Infection. *J Infect Dis* 205, no. 1 (Jan 1 2012): 152-61. DOI:10.1093/infdis/jir621.

Driehuis, E., van Hoeck, A., Moore, K., Kolders, S., Francies, H. E., Gulersonmez, M. C., Stigter, E. C. A., Burgering, B., Geurts, V., Gracanin, A., Bounova, G., Morsink, F. H., Vries, R., Boj, S., van Es, J., Offerhaus, G. J. A., Kranenburg, O., Garnett, M. J., Wessels, L., Cuppen, E., Brosens, L. A. A., and Clevers, H. Pancreatic Cancer Organoids Recapitulate Disease and Allow Personalized Drug Screening. *Proc Natl Acad Sci U S A* (Dec 9 2019). DOI:10.1073/pnas.1911273116.

Dubey, J. P. History of the Discovery of the Life Cycle of *Toxoplasma gondii*. *Int J Parasitol* 39, no. 8 (Jul 1 2009a): 877-82. DOI:10.1016/j.ijpara.2009.01.005.

Dubey, J. P. *Toxoplasmosis of Animals and Humans*. 2nd New edition. Boca Raton, FL.: CRC Press Inc., 2009b.

Dubey, J. P., Lindsay, D. S., and Speer, C. A. Structures of *Toxoplasma gondii* Tachyzoites, Bradyzoites, and Sporozoites and Biology and Development of Tissue Cysts. *Clin Microbiol Rev* 11, no. 2 (Apr 1998): 267-99. DOI:10.1128/CMR.11.2.267.

Dubey, J. P., Miller, N. L., and Frenkel, J. K. The *Toxoplasma gondii* Oocyst from Cat Feces. *J Exp Med* 132, no. 4 (Oct 1 1970): 636-62. DOI:10.1084/jem.132.4.636.

Eleftheriadis, T., Pissas, G., Antoniadi, G., Spanoulis, A., Liakopoulos, V., and Stefanidis, I. Indoleamine 2,3-Dioxygenase Increases P53 Levels in Alloreactive Human T Cells, and Both Indoleamine 2,3-Dioxygenase and P53 Suppress Glucose Uptake, Glycolysis and Proliferation. *Int Immunol* 26, no. 12 (Dec 2014): 673-84. DOI:10.1093/intimm/dxu077.

Etheridge, R. D., Alaganan, A., Tang, K., Lou, H. J., Turk, B. E., and Sibley, L. D. The Toxoplasma Pseudokinase Rop5 Forms Complexes with Rop18 and Rop17 Kinases That Synergize to Control Acute Virulence in Mice. *Cell Host Microbe* 15, no. 5 (May 14 2014): 537-50. DOI:10.1016/j.chom.2014.04.002.

Ewald, S. E., Chavarria-Smith, J., and Boothroyd, J. C. Nlrp1 Is an Inflammasome Sensor for *Toxoplasma gondii*. *Infect Immun* 82, no. 1 (Jan 2014): 460-8. DOI:10.1128/IAI.01170-13.

Fallarino, F., Grohmann, U., Hwang, K. W., Orabona, C., Vacca, C., Bianchi, R., Belladonna, M. L., Fioretti, M. C., Alegre, M. L., and Puccetti, P. Modulation of Tryptophan Catabolism by Regulatory T Cells. *Nat Immunol* 4, no. 12 (Dec 2003): 1206-12. DOI:10.1038/ni1003.

Fallarino, F., Grohmann, U., Vacca, C., Bianchi, R., Orabona, C., Spreca, A., Fioretti, M. C., and Puccetti, P. T Cell Apoptosis by Tryptophan Catabolism. *Cell Death Differ* 9, no. 10 (Oct 2002): 1069-77. DOI:10.1038/sj.cdd.4401073.

Fisch, D., Bando, H., Clough, B., Hornung, V., Yamamoto, M., Shenoy, A. R., and Frickel, E. M. Human Gbp1 Is a Microbe-Specific Gatekeeper of Macrophage Apoptosis and Pyroptosis. *EMBO J* 38, no. 13 (Jul 1 2019): e100926. DOI:10.15252/embj.2018100926.

Fontenot, J. D., Gavin, M. A., and Rudensky, A. Y. Foxp3 Programs the Development and Function of Cd4+Cd25+ Regulatory T Cells. *Nat Immunol* 4, no. 4 (Apr 2003): 330-6. DOI:10.1038/ni904.

Forstermann, U., Boissel, J. P., and Kleinert, H. Expressional Control of the 'Constitutive' Isoforms of Nitric Oxide Synthase (Nos I and Nos Iii). *FASEB J* 12, no. 10 (Jul 1998): 773-90. DOI:10.1096/fasebj.12.10.773.

Fox, B. A., Gigley, J. P., and Bzik, D. J. *Toxoplasma gondii* Lacks the Enzymes Required for De Novo Arginine Biosynthesis and Arginine Starvation Triggers Cyst Formation. *Int J Parasitol* 34, no. 3 (Mar 9 2004): 323-31. DOI:10.1016/j.ijpara.2003.12.001.

Fujigaki, S., Saito, K., Takemura, M., Maekawa, N., Yamada, Y., Wada, H., and Seishima, M. L-Tryptophan-L-Kynurenine Pathway Metabolism Accelerated by *Toxoplasma gondii* Infection Is Abolished in Gamma Interferon-Gene-Deficient Mice: Cross-Regulation between Inducible Nitric Oxide Synthase and Indoleamine-2,3-Dioxygenase. *Infect Immun* 70, no. 2 (Feb 2002): 779-86. DOI:10.1128/iai.70.2.779-786.2002.

Fukunaga, M., Yamamoto, Y., Kawasoe, M., Arioka, Y., Murakami, Y., Hoshi, M., and Saito, K. Studies on Tissue and Cellular Distribution of Indoleamine 2,3-Dioxygenase 2: The Absence of Ido1 Upregulates Ido2 Expression in the Epididymis. *J Histochem Cytochem* 60, no. 11 (Nov 2012): 854-60. DOI:10.1369/0022155412458926.

Gautam, U. S., Foreman, T. W., Bucsan, A. N., Veatch, A. V., Alvarez, X., Adekambi, T., Golden, N. A., Gentry, K. M., Doyle-Meyers, L. A., Russell-Lodrigue, K. E., Didier, P. J., Blanchard, J. L., Kousoulas, K. G., Lackner, A. A., Kalman, D., Rengarajan, J., Khader, S. A., Kaushal, D., and Mehra, S. *In vivo* Inhibition of Tryptophan Catabolism Reorganizes the Tuberculoma and Augments Immune-Mediated Control of *Mycobacterium tuberculosis*. *Proc Natl Acad Sci U S A* 115, no. 1 (Jan 2 2018): E62-E71. DOI:10.1073/pnas.1711373114.

Gay, G., Braun, L., Brenier-Pinchart, M. P., Vollaire, J., Josserand, V., Bertini, R. L., Varesano, A., Touquet, B., De Bock, P. J., Coute, Y., Tardieux, I., Bougdour, A., and Hakimi, M. A. *Toxoplasma gondii* Tgist Co-Opts Host Chromatin Repressors Dampening Stat1-Dependent Gene Regulation and IFN-Gamma-Mediated Host Defenses. *J Exp Med* 213, no. 9 (Aug 22 2016): 1779-98. DOI:10.1084/jem.20160340.

Gazzinelli, R. T., Hieny, S., Wynn, T. A., Wolf, S., and Sher, A. Interleukin 12 Is Required for the T-Lymphocyte-Independent Induction of Interferon Gamma by an Intracellular Parasite and Induces Resistance in T-Cell-Deficient Hosts. *Proc Natl Acad Sci U S A* 90, no. 13 (Jul 1 1993): 6115-9. DOI:10.1073/pnas.90.13.6115.

Gazzinelli, R. T., Mendonca-Neto, R., Lilue, J., Howard, J., and Sher, A. Innate Resistance against *Toxoplasma gondii*: An Evolutionary Tale of Mice, Cats, and Men. *Cell Host Microbe* 15, no. 2 (Feb 12 2014): 132-8. DOI:10.1016/j.chom.2014.01.004.

Gazzinelli, R. T., Wysocka, M., Hayashi, S., Denkers, E. Y., Hieny, S., Caspar, P., Trinchieri, G., and Sher, A. Parasite-Induced Il-12 Stimulates Early IFN-Gamma Synthesis and Resistance During Acute Infection with *Toxoplasma gondii*. *J Immunol* 153, no. 6 (Sep 15 1994): 2533-43. https://www.ncbi.nlm.nih.gov/pubmed/7915739.

Gillis, S., and Smith, K. A. Long Term Culture of Tumour-Specific Cytotoxic T Cells. *Nature* 268, no. 5616 (Jul 14 1977): 154-6. DOI:10.1038/268154a0.

Goldman, M., Carver, R. K., and Sulzer, A. J. Reproduction of *Toxoplasma gondii* by Internal Budding. *J Parasitol* 44, no. 2 (Apr 1958): 161-71. https://www.ncbi.nlm.nih.gov/pubmed/13539708.

Golubovskaya, V., and Wu, L. Different Subsets of T Cells, Memory, Effector Functions, and Car-T Immunotherapy. *Cancers (Basel)* 8, no. 3 (Mar 15 2016). DOI:10.3390/cancers8030036.

Gorfu, G., Cirelli, K. M., Melo, M. B., Mayer-Barber, K., Crown, D., Koller, B. H., Masters, S., Sher, A., Leppla, S. H., Moayeri, M., Saeij, J. P., and Grigg, M. E. Dual Role for Inflammasome Sensors Nlrp1 and Nlrp3 in Murine Resistance to *Toxoplasma gondii*. *mBio* 5, no. 1 (Feb 18 2014). DOI:10.1128/mBio.01117-13.

Goureau, O., Hicks, D., Courtois, Y. Human retinal pigmented epithelial cells produce nitric oxide in response to cytokines. *Biochem Biophys Res Commun*. 198 (Jan 14 1994):120–6. DOI:10.1006/bbrc.1994.1017.

Gov, L., Schneider, C. A., Lima, T. S., Pandori, W., and Lodoen, M. B. Nlrp3 and Potassium Efflux Drive Rapid Il-1beta Release from Primary Human Monocytes During *Toxoplasma gondii* Infection. *J Immunol* 199, no. 8 (Oct 15 2017): 2855-64. DOI:10.4049/jimmunol.1700245.

Grohmann, U., Fallarino, F., and Puccetti, P. Tolerance, Dcs and Tryptophan: Much Ado About Ido. *Trends Immunol* 24, no. 5 (May 2003): 242-8. DOI:10.1016/s1471-4906(03)00072-3.

Halonen, S. K., Chiu, F.-C., Weiss, L. M. Effect of Cytokines on Growth of *Toxoplasma gondii* in Murine Astrocytes. *Infect Immun* 66, no.10 (Oct 1998): 4989-93. DOI:10.1128/IAI.66.10.4989-4993.1998.

Han, Y., Duan, X., Yang, L., Nilsson-Payant, B. E., Wang, P., Duan, F., Tang, X., Yaron, T. M., Zhang, T., Uhl, S., Bram, Y., Richardson, C., Zhu, J., Zhao, Z., Redmond, D., Houghton, S., Nguyen, D. T., Xu, D., Wang, X., Jessurun, J., Borczuk, A., Huang, Y., Johnson, J. L., Liu, Y., Xiang, J., Wang, H., Cantley, L. C., tenOever, B. R., Ho, D. D., Pan, F. C., Evans, T., Chen, H. J., Schwartz, R. E., and Chen, S. Identification of Sars-Cov-2 Inhibitors Using Lung and Colonic Organoids. *Nature* 589, no. 7841 (Jan 2021): 270-75. DOI:10.1038/s41586-020-2901-9.

Hansen, A. M., Driussi, C., Turner, V., Takikawa, O., and Hunt, N. H. Tissue Distribution of Indoleamine 2,3-Dioxygenase in Normal and Malaria-Infected Tissue. *Redox Rep* 5, no. 2-3 (2000): 112-5. DOI:10.1179/135100000101535384.

Haque, S., Khan, I., Haque, A., and Kasper, L. Impairment of the Cellular Immune Response in Acute Murine Toxoplasmosis: Regulation of Interleukin 2 Production and Macrophage-Mediated Inhibitory Effects. *Infect Immun* 62, no. 7 (Jul 1994): 2908-16. DOI:10.1128/IAI.62.7.2908-2916.1994.

Hatter, J. A., Kouche, Y. M., Melchor, S. J., Ng, K., Bouley, D. M., Boothroyd, J. C., Ewald, S. E. *Toxoplasma gondii* infection triggers chronic cachexia and sustained commensal dysbiosis in mice. *PLOS ONE* 13, no. 10 (Oct 31 2018): e0204895. DOI:10.1371/journal.pone.0204895.

Hayashi, T., Beck, L., Rossetto, C., Gong, X., Takikawa, O., Takabayashi, K., Broide, D. H., Carson, D. A., and Raz, E. Inhibition of Experimental Asthma by Indoleamine 2,3-Dioxygenase. *J Clin Invest* 114, no. 2 (Jul 2004): 270-9. DOI:10.1172/JCI21275.

Heseler, K., Spekker, K., Schmidt, S. K., MacKenzie, C. R., and Daubener, W. Antimicrobial and Immunoregulatory Effects Mediated by Human Lung Cells: Role of IFN-Gamma-Induced Tryptophan Degradation. *FEMS Immunol Med Microbiol* 52, no. 2 (Mar 2008): 273-81. DOI:10.1111/j.1574-695X.2007.00374.x.

Hofer, M., and Lutolf, M. P. Engineering Organoids. *Nat Rev Mater* (Feb 19 2021): 1-19. DOI:10.1038/s41578-021-00279-y.

Holthaus, D., Delgado-Betancourt, E., Aebischer, T., Seeber, F., and Klotz, C. Harmonization of Protocols for Multi-Species Organoid Platforms to Study the Intestinal Biology of *Toxoplasma gondii* and Other Protozoan Infections. *Front Cell Infect Microbiol* 10 (2020): 610368. DOI:10.3389/fcimb.2020.610368.

Hori, S., Nomura, T., and Sakaguchi, S. Control of Regulatory T Cell Development by the Transcription Factor Foxp3. *Science* 299, no. 5609 (Feb 14 2003): 1057-61. DOI:10.1126/science.1079490.

Howe, D. K., and Sibley, L. D. *Toxoplasma gondii* Comprises Three Clonal Lineages: Correlation of Parasite Genotype with Human Disease. *J Infect Dis* 172, no. 6 (Dec 1995): 1561-6. DOI:10.1093/infdis/172.6.1561.

Hucke, C., MacKenzie, C. R., Adjogble, K. D., Takikawa, O., and Daubener, W. Nitric Oxide-Mediated Regulation of Gamma Interferon-Induced Bacteriostasis: Inhibition and Degradation of Human Indoleamine 2,3-Dioxygenase. *Infect Immun* 72, no. 5 (May 2004): 2723-30. DOI:10.1128/iai.72.5.2723-2730.2004.

Hunn, J. P., Feng, C. G., Sher, A., and Howard, J. C. The Immunity-Related Gtpases in Mammals: A Fast-Evolving Cell-Autonomous Resistance System against Intracellular Pathogens. *Mamm Genome* 22, no. 1-2 (Feb 2011): 43-54. DOI:10.1007/s00335-010-9293-3.

Hunn, J. P., Koenen-Waisman, S., Papic, N., Schroeder, N., Pawlowski, N., Lange, R., Kaiser, F., Zerrahn, J., Martens, S., and Howard, J. C. Regulatory Interactions between Irg Resistance Gtpases in the Cellular Response to *Toxoplasma gondii*. *EMBO J* 27, no. 19 (Oct 8 2008): 2495-509. DOI:10.1038/emboj.2008.176.

Hunter, C. A., Subauste, C. S., Van Cleave, V. H., and Remington, J. S. Production of Gamma Interferon by Natural Killer Cells from *Toxoplasma gondii*-Infected Scid Mice: Regulation by Interleukin-10, Interleukin-12, and Tumor Necrosis Factor Alpha. *Infect Immun* 62, no. 7 (Jul 1994): 2818-24. DOI:10.1128/IAI.62.7.2818-2824.1994.

Jackson, M. H., and Hutchison, W. M. The Prevalence and Source of Toxoplasma Infection in the Environment. *Adv Parasitol* 28 (1989): 55-105. DOI:10.1016/s0065-308x(08)60331-0.

Jakob, E., Reuland, M. S., Mackensen, F., Harsch, N., Fleckenstein, M., Lorenz, H. M., Max, R., and Becker, M. D. Uveitis Subtypes in a German Interdisciplinary Uveitis Center--Analysis of 1916 Patients. *J Rheumatol* 36, no. 1 (Jan 2009): 127-36. DOI:10.3899/jrheum.080102.

Jehangir, W., Sareen, R., Sen, S., Raoof, N., and Yousif, A. Acute Confusional State: A Manifestation of Toxoplasma and Cmv Co-Infection in Hiv Patient. *N Am J Med Sci* 6, no. 10 (Oct 2014): 545-8. DOI:10.4103/1947-2714.143290.

Jennifer, B., Berg, V., Modak, M., Puck, A., Seyerl-Jiresch, M., Kunig, S., Zlabinger, G. J., Steinberger, P., Chou, J., Geha, R. S., Ohler, L., Yachie, A., Choe, H., Kraller, M., Stockinger, H., and Stockl, J. Transferrin Receptor 1 Is a Cellular Receptor for Human Heme-Albumin. *Commun Biol* 3, no. 1 (Oct 27 2020): 621. DOI:10.1038/s42003-020-01294-5.

Johnston, A. C., Piro, A., Clough, B., Siew, M., Virreira Winter, S., Coers, J., and Frickel, E. M. Human Gbp1 Does Not Localize to Pathogen Vacuoles but Restricts *Toxoplasma gondii*. *Cell Microbiol* 18, no. 8 (Aug 2016): 1056-64. DOI:10.1111/cmi.12579.

Khan, A., Dubey, J. P., Su, C., Ajioka, J. W., Rosenthal, B. M., and Sibley, L. D. Genetic Analyses of Atypical *Toxoplasma gondii* Strains Reveal a Fourth Clonal Lineage in North America. *Int J Parasitol* 41, no. 6 (May 2011): 645-55. DOI:10.1016/j.ijpara.2011.01.005.

Khan, I. A., Hwang, S., and Moretto, M. *Toxoplasma gondii*: Cd8 T Cells Cry for Cd4 Help. *Front Cell Infect Microbiol* 9 (2019): 136. DOI:10.3389/fcimb.2019.00136.

Khan, I. A., Matsuura, T., and Kasper, L. H. Activation-Mediated Cd4+ T Cell Unresponsiveness During Acute *Toxoplasma gondii* Infection in Mice. *Int Immunol* 8, no. 6 (Jun 1996): 887-96. DOI:10.1093/intimm/8.6.887.

Khan, I. A., Murphy, P. M., Casciotti, L., Schwartzman, J. D., Collins, J., Gao, J. L., and Yeaman, G. R. Mice Lacking the Chemokine Receptor Ccr1 Show Increased Susceptibility to *Toxoplasma gondii* Infection. *J Immunol* 166, no. 3 (Feb 1 2001): 1930-7. DOI:10.4049/jimmunol.166.3.1930.

Khan, I. A., Schwartzman, J. D., Matsuura, T., and Kasper, L. H. A Dichotomous Role for Nitric Oxide During Acute *Toxoplasma gondii* Infection in Mice. *Proc Natl Acad Sci U S A* 94, no. 25 (Dec 9 1997): 13955-60. DOI:10.1073/pnas.94.25.13955.

Khan, I. A., Thomas, S. Y., Moretto, M. M., Lee, F. S., Islam, S. A., Combe, C., Schwartzman, J. D., and Luster, A. D. Ccr5 Is Essential for Nk Cell Trafficking and Host Survival Following *Toxoplasma gondii* Infection. *PLoS Pathog* 2, no. 6 (Jun 2006): e49. DOI:10.1371/journal.ppat.0020049.

Kim, B. H., Chee, J. D., Bradfield, C. J., Park, E. S., Kumar, P., MacMicking J. D. Interferon-induced guanylate-binding proteins in inflammasome activation and host defense. *Nat Immunol* 17 (May 2016a):481–9. DOI:10.1038/ni.3440.

Kim, E. W., Nadipuram, S. M., Tetlow, A. L., Barshop, W. D., Liu, P. T., Wohlschlegel, J. A., and Bradley, P. J. The Rhoptry Pseudokinase Rop54 Modulates *Toxoplasma gondii* Virulence and Host Gbp2 Loading. *mSphere* 1, no. 2 (Mar-Apr 2016b). DOI:10.1128/mSphere.00045-16.

Knox, W. E. The Regulation of Tryptophan Pyrrolase Activity by Tryptophan. *Adv Enzyme Regul* 4 (1966): 287-97. DOI:10.1016/0065-2571(66)90023-9.

Knubel, C. P., Martinez, F. F., Fretes, R. E., Diaz Lujan, C., Theumer, M. G., Cervi, L., and Motran, C. C. Indoleamine 2,3-Dioxigenase (Ido) Is Critical for Host Resistance against *Trypanosoma cruzi*. *FASEB J* 24, no. 8 (Aug 2010): 2689-701. DOI:10.1096/fj.09-150920.

Le, V. T. K., Trilling, M., Wilborn, M., Hengel, H., and Zimmermann, A. Human Cytomegalovirus Interferes with Signal Transducer and Activator of Transcription (Stat) 2 Protein Stability and Tyrosine Phosphorylation. *J Gen Virol* 89, no. Pt 10 (Oct 2008): 2416-26. DOI:10.1099/vir.0.2008/001669-0.

Lee, S. M., Lee, Y. S., Choi, J. H., Park, S. G., Choi, I. W., Joo, Y. D., Lee, W. S., Lee, J. N., Choi, I., and Seo, S. K. Tryptophan Metabolite 3-Hydroxyanthranilic Acid Selectively Induces Activated T Cell Death Via Intracellular Gsh Depletion. *Immunol Lett* 132, no. 1-2 (Aug 16 2010): 53-60. DOI:10.1016/j.imlet.2010.05.008.

Lee, S. M., Park, H. Y., Suh, Y. S., Yoon, E. H., Kim, J., Jang, W. H., Lee, W. S., Park, S. G., Choi, I. W., Choi, I., Kang, S. W., Yun, H., Teshima, T., Kwon, B., and Seo, S. K. Inhibition of Acute Lethal Pulmonary Inflammation by the Ido-Ahr Pathway. *Proc Natl Acad Sci U S A* 114, no. 29 (Jul 18 2017): E5881-E90. DOI:10.1073/pnas.1615280114.

Legewie, L., Loschwitz, J., Steffens, N., Prescher, M., Wang, X., Smits, S. H. J., Schmitt, L., Strodel, B., Degrandi, D., and Pfeffer, K. Biochemical and Structural Characterization of Murine Gbp7, a Guanylate Binding Protein with an Elongated C-Terminal Tail. *Biochem J* 476, no. 21 (Nov 15 2019): 3161-82. DOI:10.1042/BCJ20190364.

Lekutis, C., Ferguson, D. J., and Boothroyd, J. C. *Toxoplasma gondii*: Identification of a Developmentally Regulated Family of Genes Related to Sag2. *Exp Parasitol* 96, no. 2 (Oct 2000): 89-96. DOI:10.1006/expr.2000.4556.

Leonhardt, R. M., Lee, S. J., Kavathas, P. B., and Cresswell, P. Severe Tryptophan Starvation Blocks Onset of Conventional Persistence and Reduces Reactivation of *Chlamydia trachomatis*. *Infect Immun* 75, no. 11 (Nov 2007): 5105-17. DOI:10.1128/IAI.00668-07.

Liao, W., Lin, J. X., and Leonard, W. J. Il-2 Family Cytokines: New Insights into the Complex Roles of Il-2 as a Broad Regulator of T Helper Cell Differentiation. *Curr Opin Immunol* 23, no. 5 (Oct 2011): 598-604. DOI:10.1016/j.coi.2011.08.003.

Lieberman, L. A., Banica, M., Reiner, S. L., and Hunter, C. A. Stat1 Plays a Critical Role in the Regulation of Antimicrobial Effector Mechanisms, but Not in the Development of Th1-Type Responses During Toxoplasmosis. *J Immunol* 172, no. 1 (Jan 1 2004): 457-63. DOI:10.4049/jimmunol.172.1.457.

Lilue, J., Muller, U. B., Steinfeldt, T., and Howard, J. C. Reciprocal Virulence and Resistance Polymorphism in the Relationship between *Toxoplasma gondii* and the House Mouse. *Elife* 2 (Oct 29 2013): e01298. DOI:10.7554/eLife.01298.

Lippens, C., Duraes, F. V., Dubrot, J., Brighouse, D., Lacroix, M., Irla, M., Aubry-Lachainaye, J. P., Reith, W., Mandl, J. N., and Hugues, S. Ido-Orchestrated Crosstalk between Pdcs and Tregs Inhibits Autoimmunity. *J Autoimmun* 75 (Dec 2016): 39-49. DOI:10.1016/j.jaut.2016.07.004.

Liversidge, J., McKay, D., Mullen, G., and Forrester, J. V. Retinal Pigment Epithelial Cells Modulate Lymphocyte Function at the Blood-Retina Barrier by Autocrine Pge2 and Membrane-Bound Mechanisms. *Cell Immunol* 149, no. 2 (Jul 1993): 315-30. DOI:10.1006/cimm.1993.1158.

Lob, S., Konigsrainer, A., Rammensee, H. G., Opelz, G., and Terness, P. Inhibitors of Indoleamine-2,3-Dioxygenase for Cancer Therapy: Can We See the Wood for the Trees? , *Nat Rev Cancer* 9, no. 6 (Jun 2009): 445-52. DOI:10.1038/nrc2639.

Lopez-Yglesias, A. H., Camanzo, E., Martin, A. T., Araujo, A. M., and Yarovinsky, F. Tlr11-Independent Inflammasome Activation Is Critical for Cd4+ T Cell-Derived IFN-Gamma Production and Host Resistance to *Toxoplasma gondii*. *PLoS Pathog* 15, no. 6 (Jun 2019): e1007872. DOI:10.1371/journal.ppat.1007872.

Loughman, J. A., and Hunstad, D. A. Induction of Indoleamine 2,3-Dioxygenase by Uropathogenic Bacteria Attenuates Innate Responses to Epithelial Infection. *J Infect Dis* 205, no. 12 (Jun 15 2012): 1830-9. DOI:10.1093/infdis/jis280.

Luder, C. G. K., and Rahman, T. Impact of the Host on Toxoplasma Stage Differentiation. *Microb Cell* 4, no. 7 (Jun 22 2017): 203-11. DOI:10.15698/mic2017.07.579.

Luft, B. J., Conley, F., Remington, J. S., Laverdiere, M., Wagner, K. F., Levine, J. F., Craven, P. C., Strandberg, D. A., File, T. M., Rice, N., and Meunier-Carpentier, F. Outbreak of Central-Nervous-System Toxoplasmosis in Western Europe and North America. *Lancet* 1, no. 8328 (Apr 9 1983): 781-4. DOI:10.1016/s0140-6736(83)91847-0.

Lunde, M. N., and Jacobs, L. Antigenic Differences between Endozoites and Cystozoites of *Toxoplasma gondii*. *J Parasitol* 69, no. 5 (Oct 1983): 806-8. DOI:10.2307/3281034.

Macedo, M. F., de Sousa, M., Ned, R. M., Mascarenhas, C., Andrews, N. C., and Correia-Neves, M. Transferrin Is Required for Early T-Cell Differentiation. *Immunology* 112, no. 4 (Aug 2004): 543-9. DOI:10.1111/j.1365-2567.2004.01915.x.

MacKenzie, C. R., Hadding, U., and Daubener, W. Interferon-Gamma-Induced Activation of Indoleamine 2,3-Dioxygenase in Cord Blood Monocyte-Derived Macrophages Inhibits the Growth of Group B Streptococci. *J Infect Dis* 178, no. 3 (Sep 1998): 875-8. DOI:10.1086/515347.

MacMicking, J. D. Interferon-Inducible Effector Mechanisms in Cell-Autonomous Immunity. *Nat Rev Immunol* 12, no. 5 (Apr 25 2012): 367-82. DOI:10.1038/nri3210.

Maenz, M., Schluter, D., Liesenfeld, O., Schares, G., Gross, U., and Pleyer, U. Ocular Toxoplasmosis Past, Present and New Aspects of an Old Disease. *Prog Retin Eye Res* 39 (Mar 2014): 77-106. DOI:10.1016/j.preteyeres.2013.12.005.

Majumdar, T., Sharma, S., Kumar, M., Hussain, M. A., Chauhan, N., Kalia, I., Sahu, A. K., Rana, V. S., Bharti, R., Haldar, A. K., Singh, A. P., and Mazumder, S. Tryptophan-Kynurenine Pathway Attenuates Beta-Catenin-Dependent Pro-Parasitic Role of Sting-Ticam2-Irf3-Ido1 Signalosome in *Toxoplasma gondii* Infection. *Cell Death Dis* 10, no. 3 (Feb 15 2019): 161. DOI:10.1038/s41419-019-1420-9.

Martens, S., Parvanova, I., Zerrahn, J., Griffiths, G., Schell, G., Reichmann, G., and Howard, J. C. Disruption of *Toxoplasma gondii* Parasitophorous Vacuoles by the Mouse P47-Resistance Gtpases. *PLoS Pathog* 1, no. 3 (Nov 2005): e24. DOI:10.1371/journal.ppat.0010024.

Martorelli Di Genova, B., Wilson, S. K., Dubey, J. P., and Knoll, L. J. Intestinal Delta-6-Desaturase Activity Determines Host Range for Toxoplasma Sexual Reproduction. *PLoS Biol* 17, no. 8 (Aug 2019): e3000364. DOI:10.1371/journal.pbio.3000364.

McAuley, J., Boyer, K. M., Patel, D., Mets, M., Swisher, C., Roizen, N., Wolters, C., Stein, L., Stein, M., Schey, W., and *et al.* Early and Longitudinal Evaluations of Treated Infants and Children and Untreated Historical Patients with Congenital Toxoplasmosis: The Chicago Collaborative Treatment Trial. *Clin Infect Dis* 18, no. 1 (Jan 1994): 38-72. DOI:10.1093/clinids/18.1.38.

Mehta, S. J., Miller, R. D., Ramirez, J. A., and Summersgill, J. T. Inhibition of *Chlamydia pneumoniae* Replication in Hep-2 Cells by Interferon-Gamma: Role of Tryptophan Catabolism. *J Infect Dis* 177, no. 5 (May 1998): 1326-31. DOI:10.1086/515287.

Meisel, R., Brockers, S., Heseler, K., Degistirici, Ö., Bülle, H., Woite, E., Stuhlsatz, S., Schwippert, W., Jäger, M., Sorg, R., Henschler, R., Seissler, J., Dilloo, D., Däubener, W. Human but not murine multipotent mesenchymal stromal cells exhibit broad-spectrum antimicrobial effector function mediated by indoleamine 2,3-dioxygenase. *Leukemia* 25, (2011): 648–54. DOI:10.1038/leu.2010.310.

Melchor, S. J., Hatter, J. A., Castillo, É. A. L., Saunders, C. M., Byrnes, K. A., Sanders, I., Abebayehu, D., Barker, T. H., Ewald, S. E. *T. gondii* infection induces IL-1R dependent chronic cachexia and perivascular fibrosis in the liver and skeletal muscle. *Sci Rep* 10, (2020):15724. DOI:10.1038/s41598-020-72767-0.

Melendez-Munoz, R., Marchalik, R., Jerussi, T., Dimitrova, D., Nussenblatt, V., Beri, A., Rai, K., Wilder, J. S., Barrett, A. J., Battiwalla, M., Childs, R. W., Fitzhugh, C. D., Fowler, D. H., Fry, T. J., Gress, R. E., Hsieh, M. M., Ito, S., Kang, E. M., Pavletic, S. Z., Shah, N. N., Tisdale, J. F., Gea-Banacloche, J., Kanakry, C. G., and Kanakry, J. A. Cytomegalovirus Infection Incidence and Risk Factors across Diverse Hematopoietic Cell Transplantation Platforms Using a Standardized Monitoring and Treatment Approach: A Comprehensive Evaluation from a Single Institution. *Biol Blood Marrow Transplant* 25, no. 3 (Mar 2019): 577-86. DOI:10.1016/j.bbmt.2018.10.011.

Mellor, A. L., Baban, B., Chandler, P., Marshall, B., Jhaver, K., Hansen, A., Koni, P. A., Iwashima, M., and Munn, D. H. Cutting Edge: Induced Indoleamine 2,3 Dioxygenase Expression in Dendritic Cell Subsets Suppresses T Cell Clonal Expansion. *J Immunol* 171, no. 4 (Aug 15 2003): 1652-5. DOI:10.4049/jimmunol.171.4.1652.

Mellor, A. L., and Munn, D. H. Ido Expression by Dendritic Cells: Tolerance and Tryptophan Catabolism. *Nat Rev Immunol* 4, no. 10 (Oct 2004): 762-74. DOI:10.1038/nri1457.

Mellor, A. L., and Munn, D. H. Tryptophan Catabolism and T-Cell Tolerance: Immunosuppression by Starvation? , *Immunol Today* 20, no. 10 (Oct 1999): 469-73. DOI:10.1016/s0167-5699(99)01520-0.

Miller, D. M., Rahill, B. M., Boss, J. M., Lairmore, M. D., Durbin, J. E., Waldman, J. W., and Sedmak, D. D. Human Cytomegalovirus Inhibits Major Histocompatibility Complex Class Ii Expression by Disruption of the Jak/Stat Pathway. *J Exp Med* 187, no. 5 (Mar 2 1998): 675-83. DOI:10.1084/jem.187.5.675.

Miyajima, M., Zhang, B., Sugiura, Y., Sonomura, K., Guerrini, M. M., Tsutsui, Y., Maruya, M., Vogelzang, A., Chamoto, K., Honda, K., Hikida, T., Ito, S., Qin, H., Sanuki, R., Suzuki, K., Furukawa, T., Ishihama, Y., Matsuda, F., Suematsu, M., Honjo, T., and Fagarasan, S. Metabolic Shift Induced by Systemic Activation of T Cells in Pd-1-Deficient Mice Perturbs Brain Monoamines and Emotional Behavior. *Nat Immunol* 18, no. 12 (Dec 2017): 1342-52. DOI:10.1038/ni.3867.

Mogensen, T. H. Pathogen Recognition and Inflammatory Signaling in Innate Immune Defenses. *Clin Microbiol Rev* 22, no. 2 (Apr 2009): 240-73, Table of Contents. DOI:10.1128/CMR.00046-08.

Montoya, J. G., and Liesenfeld, O. Toxoplasmosis. *Lancet* 363, no. 9425 (Jun 12 2004): 1965-76. DOI:10.1016/S0140-6736(04)16412-X.

Mordue, D. G., Monroy, F., La Regina, M., Dinarello, C. A., and Sibley, L. D. Acute Toxoplasmosis Leads to Lethal Overproduction of Th1 Cytokines. *J Immunol* 167, no. 8 (Oct 15 2001): 4574-84. DOI:10.4049/jimmunol.167.8.4574.

Mukhopadhyay, D., Arranz-Solis, D., and Saeij, J. P. J. Influence of the Host and Parasite Strain on the Immune Response During Toxoplasma Infection. *Front Cell Infect Microbiol* 10 (2020): 580425. DOI:10.3389/fcimb.2020.580425.

Mullen, A. C., High, F. A., Hutchins, A. S., Lee, H. W., Villarino, A. V., Livingston, D. M., Kung, A. L., Cereb, N., Yao, T. P., Yang, S. Y., and Reiner, S. L. Role of T-Bet in Commitment of Th1 Cells before Il-12-Dependent Selection. *Science* 292, no. 5523 (Jun 8 2001): 1907-10. DOI:10.1126/science.1059835.

Munn, D. H., Shafizadeh, E., Attwood, J. T., Bondarev, I., Pashine, A., and Mellor, A. L. Inhibition of T Cell Proliferation by Macrophage Tryptophan Catabolism. *J Exp Med* 189, no. 9 (May 3 1999): 1363-72. DOI:10.1084/jem.189.9.1363.

Munn, D. H., Sharma, M. D., Hou, D., Baban, B., Lee, J. R., Antonia, S. J., Messina, J. L., Chandler, P., Koni, P. A., and Mellor, A. L. Expression of Indoleamine 2,3-Dioxygenase by Plasmacytoid Dendritic Cells in Tumor-Draining Lymph Nodes. *J Clin Invest* 114, no. 2 (Jul 2004): 280-90. DOI:10.1172/JCI21583.

Munn, D. H., Sharma, M. D., Lee, J. R., Jhaver, K. G., Johnson, T. S., Keskin, D. B., Marshall, B., Chandler, P., Antonia, S. J., Burgess, R., Slingluff, C. L., Jr., and Mellor, A. L. Potential Regulatory Function of Human Dendritic Cells Expressing Indoleamine 2,3-Dioxygenase. *Science* 297, no. 5588 (Sep 13 2002): 1867-70. DOI:10.1126/science.1073514.

Munn, D. H., Zhou, M., Attwood, J. T., Bondarev, I., Conway, S. J., Marshall, B., Brown, C., and Mellor, A. L. Prevention of Allogeneic Fetal Rejection by Tryptophan Catabolism. *Science* 281, no. 5380 (Aug 21 1998): 1191-3. DOI:10.1126/science.281.5380.1191.

Munoz, M., Liesenfeld, O., and Heimesaat, M. M. Immunology of *Toxoplasma gondii*. *Immunol Rev* 240, no. 1 (Mar 2011): 269-85. DOI:10.1111/j.1600-065X.2010.00992.x.

Murakami, Y., Hoshi, M., Hara, A., Takemura, M., Arioka, Y., Yamamoto, Y., Matsunami, H., Funato, T., Seishima, M., and Saito, K. Inhibition of Increased Indoleamine 2,3-Dioxygenase Activity Attenuates *Toxoplasma gondii* Replication in the Lung During Acute Infection. *Cytokine* 59, no. 2 (Aug 2012): 245-51. DOI:10.1016/j.cyto.2012.04.022.

Murphy, Kenneth, and Weaver, Casey. *Janeway's Immunobiology*. 9th edition ed., edited by Allan Mowat, Leslie Berg, and David Chaplin: Garland Science, Taylor & Francis Group, LLC, 2019.

Nagineni, C. N., Pardhasaradhi, K., Martins, M. C., Detrick, B., and Hooks, J. J. Mechanisms of Interferon-Induced Inhibition of *Toxoplasma gondii* Replication in Human Retinal Pigment Epithelial Cells. *Infect Immun* 64, no. 10 (Oct 1996): 4188-96. DOI:10.1128/IAI.64.10.4188-4196.1996.

Nast, R., Staab, J., Meyer, T., and Luder, C. G. K. *Toxoplasma gondii* Stabilises Tetrameric Complexes of Tyrosine-Phosphorylated Signal Transducer and Activator of Transcription-1 and Leads to Its Sustained and Promiscuous DNA Binding. *Cell Microbiol* 20, no. 11 (Nov 2018): e12887. DOI:10.1111/cmi.12887.

Neurath, M. F., Weigmann, B., Finotto, S., Glickman, J., Nieuwenhuis, E., Iijima, H., Mizoguchi, A., Mizoguchi, E., Mudter, J., Galle, P. R., Bhan, A., Autschbach, F., Sullivan, B. M., Szabo, S. J., Glimcher, L. H., and Blumberg, R. S. The Transcription Factor T-Bet Regulates Mucosal T Cell Activation in Experimental Colitis and Crohn's Disease. *J Exp Med* 195, no. 9 (May 6 2002): 1129-43. DOI:10.1084/jem.20011956.

Ng, T. H., Britton, G. J., Hill, E. V., Verhagen, J., Burton, B. R., and Wraith, D. C. Regulation of Adaptive Immunity; the Role of Interleukin-10. *Front Immunol* 4 (2013): 129. DOI:10.3389/fimmu.2013.00129.

Nicola, M., Alsafi, Z., Sohrabi, C., Kerwan, A., Al-Jabir, A., Iosifidis, C., Agha, M., and Agha, R. The Socio-Economic Implications of the Coronavirus Pandemic (Covid-19): A Review. *Int J Surg* 78 (Jun 2020): 185-93. DOI:10.1016/j.ijsu.2020.04.018.

Nicolle, C., and Manceaux, L. Sur Un Protozoaire Nouveau Du Gondi., *C. R. Acad. Sci.* 148 (1909): 369-72.

Nikolich-Zugich, J., Slifka, M. K., and Messaoudi, I. The Many Important Facets of T-Cell Repertoire Diversity. *Nat Rev Immunol* 4, no. 2 (Feb 2004): 123-32. DOI:10.1038/nri1292.

Nino-Castro, A., Abdullah, Z., Popov, A., Thabet, Y., Beyer, M., Knolle, P., Domann, E., Chakraborty, T., Schmidt, S. V., and Schultze, J. L. The Ido1-Induced Kynurenines Play a Major Role in the Antimicrobial Effect of Human Myeloid Cells against *Listeria monocytogenes*. *Innate Immun* 20, no. 4 (May 2014): 401-11. DOI:10.1177/1753425913496442.

Obojes, K., Andres, O., Kim, K. S., Daubener, W., and Schneider-Schaulies, J. Indoleamine 2,3-Dioxygenase Mediates Cell Type-Specific Anti-Measles Virus Activity of Gamma Interferon. *J Virol* 79, no. 12 (Jun 2005): 7768-76. DOI:10.1128/JVI.79.12.7768-7776.2005.

Oh, J. S., Seo, H. S., Kim, K. H., Pyo, H., Chung, B. C., and Lee, J. Urinary Profiling of Tryptophan and Its Related Metabolites in Patients with Metabolic Syndrome by Liquid Chromatography-Electrospray Ionization/Mass Spectrometry. *Anal Bioanal Chem* 409, no. 23 (Sep 2017): 5501-12. DOI:10.1007/s00216-017-0486-4.

Ohshima, J., Lee, Y., Sasai, M., Saitoh, T., Su Ma, J., Kamiyama, N., Matsuura, Y., Pann-Ghill, S., Hayashi, M., Ebisu, S., Takeda, K., Akira, S., and Yamamoto, M. Role of Mouse and Human Autophagy Proteins in IFN-Gamma-Induced Cell-Autonomous Responses against *Toxoplasma gondii*. *J Immunol* 192, no. 7 (Apr 1 2014): 3328-35. DOI:10.4049/jimmunol.1302822.

Ohtaki, H., Ito, H., Ando, K., Ishikawa, T., Hoshi, M., Tanaka, R., Osawa, Y., Yokochi, T., Moriwaki, H., Saito, K., and Seishima, M. Interaction between Lps-Induced No Production and Ido Activity in Mouse Peritoneal Cells in the Presence of Activated Valpha14 Nkt Cells. *Biochem Biophys Res Commun* 389, no. 2 (Nov 13 2009): 229-34. DOI:10.1016/j.bbrc.2009.08.120.

Okazaki, T., Chikuma, S., Iwai, Y., Fagarasan, S., Honjo, T. A rheostat for immune responses: the unique properties of PD-1 and their advantages for clinical application. *Nat Immunol* 14, (Dec 2013):1212–8. DOI:10.1038/ni.2762.

Oldenhove, G., Bouladoux, N., Wohlfert, E. A., Hall, J. A., Chou, D., Dos Santos, L., O'Brien, S., Blank, R., Lamb, E., Natarajan, S., Kastenmayer, R., Hunter, C., Grigg, M. E., and Belkaid, Y. Decrease of Foxp3+ Treg Cell Number and Acquisition of Effector Cell Phenotype During Lethal Infection. *Immunity* 31, no. 5 (Nov 20 2009): 772-86. DOI:10.1016/j.immuni.2009.10.001.

Olias, P., Etheridge, R. D., Zhang, Y., Holtzman, M. J., and Sibley, L. D. Toxoplasma Effector Recruits the Mi-2/Nurd Complex to Repress Stat1 Transcription and Block IFN-Gamma-Dependent Gene Expression. *Cell Host Microbe* 20, no. 1 (Jul 13 2016): 72-82. DOI:10.1016/j.chom.2016.06.006.

Olson, W. J., Martorelli Di Genova, B., Gallego-Lopez, G., Dawson, A. R., Stevenson, D., Amador-Noguez, D., and Knoll, L. J. Dual Metabolomic Profiling Uncovers Toxoplasma Manipulation of the Host Metabolome and the Discovery of a Novel Parasite Metabolic Capability. *PLoS Pathog* 16, no. 4 (Apr 2020): e1008432. DOI:10.1371/journal.ppat.1008432.

Pandiyan, P., Zheng, L., Ishihara, S., Reed, J., and Lenardo, M. J. Cd4+Cd25+Foxp3+ Regulatory T Cells Induce Cytokine Deprivation-Mediated Apoptosis of Effector Cd4+ T Cells. *Nat Immunol* 8, no. 12 (Dec 2007): 1353-62. DOI:10.1038/ni1536.

Park, J., Wetzel, I., Marriott, I., Dreau, D., D'Avanzo, C., Kim, D. Y., Tanzi, R. E., and Cho, H. A 3d Human Triculture System Modeling Neurodegeneration and Neuroinflammation in Alzheimer's Disease. *Nat Neurosci* 21, no. 7 (Jul 2018): 941-51. DOI:10.1038/s41593-018-0175-4.

Parker, K. E. R., Fairweather, S. J., Rajendran, E., Blume, M., McConville, M. J., Broer, S., Kirk, K., and van Dooren, G. G. The Tyrosine Transporter of *Toxoplasma gondii* Is a Member of the Newly Defined Apicomplexan Amino Acid Transporter (Apiat) Family. *PLoS Pathog* 15, no. 2 (Feb 2019): e1007577. DOI:10.1371/journal.ppat.1007577.

Paterson, D. J., Jefferies, W. A., Green, J. R., Brandon, M. R., Corthesy, P., Puklavec, M., and Williams, A. F. Antigens of Activated Rat T Lymphocytes Including a Molecule of 50,000 Mr Detected Only on Cd4 Positive T Blasts. *Mol Immunol* 24, no. 12 (Dec 1987): 1281-90. DOI:10.1016/0161-5890(87)90122-2.

Patton, E. A., La Flamme, A. C., Pedras-Vasoncelos, J. A., and Pearce, E. J. Central Role for Interleukin-4 in Regulating Nitric Oxide-Mediated Inhibition of T-Cell Proliferation and Gamma Interferon Production in Schistosomiasis. *Infect Immun* 70, no. 1 (Jan 2002): 177-84. DOI:10.1128/iai.70.1.177-184.2002.

Peixoto, L., Chen, F., Harb, O. S., Davis, P. H., Beiting, D. P., Brownback, C. S., Ouloguem, D., and Roos, D. S. Integrative Genomic Approaches Highlight a Family of Parasite-Specific Kinases That Regulate Host Responses. *Cell Host Microbe* 8, no. 2 (Aug 19 2010): 208-18. DOI:10.1016/j.chom.2010.07.004.

Pelloux, H., Guy, E., Angelici, M. C., Aspock, H., Bessieres, M. H., Blatz, R., Del Pezzo, M., Girault, V., Gratzl, R., Holberg-Petersen, M., Johnson, J., Kruger, D., Lappalainen, M., Naessens, A., and Olsson, M. A Second European Collaborative Study on Polymerase Chain Reaction for *Toxoplasma gondii*, Involving 15 Teams. *FEMS Microbiol Lett* 165, no. 2 (Aug 15 1998): 231-7. DOI:10.1111/j.1574-6968.1998.tb13151.x.

Pernas, L., Adomako-Ankomah, Y., Shastri, A. J., Ewald, S. E., Treeck, M., Boyle, J. P., and Boothroyd, J. C. Toxoplasma Effector Maf1 Mediates Recruitment of Host Mitochondria and Impacts the Host Response. *PLoS Biol* 12, no. 4 (Apr 2014): e1001845. DOI:10.1371/journal.pbio.1001845.

Pernas, L., Bean, C., Boothroyd, J. C., and Scorrano, L. Mitochondria Restrict Growth of the Intracellular Parasite *Toxoplasma gondii* by Limiting Its Uptake of Fatty Acids. *Cell Metab* 27, no. 4 (Apr 3 2018): 886-97 e4. DOI:10.1016/j.cmet.2018.02.018.

Pestka, S., Kotenko, S. V., Muthukumaran, G., Izotova, L. S., Cook, J. R., and Garotta, G. The Interferon Gamma (IFN-Gamma) Receptor: A Paradigm for the Multichain Cytokine Receptor. *Cytokine Growth Factor Rev* 8, no. 3 (Sep 1997): 189-206. DOI:10.1016/s1359-6101(97)00009-9.

Pestka, S., Krause, C. D., and Walter, M. R. Interferons, Interferon-Like Cytokines, and Their Receptors. *Immunol Rev* 202 (Dec 2004): 8-32. DOI:10.1111/j.0105-2896.2004.00204.x.

Pfefferkorn, E. R. Interferon Gamma Blocks the Growth of *Toxoplasma gondii* in Human Fibroblasts by Inducing the Host Cells to Degrade Tryptophan. *Proc Natl Acad Sci U S A* 81, no. 3 (Feb 1984): 908-12. DOI:10.1073/pnas.81.3.908.

Pfefferkorn, E. R., Eckel, M., and Rebhun, S. Interferon-Gamma Suppresses the Growth of *Toxoplasma gondii* in Human Fibroblasts through Starvation for Tryptophan. *Mol Biochem Parasitol* 20, no. 3 (Sep 1986): 215-24. DOI:10.1016/0166-6851(86)90101-5.

Pfefferkorn, E. R., and Pfefferkorn, L. C. Specific Labeling of Intracellular *Toxoplasma gondii* with Uracil. *J Protozool* 24, no. 3 (Aug 1977): 449-53. DOI:10.1111/j.1550-7408.1977.tb04774.x.

Pfefferkorn, E. R., Pfefferkorn, L. C., and Colby, E. D. Development of Gametes and Oocysts in Cats Fed Cysts Derived from Cloned Trophozoites of *Toxoplasma gondii*. *J Parasitol* 63, no. 1 (Feb 1977): 158-9. DOI:10.2307/3280129.

Platanias, L. C. Mechanisms of Type-I- and Type-Ii-Interferon-Mediated Signalling. *Nat Rev Immunol* 5, no. 5 (May 2005): 375-86. DOI:10.1038/nri1604.

Plattner, F., Yarovinsky, F., Romero, S., Didry, D., Carlier, M. F., Sher, A., and Soldati-Favre, D. Toxoplasma Profilin Is Essential for Host Cell Invasion and Tlr11-Dependent Induction of an Interleukin-12 Response. *Cell Host Microbe* 3, no. 2 (Feb 14 2008): 77-87. DOI:10.1016/j.chom.2008.01.001.

Pleyer, U., Gross, U., Schluter, D., Wilking, H., and Seeber, F. Toxoplasmosis in Germany. *Dtsch Arztebl Int* 116, no. 25 (Jun 21 2019): 435-44. DOI:10.3238/arztebl.2019.0435.

Praefcke, G. J., and McMahon, H. T. The Dynamin Superfamily: Universal Membrane Tubulation and Fission Molecules? , *Nat Rev Mol Cell Biol* 5, no. 2 (Feb 2004): 133-47. DOI:10.1038/nrm1313.

Prolo, C., Alvarez, M. N., and Radi, R. Peroxynitrite, a Potent Macrophage-Derived Oxidizing Cytotoxin to Combat Invading Pathogens. *Biofactors* 40, no. 2 (Mar-Apr 2014): 215-25. DOI:10.1002/biof.1150.

Rad Pour, S., Morikawa, H., Kiani, N. A., Yang, M., Azimi, A., Shafi, G., Shang, M., Baumgartner, R., Ketelhuth, D. F. J., Kamleh, M. A., Wheelock, C. E., Lundqvist, A., Hansson, J., and Tegner, J. Exhaustion of Cd4+ T-Cells Mediated by the Kynurenine Pathway in Melanoma. *Sci Rep* 9, no. 1 (Aug 21 2019): 12150. DOI:10.1038/s41598-019-48635-x.

Raetz, M., Kibardin, A., Sturge, C. R., Pifer, R., Li, H., Burstein, E., Ozato, K., Larin, S., and Yarovinsky, F. Cooperation of Tlr12 and Tlr11 in the Irf8-Dependent Il-12 Response to *Toxoplasma gondii* Profilin. *J Immunol* 191, no. 9 (Nov 1 2013): 4818-27. DOI:10.4049/jimmunol.1301301.

Ramani, A., Müller, L., Ostermann, P. N., Gabriel, E., Abida-Islam, P., Müller-Schiffmann, A., Mariappan, A., Goureau, O., Gruell, H., Walker, A., Andrée, M., Hauka, S., Houwaart, T., Dilthey, A., Wohlgemuth, K., Omran, H., Klein, F., Wieczorek, D., Adams, O., Timm, J., Korth, C., Schaal, H., Gopalakrishnan, J. SARS-CoV-2 targets neurons of 3D human brain organoids. *EMBO J*. 39, no. 20 (Oct 15 2020):e106230. DOI:10.15252/embj.2020106230.

Ravishankar, B., Liu, H., Shinde, R., Chandler, P., Baban, B., Tanaka, M., Munn, D. H., Mellor, A. L., Karlsson, M. C., and McGaha, T. L. Tolerance to Apoptotic Cells Is Regulated by Indoleamine 2,3-Dioxygenase. *Proc Natl Acad Sci U S A* 109, no. 10 (Mar 6 2012): 3909-14. DOI:10.1073/pnas.1117736109.

Ray, A., and Dittel, B. N. Isolation of Mouse Peritoneal Cavity Cells. *J Vis Exp*, no. 35 (Jan 28 2010). DOI:10.3791/1488.

Riley, J. L. Pd-1 Signaling in Primary T Cells. *Immunol Rev* 229, no. 1 (May 2009): 114-25. DOI:10.1111/j.1600-065X.2009.00767.x.

Robinson, C. M., Shirey, K. A., and Carlin, J. M. Synergistic Transcriptional Activation of Indoleamine Dioxygenase by IFN-Gamma and Tumor Necrosis Factor-Alpha. *J Interferon Cytokine Res* 23, no. 8 (Aug 2003): 413-21. DOI:10.1089/107999003322277829.

Ronchetti, S., Ricci, E., Petrillo, M. G., Cari, L., Migliorati, G., Nocentini, G., and Riccardi, C. Glucocorticoid-Induced Tumour Necrosis Factor Receptor-Related Protein: A Key Marker of Functional Regulatory T Cells. *J Immunol Res* 2015 (2015): 171520. DOI:10.1155/2015/171520.

Roshick, C., Wood, H., Caldwell, H. D., and McClarty, G. Comparison of Gamma Interferon-Mediated Antichlamydial Defense Mechanisms in Human and Mouse Cells. *Infect Immun* 74, no. 1 (Jan 2006): 225-38. DOI:10.1128/IAI.74.1.225-238.2006.

Rosowski, E. E., Lu, D., Julien, L., Rodda, L., Gaiser, R. A., Jensen, K. D., and Saeij, J. P. Strain-Specific Activation of the Nf-Kappab Pathway by Gra15, a Novel *Toxoplasma gondii* Dense Granule Protein. *J Exp Med* 208, no. 1 (Jan 17 2011): 195-212. DOI:10.1084/jem.20100717.

Rosowski, E. E., Nguyen, Q. P., Camejo, A., Spooner, E., and Saeij, J. P. *Toxoplasma gondii* Inhibits Gamma Interferon (IFN-Gamma)- and IFN-Beta-Induced Host Cell Stat1 Transcriptional Activity by Increasing the Association of Stat1 with DNA. *Infect Immun* 82, no. 2 (Feb 2014): 706-19. DOI:10.1128/IAI.01291-13.

Rosowski, E. E., and Saeij, J. P. *Toxoplasma gondii* Clonal Strains All Inhibit Stat1 Transcriptional Activity but Polymorphic Effectors Differentially Modulate Ifngamma Induced Gene Expression and Stat1 Phosphorylation. *PLoS One* 7, no. 12 (2012): e51448. DOI:10.1371/journal.pone.0051448.

Sabin, A. Toxoplasmic Encephalitis in Children. *JAMA* 116, no. 9 (1941): 801-07. DOI:10.1001/jama.1941.02820090001001.

Saeij, J. P., Boyle, J. P., Coller, S., Taylor, S., Sibley, L. D., Brooke-Powell, E. T., Ajioka, J. W., and Boothroyd, J. C. Polymorphic Secreted Kinases Are Key Virulence Factors in Toxoplasmosis. *Science* 314, no. 5806 (Dec 15 2006): 1780-3. DOI:10.1126/science.1133690.

Safronova, A., Araujo, A., Camanzo, E. T., Moon, T. J., Elliott, M. R., Beiting, D. P., and Yarovinsky, F. Alarmin S100a11 Initiates a Chemokine Response to the Human Pathogen *Toxoplasma gondii*. *Nat Immunol* 20, no. 1 (Jan 2019): 64-72. DOI:10.1038/s41590-018-0250-8.

Salinas, N., Olguin, J. E., Castellanos, C., and Saavedra, R. T Cell Suppression *in vitro* During *Toxoplasma gondii* Infection Is the Result of Il-2 Competition between Tregs and T Cells Leading to Death of Proliferating T Cells. *Scand J Immunol* 79, no. 1 (Jan 2014): 1-11. DOI:10.1111/sji.12120.

Samelson-Jones, B. J., and Yeh, S. R. Interactions between Nitric Oxide and Indoleamine 2,3-Dioxygenase. *Biochemistry* 45, no. 28 (Jul 18 2006): 8527-38. DOI:10.1021/bi060143j.

Sasai, M., and Yamamoto, M. Innate, Adaptive, and Cell-Autonomous Immunity against *Toxoplasma gondii* Infection. *Exp Mol Med* 51, no. 12 (Dec 11 2019): 1-10. DOI:10.1038/s12276-019-0353-9.

Scharton-Kersten, T. M., Wynn, T. A., Denkers, E. Y., Bala, S., Grunvald, E., Hieny, S., Gazzinelli, R. T., and Sher, A. In the Absence of Endogenous IFN-Gamma, Mice Develop Unimpaired Il-12 Responses to *Toxoplasma gondii* While Failing to Control Acute Infection. *J Immunol* 157, no. 9 (Nov 1 1996): 4045-54. https://www.ncbi.nlm.nih.gov/pubmed/8892638.

Scharton-Kersten, Tanya M., Yap, George, Magram, Jeanne, and Sher, Alan. Inducible Nitric Oxide Is Essential for Host Control of Persistent but Not Acute Infection with the Intracellular Pathogen *Toxoplasma gondii*. *Journal of Experimental Medicine* 185, no. 7 (1997): 1261-74. Accessed 12/20/2020. DOI:10.1084/jem.185.7.1261.

Scheu, S., Dresing, P., and Locksley, R. M. Visualization of Ifnbeta Production by Plasmacytoid Versus Conventional Dendritic Cells under Specific Stimulation Conditions *in vivo*. *Proc Natl Acad Sci U S A* 105, no. 51 (Dec 23 2008): 20416-21. DOI:10.1073/pnas.0808537105.

Schimke, R. T., Sweeney, E. W., and Berlin, C. M. The Roles of Synthesis and Degradation in the Control of Rat Liver Tryptophan Pyrrolase. *J Biol Chem* 240 (Jan 1965): 322-31. DOI:doi.org/10.1016/S0021-9258(18)97652-0.

Schluter, D., Daubener, W., Schares, G., Gross, U., Pleyer, U., and Luder, C. Animals Are Key to Human Toxoplasmosis. *Int J Med Microbiol* 304, no. 7 (Oct 2014): 917-29. DOI:10.1016/j.ijmm.2014.09.002.

Schmid, M., Heitlinger, E., Spork, S., Mollenkopf, H. J., Lucius, R., and Gupta, N. Eimeria Falciformis Infection of the Mouse Caecum Identifies Opposing Roles of Ifngamma-Regulated Host Pathways for the Parasite Development. *Mucosal Immunol* 7, no. 4 (Jul 2014): 969-82. DOI:10.1038/mi.2013.115.

Schmid, M., Lehmann, M. J., Lucius, R., and Gupta, N. Apicomplexan Parasite, Eimeria Falciformis, Co-Opts Host Tryptophan Catabolism for Life Cycle Progression in Mouse. *J Biol Chem* 287, no. 24 (Jun 8 2012): 20197-207. DOI:10.1074/jbc.M112.351999.

Schmidt, A., Oberle, N., and Krammer, P. H. Molecular Mechanisms of Treg-Mediated T Cell Suppression. *Front Immunol* 3 (2012): 51. DOI:10.3389/fimmu.2012.00051.

Schmidt, S. K., Muller, A., Heseler, K., Woite, C., Spekker, K., MacKenzie, C. R., and Daubener, W. Antimicrobial and Immunoregulatory Properties of Human Tryptophan 2,3-Dioxygenase. *Eur J Immunol* 39, no. 10 (Oct 2009): 2755-64. DOI:10.1002/eji.200939535.

Schroder, K., Hertzog, P. J., Ravasi, T., and Hume, D. A. Interferon-Gamma: An Overview of Signals, Mechanisms and Functions. *J Leukoc Biol* 75, no. 2 (Feb 2004): 163-89. DOI:10.1189/jlb.0603252.

Schumann, J., Stanko, K., Schliesser, U., Appelt, C., and Sawitzki, B. Differences in Cd44 Surface Expression Levels and Function Discriminates Il-17 and IFN-Gamma Producing Helper T Cells. *PLoS One* 10, no. 7 (2015): e0132479. DOI:10.1371/journal.pone.0132479.

Sedlmayr, P., Blaschitz, A., Wintersteiger, R., Semlitsch, M., Hammer, A., MacKenzie, C. R., Walcher, W., Reich, O., Takikawa, O., and Dohr, G. Localization of Indoleamine 2,3-Dioxygenase in Human Female Reproductive Organs and the Placenta. *Mol Hum Reprod* 8, no. 4 (Apr 2002): 385-91. DOI:10.1093/molehr/8.4.385.

Seif, F., Khoshmirsafa, M., Aazami, H., Mohsenzadegan, M., Sedighi, G., and Bahar, M. The Role of Jak-Stat Signaling Pathway and Its Regulators in the Fate of T Helper Cells. *Cell Commun Signal* 15, no. 1 (Jun 21 2017): 23. DOI:10.1186/s12964-017-0177-y.

Selleck, E. M., Fentress, S. J., Beatty, W. L., Degrandi, D., Pfeffer, K., Virgin, H. W. th, Macmicking, J. D., and Sibley, L. D. Guanylate-Binding Protein 1 (Gbp1) Contributes to Cell-Autonomous Immunity against *Toxoplasma gondii*. *PLoS Pathog* 9, no. 4 (2013): e1003320. DOI:10.1371/journal.ppat.1003320.

Selleck, E.M., Orchard, R. C., Lassen, K. G., Beatty, W. L., Xavier, R. J., Levine, B., Virgin, H. W., Sibley, L. D. A Noncanonical Autophagy Pathway Restricts *Toxoplasma gondii* Growth in a Strain-Specific Manner in IFN-γ-Activated Human Cells. *mBio* 6, no. 5 (Sep 8 2015):e01157-15. DOI:10.1128/mBio.01157-15.

Seo, H. H., Han, H. W., Lee, S. E., Hong, S. H., Cho, S. H., Kim, S. C., Koo, S. K., and Kim, J. H. Modelling *Toxoplasma gondii* Infection in Human Cerebral Organoids. *Emerg Microbes Infect* 9, no. 1 (Dec 2020): 1943-54. DOI:10.1080/22221751.2020.1812435.

Sharma, M. D., Baban, B., Chandler, P., Hou, D. Y., Singh, N., Yagita, H., Azuma, M., Blazar, B. R., Mellor, A. L., and Munn, D. H. Plasmacytoid Dendritic Cells from Mouse Tumor-Draining Lymph Nodes Directly Activate Mature Tregs Via Indoleamine 2,3-Dioxygenase. *J Clin Invest* 117, no. 9 (Sep 2007): 2570-82. DOI:10.1172/JCI31911.

Sheffield, H. G., and Melton, M. L. The Fine Structure and Reproduction of *Toxoplasma gondii*. *J Parasitol* 54, no. 2 (Apr 1968): 209-26. DOI:10.2307/3276925.

Sibley, L. D., Adams, L. B., Fukutomi, Y., and Krahenbuhl, J. L. Tumor Necrosis Factor-Alpha Triggers Antitoxoplasmal Activity of IFN-Gamma Primed Macrophages. *J Immunol* 147, no. 7 (Oct 1 1991): 2340-5. https://www.ncbi.nlm.nih.gov/pubmed/1918966.

Sibley, L. D., and Boothroyd, J. C. Virulent Strains of *Toxoplasma gondii* Comprise a Single Clonal Lineage. *Nature* 359, no. 6390 (Sep 3 1992): 82-5. DOI:10.1038/359082a0.

Silva, N. M., Rodrigues, C. V., Santoro, M. M., Reis, L. F., Alvarez-Leite, J. I., and Gazzinelli, R. T. Expression of Indoleamine 2,3-Dioxygenase, Tryptophan Degradation, and Kynurenine Formation During *in vivo* Infection with *Toxoplasma gondii*: Induction by Endogenous Gamma Interferon and Requirement of Interferon Regulatory Factor 1. *Infect Immun* 70, no. 2 (Feb 2002): 859-68. DOI:10.1128/iai.70.2.859-868.2002.

Sinzger, C., Hahn, G., Digel, M., Katona, R., Sampaio, K. L., Messerle, M., Hengel, H., Koszinowski, U., Brune, W., and Adler, B. Cloning and Sequencing of a Highly Productive, Endotheliotropic Virus Strain Derived from Human Cytomegalovirus Tb40/E. *J Gen Virol* 89, no. Pt 2 (Feb 2008): 359-68. DOI:10.1099/vir.0.83286-0.

Sinzger, C., Schmidt, K., Knapp, J., Kahl, M., Beck, R., Waldman, J., Hebart, H., Einsele, H., and Jahn, G. Modification of Human Cytomegalovirus Tropism through Propagation *in vitro* Is Associated with Changes in the Viral Genome. *J Gen Virol* 80 (Pt 11) (Nov 1999): 2867-77. DOI:10.1099/0022-1317-80-11-2867.

Smith, D. A., Parish, T., Stoker, N. G., and Bancroft, G. J. Characterization of Auxotrophic Mutants of *Mycobacterium tuberculosis* and Their Potential as Vaccine Candidates. *Infect Immun* 69, no. 2 (Feb 2001): 1142-50. DOI:10.1128/IAI.69.2.1442-1150.2001.

Soares, A., Govender, L., Hughes, J., Mavakla, W., de Kock, M., Barnard, C., Pienaar, B., Janse van Rensburg, E., Jacobs, G., Khomba, G., Stone, L., Abel, B., Scriba, T. J., and Hanekom, W. A. Novel Application of Ki67 to Quantify Antigen-Specific *in vitro* Lymphoproliferation. *J Immunol Methods* 362, no. 1-2 (Oct 31 2010): 43-50. DOI:10.1016/j.jim.2010.08.007.

Sotero-Esteva, W. D., Wolfe, D., Ferris, M., and Taylor, M. W. An Indoleamine 2,3-Dioxygenase-Negative Mutant Is Defective in Stat1 DNA Binding: Differential Response to IFN-Gamma and IFN-Alpha. *J Interferon Cytokine Res* 20, no. 7 (Jul 2000): 623-32. DOI:10.1089/107999000414790.

Spekker, K., Czesla, M., Ince, V., Heseler, K., Schmidt, S. K., Schares, G., and Daubener, W. Indoleamine 2,3-Dioxygenase Is Involved in Defense against Neospora Caninum in Human and Bovine Cells. *Infect Immun* 77, no. 10 (Oct 2009): 4496-501. DOI:10.1128/IAI.00310-09.

Spekker, K., Leineweber, M., Degrandi, D., Ince, V., Brunder, S., Schmidt, S. K., Stuhlsatz, S., Howard, J. C., Schares, G., Degistirici, O., Meisel, R., Sorg, R. V., Seissler, J., Hemphill, A., Pfeffer, K., Däubener, W. Antimicrobial effects of murine mesenchymal stromal cells directed against *Toxoplasma gondii* and *Neospora caninum*: role of immunity-related GTPases (IRGs) and guanylate-binding proteins (GBPs). *Med Microbiol Immunol*. 202 no. 3 (Jun 2013):197-206. DOI:10.1007/s00430-012-0281-y.

Spekker-Bosker, K., Ufermann, C. M., Maywald, M., Zimmermann, A., Domrose, A., Woite, C., Daubener, W., and Eller, S. K. Hcmv-Mediated Immune Escape Mechanisms Favor Pathogen Growth and Disturb the Immune Privilege of the Eye. *Int J Mol Sci* 20, no. 4 (Feb 16 2019). DOI:10.3390/ijms20040858.

Spekker-Bosker, K., Ufermann, C. M., Oldenburg, M., Daubener, W., and Eller, S. K. Interplay between Ido1 and Inos in Human Retinal Pigment Epithelial Cells. *Med Microbiol Immunol* 208, no. 6 (Dec 2019): 811-24. DOI:10.1007/s00430-019-00627-4.

Servier (2017) Servier Medical Art, http://smart.servier.com

Sprent, J., and Surh, C. D. Normal T Cell Homeostasis: The Conversion of Naive Cells into Memory-Phenotype Cells. *Nat Immunol* 12, no. 6 (Jun 2011): 478-84. DOI:10.1038/ni.2018.

Steffens, N., Beuter-Gunia, C., Kravets, E., Reich, A., Legewie, L., Pfeffer, K., and Degrandi, D. Essential Role of Mgbp7 for Survival of *Toxoplasma gondii* Infection. *mBio* 11, no. 1 (Jan 21 2020). DOI:10.1128/mBio.02993-19.

Strauss, O. The Retinal Pigment Epithelium in Visual Function. *Physiol Rev* 85, no. 3 (Jul 2005): 845-81. DOI:10.1152/physrev.00021.2004.

Streilein, J. W., Ma, N., Wenkel, H., Ng, T. F., and Zamiri, P. Immunobiology and Privilege of Neuronal Retina and Pigment Epithelium Transplants. *Vision Res* 42, no. 4 (Feb 2002): 487-95. DOI:10.1016/s0042-6989(01)00185-7.

Strikoudis, A., Cieslak, A., Loffredo, L., Chen, Y. W., Patel, N., Saqi, A., Lederer, D. J., and Snoeck, H. W. Modeling of Fibrotic Lung Disease Using 3d Organoids Derived from Human Pluripotent Stem Cells. *Cell Rep* 27, no. 12 (Jun 18 2019): 3709-23 e5. DOI:10.1016/j.celrep.2019.05.077.

Sturge, C. R., Benson, A., Raetz, M., Wilhelm, C. L., Mirpuri, J., Vitetta, E. S., and Yarovinsky, F. Tlr-Independent Neutrophil-Derived IFN-Gamma Is Important for Host Resistance to Intracellular Pathogens. *Proc Natl Acad Sci U S A* 110, no. 26 (Jun 25 2013): 10711-6. DOI:10.1073/pnas.1307868110.

Su, C., Khan, A., Zhou, P., Majumdar, D., Ajzenberg, D., Darde, M. L., Zhu, X. Q., Ajioka, J. W., Rosenthal, B. M., Dubey, J. P., and Sibley, L. D. Globally Diverse *Toxoplasma gondii* Isolates Comprise Six Major Clades Originating from a Small Number of Distinct Ancestral Lineages. *Proc Natl Acad Sci U S A* 109, no. 15 (Apr 10 2012): 5844-9. DOI:10.1073/pnas.1203190109.

Sudharshan, S., Nair, N., Curi, A., Banker, A., and Kempen, J. H. Human Immunodeficiency Virus and Intraocular Inflammation in the Era of Highly Active Anti Retroviral Therapy - an Update. *Indian J Ophthalmol* 68, no. 9 (Sep 2020): 1787-98. DOI:10.4103/ijo.IJO_1248_20.

Sugita, S., Futagami, Y., Smith, S. B., Naggar, H., and Mochizuki, M. Retinal and Ciliary Body Pigment Epithelium Suppress Activation of T Lymphocytes Via Transforming Growth Factor Beta. *Exp Eye Res* 83, no. 6 (Dec 2006): 1459-71. DOI:10.1016/j.exer.2006.08.005.

Sun, X., and Kaufman, P. D. Ki-67: More Than a Proliferation Marker. *Chromosoma* 127, no. 2 (Jun 2018): 175-86. DOI:10.1007/s00412-018-0659-8.

Suzuki, Y., Orellana, M. A., Schreiber, R. D., and Remington, J. S. Interferon-Gamma: The Major Mediator of Resistance against *Toxoplasma gondii*. *Science* 240, no. 4851 (Apr 22 1988): 516-8. DOI:10.1126/science.3128869.

Suzuki, Y., Wang, X., Jortner, B. S., Payne, L., Ni, Y., Michie, S. A., Xu, B., Kudo, T., and Perkins, S. Removal of *Toxoplasma gondii* Cysts from the Brain by Perforin-Mediated Activity of Cd8+ T Cells. *Am J Pathol* 176, no. 4 (Apr 2010): 1607-13. DOI:10.2353/ajpath.2010.090825.

Takikawa, O. Biochemical and Medical Aspects of the Indoleamine 2,3-Dioxygenase-Initiated L-Tryptophan Metabolism. *Biochem Biophys Res Commun* 338, no. 1 (Dec 9 2005): 12-9. DOI:10.1016/j.bbrc.2005.09.032.

Takikawa, O., Kuroiwa, T., Yamazaki, F., and Kido, R. Mechanism of Interferon-Gamma Action. Characterization of Indoleamine 2,3-Dioxygenase in Cultured Human Cells Induced by Interferon-Gamma and Evaluation of the Enzyme-Mediated Tryptophan Degradation in Its Anticellular Activity. *J Biol Chem* 263, no. 4 (Feb 5 1988): 2041-8. DOI:doi.org/10.1016/S0021-9258(19)77982-4.

Takikawa, O., Tagawa, Y., Iwakura, Y., Yoshida, R., and Truscott, R. J. Interferon-Gamma-Dependent/Independent Expression of Indoleamine 2,3-Dioxygenase. Studies with Interferon-Gamma-Knockout Mice. *Adv Exp Med Biol* 467 (1999): 553-7. DOI:10.1007/978-1-4615-4709-9_68.

Talabani, H., Mergey, T., Yera, H., Delair, E., Brezin, A. P., Langsley, G., and Dupouy-Camet, J. Factors of Occurrence of Ocular Toxoplasmosis. A Review. *Parasite* 17, no. 3 (Sep 2010): 177-82. DOI:10.1051/parasite/2010173177.

Tenopoulou, M., and Doulias, P. T. Endothelial Nitric Oxide Synthase-Derived Nitric Oxide in the Regulation of Metabolism. *F1000Res* 9 (2020). DOI:10.12688/f1000research.19998.1.

Tenorio, E. P., Fernandez, J., Castellanos, C., Olguin, J. E., and Saavedra, R. Cd4+ Foxp3+ Regulatory T Cells Mediate *Toxoplasma gondii*-Induced T-Cell Suppression through an Il-2-Related Mechanism but Independently of Il-10. *Eur J Immunol* 41, no. 12 (Dec 2011): 3529-41. DOI:10.1002/eji.201141507.

Thomas, S. R., and Stocker, R. Redox Reactions Related to Indoleamine 2,3-Dioxygenase and Tryptophan Metabolism Along the Kynurenine Pathway. *Redox Rep* 4, no. 5 (1999): 199-220. DOI:10.1179/135100099101534927.

Thomas, S. R., Terentis, A. C., Cai, H., Takikawa, O., Levina, A., Lay, P. A., Freewan, M., and Stocker, R. Post-Translational Regulation of Human Indoleamine 2,3-Dioxygenase Activity by Nitric Oxide. *J Biol Chem* 282, no. 33 (Aug 17 2007): 23778-87. DOI:10.1074/jbc.M700669200.

Torgerson, P. R., and Mastroiacovo, P. The Global Burden of Congenital Toxoplasmosis: A Systematic Review. *Bull World Health Organ* 91, no. 7 (Jul 1 2013): 501-8. DOI:10.2471/BLT.12.111732.

Tretina, K., Park, E.-S., Maminska, A., MacMicking, J. D. Interferon-induced guanylate-binding proteins: Guardians of host defense in health and disease. *J Exp Med* 216, no. 3 (Mar 4 2019): 482-500. DOI:10.1084/jem.20182031.

Ufermann, C. M., Domrose, A., Babel, T., Tersteegen, A., Cengiz, S. C., Eller, S. K., Spekker-Bosker, K., Sorg, U. R., Forster, I., and Daubener, W. Indoleamine 2,3-Dioxygenase Activity During Acute Toxoplasmosis and the Suppressed T Cell Proliferation in Mice. *Front Cell Infect Microbiol* 9 (2019): 184. DOI:10.3389/fcimb.2019.00184.

Union., European Parliament and the Council of the European, European Union. Directive 2010/63/Eu of the European Parliament and of the Council of 22 September 2010 on the Protection of Animals Used for Scientific Purposes. L276, 20.10.2010, P. 33-79. 2010.

van der Veen, R. C. Nitric Oxide and T Helper Cell Immunity. *Int Immunopharmacol* 1, no. 8 (Aug 2001): 1491-500. DOI:10.1016/s1567-5769(01)00093-5.

Virok, D. P., Raffai, T., Kokai, D., Paroczai, D., Bogdanov, A., Veres, G., Vecsei, L., Poliska, S., Tiszlavicz, L., Somogyvari, F., Endresz, V., and Burian, K. Indoleamine 2,3-Dioxygenase Activity in *Chlamydia muridarum* and *Chlamydia pneumoniae* Infected Mouse Lung Tissues. *Front Cell Infect Microbiol* 9 (2019): 192. DOI:10.3389/fcimb.2019.00192.

Wagstaff, P. E., Ten Asbroek, Alma, Ten Brink, J. B., Jansonius, N. M., and Bergen, A. A. B. An Alternative Approach to Produce Versatile Retinal Organoids with Accelerated Ganglion Cell Development. *Sci Rep* 11, no. 1 (Jan 13 2021): 1101. DOI:10.1038/s41598-020-79651-x.

Wang, Y., Zhu, J., Cao, Y., Shen, J., Yu, L. Insight Into Inflammasome Signaling: Implications for *Toxoplasma gondii* Infection. *Front Immunol*.11 (Dec 16 2020): 583193. DOI:10.3389/fimmu.2020.583193.

Wilking, H., Thamm, M., Stark, K., Aebischer, T., and Seeber, F. Prevalence, Incidence Estimations, and Risk Factors of *Toxoplasma gondii* Infection in Germany: A Representative, Cross-Sectional, Serological Study. *Sci Rep* 6 (Mar 3 2016): 22551. DOI:10.1038/srep22551.

Witola, W. H., Mui, E., Hargrave, A., Liu, S., Hypolite, M., Montpetit, A., Cavailles, P., Bisanz, C., Cesbron-Delauw, M. F., Fournie, G. J., and McLeod, R. Nalp1 Influences Susceptibility to Human Congenital Toxoplasmosis, Proinflammatory Cytokine Response, and Fate of *Toxoplasma gondii*-Infected Monocytic Cells. *Infect Immun* 79, no. 2 (Feb 2011): 756-66. DOI:10.1128/IAI.00898-10.

World Health Organization. "Who Coronavirus (Covid-19) Dashboard." 2021. Accessed 25.04.2021, 2021. https://covid19.who.int.

World Health Organization. Who Estimates of the Global Burden of Foodborne Diseases: Foodborne Disease Burden Epidemiology Reference Group 2007-2015.: World Health Organization, 2015. https://apps.who.int/iris/handle/10665/199350.

Wu, G., and Morris, S. M., Jr. Arginine Metabolism: Nitric Oxide and Beyond. *Biochem J* 336 (Pt 1) (Nov 15 1998): 1-17. DOI:10.1042/bj3360001.

Yamamoto, M., Okuyama, M., Ma, J. S., Kimura, T., Kamiyama, N., Saiga, H., Ohshima, J., Sasai, M., Kayama, H., Okamoto, T., Huang, D. C., Soldati-Favre, D., Horie, K., Takeda, J., and Takeda, K. A Cluster of Interferon-Gamma-Inducible P65 Gtpases Plays a Critical Role in Host Defense against *Toxoplasma gondii*. *Immunity* 37, no. 2 (Aug 24 2012): 302-13. DOI:10.1016/j.immuni.2012.06.009.

Yap, G. S., and Sher, A. Effector Cells of Both Nonhemopoietic and Hemopoietic Origin Are Required for Interferon (Ifn)-Gamma- and Tumor Necrosis Factor (Tnf)-Alpha-Dependent Host Resistance to the Intracellular Pathogen, *Toxoplasma gondii*. *J Exp Med* 189, no. 7 (Apr 5 1999): 1083-92. DOI:10.1084/jem.189.7.1083.

Yarovinsky, F. Innate Immunity to *Toxoplasma gondii* Infection. *Nat Rev Immunol* 14, no. 2 (Feb 2014): 109-21. DOI:10.1038/nri3598.

Yarovinsky, F., Zhang, D., Andersen, J. F., Bannenberg, G. L., Serhan, C. N., Hayden, M. S., Hieny, S., Sutterwala, F. S., Flavell, R. A., Ghosh, S., and Sher, A. Tlr11 Activation of Dendritic Cells by a Protozoan Profilin-Like Protein. *Science* 308, no. 5728 (Jun 10 2005): 1626-9. DOI:10.1126/science.1109893.

Ye, Q. X., Xu, L. H., Shi, P. J., Xia, T., and Fang, J. P. Indoleamine 2,3-Dioxygenase and Inducible Nitric Oxide Synthase Mediate Immune Tolerance Induced by Ctla4ig and Anti-Cd154 Hematopoietic Stem Cell Transplantation in a Sensitized Mouse Model. *Exp Ther Med* 14, no. 3 (Sep 2017): 1884-91. DOI:10.3892/etm.2017.4722.

Yeung, A. W., Terentis, A. C., King, N. J., and Thomas, S. R. Role of Indoleamine 2,3-Dioxygenase in Health and Disease. *Clin Sci (Lond)* 129, no. 7 (Oct 2015): 601-72. DOI:10.1042/CS20140392.

Zamanakou, M., Germenis, A. E., and Karanikas, V. Tumor Immune Escape Mediated by Indoleamine 2,3-Dioxygenase. *Immunol Lett* 111, no. 2 (Aug 15 2007): 69-75. DOI:10.1016/j.imlet.2007.06.001.

Zhang, M., Joyce, B. R., Sullivan, W. J., Jr., and Nussenzweig, V. Translational Control in Plasmodium and Toxoplasma Parasites. *Eukaryot Cell* 12, no. 2 (Feb 2013a): 161-7. DOI:10.1128/EC.00296-12.

Zhang, Y. J., Reddy, M. C., Ioerger, T. R., Rothchild, A. C., Dartois, V., Schuster, B. M., Trauner, A., Wallis, D., Galaviz, S., Huttenhower, C., Sacchettini, J. C., Behar, S. M., and Rubin, E. J. Tryptophan Biosynthesis Protects Mycobacteria from Cd4 T-Cell-Mediated Killing. *Cell* 155, no. 6 (Dec 5 2013b): 1296-308. DOI:10.1016/j.cell.2013.10.045.

Zhang, Y., Jiang, N., Zhang, T., Wang, D., Feng, Y., Sang, X., Yang, N., and Chen, Q. *Toxoplasma gondii* Genotype Determines Tim-3 Expression Levels in Splenic and Circulatory T Cells in Mice. *Front Microbiol* 9 (2018): 2967. DOI:10.3389/fmicb.2018.02967.

Zhao, D., Yu, Y., Shen, Y., Liu, Q., Zhao, Z., Sharma, R., and Reiter, R. J. Melatonin Synthesis and Function: Evolutionary History in Animals and Plants. *Front Endocrinol (Lausanne)* 10 (2019): 249. DOI:10.3389/fendo.2019.00249.

Zhou, T., Tan, L., Cederquist, G. Y., Fan, Y., Hartley, B. J., Mukherjee, S., Tomishima, M., Brennand, K. J., Zhang, Q., Schwartz, R. E., Evans, T., Studer, L., and Chen, S. High-Content Screening in Hpsc-Neural Progenitors Identifies Drug Candidates That Inhibit Zika Virus Infection in Fetal-Like Organoids and Adult Brain. *Cell Stem Cell* 21, no. 2 (Aug 3 2017): 274-83 e5. DOI:10.1016/j.stem.2017.06.017.

Zhu, J., Yamane, H., and Paul, W. E. Differentiation of Effector Cd4 T Cell Populations (*). *Annu Rev Immunol* 28 (2010): 445-89. DOI:10.1146/annurev-immunol-030409-101212.

Zimmermann, A., Hauka, S., Maywald, M., Le, V. T. K., Schmidt, S. K., Daubener, W., and Hengel, H. Checks and Balances between Human Cytomegalovirus Replication and Indoleamine-2,3-Dioxygenase. *J Gen Virol* 95, no. Pt 3 (Mar 2014): 659-70. DOI:10.1099/vir.0.061994-0.

Zuhair, M., Smit, G. S. A., Wallis, G., Jabbar, F., Smith, C., Devleesschauwer, B., and Griffiths, P. Estimation of the Worldwide Seroprevalence of Cytomegalovirus: A Systematic Review and Meta-Analysis. *Rev Med Virol* 29, no. 3 (May 2019): e2034. DOI:10.1002/rmv.2034.

Appendix

Appx. A: miNOS immunoblot of murine lung tissue.

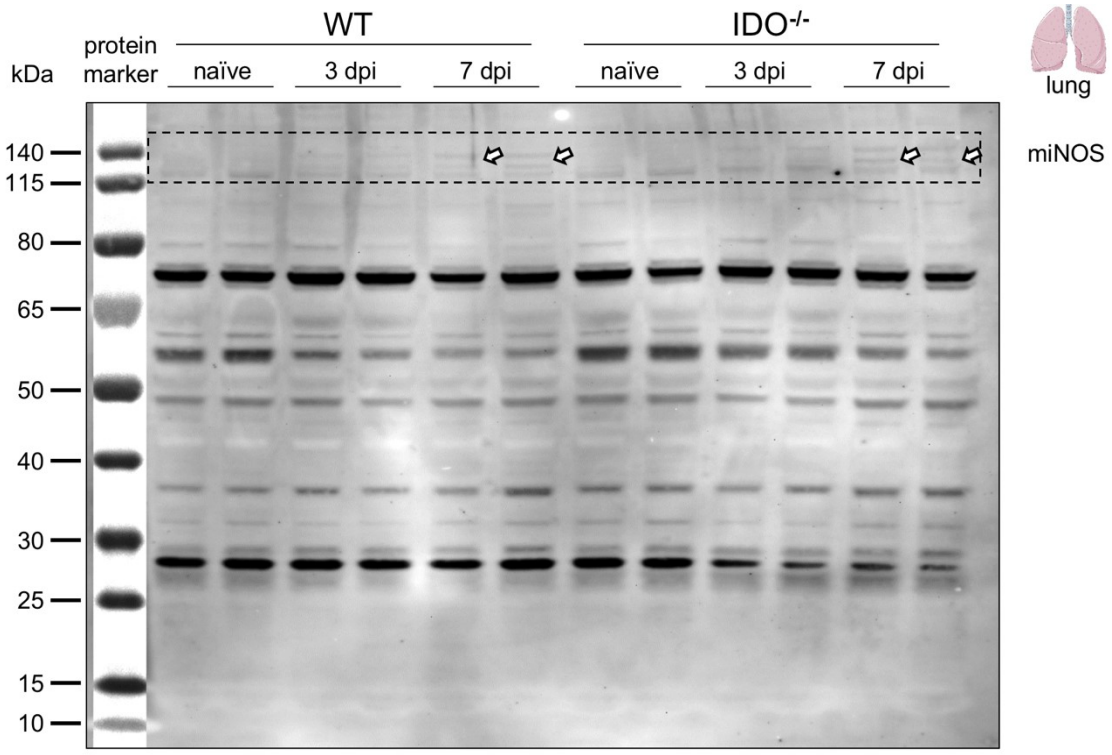

Appendix A: miNOS immunoblot of murine lung tissue.
Immunoblot of lung samples from naïve and *Toxoplasma gondii* (*T. gondii*; ME49 strain) infected wild type (WT) and indoleamine 2,3-dioxygenase 1 deficient ($IDO^{-/-}$) mice. Lung samples origin from two independent experiments. Samples (10 µg/lane) and protein marker were run on a 4 %–12 % Bis-Tris gel. Protein marker bands are indicated with a line and the band size in kilo dalton (kDa) on the left side of the blot. A commercial antibody (LOT no. D00040543; order no. 482728; CalBiochem®, Merck) was used to detect murine inducible nitric oxide synthase (miNOS). The arrows point towards the bands that are at the expected miNOS protein size (130 kDa). The dashed box highlights the part of the blot that is illustrated in Figure 14. (dpi - days post infection).

Appx. B: Gating strategy to identify effector T cells.

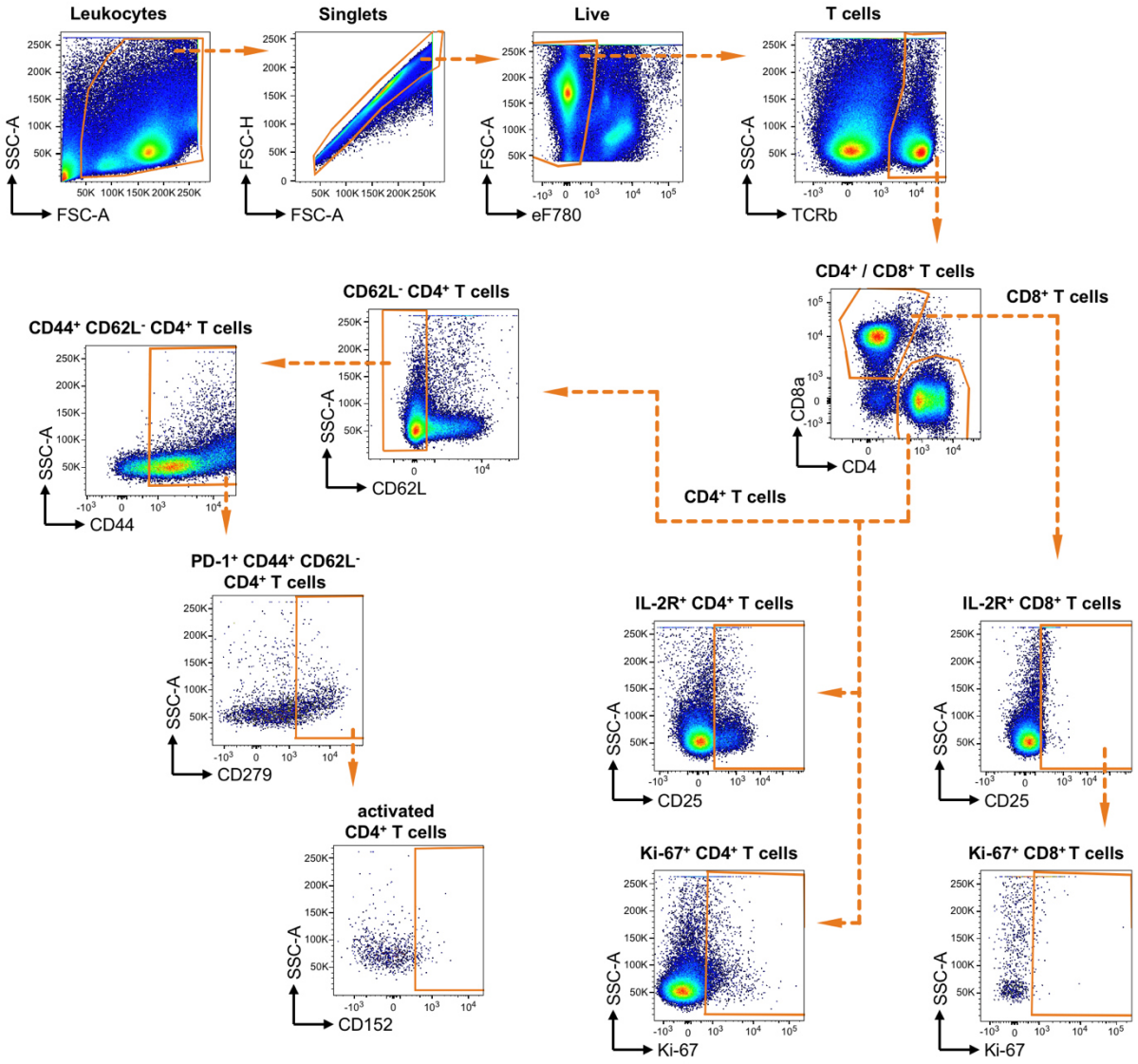

Appendix B: Gating strategy to identify effector T cells.
Representative illustration of the gating strategy for effector T cell identification via pseudo color plots of splenocytes from a naïve wild type mouse. Leukocytes were gated based on granulocytic (SSC-A) and cell size (FSC-A) followed by definition of single cells (singlets). Alive singlets (live) were determined with the viability stain eFluor™780 (labels dead/dying cells). T cells were gated based on the presence of T cell receptor beta chain (TCRb) and were further separated into $CD4^+$ and $CD8^+$ T cells. Interleukin-2 receptor (IL-2R; CD25) positive $CD8^+$ T cells were analyzed for expression of the proliferation marker Ki-67. $CD4^+$ T cells were analyzed for the surface expression of IL-2R and Ki-67. Activated $CD4^+$ T cells were identified by gating on L-selectin (CD62L) negative $CD4^+$ T cells, followed by gating this cell population based on the presence of the surface adhesion receptor (CD44). This cell population was analyzed for PD-1 (CD279) positive cells and next CTLA4 (CD152) positive cells. (SSC - sideward scatter; FSC - forward scatter; A - area; H - height).

Appx. C: Gating strategy to identify regulatory T cells.

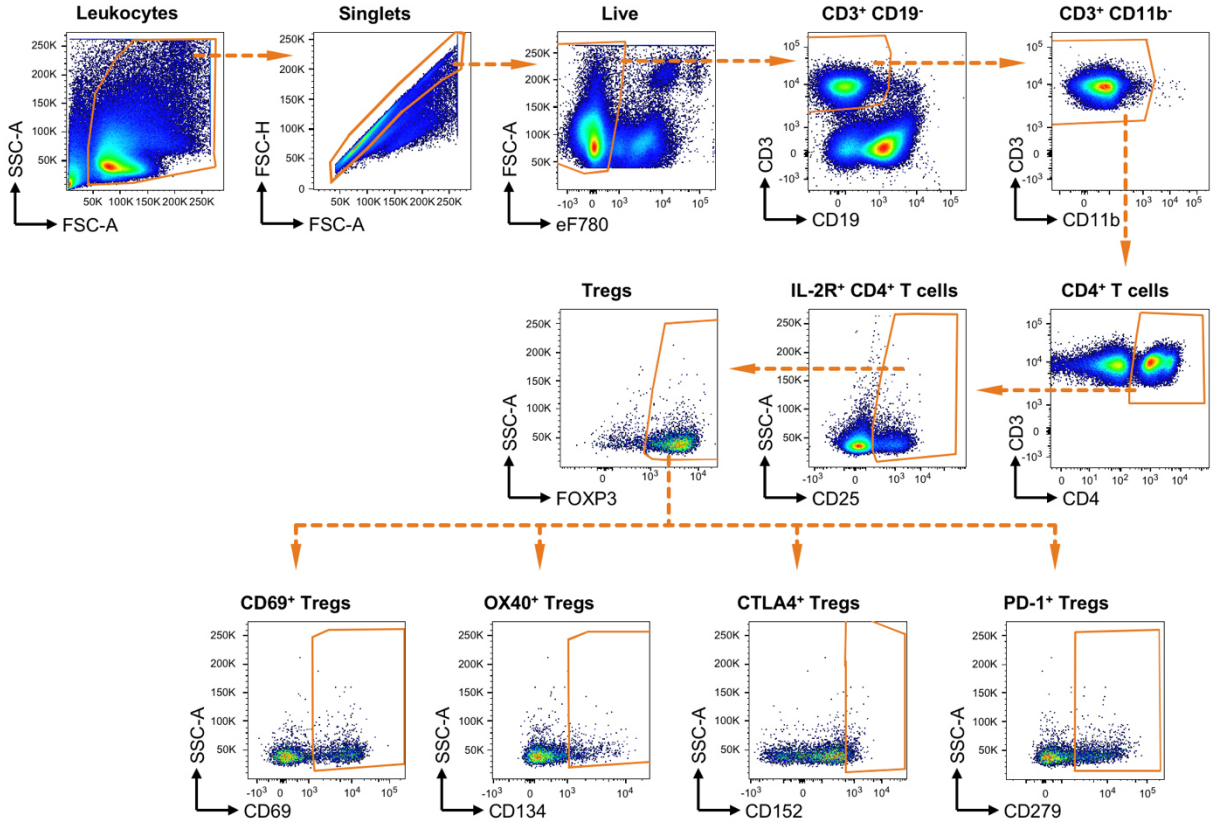

Appendix C: Gating strategy to identify regulatory T cells.
Representative illustration of the gating strategy for regulatory T cells (Tregs) via pseudo color plots of splenocytes from a naïve wild type mouse. Leukocytes were gated based on granulocytic (SSC-A) and cell size (FSC-A) followed by definition of single cells (singlets). Alive singlets (live) were determined with the viability stain eFluor™780 (labels dead/dying cells). T cells were gated based on the presence of CD3 and the absence of CD19 and CD11b. $CD4^+$ T cells were gated and analyzed the expression of the interleukin-2 receptor (IL-2R; CD25). Tregs were then identified in the following gate by detection of the transcription factor FOXP3. $FOXP3^+$ cells were further analyzed for the expression of the activation markers CD69, OX40 (CD134), CTLA4 (CD152) and PD-1 (CD279). (SSC - sideward scatter; FSC - forward scatter; A - area; H - height).

Appx. D: List of figures.

Appx. E: List of tables.

Appx. F: List of abbreviations.

A

A	area
AAPOS	American Association of Pediatric Ophthalmology & Strabismus
Appx.	appendix
AIDS	acquired immune deficiency syndrome
ANOVA	analysis of variance
APC(s)	antigen presenting cell(s) or allophycocyanin (fluorophore)
ApiAT	apicomplexan amino acid transporters
Arg	arginine (L-)
AU	Australia or arbitrary unit

B

β-actin	beta actin
BAC	bacterial artificial chromosome
BCA	bicinchoninic acid
BE	Belgium
BHQ	Black hole quencher ®
Bis-Tris	bis(2-hydroxyethyl)amino-tris(hydroxymethyl)-methane
BM	Bruch's membrane
BMDM	bone marrow derived macrophage
bp	base pair(s)
Bq (kBq, MBq)	becquerel (kilo, mega becquerel)
BSA	bovine serum albumin
BV™	Brilliant Violet™

C

C. spp.	Chlamydia species
CC BY 4.0	Creative Commons Attribution 4.0 International license
CCL	CC chemokine ligand
CCR	CC chemokine receptor
CD	cluster of differentiation
CD134	OX40
CD152	compare CTLA4
CD25	high affinity interleukin 2 receptor
CD279	compare PD-1
CD375	compare GITR
CD62L	L-selectin
cDNA	complementary DNA
cfu	colony-forming units
CH	Switzerland or choroid
CO_2	carbon dioxide
ConA	concanavalin A
CpG B	class B CpG-oligonucleotide ODN1826
cpm	counts per minute
CRISPR	clustered regularly interspaced short palindromic repeats
CT(s)	cycle threshold(s)
CTL(s)	cytotoxic T lymphocyte(s)
CTLA4	cytotoxic T lymphocyte antigen 4
Cy	cyanine

D

d	day (s)
Da (kDa)	dalton (kilo dalton)
DC(s)	dendritic cell(s)
ddH_2O	double-distilled water
DMSO	dimethylsulfoxid
DNA	deoxyribonucleic acid
dNTPs	deoxynucleoside triphosphates
DPBS	Dulbecco's phosphate buffered saline
dpi	days post infection
DTT	dithiothreitol
dTTP	deoxythymidine triphosphate

E

E. falciformis	*Eimeria falciformis*
e.g.	*exempli grata* – for example
EBE	endogenous bacterial endophthalmitis
ECL	enhanced chemiluminescence
EDTA	ethylenediaminetetraacetic acid
eNOS	endothelial NOS (NOS3)
et al.	*et alii* – and others
EU	European Union

F

F- / U- / V-bottom	flat (F) / round (U) / conically shaped (V) bottom
FA	fatty acid(s)
FACS	fluorescence-activated cell sorting
FAM	fluorescein
FBS	fetal bovine serum
FC	fovea centralis
FITC	fluorescein isothiocyanate
FMO	fluorescence minus one
FOXP3	forkhead box P3
FSC	forward scatter
fw	forward

G

g	gravity
G	gauge
g (mg, µg)	gram (milligram, microgram)
GAS	gamma-activated sequence
GBP(s)	guanylate binding protein(s)
(m/hGBP)	(murine/human GBP); p65 GTPases
GER	Germany
GITR	glucocorticoid-induced tumor necrosis factor receptor related protein
GRA	dense granule derived protein(s)
group B *Streptococcus*	*Streptococcus agalactiae*
GTPase(s)	guanosine triphosphatase(s)

H

h	hour
H	height
HAART	highly active antiretroviral therapy
HBI agar	brain heart infusion agar
HCl	hydrochloric acid
hCMV	human cytomegalovirus
HEPES	4-(2-hydroxyethyl)-1-piperazineethanesulfonic acid
HFF	human foreskin fibroblast
HHU	Heirnich Heine University
HIV	human immunodeficiency virus
hpi	hour(s) post infection
HPLC	high-performance liquid chromatography
HRP	horseradish peroxidase

I

i.e.	*id est* – that is
IDO1/2	indoleamine 2,3-dioxygenase 1 / 2
(m/hIDO1/2)	(murine/human IDO1/2)
$IDO^{-/-}$	mIDO1 deficient C57BL/6J mouse
IFN (-α /-β /-γ)	interferon alpha / beta / gamma
IFNGR (IFN-γR1/2)	interferon gamma receptor (1/2)
IgG	immunoglobulin G
IL	interleukin
IL-12R	interleukin 12 receptor
IMDM	Iscove's modified Dulbecco's medium
iNOS / miNOS	inducible NOS (NOS2) / murine iNOS
ip	intraperitoneal
IRF	interferon response factor
IRG(s) / mIRG	immunity related GTPase(s) / murine IRG (p47 GTPases)
ISG(s)	interferon stimulated gene(s)
ISRE(s)	interferon-stimulated response element(s)
IQR	interquartile range

J

JAKs	Janus kinases

K

KO	knock out (of a gen)
Kyn	kynurenine (L-)

L

L (mL, µL)	liter (milliliter, microliter)
LAT (LAT1)	L-amino acid transporter (for neutral amino acids)
LPS	lipopolysaccharide

M

m (nm, µm)	meter (nanometer, micrometer)
M (mM, µM)	molar (millimolar, micromolar)
M-CSF	macrophage colony-stimulating factor
M-MLV	moloney murine leukemia virus
1-MT	1-methyl tryptophan
1-D-MT	1-methyl-D-tryptophan
1-DL-MT	1-methyl-DL-tryptophan
1-L-MT	1-methyl-L-tryptophan
M. tuberculosis	*Mycobacterium tuberculosis*
mA	milliampere
mAb / pAb	monoclonal / polyclonal antibody
MACS®	magnetic-activated cell sorting
MAF1	mitochondrial association factor 1
MFI	mean fluorescence intensity
MHCI/II	major histocompatibility complex class I / II
min	minute
ML	macula lutea
MLN	mesenteric lymph nodes
MOI	multiplicity of infection
MOPS	3-(*N*-morpholino)propanesulfonic acid
MP	skim milk powder
MyD88	myeloid differentiation primary response 88

N

NaCl	sodium chloride
$NaHCO_3$	Sodium bicarbonate
nc	neomycin cassette
nd	not detected
NFκB	nuclear factor kappa (κ) B
N^GMMA	N^G-monomethyl-L-arginine
NK cell(s)	natural killer cell(s)
NLRP	nucleotide binding oligomerization domain, leucine rich repeat and pyrin domain containing (protein)
nNOS	neuronal NOS (NOS1)
no.	number
NO	nitric oxide
NOS	nitric oxide synthase
ns	not significant

O

OD	optic disc or optical density

P

p. / pp.	page / pages
P. brasiliensis	*Paracoccidioides brasiliensis*
PAMP(s)	pathogen associated molecular pattern(s)
PBL	peripheral blood lymphocytes
PBS	phosphate buffered saline
PCR	polymerase chain reaction
PD-1	programmed cell death 1
PE	phycoerythrin
PECs	peritoneal exudate cells
PERCP	peridinin chlorophyll protein
PGE2	prostaglandin E2
PR	photoreceptors
PRR (s)	pattern recognition receptor(s)
P/S	penicillin/streptomycin
PV	parasitophorous vacuole

Q

qPCR	quantitative real-time PCR

R

RG	research group
rh / rm	recombinant human / murine (protein)
RNA (mRNA)	ribonucleic acid (messenger RNA)
ROP	rhoptry derived protein(s)
RPE / hRPE	retinal pigment epithelium / human RPE
rpm	revolutions per minute
RT	room temperature
rv	reverse

S

s	second
S. aureus	*Staphylococcus aureus*
SARS-CoV-2	severe acute respiratory syndrome coronavirus 2
SD	standard deviation
SDS	sodium dodecyl sulfate
SEM	standard error of the mean
SOCS	suppressor of cytokine signaling
SPF	specific pathogen-free
spp.	species
SSC	sideward scatter
STAT1(pSTAT1)/ STAT3(pSTAT3)	signal transducer and activator of transcription 1 / 3 (phosphorylated)

T

T. gondii	*Toxoplasma gondii*
TAE	tris base, acetic acid and EDTA
TBS	tris buffered saline
TBS-T	TBS with 0.1 % Tween® 20
TCA	trichloroacetic acid
TCR (TCRb)	T cell receptor (TCR beta chain)
TDO (m/hTDO)	tryptophan 2,3-dioxygenase (murine/human TDO)
*Tg*ApiAT5-3	apicomplexan amino acid transporter of *T. gondii*
*Tg*B1	35-fold repetitive B1 gen of *T. gondii*
TGF-β	transforming growth factor beta
*Tg*IST	*T. gondii* inhibitor of STAT1 transcription activity
*Tg*SAG2	surface antigen 2 of *T. gondii*
Th cell(s)	T helper cell(s)
Th1 cell(s)	type 1 T helper cell(s)
TLA	Toxoplasma lysate antigen
TLR	Toll-like receptor
TNF(-α)	tumor necrosis factor (-alpha)
Treg(s)	regulatory T cell(s)
TRIS	tris(hydroxymethyl)aminomethane
Trp	Tryptophan (L-)

U

U	unit
UK	United Kingdom
USA	United States of America

V

V	volt
v/v	volume per volume

W

w/	with
w/o	without
w/v	weight per volume
WHO	World Health Organization
WT	wild type C57BL/6J mouse

others

°C	degree Celsius
^{3}H-thymidine	tritiated thymidine
^{3}H-uracil	tritiated uracil

Affidavit

I declare under oath that I have produced my thesis independently and without any undue assistance by third parties under consideration of the ‘Principles for the Safeguarding of Good Scientific Practice at Heinrich Heine University Düsseldorf'.

I further declare that my thesis has not already been submitted to another institution, either in the form presented or in a similar form.

Düsseldorf, _____

Christoph-Martin Ufermann

Acknowledgement

This goes to my colleagues, friends and family, because only with your support such a project is possible.

First and foremost, I would like to thank Walter Däubener for providing me with this research topic, as well as for his support and trust that he has shown me throughout the entire period of my doctoral thesis. Special thanks also go to Lutz Schmitt for accompanying my work as the second supervisor.

I would like to thank the Jürgen Manchot Foundation and the Manchot Graduate School 'Molecules of Infection' (MOI) for funding my research project. Thanks to all the members of MOI III for the pleasant time and the lively scientific discussions.
My thanks also go to the relentless proofreaders who have meticulously reviewed my thesis.

I would like to thank all active and former members of my workgroup (including the ‘HPLC-whisperer’) for the support in the past years. In particular, I would like to thank Claudia and Winni, because without their vigorous assistance, even early in the morning and on weekends, this would not have been possible.
Thanks to my colleagues and cooperation partners for their fruitful and productive work. I would like to thank Klaus Pfeffer for the pleasant working atmosphere at his institute.

In this context, I would like to thank, among others, the coffee and breakfast groups, the ‘Brunch & Escape Room’-Team and the 'AA's'. The conference trips to Erlangen, Sardinia and San Diego are not to be neglected, where we learned a lot and created wonderful memories together.
However, I would like to point out one person in particular, Anne, because without her early and continuing friendship and support in virtually all matters, scientific, practical and also mental, I could not have brought this work so far.

From the bottom of my heart, I thank my family and friends for their interest in my academic life and their ‘distractions’ to get me back on track. I would not want to miss any of them. In particular I thank my mother and my sister, who have always supported and motivated me and were proud of every single goal I achieved during my studies and doctorate.

Finally, I would like to thank my wife Vanessa for supporting me in my scientific endeavors, taking care of our lovely son and of things at home, and organizing our social gatherings with friends - without her, this would not be possible. Many thanks to Leon for the joy of life and the balance he gives me day after day.